POWER FLUCTUATION MINIMIZATION IN RENEWABLE SOURCES USING ENERGY STORAGE SYSTEMS

BY

MUHAMMED YIBRE WORKU

A Dissertation Presented to the

DEANSHIP OF GRADUATE STUDIES

KING FAHD UNIVERSITY OF PETROLEUM & MINERALS

DHAHRAN, SAUDI ARABIA

In Partial Fulfillment of the

Requirements for the Degree of

DOCTOR OF PHILOSOPHY

In

ELECTRICAL ENGINEERING

JUNE 2015

KING FAHD UNIVERSITY OF PETROLEUM & MINERALS

DHAHRAN- 31261, SAUDI ARABIA

DEANSHIP OF GRADUATE STUDIES

This dissertation, written by **MUHAMMED YIBRE WORKU** under the direction of his dissertation advisor and approved by his dissertation committee, has been presented and accepted by the Dean of Graduate Studies, in partial fulfillment of the requirements for the degree of **DOCTOR OF PHILOSOPHY IN ELECTRICAL ENGINEERING.**

Dr. MOHAMMAD A. ABIDO
(Advisor)

Dr. ALI AHMAD AL-SHAIKHI
Department Chairman

Dr. IBRAHIM EL-AMIN
(Member)

Dr. SALAM A. ZUMMO
Dean of Graduate Studies

Dr. MAHMOUD KASSAS
(Member)

16/6/15
Date

Dr. IBRAHIM HABIBALLAH
(Member)

Dr. SALIM IBRIR
(Member)

Dedicated To

My Parents

My Sisters

My Brothers

My Wife and Child

ACKNOWLEDGMENTS

All praise is due to Allah the most merciful the most gracious. I am very thankful to Allah for giving me the courage, the guidance and the knowledge to accomplish this work.

I would like to acknowledge the support provided by King Fahd University of Petroleum and Minerals.

I would like to express my special and deepest thanks and appreciation to my supervisor Dr. Mohammad A. Abido for his continuous support, motivation and enthusiasm. He has spent a tremendous effort in mentoring me in how to do novel research and how to write research paper. His advices on the research as well as on my carrier have been priceless. He has been looking after me and the research in every possible way. His welcoming office, listening skill and vast knowledge make working with him an exciting opportunity. I could not have imagined having a better advisor and mentor for my PhD thesis than him. Without his supervision and constant help this dissertation would have not been possible.

I would like to thank Professor Abido and Professor Ibrahim El. Amin for being the best lecturers for my courses. I have really enjoyed the course I took with them.

My special thanks also go to my dissertation committee members; Dr. Ibrahim El. Amin, Dr. A.H Abdurahim, Dr. Mahmoud Kassas, Dr. Ibrahim Habiballah, Dr. Samir Ibrir for their continuous support and positive comments that help improve the dissertation. I

would also like to thank the power research group for discussing issues related to my research work.

Last but not least, I would like to thank my sisters and brothers for their support throughout my studies. My acknowledgment will not be full without thanking my wife Halima and my daughter Tesnim for giving me a freedom to work on the research by scarifying their precious weekends.

TABLE OF CONTENTS

LIST OF TABLES

LIST OF FIGURES

LIST OF ABBREVIATIONS

DG	:	Distribution Generation
RES	:	Renewable Energy Source
SCESS	:	Supercapacitor Energy Storage System
RTDS	:	Real Time Digital Simulator
SMES	:	Superconducting Magnetic Energy Storage
PV	:	Photovoltaic
BESS	:	Battery Energy Storage Systems
FES	:	Flywheel Energy Storage
CAES	:	Compressed Air Energy Storage
PMSG	:	Permanent Magnet Synchronous Generator
WTG	:	Wind Turbine Generator
DER	:	Distributed Energy Resource
MPPT	:	Maximum Power Point Tracking
MPP	:	Maximum Power Point
P&O	:	Perturb and Observe
IC	:	Incremental Conductance

ANN	:	Artificial Neural Network
ANFIS	:	Adaptive Network-Based Fuzzy Inference System
DFIG	:	Double Fed Induction Generator
FRT	:	Fault Ride Through
LVRT	:	Low Voltage Ride Through
PWM	:	Pulse Width Modulation
D-Q	:	Direct and Quadrature axis
PLL	:	Phase Locked Loop
PI	:	Proportional Integral
PSO	:	Particle Swarm Optimization
VSC	:	Voltage Source Converter
MSC	:	Machine Side Converter
GSC	:	Grid Side Converter
NPC	:	Neutral Point-Clamped

ABSTRACT

Full Name : [Muhammed Yibre Worku]

Thesis Title : [Power Fluctuation Minimization in Renewable Sources Using Energy Storage Systems]

Major Field : [Electrical Engineering]

Date of Degree : [June 2015]

Recently the world has seen a shift from the conventional power generation to renewable generation to tackle problems associated with price volatility and carbon impact of fossil fuels. The development of renewable energy based Distributed Generation (DG) is moving fast to meet the worldwide urgent needs of utilizing clean energy sources to create a clean energy future and minimizing costs. Among the renewable energy sources, solar and wind energy are promising to generate electrical energy without environmental contamination. The increasing penetration of renewable and clean DG in utility distribution grids gives rise to the concept of microgrids.

Microgrids which consist of renewable DG play an important role in minimizing the transmission line stress as they are located near the loads and consumers. The disadvantage of these renewable energy sources is that they are intermittent in nature and their output is unpredictable. In order to maintain microgrid internal instantaneous power balance and ensure user load power supply reliability, energy storage device with charging and discharging frequently needs to be equipped to suppress the power fluctuation and provide backup power supply for sensitive load when microgrid is islanded.

This dissertation proposes a control strategy that can minimize the power fluctuations in microgrids consisting of renewable energy sources such as wind and solar. Among the energy storage systems supercapacitor energy storage system (SCESS) is used as it has high power density, maintenance free, higher efficiency, high life time and can be charged and discharged continuously without deterioration. Linear and non-linear models of both grid connected PV and wind systems are developed and optimal design of the control parameters are carried out. The power electronics blocks that are used to integrate the renewable sources to the grid are designed. The optimal size of the SCESS and its control strategy are developed for continuously charging and discharging SCESS to achieve its objectives. The proposed control strategy is implemented in Real Time Digital Simulator (RTDS) and the stability of the microgrid equipped with SCESS has been investigated. The fault ride through capability of the microgrid with and without SCESS is investigated and results are provided to verify the efficiency of the proposed controller. The results provided show that the fluctuation of the power generated from the renewable sources is minimized. During grid faults the proposed controller stores the power generated during the fault duration.

ملخص الرسالة

الاسم الكامل : محمد ايبري واركو

عنوان الرسالة : تقليص التذبذب فى القدرة لمصادر الطاقة المتجددة باستخدام أنظمة تخزين الطاقة

التخصص: : الهندسة الكهربية

تاريخ الدرجة العلمية : مايو 2015

لقد شهد العالم مؤخرا تحولا من الأعتماد على توليد الطاقة التقليدية إلى توليد الطاقة المتجددة و ذلك للتصدى للمشاكل المرتبطة بارتفاع الأسعار و الأنبعاثات الكربونية للوقود الحفرى. نتيجة لذلك يتسارع التطوير لنظم التوليد الموزعة المعتمدة على الطاقة المتجددة لتلبية الحاجات الملحة لمصادر طاقة نظيفة لخلق مستقبل نظيف للطاقة و لتقليل التكاليف. و تعد الطاقة الشمسية و طاقة الرياح من مصادر الطاقة المتجددة الواعدة لتوليد الطاقة الكهربية دون التسبب فى تلوث البيئة. ولقد أدى زيادة انتشارأنظمة التوليد الموزع المعتمد على الطاقة المتجددة فى شبكات التوزيع الكهربية لظهور مفهوم الشبكات الدقيقة. حيث تلعب الشبكات الدقيقة المعتمدة على مصادر الطاقة المتجددة دورا كبيرا فى تقليل الضغط على خطوط نقل الطاقة حيث تتواجد بالقرب من الأحمال و المستهلكين. و لكن يعاب على مصادر الطاقة المتجددة أنها خرجها متقطع بطبيعته و لا يمكن التنبؤ به. و للحفاظ على توازن الطاقة اللحظى للشبكات الدقيقة و لضمان الأعتمادية بين مصدر الطاقة و الأحمال فيجب تزويدها بمصادر تخزين الطاقة, وذلك لإخماد التذبذب فى الطاقة كما أنها تعمل كدعم لتغذية الأحمال عالية الحساسية فى حالة الفصل الأضطراى للشبكة الدقيقة.

تقدم هذة الأطروحة طريقة تحكم لتقليل التذبذب فى الطاقة للشبكات الدقيقة المعتمدة على مصادر الطاقة الجديدة مثل طاقة الرياح و الطاقة الشمسية لأدنى قيمة. وقد تم استخدام نظام التخزين المعتمد على المكثفات الفائقة من بين أنظمة تخزين الطاقة المختلفة حيث أنها تتميز بكثافة عالية للطاقة. تم عرض كل من النماذج الخطية و الغير خطية للشبكة المتصلة بمصادر الطاقة المعتمدة على الطاقة الشمسية و الرياح مع تنفيذ التصميم الأمثل للعوامل المؤثرة فى التحكم. كذلك تم تصميم وحدات الكترونيات القوى اللازمة لتوصيل مصادر الطاقة المتجددة مع الشبكة. تم اختيار الحجم الأمثل لنظام التخزين المعتمد على المكثفات الفائقة و تصميم استراتيجية التحكم بها لضمان استمرارية الشحن و

التفريغ لهذه الأنظمة بما يحقق أهدافها. تم تنفيذ استراتيجية التحكم عمليا على نظام (RTDS) و تم التحرى من استقرار الشبكة المزودة بنظام التخزين المعتمد على المكثفات الفائقة. كذلك تم التحرى من قدرة الشبكة على التغلب على الأخطاء بوجود و بدون نظام التخزين المعتمد على المكثفات الفائقة و قد أوضحت النتائج كفاءة طريقة التحكم المقترحة.

CHAPTER 1

INTRODUCTION

1.1 Background

The electric power systems are generally experiencing different trends which may imply major changes in their architecture and operation. They are facing several issues because of integration of renewable energy sources, energy market restructuring, increasing environmental awareness and rising concerns about security of energy supply. Furthermore, the constant growth in electricity demand and general increase of inter and intra zonal power transactions put the electric system under strain and force it to operate close to its physical limits. Such issues have been traditionally addressed by adding new capacity, with investments particularly in the field of large size generation and transmission infrastructures. Nowadays, increasing the power system capacity is frequently a challenging option due to economic, environmental, and political constraints that hinder the construction of large power plants and high voltage lines [1]. The aforementioned concerns encourage the use of distributed generation (DG) in which the energy sources are installed close to the end users. Renewable energies with their infinite sources (like sun and wind) and the lowest impact on the environment are the first choice for the primary power of DG units. The increasing penetration of renewable and clean DG in utility distribution grids gives rise to the concept of microgrids.

Microgrids which consist of renewable DG play an important role in minimizing the transmission line stress as they are located near the loads and consumers. The disadvantage of these renewable energy sources is that they are intermittent in nature and their output is unpredictable. Microgrids need to be equipped with energy storage devices with frequent charging and discharging to reduce the intermittency in the generated power and to maintain microgrid internal instantaneous power balance, improve power quality, and ensure user load power supply reliability.

In a Microgrid with renewable energy sources, the objective is to transfer the maximum possible power. In grid connected mode, since the voltage magnitude and frequency are adapted from the main grid, the controller objectives are different from autonomous operation mode. In grid connected mode the output active and reactive power or input DC–link voltage magnitude can be controlled. In autonomous mode, along with the power balance between the loads and the sources, the voltage magnitude and frequency should be controlled.

Wind turbines produce AC voltage using different kinds of generators and are normally connected with an AC-DC-AC back-to-back converter. In this condition, the input AC voltage is converted to DC voltage and is then converted to an AC voltage with a desirable voltage magnitude and frequency. In addition, the active and reactive power in both sides can also be controlled. The PV system, as a DC source, can be connected to the loads in either single stage or double stage mode. In single stage mode, the PV system is connected to the grid using three phase or single phase inverter which directly converts the DC input to AC output. The other combination, due to the nonlinear characteristics of

the PV system, uses a DC/DC converter to control and normally boost the input source voltage while another inverter converts the DC voltage to AC voltage.

Recent developments and advances in energy storage and power electronics technologies are making the application of energy storage technologies a viable solution for microgrid applications [3, 4]. With the four quadrant operating capacity of the energy storage, the microgrid can easily control the bidirectional power flow and maintain system instantaneous power balance. The energy storage systems in microgrid can be batteries, flywheels, super-conducting magnetic energy storage (SMES) or supercapacitor energy storage system (SCESS). An energy storage technology usually includes a power conversion unit to convert the energy from one form to another. Two factors characterize the application of an energy storage technology. One is the amount of energy that can be stored in the device which is a characteristic of the storage device itself. Another is the rate at which energy can be transferred into or out of the storage device.

Given this brief background, this dissertation proposes a control strategy that can minimize the power fluctuations in microgrids consisting of renewable energy sources such as wind and solar. Among the energy storage systems supercapacitor energy storage system (SCESS) is proposed as it has high power density. Linear and non-linear models of both grid connected PV and wind systems are developed and optimal design of the control parameters are carried out. The power electronics blocks that are used to integrate the renewable sources to the grid are designed. The optimal SCESS to minimize the fluctuation and the charging and discharging controllers are designed. The proposed control strategy is implemented in Real Time Digital Simulator (RTDS) and the stability of the microgrid equipped with SCESS has been investigated. The fault ride through

capability of the microgrid with and without SCESS is investigated and results are provided to verify the efficiency of the proposed controllers.

1.2 Dissertation Motivations

The increasing penetration of renewable and clean distribution generation (DG) in utility distribution grids gives rise to the concept of microgrids. A typical microgrid can be viewed as a cluster of DG units capable of operating either islanded or connected to the main grid. Microgrids can provide grid reinforcement without the need for more generation expansion and can increase the service reliability. But the output of microgrids consisting of renewable energy sources such as wind and solar are unpredictable and difficult to dispatch.

The motivation of this dissertation work is inspired from some of the unresolved issues found in related works on the problems of power fluctuations in microgrids using renewable energy sources. With increasing level of renewable energy sources especially wind and solar power, the intermittent and fluctuating features of these resources increase the uncertainties and challenges for future smart grids. Minimizing the power fluctuation and controlling the power flow in the microgrid is the motivations of this dissertation. Energy storage systems can play a viable role in minimizing these fluctuations. A supercapacitor energy storage system (SCESS) is used to aid the microgrid to minimize the power fluctuations from renewable energy sources. A buck boost converter is used to connect the energy storage to the DC link of the inverter. The inverter is controlled to exchange active and reactive power making the microgrid more reliable.

1.3 Dissertation Objectives

This dissertation aims at developing a new control strategy to minimize the power fluctuation caused by renewable energy sources in microgrids working in grid connected mode. The developed controller is implemented in real time using Real Time Digital Simulator (RTDS). The developed control unit minimizes the intermittency caused by renewable energy sources in the microgrid. The specific objectives are as follows:

1. Developing a dynamic model of a microgrid consisting of renewable energy sources of photovoltaic (PV) and wind, buck converter, inverter, buck-boost converter, and supercapacitor.
2. Developing intelligent control strategies for the developed model so that the power fluctuation is minimized. The developed model with its controllers is implemented in RTDS.
3. Testing the developed system under different scenarios in order to assess the effectiveness of the proposed control strategies.
4. Investigating the fault ride through capability of the system equipped with supercapacitor energy storage.

1.4 Dissertation Methodology

The aim of this dissertation is to develop and implement an intelligent real time control of a microgrid with energy storage system so that the power fluctuation is minimized. To do

so, a comprehensive theoretical investigation, controller implementation and experimental validation are required to accomplish the dissertation. The phases required for the execution of the dissertation are:

1. Comprehensive Literature Review on: microgrid, distribution generation, inverters used in microgrids, energy storage to minimize power fluctuation in microgrids, superconducting magnetic energy storage (SMES), battery energy storage systems (BESS), flywheel energy storage (FES), compressed air energy storage (CAES), supercapacitor energy storage system (SCESS).
2. System Modeling: developing models for the microgrid with renewable energy source, developing models for buck-boost converter, inverter, buck boost converter, supercapacitor and battery, integration of the whole system.
3. Developing Control Strategy: developing a controller for each developed block. The optimal control parameters are determined using the linearized model. Linear objective function is proposed to determine the control parameters and to check the system stability. Testing each controller and integrating the whole controller to the system.
4. Investigation of the developed model under different operating scenarios: verification of the model in minimizing the power fluctuation from renewable sources.

1.5 Summary of Contributions

The main contribution of this dissertation is proposing an efficient control technique to minimize the fluctuation and enhance fault ride through capability of renewable sources such as PV and wind. Both PV and wind with supercapacitor energy storage system are implemented and a controller is developed to continuously charge and discharge the supercapacitors to minimize the fluctuation for both wind and PV. The generated power from the renewable sources is integrated to the grid using an inverter. An independent P-Q controller is developed and implemented for the inverter to transfer the DC link power to the grid for both wind and PV. To generate maximum power from the PV array, a controller is proposed for the buck converter to continuously locate the maximum power point.

Renewable power sources need to have fault ride through capability. A controller is proposed and implemented to help the system to ride through grid faults and make the system alive during the fault duration. The optimal supercapacitance to minimize the fluctuation of the generated power and for fault ride through for both PV and wind is determined. Both PV and wind systems are implemented in RTDS. The controllers efficiency is examined by applying different disturbances and results are provided for verification.

1.6 Dissertation Organization

This dissertation consists of seven chapters as outlined below.

- The first chapter is an introduction chapter introducing the dissertation work, motivation and objectives.
- Chapter 2 deals with detailed literature review of power fluctuation minimization in renewable sources using energy storage system. Different energy storage systems are explained in this chapter. The fault ride through technique is also explained.
- Chapter 3 focuses on the modeling and control of grid connected PV system. Non-linear and linear model of the system is developed and control parameters are designed. The generated power from the PV array is transferred directly to the grid. RTDS based simulation results are provided by varying the input irradiation and temperature.
- Chapter 4 deals with power fluctuation minimization in PV systems by using supercapacitor energy storage system (SCESS). The SCESS is used to store the power from the PV array during off-peak loads and is then used later when the power demand is peak. The system parameters of the SCESS and the optimal supercapacitance are designed in this chapter. The system performance is evaluated by applying a disturbance and RTDS based simulation results are provided.
- Chapter 5 presents the power fluctuation minimization in wind based renewable energy source. The dynamic model and control of permanent

magnet synchronous generator (PMSG) based wind turbine generator (WTG) is presented. The model is tested to minimize the fluctuation of the power by varying the wind speed and results are provided for verification.

- Chapter 6 deals with the fault ride through capability of renewable sources equipped with SCESS. This chapter explains how the power generated during grid faults is stored in the SCESS. Three phase grid faults are applied for both PV and wind systems and results are presented at the end of the chapter.
- Chapter 7 concludes the dissertation by pointing the findings of the work and highlighting the scope of future work.

CHAPTER 2

LITERATURE REVIEW

This chapter presents a comprehensive literature review of grid connected PV and wind system together with power fluctuation minimization, maximum power point tracking, and energy storage systems. In addition the chapter contains control strategies for fault ride through by equipping the renewable sources with energy storage systems.

2.1 Overview

In the near future, the demand of electric energy is expected to increase rapidly due to the global population growth and industrialization. This increase in energy demand requires electric utilities to increase their generation. Currently, a large share of electricity is generated from fossil fuels, especially coal due to its low prices. However, the increasing use of fossil fuels accounts for a significant portion of environmental pollution and greenhouse gas emissions, which are considered the main reason behind global warming. To overcome the problems associated with generation of electricity from fossil fuels, Renewable Energy Sources (RES) can participate in the energy mix. Also the deregulation in electricity markets and the development of the distributed generation (DG) technologies are promoting the use of RES in power generation [1]. A complete literature review of integration of DG in terms of control, protection and stability is reported in [2], [3]. Hardware in the loop simulation for testing the operation and control of microgrid is presented in [4]. A method of controlling the power flow between the utility and the microgrid using back to back controlled converter is reported in [5], [6].

The size and location of DGs in distribution systems with different local loads can be determined using a multi-objective optimization as reported in [7]. But one disadvantage of using RES such as PV and wind is that their output power is fluctuating and unpredictable and hence they are undispatchable [8]. To minimize this fluctuation different energy storage systems can be integrated to the RES [9]. Recent developments and advances in energy storage and power electronics technologies are making the application of energy storage technologies a viable solution for microgrid applications [10], [11].

2.2 Energy Storage Systems

Electrical energy in an AC system cannot be stored electrically. However, energy can be stored by converting the AC electricity and storing it electromagnetically, electrochemically, kinetically, or as potential energy. Each energy storage technology usually includes a power conversion unit to convert the energy from one form to another. Energy storage technology is used to make the electric power systems more reliable as well as making the broader use of renewable energy a reality. They can provide a wide array of solutions to key issues that are affecting the power system. Depending on the technology selected, they can provide spinning reserves, load leveling and shifting, load forecasting, frequency control, VAR support and voltage regulation, relief of overloaded transmission lines, release of system capacity, and enhance power quality. It also increases the overall efficiency of the power system.

There are a variety of storage devices such as batteries, supercapacitors, superconducting materials, flywheels, and water pumping. These devices vary in their characteristics, method of operation, and accordingly, the tasks that they can perform. Thus, choosing a

storage device that can perform the required function efficiently is a preliminary step. Moreover, due to the fact that the majority of storage devices are expensive, it is essential to study the economical value of using these devices.

2.2.1 Superconducting Magnetic Energy Storage (SMES)

Although superconductivity was discovered in 1911, it was not utilized until the 1970s that SMES was first proposed as an energy storage technology for power systems. SMES systems have attracted the attention of both electric utilities and the military due to their fast response and high efficiency (charge–discharge efficiency over 95%). The SMES unit is designed to store electric power in low loss superconducting magnetic coil. Power can be absorbed by or released from the coil according to system requirements. Besides stability improvement of interconnected systems, SMES units have been reported to be used in isolated systems for load leveling and damping control and also for load frequency control of power systems [12]–[16]. One of the main components of a SMES unit is the converter bridge where the voltage impressed on the superconducting coil can be moved up and down in order to achieve the desired power interchange.

2.2.2 Battery Energy Storage Systems (BESS)

Batteries are one of the most cost effective energy storage technologies available with energy stored electrochemically. A battery system is made up of a set of low voltage/power battery modules connected in parallel and series to achieve a desired electrical characteristic. They store DC charge, so power conversion is required to interface a battery with an AC system. Key factors of batteries for storage applications include: high energy density, high energy capability, round trip efficiency, cycling capability, life span, and initial cost [17]. Batteries can be designed for bulk energy

storage or for rapid charge/discharge. Improvements in energy density and charging characteristics are still an active research area, with different additives under consideration. Due to the chemical kinetics involved, batteries cannot operate at high power levels for long time periods. In addition, rapid, deep discharges may lead to early replacement of the battery, since heating resulting in this kind of operation reduces battery lifetime. There are also environmental concerns related to battery storage due to toxic gas generation during battery charge/discharge. The disposal of hazardous materials presents some battery disposal problems.

As solar photovoltaic power generation becomes more commonplace, the inherent intermittency of the solar resource poses one of the great challenges to those who would design and implement the next generation smart grid. Specifically, grid-tied solar power generation is a distributed resource whose output can change extremely rapidly, resulting in many issues for the distribution system operator with a large quantity of installed photovoltaic devices. Battery energy storage systems are increasingly being used to help integrate solar power into the grid. These systems are capable of absorbing and delivering both real and reactive power with sub-second response times. With these capabilities, battery energy storage systems can mitigate such issues with solar power generation as ramp rate, frequency, and voltage issues. Beyond these applications focusing on system stability, energy storage control systems can also be integrated with energy markets to make the solar resource more economical [18].

2.2.3 Flywheel Energy Storage (FES)

Flywheel energy storage works by accelerating a cylindrical assembly called a rotor (flywheel) to a very high speed and maintaining the energy in the system as rotational

energy. Energy is stored as kinetic energy using a rotor that rotates with high angular speed. The energy storage capacity depends on the mass and shape of the rotor and on the maximum available angular velocity. Mechanical inertia is the basis of this storage method. A heavy rotating disc is accelerated by an electric motor, which acts as a generator on reversal, slowing down the disc and producing electricity. Electricity is stored as the kinetic energy of the disc. Friction must be kept to a minimum to prolong the storage time. This is often achieved by placing the flywheel in a vacuum and using magnetic bearings, tending to make the method expensive. Due to their simplicity, FES has been widely used in commercial small units (about 3 kWh) in the range of from 1 kW – 3 hours to 100 kW – 3 seconds [19].

2.2.4 Compressed Air Energy Storage (CAES)

CAES uses the peaks of energy generated by renewable energy plants to run a compressor that compresses the air into a hermetic underground reservoir or surface vessel/piping. The compressed air is used, combined with a variety of fuels in a combustion turbine to generate electric energy when demand is high. The energy storage capacity depends on deposit volume and maximum storage pressure of the compressed air. Start up time is usually high. CAES is used for large and medium (micro CAES) scale systems [20]–[22].

During off-peak hours, electricity from the grid powers compressors that drive air into the underground storage vessel. When demand increases, the air is released to the surface and heated with clean burning natural gas to expand its volume and velocity. The air-gas mixture is used to drive a specialized combustion turbine that can generate up to 300MW of power. Because off-peak electricity rather than gas is used to compress the air, a

CAES plant uses less than half the amount of natural gas required by a conventional combustion turbine. By using this excess energy to run a compression unit which compresses fresh air and securely stored underground, we can make sure that most of the renewable energy generated can be used if not immediately, then at a time when there is increased demand, or when renewable resources are experiencing periods of low production. Storing fresh air in salt caverns is a proven, reliable and safe method of ensuring that excess energy is not wasted.

2.2.5 Supercapacitor Energy Storage System (SCESS)

There are no chemical reactions involved in the supercapacitor energy storage mechanisms. The principal supercapacitor characteristic that makes it suitable for using in energy storage system is the possibility of fast charge and discharge without loss of efficiency for thousands of cycles as they store electrical energy directly. They can recharge in a very short time having a great facility to supply high and frequent power demand peaks. They are well suited to replace batteries in many applications because at the moment their scale is comparable to that of batteries, from small ones used in cellular phones to large ones that can be found in cars. Even though super capacitors have a lower energy density compared to batteries, they avoid many of the battery's disadvantages [23], [24].

They can be used for short term ride through capabilities as well as voltage regulation, frequency control and other power quality issues [25]–[27]. The supercapacitor offers great promise because it has the great attributes of a battery without the undesirable traits and offers a round trip efficiency of 84-95%. This combined with the ability of modular,

quiet, non-polluting, quick charge and discharge capability, long life (10 to 12 years) and very high cycle life makes the supercapacitor a very desirable energy storage device [28].

The comparison of different energy storage systems in terms of power density, energy density, response time and efficiency is tabulated in Table 2.1.

Table 2.1 Comparison of Different Energy Storage Systems

Technology	Power	Energy Density	Back-Uptime	Response Time	Efficiency (%)
Pumped hydro	100MW-2GW	400MWh-20GWh	hours	12 minutes	70-80
CAES	110-290(MW)	1.16-3 (GWh)	hours	12 minutes	99
BESS	100W-100MW	1kWh-200MWh	hours	seconds	60-80
Flywheels	5kW-90MW	5-200 (kWh)	minutes	12 minutes	80-95
SMES	170kW-100MW	110Wh-27kWh	seconds	milliseconds	95
Supercapacitor	<1MW	1Wh-1kWh	seconds	milliseconds	>95

2.3 Standards for Microgrid Generation

The following standards are considered as guidelines during the design process of the power conditioning unit (PCU) and control thereof:

IEEE 519 – 1992 (Harmonics) [29]

IEEE 929 – 2000 (islanding detection) [30]

IEEE 1547 – 2003 [31]–[33]

These standards provide guidelines and specifications for the interconnection and control of distributed energy resources (DERs) to the utility grid. A brief summary of each standard is given below.

IEEE 519 – 1992 gives recommended practices and requirements for the harmonic control of electrical power systems. It sets maximum Total Harmonic Distortion (THD)

limits on voltages and currents that a power system is allowed; therefore the power conditioning unit cannot inject harmonics into the grid that cause the system to go above these limits set forth by the standard, and if at all possible, the power conditioning unit should filter these harmonics.

IEEE 929 – 2000 presents recommended practices for the utility interface of photovoltaic (PV) systems. Though written for PV inverters, the guidelines and specifications can be adapted to be used for an inverter connecting a DER to the utility.

IEEE 1547 – 2003 is the standard for the interconnection of distributed resources to the utility grid. This standard outlines requirements and specifications that the conversion systems of the DER have to meet to be allowed to connect to the utility. This standard does not deal with the concepts and issues of intentional islanding, and currently dictates that the DER shall disconnect from the distribution system when islanding events occur.

An analysis of 1547 raising questions to issues proposed by it can be found in [33].

The IEEE 1547 is compatible with the Saudi distribution code provided by the Electricity and Cogeneration Regulatory Authority (ECRA) [34].

2.4 Power Fluctuation Minimization Using Energy Storage

Recently, the world has seen a shift from the conventional power generation to renewable generation to tackle problems associated with price volatility and carbon impact of fossil fuels. The development of renewable energy based DG is moving fast to meet the worldwide urgent needs of utilizing clean energy sources to create a clean energy future and minimizing costs. Among the renewable energy sources, wind and solar energy are promising power sources. Photovoltaic (PV) system provides the most direct method to convert solar energy into electrical energy without environmental contamination.

2.4.1 PV Systems

The power generated from a PV cell varies depending on the irradiation and temperature received at any instant of time. Since these input parameters vary throughout the day, different maximum power point tracking (MPPT) design methods have been reported over the years to locate the best operating point [35]–[50]. These include Perturb and observe (P&O) [48], Incremental Conductance (IC) [39], artificial intelligence techniques such as Artificial Neural Networks (ANNs) [43] and Fuzzy Logic control [41]. The widely used methods by many researchers are IC and P&O due to their simplicity. On the other hand, the fuzzy-inference system (FIS) based MPPT has been proposed and used recently. Integrating FIS with ANN results in a powerful Artificial Intelligence technique known as Adaptive Network-Based Fuzzy Inference System (ANFIS) [45], [46].

The power generated from the PV array can be integrated to the grid in a single stage using an inverter or multistage using a buck or boost DC-DC converter and an inverter. Single stage grid connected PV system is studied in [51]–[54] where as a multistage grid connected PV system is reported in [55]–[58]. Multistage scheme provides the flexibility in designing the control architecture as it has more control variables and multiple control objectives.

Generally, PV output power fluctuates as a result of varying irradiation and temperature. When the irradiation fluctuates, the generated power from the PV array fluctuates and power system is very sensitive to medium frequency power fluctuations ranging from 0.01 Hz to 1 Hz [59]. Voltage fluctuation in PV systems caused by change in irradiation at the point of common coupling is reported in [60]. Attenuating this power fluctuation helps the power system to be more stable. Besides this, fluctuation of the generated

power from PV source based DG affects local loads connected to the system. Hence, minimizing this fluctuation by storing the generated power during off peak loads and using it later during peak loads increases the reliability of the DG system. To overcome this fluctuation, different energy storage devices are integrated to the PV system. A review of energy storage systems for microgrid is reported in [61]. Among these, battery and supercapacitor energy storage system (SCESS) are used in the literature because of their high energy and power densities respectively [61]–[64]. Some work has been done to integrate SCESS with STATCOM for low voltage and fault ride through of wind energy system as well as smoothing power fluctuation [65]–[66]. Fuel cell is used to reduce the intermittent nature of wind and photovoltaic systems in [68]. The optimal size of a battery and battery-supercapacitor hybrid energy storage system for microgrid application is proposed in [69]-[70]. Different linear and nonlinear control techniques have been proposed recently on isolated and grid connected PV with energy storage system [71]–[74]. Model predictive control to forecast grid connected PV and to use energy storage to participate in power market is studied in [73].

2.4.2 Wind System

One way of generating electricity from renewable sources is to use wind turbines that convert the energy contained in flowing air into electricity [75]. Wind turbines have been in use for more than 1,000 years. The earliest wind turbine designs were extremely simple; turbines were allowed to rotate at a rate proportional to the velocity of the wind. They were used to pump water, grind grain, cut lumber, and perform a myriad of other tasks. For these purposes, varying speed seldom impacted the effectiveness of the windmill enough to justify the complications of closely controlling rotational speed.

Allowing the machines to run at variable speed was in fact highly advantageous as it greatly increases the total energy that could be extracted from the wind.

Induction generator including squirrel cage and double fed induction generator (DFIG) are commonly used to extract power from wind speed. Since the output voltage and frequency from the variable speed wind turbine system is variable, power electronics components are used to convert and interface these values to meet the grid codes. Vector control of variable speed wind power generation using DFIG is reported in [76]–[78].

Variable speed wind turbines using direct drive permanent magnet synchronous generator (PMSG) is getting more attention in wind turbine applications because it is gear box free, does not need field excitation, has full controllability of the system [79]–[82]. As compared to double fed induction generator (DFIG) wind turbine, PMSG wind turbine has better efficiency and reliability [75], [83], [84].

Similar to PV, the output power from wind turbine generators (WTG) varies depending on wind speed. Application of battery storage for wind power dispatchability is used in [85]–[87], flywheel is used in [88]-[89] where as superconducting magnetic energy storage system is studied in [90]–[92] . Sliding mode and neural network control techniques for DFIG using fly wheel energy storage system are reported in [93], [94]. A review of energy storage for wind based microgrid is reported in [95]. To minimize the intermittency of renewable sources, assessment of energy storage options is presented in [96], [97]. A hybrid energy storage system with supercapacitor and battery to study the stability of a micrigrid with high penetration of renewable sources is studied using simulation and experiments in [98]. Supercapacitors have high power density and fast response time which make them suitable to be used in minimizing short term fluctuation

in renewable sources. One such application is reported in [99]–[101] and authors in [102],[103] reported the use of supercapacitor based DFIG to provide constant power to the grid. The SCESS can be connected to the system at the AC side or DC link side. Buck boost converter is used to integrate the SCESS to the DC link. Authors in [103] used the SCESS at the AC side to minimize the fluctuation of permanent magnet synchronous generator (PMSG). But this type of topology needs more converters and is expensive to implement as compared to the SCESS connected at the DC link side. Conventional and novel control designs for direct driven PMSG based wind turbine is reported in [104] where as in [105], the authors proposed a control scheme for variable speed wind turbine using a full scale converter. Two level converters are commonly used to integrate the power generated from wind turbines to the grid but for higher voltage raring three level converters can be used. Authors in [106] used a three level neutral point clamped (NPC) converters to integrate PMSG based WTG to the grid. The stability of NPC based PMSG for weak grid is reported in [107].

However, most of the literature address how to use the energy storage for other issues and control techniques. Issues related to power fluctuation minimization using the energy storage has not been extensively discussed.

2.5 Fault Ride Through (FRT)

The increasing penetration of PV and wind power into electric power grids raises the concern that wide spread tripping of these systems due to grid disturbances, could lead to local or system wide instabilities [108]. Therefore, many countries have developed or revised grid operating codes for PV arrays and wind farms, specifying the fault

conditions under which these systems should remain connected to the electricity grid [109].

Energy storage systems can play a great role in managing the power generated during grid faults and help the system ride through fault [110], [111]. There should be proper voltage control in grid connected WTG system using DFIGs as they are very sensitive to voltage ride or fall. Authors in [112]–[115] reported a low voltage ride through technique for such application. The low voltage ride through (LVRT) of fixed speed wind turbines using STATCOM using energy storage system is reported in [116],[117]. Advanced FRT technique using electric double layer capacitor (EDLC) is proposed in [118]. The authors proposed that during grid fault the DC link voltage is controlled by the buck-boost converter and the grid side converter acts as STATCOM to inject the required reactive power. Authors in [119],[120] used a superconducting fault current limiter (SFCL) to improve the FRT capability of DFIG based wind turbine generation system without using energy storage system but authors in [121],[122] used a SMES to improve the FRT.

2.6 Control of Microgrids

Microgrids are controlled to be operated in two modes: grid connected and islanded modes. In grid connected mode, the frequency and the voltage are controlled by the grid. The objective of the microgrid is to transfer a specified active and reactive power to the grid. In the island mode, the microgrid has to control the voltage, frequency together with controlling the active and reactive power supplied to the load. Survey of control strategies for island mode operation of microgrids is presented in [123], [124]. The authors in [125] addressed both grid connected and islanded mode microgrids based on potential function. Autonomous electricity networks to integrate distributed energy sources using droop

control is presented in [126]. A controller to detect the intentional islanding of a microgrid from grid connected mode to island mode is studied in [127]. The authors in [128]–[130] presented control of voltage source inverters used to integrate distribution generation to the grid.

CHAPTER 3

GRID CONNECTED PV SYSTEM

This chapter presents the power electronics components and the controllers used to integrate the power generated from the PV array directly to the grid. Furthermore, it presents the small signal model of the system to check the system stability and to design the control parameters. RTDS based results are provided to check the controller in transferring the generated power to the grid by applying a different disturbance in the input irradiation and temperature.

3.1 Overview

The growth of world energy demand and the environmental concerns lead to an increase of the renewable energy production over the last decade. Energy sources such as solar or wind become more popular mainly because they produce no emissions and are inexhaustible. Photovoltaic (PV) cells generate electricity directly from light hence the name, photo relating to the light source and voltaic relating to the electrical output. PV energy is the fastest growing renewable source with a history dating since it has been first used as power supply for space satellites. It is one of the most promising sources of electricity for the future and it can be used as a distributed generator (DG) to play its role in smart grids of the future. The conversion process produces no harmful by-products and with no moving parts, the photovoltaic cell should last practically longer period.

PV cells which are usually made of semiconductor material generate low output dc voltage (current) and have a nonlinear I-V / P-V characteristic. These cells are connected in series and parallel to form a module, and several of these modules are combined to form a panel which finally forms an array of panels. In order to power the utility, the PV panels require power electronic converters to condition this varying DC voltage to the grid. Each of these power electronic converters in an inverter system can comprise of a DC-AC converter, a DC-DC buck or boost converter, maximum power point tracker (MPPT) and filter circuit linking the DC source to the local load and grid.

Figure 3.1 depicts the configuration of grid integrated PV system used in this dissertation. The PV array which is formed from a number of modules converts the solar irradiation into DC current and voltage. This constant voltage and current is converted to AC using three phase inverter that can deliver the energy either to AC load connected or to the main grid. To make the DC power generated from the PV array suitable for the inverter and implement MPPT, a buck converter with its duty cycle adjusted continuously under varying irradiation and temperature to instantly locate the maximum voltage or current output from the PV arrays is used. We have a physical hardware in the power laboratory that works with a reduced DC link voltage. The choice of the buck converter is justified to meet the DC link voltage requirement of the hardware.

In Figure 3.1,

I_{PV}, V_{PV} and P_{PV} : represent the current, voltage and power generated from the PV array respectively.

I_{DC} and V_{DC} : are the DC link current and voltage respectively.

I, V_g and P_g : are the grid current, grid voltage and power delivered to the grid

respectively.

T_r : is the coupling transformer.

L : is the grid coupling inductance.

D : is the duty of the buck converter.

m_D : is the D-axis inverter control signal.

m_Q : is the Q-axis inverter control signal.

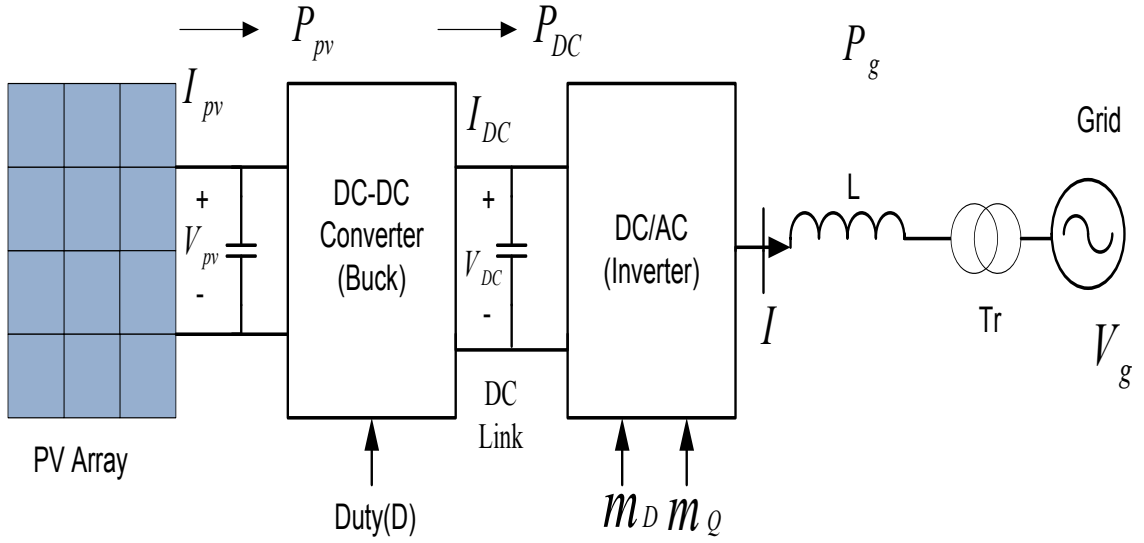

Figure 3.1: Grid connected PV system

3.2 PV Array Modeling

Figure 3.2 shows the equivalent electric circuit model of PV device used in this dissertation [131]–[134]. It consists of a current source, which is light dependent, a p-n junction diode, one series and parallel resistances.

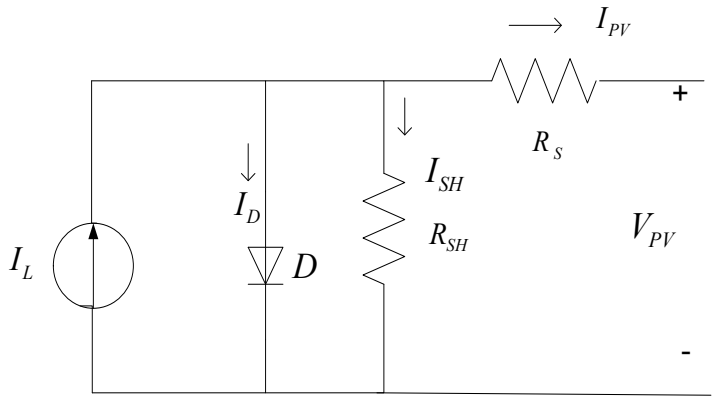

Figure 3.2: Five parameter equivalent electric circuit model of PV panel

Using simple Kirchhoff's current law:

$$I_{PV} = I_L - I_D - I_{SH} \tag{3.1}$$

I_D and I_{SH} depict the diode and shunt branch currents, respectively given by:

$$I_D = I_0\{\exp[\frac{V_{PV} + I_{PV}R_S}{a}] - 1\} \tag{3.2}$$

$$I_{SH} = \frac{V_{PV} + I_{PV}R_S}{R_{SH}} \tag{3.3}$$

Putting these expressions of I_D and I_{SH} in to equation (3.1) gives the complete I-V relationships of a PV panel:

$$I_D = I_L - I_0\{\exp[\frac{V_{PV} + I_{PV}R_S}{a}] - 1\} - \frac{V_{PV} + I_{PV}R_S}{R_{SH}} \tag{3.4}$$

where,

I_L : is the light generated current,

I_0 : is the diode saturation current,

R_S and R_{SH} : are the series and parallel resistance respectively and

a : is the diode modified ideality factor given as:

$$a = \frac{N_s n k T}{q} \tag{3.5}$$

where,

N_S : is the number of cells in the PV panel,

n : is the ideality factor (it has a value between 1 to 2 for real diode),

k : is the Boltzmann's constant,

T : is the cell temperature and

q : is the electronic charge

Equation (3.2) can be solved using numerical solution technique like Newton Raphson method. To get the required voltage and current, PV panels can be connected either in series, parallel or combination of series and parallel. The series-parallel array is the most commonly used because of its flexibility in maintaining the required output voltage and current and better performance in the partial shading conditions [135]–[137]. Eq. (3.4) can be modified to represent the I-V relationship of the array as follows.

$$I_{PV} = N_{PP} I_L - N_{PP} I_0 \{\exp[\frac{V_{PV} + I_{PV} R_S N}{N_{SS} a}] - 1\} - (\frac{V_{PV} + I_{PV} R_S N}{R_{SH} N}) \tag{3.6}$$

$$N = \frac{N_{SS}}{N_{PP}} \tag{3.7}$$

where,

N_{SS} and N_{PP} are the number of series and parallel connected panels, respectively.

3.3 Buck Converter Model

The purpose of the buck converter is to convert unregulated DC input to regulated or controlled DC output at a desired voltage level. Since the input of the PV array is irradiation and temperature that varies throughout the day, the output voltage and current are unregulated. The buck converter is actually controlling the input by considering the unregulated output by the help of MPPT by adjusting its operation according to the output value to find the optimal operating voltage of the PV module. Buck or boost converter can be used for this operation. For this dissertation buck converter is used.

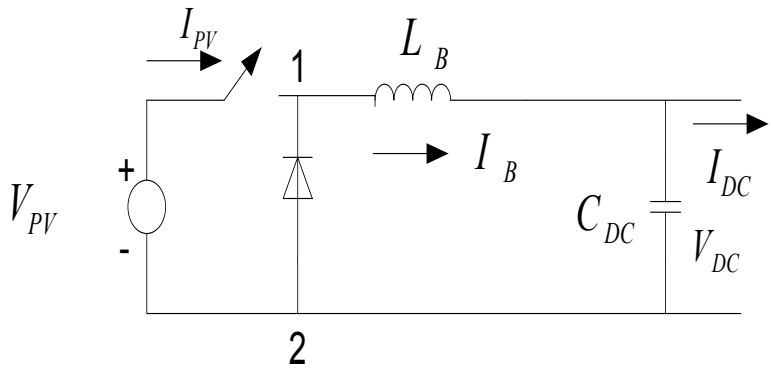

Figure 3.3: Buck converter

From Figure 3.3, when the switch is on, the input voltage V_{PV} leads to a linear increase in the inductor current. As the switch is turned off, the diode becomes forward biased and the stored energy in the inductor makes the current continue to flow. But as the energy is transferred from the inductor to the DC link, the current is decreasing again.

Application of KVL to the buck converter circuit in Figure 3.3 yields the dynamical relations involved in the converter model. The current flowing through energy storing inductor can be taken as a state variable. The differential equation describing the DC buck converter model is obtained as [138]:

$$V_{PV} - V_{DC} - \frac{L_B dI_B}{dt} = 0 \tag{3.8}$$

$$\frac{dI_B}{dt} = \frac{1}{L_B}(V_{PV} - V_{DC}) \tag{3.9}$$

$$V_{12} = V_{PV} D \tag{3.10}$$

$$I_B = I_{PV} D \tag{3.11}$$

Substituting (3.11) into (3.9) yields:

$$\frac{dI_{PV}}{dt} = \frac{1}{L_B D}(V_{PV} - V_{DC}) \tag{3.12}$$

The DC link capacitor acts as a link between the buck converter and the DC-AC inverter.

where,

L_B : is the buck converter inductor

I_B : the buck converter inductor current

D : duty of the buck converter

V_{DC} : is the DC link voltage

C_{DC} : is the DC link capacitor

I_{DC} : is the DC link current input to the inverter

The buck converter inductor is designed as follows:

The maximum power that can be generated from the PV array is P_{PVMAX} with a maximum voltage of V_{PVMAX}. The DC link voltage is designed to have a reference voltage of V_{DCREF}. The DC current flowing out of the buck converter is given by:

$$I_B = \frac{P_{PVMAX}}{V_{DCREF}} \tag{3.13}$$

Resistance seen by the buck converter is

$$R_B = \frac{V_{DCREF}}{I_B} \tag{3.14}$$

For the DC link voltage of V_{DCREF} and input PV array voltage of V_{PVMAX}, the duty is calculated as:

$$D = \frac{V_{DC}}{V_{PV}} \tag{3.15}$$

The inductor L_B is designed using the following equation

$$L_B = (V_{PV} - V_{DC}) \frac{V_{DC}}{V_{PV}} \frac{1}{f} \frac{1}{LIRI_B} \tag{3.16}$$

Where,

f : is the switching frequency of the buck converter

LIR : is the inductor current ratio expressed as a percentage of I_B

An LIR of 0.3 represents a good trade of between efficiency and load transient response.

Substituting the values in equation (3.16) the inductor value can be calculated.

The DC link capacitor C_{DC} is designed using the formula,

$$C_{DC} = \frac{P_{PV}}{2\omega V_{DC} \Delta V_{DC}} \tag{3.17}$$

where,

ΔV_{DC} : is the ripple capacitor voltage

ω : is the grid frequency

Having Δ_{VDC}, V_{DC}, P_{PV}, known, the DC link capacitor can be determined.

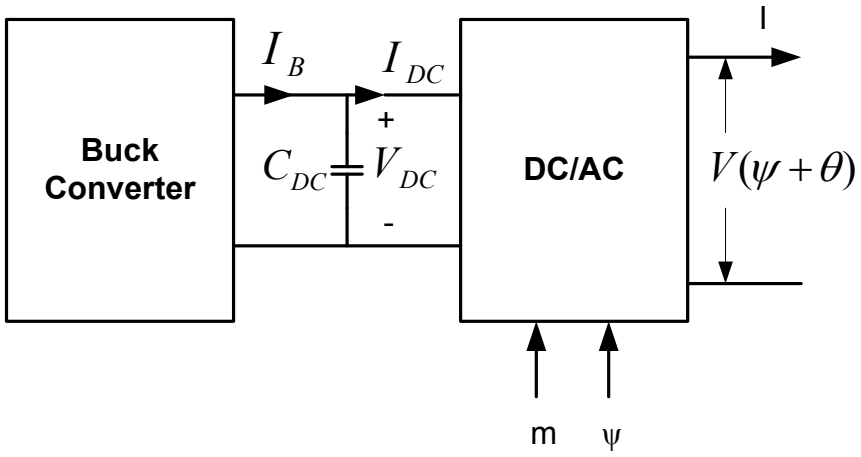

Figure 3.4: Buck converter and inverter interface

The dynamic equation relating the buck converter and the inverter shown in Figure 3.4 is given as:

$$I_B - I_{DC} = C_{DC}\frac{dV_{DC}}{dt} \tag{3.18}$$

Substituting equation (3.10) into (3.17) yields:

$$I_{DC} = I_{PV}D - C_{DC}\frac{dV_{DC}}{dt} \tag{3.19}$$

Voltage across the DC-link capacitor V_{DC} depicts its dynamics and is taken as a state variable.

$$\frac{dV_{DC}}{dt} = \frac{1}{C_{DC}}(I_{PV}D - I_{DC}) \tag{3.20}$$

The inverter input current I_{DC} could also be written in terms of inverter output current. The input DC power to the inverter and the instantaneous inverter output are equal neglecting losses.

$$P_{dc} = V_{DC}I_{DC} \tag{3.21}$$

$$P_g = \mathrm{Re}(VI^*) \tag{3.22}$$

Equation (3.22) can be decomposed into *DQ* components as:

$$P_g = V_{LD} I_{LD} + V_{LQ} I_{LQ} \tag{3.23}$$

Now, since the inverter is assumed to be lossless:

$$\begin{aligned} P_{dc} &= P_g \\ V_{DC} I_{DC} &= V_{LD} I_{LD} + V_{LQ} I_{LQ} \end{aligned} \tag{3.24}$$

where,

P_{dc} : is the DC link capacitor power

P_g : is the grid side active power respectively.

V_{LD}, V_{LQ} : are *D* and *Q* components of grid side voltage respectively.

I_{LD}, I_{LQ} : are *D* and *Q* components of grid side current respectively.

If the inverter works in the pulse width modulation (PWM) mode with a modulation index of *m* and phase angle of ψ, the inverter output voltage can be expressed in terms of the input DC link voltage.

$$V = m V_{DC} \angle \psi \tag{3.25}$$

The DQ component of equation (3.25) is given by:

$$\begin{aligned} V_D &= m V_{DC} \cos(\psi + \theta) \\ V_Q &= m V_{DC} \sin(\psi + \theta) \end{aligned} \tag{3.26}$$

where, θ is the phase shift angle of the voltage.

Substituting equation (3.26) into (3.24) yields,

$$I_{DC} = m I_D \cos(\psi + \theta) + m I_Q \sin(\psi + \theta) \tag{3.27}$$

Further substituting equation (3.27) into (3.20), the dynamic equation of the capacitor voltage is expressed in terms of the inverter output current.

$$\frac{dV_{DC}}{dt} = \frac{1}{C_{DC}} (I_{PV} D - mI_D \cos(\psi + \theta) + mI_Q \sin(\psi + \theta) \quad (3.28)$$

The duty is generated from the maximum power point tracking (MPPT) controller discussed below.

3.4 Incremental Conductance (IC) MPPT for the Buck converter

MPPT controller is a crucial element of the PV system. It tracks and extracts the maximum possible power from the PV array under different operating conditions and improves the overall efficiency of a complete PV system. Figure 3.5 shows the power-voltage (P-V) and current-voltage (I-V) curves to allocate the maximum power point (MPP).

In Figure 3.5,

V_{oc} and I_{sc} : are the short circuit voltage and current respectively.

V_{mp} and I_{mp} : are the best operating voltage and current that provide the maximum power P_{mp}.

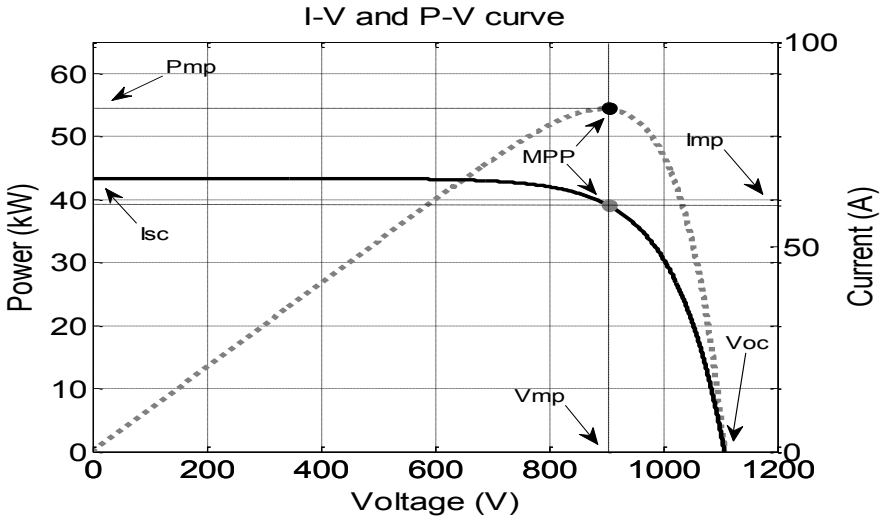

Figure 3.5: Maximum power point for a PV array

The output voltage and current generated from a PV array varies depending on irradiation and temperature. The I-V and P-V characteristics of a PV array under different irradiation and temperature are shown in Figures 3.6 and 3.7 respectively.

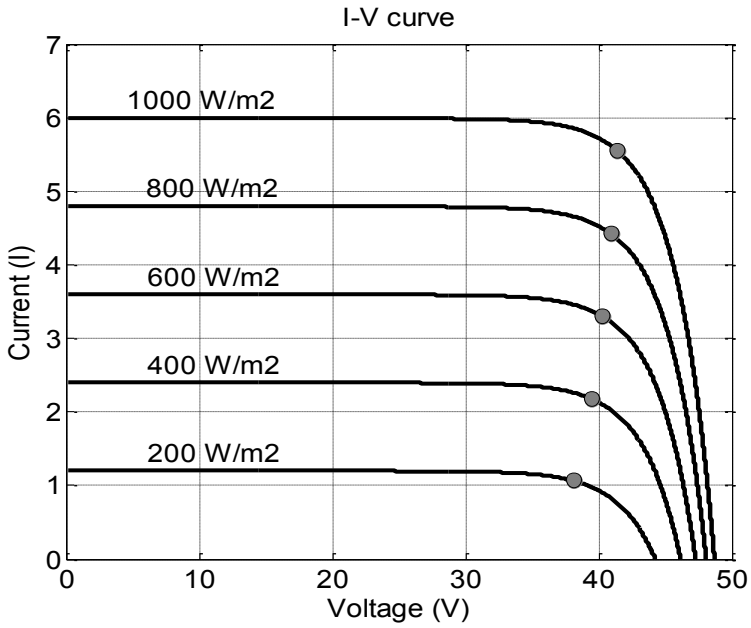

(a)

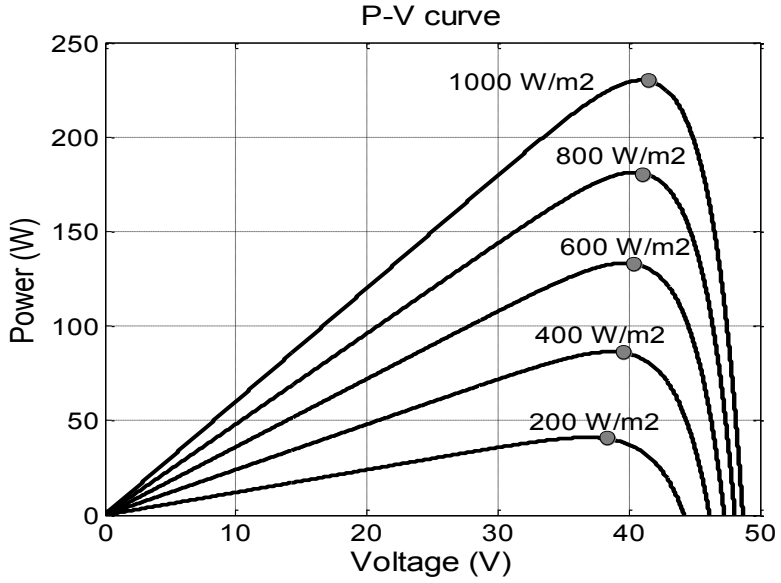

(b)

Figure 3.6: Effect of irradiation on PV characteristics (a) I-V curve (b) P-V curve

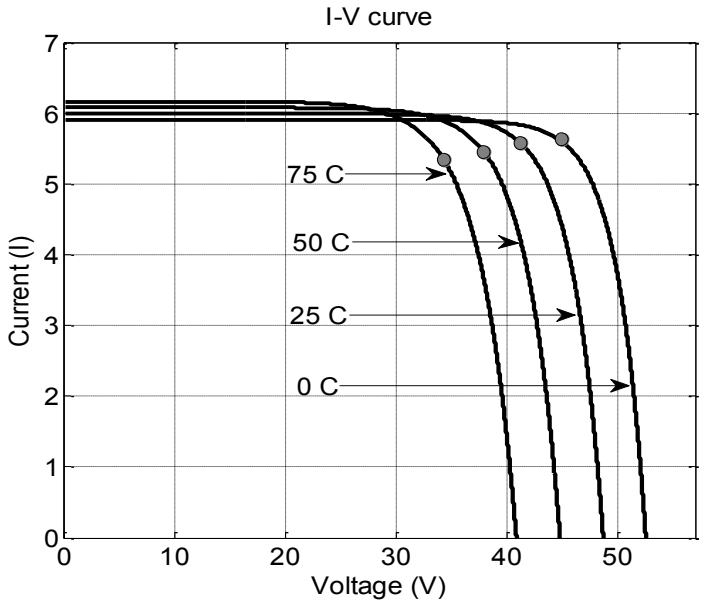

(a)

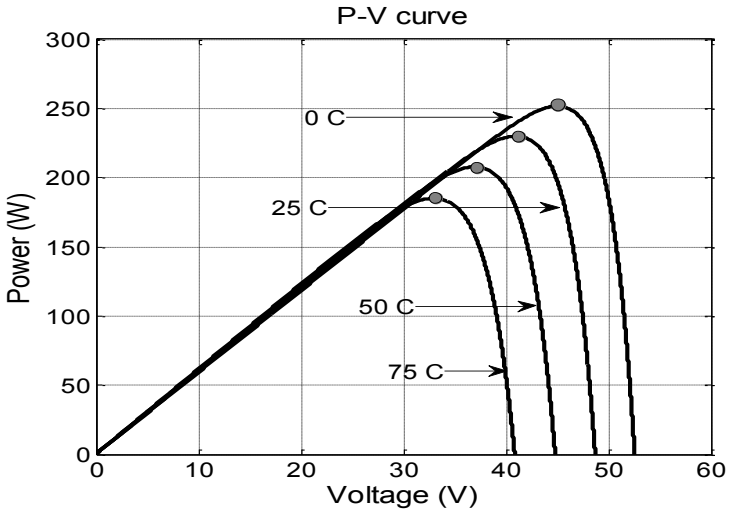

(b)

Figure 3.7: Effect of temperature on PV characteristics (a) I-V curve (b) P-V curve

Since the input to the PV array, irradiation and temperature, are varying throughout the day, the incremental conductance method calculates the PV power at each instant and changes the operating point of the PV array to capture the maximum available power [139]. The PV output power is given by:

$$P_{PV} = V_{PV} I_{PV} \tag{3.29}$$

The derivative of the PV power P is zero at the maximum operating point, as shown in Figure 3.8. Applying the chain rule of derivative yields,

$$\frac{\partial P_{pv}}{\partial V_{pv}} = \frac{\partial (V_{pv} I_{pv})}{\partial V_{pv}} = 0 \tag{3.30}$$

Rearranging the terms, equation (3.30) could be written as

$$\frac{\partial I_{pv}}{\partial V_{pv}} = \frac{-I_{pv}}{V_{pv}} \tag{3.31}$$

The buck converter's duty cycle is controlled by the IC based MPPT until equation (3.31) is satisfied. The flow chart for the IC based MPPT is shown in Figure 3.9.

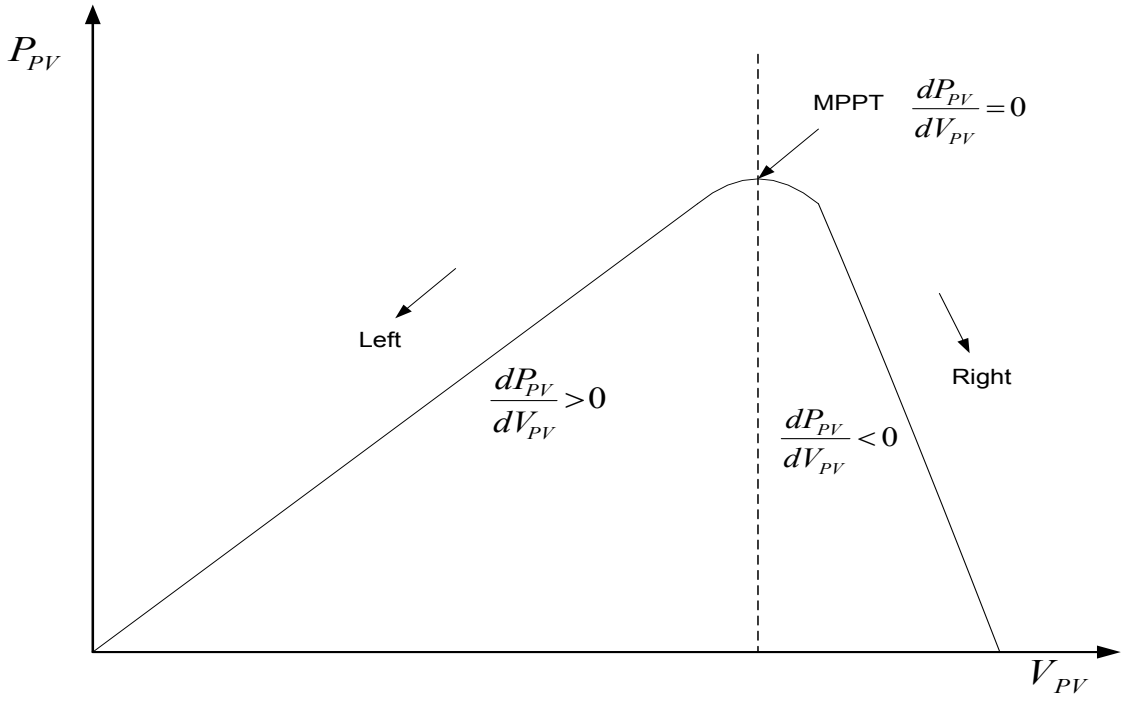

Figure 3.8: P-V curve showing the MPP

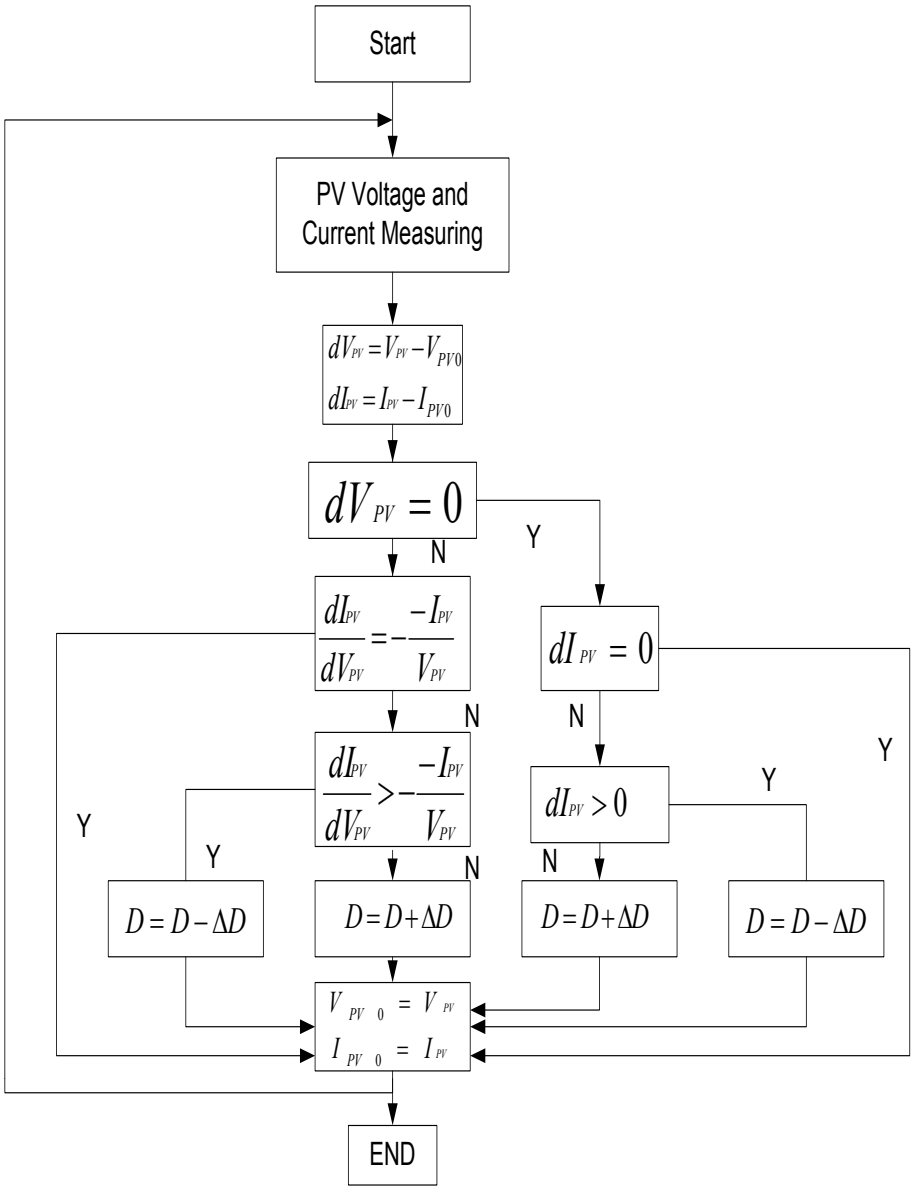

Figure 3.9: Flow chart of IC MPPT method

Input of the IC based MPPT is the output voltage and current of the PV array and its output is the reference voltage, V_{ref} as shown in Figure 3.10. This voltage is compared with the PV array output and the difference is processed by a PI regulator. After comparison of a high frequency carrier signal with the output of the PI (which is the modulating signal), firing pulse is generated for the buck converter. The DC link voltage

V_{DC} is the Duty (D) multiplied by the PV array output voltage, V_{PV}. The DC link capacitor C_{DC} removes the offset of this voltage.

Figure 3.11 shows the buck converter controller implemented to track the maximum power from the PV array.

$$\text{Let} \qquad \dot{V}_{PVerr} = (V_{ref} - V_{PV}) \tag{3.32}$$

Then the Duty, D, of the buck converter is computed as:

$$D = K_{PB}(V_{ref} - V_{PV}) + K_{IB}V_{PVerr} \tag{3.33}$$

where,

K_{PB} and K_{IB} : are the proportional and integral constants of the buck converter PI controller.

V_{PV} : output voltage from the PV array

V_{ref} : the reference voltage from the MPPT controller

V_{PVerr} : is the state of the buck converter controller

D : is the duty cycle of the buck converter

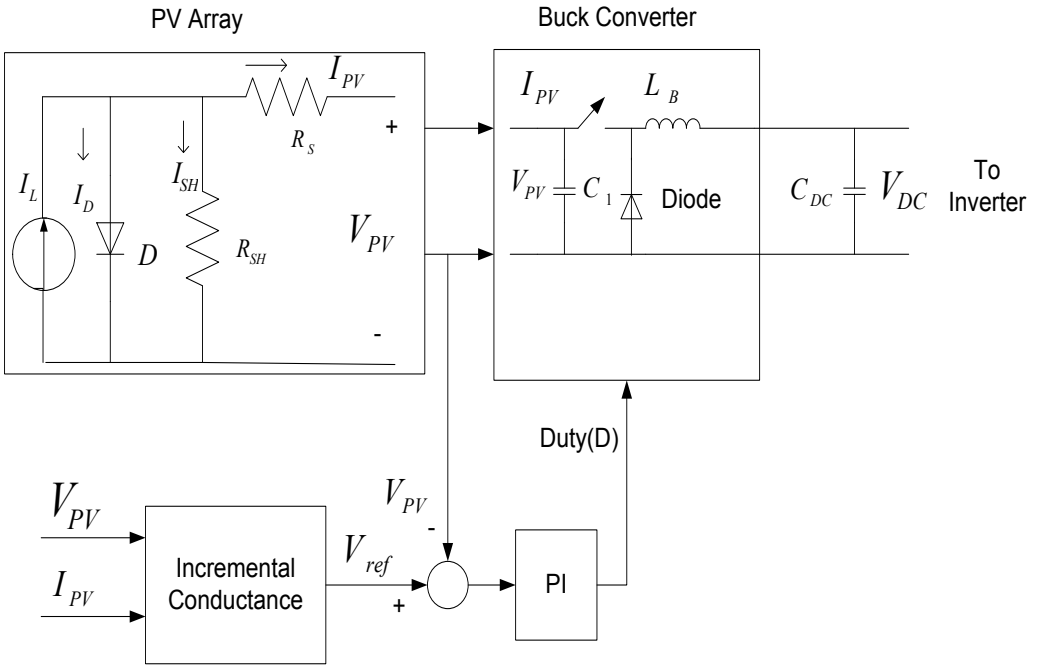

Figure 3.10: IC Based MPPT and buck converter controller

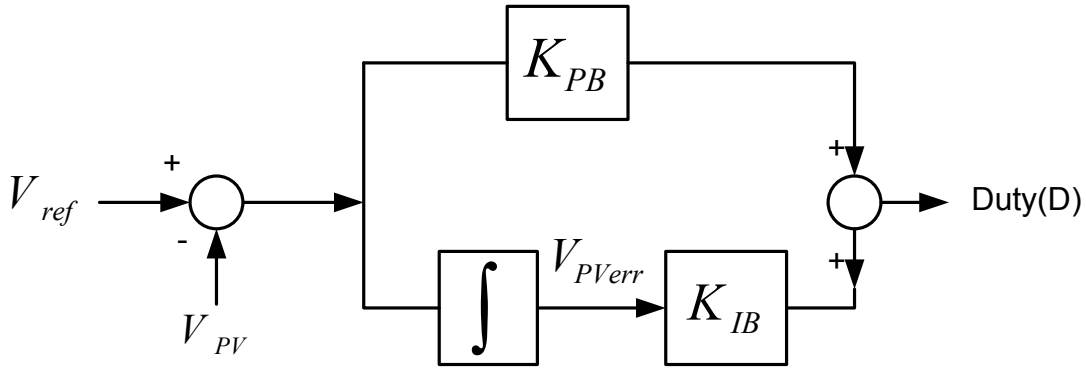

Figure 3.11: Buck converter PI controller

3.5 DC-AC Inverter Model and Controller

The DC power coming from the buck converter has to be converted to three-phase AC power to supply either AC loads or for grid integration using a two level inverter where the DC link capacitor has one positive and negative terminal shown in Figure 3.12.

Voltage and current control are two types of waveform generation control schemes used for grid-connected inverters. PV inverters inject energy directly into the grid and are controlled as power sources that is, they inject constant power into the grid at close to unity power factor. The control system constantly monitors power extracted from the PV array and adjusts the magnitude and phase of the AC voltage (in voltage control mode) or current (in current control mode) to export the power extracted from the PV array.

In this dissertation current control scheme is used to inject the generated power from the PV array to the grid. The first function of the inverter controller is to keep the DC voltage constant for real power delivery to the grid. Proper control of the magnitude and angle of the inverter output voltage controls the reactive and active power exchanged between the DC link and the grid.

The DC voltage input is subjected to variation depending on the power extracted from the photovoltaic source. The DC link voltage is also subjected to variation depending on the power available and the amount of power extracted. The increase of power results in voltage overshoot and decrease in power results in voltage undershoot at the DC link. Either way control of DC link voltage is essential to deliver power to the grid and to apply a PWM control to the inverter.

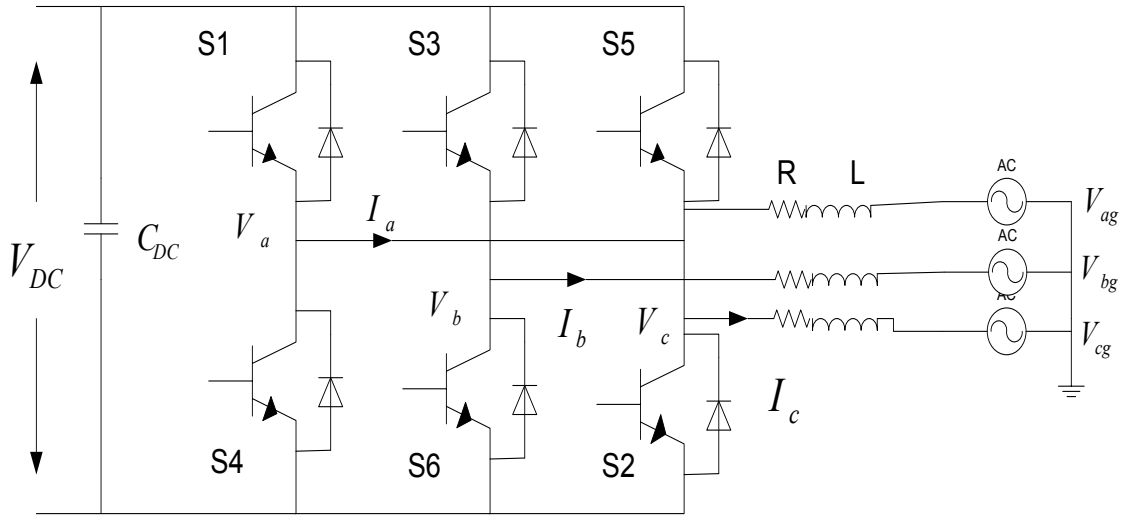

Figure 3.12: Two level three phase inverter

The three phase output voltage equations can be written as:

$$\begin{aligned} RI_a + L\frac{dI_a}{dt} &= V_a - V_{ag} \\ RI_b + L\frac{dI_b}{dt} &= V_b - V_{bg} \\ RI_c + L\frac{dI_c}{dt} &= V_c - V_{cg} \end{aligned} \tag{3.34}$$

where,

R and L : are resistance and inductance of the distribution line respectively.

I_a, I_b and I_c : are the distribution line currents;

V_a,V_b, V_c : are the inverter output voltages;

V_{ag}, V_{bg}, V_{cg} : are the grid voltages.

The inductor L is chosen to limit the inductor ripple current.

Using synchronous rotating reference frame (D-Q axis), decoupled active and reactive current control technique is implemented using a standard PI controller. The reference

angle for the synchronous rotating reference frame is provided by a phase locked loop (PLL) [140]. The transformation matrix T is given by:

$$T = \sqrt{2/3}\begin{bmatrix} \cos\theta & \cos(\theta - \frac{2\pi}{3}) & \cos(\theta + \frac{2\pi}{3}) \\ -\sin\theta & -\sin(\theta - \frac{2\pi}{3}) & -\sin(\theta - \frac{2\pi}{3}) \\ \frac{1}{\sqrt{2}} & \frac{1}{\sqrt{2}} & \frac{1}{\sqrt{2}} \end{bmatrix} \tag{3.35}$$

The PLL model used is shown in Figure 3.13 and is based on aligning the angle of the DQ transformation such that the voltage at the connection point has no Q-axis component. A PI regulator acts on the alignment error to set the rotation frequency. This frequency is used to obtain the transformation angle Θ.

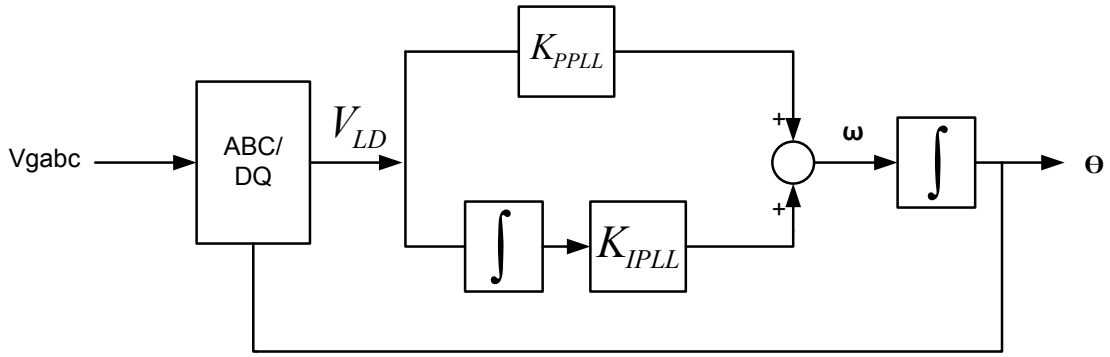

Figure 3.13: PLL Model

Using ABC to DQ transformation the grid side measured voltage is expressed as:

$$\begin{bmatrix} V_{LD} \\ V_{LQ} \\ V_{L0} \end{bmatrix} = T \begin{bmatrix} V_{ag} \\ V_{bg} \\ V_{cg} \end{bmatrix} \tag{3.36}$$

The grid side current is converted to *DQ* reference frame using the transformation matrix of 3.35.

$$\begin{bmatrix} I_{LD} \\ I_{LQ} \\ I_{L0} \end{bmatrix} = T \begin{bmatrix} I_a \\ I_b \\ I_c \end{bmatrix} \tag{3.37}$$

In the current control technique, the active current component I_D controls the active power and reactive power flow is regulated by controlling I_Q. The PI controllers force these currents to track certain reference commands I_{DREF} and I_{QREF}, respectively. The reference input power to the DC link is the output power from the PV array. Utilizing the instantaneous power theory [141]:

$$P_{dc} = P_g \tag{3.38}$$

$$P_g = \frac{3}{2}(V_{LD}I_{LD} + V_{LQ}I_{LQ}) \tag{3.39}$$

$$Q_g = \frac{3}{2}(V_{LQ}I_{LD} - V_{LD}I_{LQ}) \tag{3.40}$$

where, Q_g is the grid side reactive power.

Aligning the phase voltage of the grid to the *D*-axis reference frame will make $V_{LQ} = 0$, so the equation can be further reduced to:

$$P_g = \frac{3}{2}(V_{LD}I_{LD}) \tag{3.41}$$

$$Q_g = -\frac{3}{2}(V_{LD}I_{LQ}) \tag{3.42}$$

Two PI loops are incorporated for the VSC controller. The inner current loop controls the AC current, and the reference current is provided by the outer loop. The outer controller

includes the DC voltage controller and for unity power factor operation I_{QREF} is kept zero. Since the D and Q components are coupled, cross-coupling term and a feed forward voltage are used to improve the performance of the PI current controllers as shown in Figure 3.14.

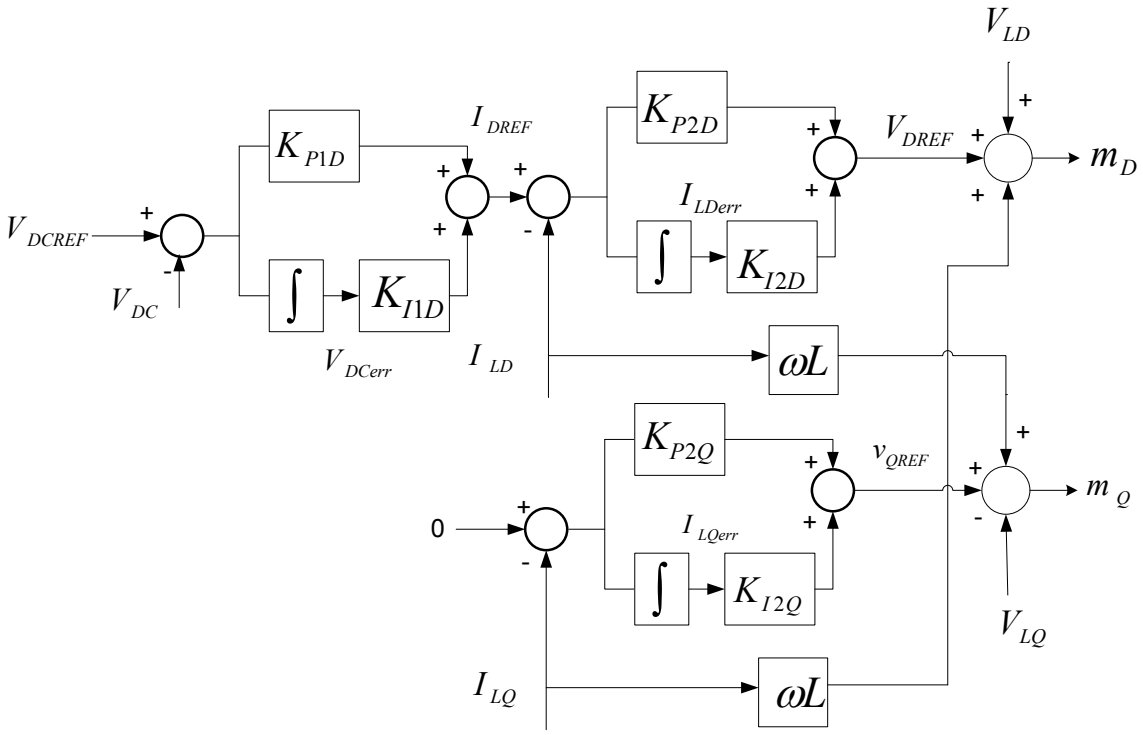

Figure 3.14: Decoupled inverter control

Let $\dot{V}_{DCerr} = V_{DCREF} - V_{DC}$

$$\dot{I}_{LDerr} = I_{LDREF} - I_{LD}$$

$$\dot{I}_{LQerr} = 0 - I_{LQ}$$

where,

V_{DCerr} : is the state variable for the outer voltage controller

I_{LDerr} : D-axis state variable for the inner current controller

I_{LQerr} : Q-axis state variable for the inner current controller

The D-axis outer voltage loop controller in the Laplace domain is:

$$I_{DREF} = K_{P1D}(V_{DC} - V_{DCREF}) + K_{I1D}V_{DCerr} \tag{3.43}$$

The inner loop current controller will be:

$$V_{DREF} = K_{P2D}(I_{DREF} - I_{LD}) + K_{I2D}I_{LDerr} \tag{3.44}$$

Similarly, the Q-axis current controller in Laplace domain is given by:

$$V_{QREF} = K_{P2Q}(I_{LQREF} - I_{LQ}) + K_{I2Q}I_{LQerr} \tag{3.45}$$

The control signals m_D and m_Q are then given by:

$$m_D = V_{DREF} - wLI_Q + V_{LD} \tag{3.46}$$

$$m_Q = V_{QREF} + wLI_D + V_{LQ} \tag{3.47}$$

where,

K_{P1D} and K_{I1D} : are the D-axis PI proportional and integral gains of the outer loop voltage controller.

K_{P2D} and K_{I2D} : are the D-axis PI proportional and integral gains of the inner current controller.

K_{P2Q} and K_{I2Q} : are the Q-axis PI proportional and integral gains of the inner current controller.

V_{DCREF} and V_{DC} : are the reference and measured DC link voltages.

I_{DREF} : is the output current from the outer voltage controller

I_{LQREF} : is the Q-axis reference current and for unity power factor this reference current is kept 0

The total state variables including the PV array, buck converter and inverter are:

$$x=[I_{PV}\ V_{DC}\ V_{PVerr}\ V_{DCerr}\ I_{LDerr}\ I_{LQerr}]^T \tag{3.48}$$

3.6 Small Signal Model of Grid Connected PV System

The non-linear equations obtained for the grid connected PV system are linearized around an operating point using the standard test conditions (STC) from the data sheet of the PV array provided by the manufacturer to determine the small signal models which is used to analyze the dynamic performance and to design the control parameters of the PI regulators.

The small signal model of the PV array, the power electronics blocks with their controllers constitute the linearized model of the grid connected PV system.

By selecting an output variable *y*, the linearized system equations are written as,

$$\begin{aligned} \dot{x} &= Ax + Bu \\ y &= Cx \end{aligned} \tag{3.49}$$

The equation given in (3.12) relating the PV array voltage current and the DC link voltage is linearized. The duty cycle, *D* from the equation is generated using the buck converter controller given in eqn. (3.33).

$$\begin{aligned} \Delta \dot{I}_{PV} = &\left(\frac{(K_{PB}(V_{ref}-V_{PV})+K_{IB}V_{PVerr})+(V_{PV0}-V_{DC0})K_{PB}}{L_B(K_{PB}(V_{ref}-V_{PV})+K_{IB}V_{PVerr})^2}\right)\Delta V_{PV} - \frac{1}{L_B(K_{PB}(V_{ref}-V_{PV})+K_{IB}V_{PVerr})}\Delta V_{DC} \\ &- \frac{(V_{PV0}-V_{DC0})K_{IB}}{L_B(K_{PB}(V_{ref}-V_{PV})+K_{IB}V_{PVerr})^2}\Delta V_{PVerr} \end{aligned} \tag{3.50}$$

The dynamics of the DC link voltage given in eqn. (3.20) can be expressed using the duty cycle of the buck converter as:

$$\frac{dV_{DC}}{dt} = \frac{1}{C_{DC}} \left(I_{PV} \left(K_{PB} (V_{ref} - V_{PV}) + K_{IB} V_{PVerr} \right) - I_{DC} \right) \tag{3.51}$$

After linearization:

$$C_{DC} \Delta \dot{V}_{DC} = (K_{PB} V_{ref\,0} - K_{PB} V_{PV\,0}) \Delta I_{PV} - K_{PB} I_{PV\,0} \Delta V_{PV} + K_{IB} \Delta V_{PVerr} - \Delta I_{DC} \tag{3.52}$$

The state variable of the buck converter given in eqn. (3.32) is linearized to provide the following expression:

$$\Delta \dot{V}_{PVerr} = \Delta V_{ref} - \Delta V_{PV} \tag{3.53}$$

Similarly, the state variables of the inverter controller shown in Figure 3.14 are linearized and are given below:

$$\Delta \dot{V}_{DCerr} = -\Delta V_{DC} \tag{3.54}$$

$$\Delta \dot{I}_{LDerr} = K_{P1D} \Delta V_{DC} + K_{I1D} \Delta V_{DCerr} - \Delta I_{LD} \tag{3.55}$$

$$\Delta \dot{I}_{LQerr} = -\Delta I_{LQ} \tag{3.56}$$

The linearized model can be expressed in matrix form as:

$$\begin{bmatrix} \dot{\Delta I_{PV}} \\ \dot{\Delta V_{DC}} \\ \dot{\Delta V_{PVerr}} \\ \dot{\Delta V_{DCerr}} \\ \dot{\Delta I_{LDerr}} \\ \dot{\Delta I_{LQerr}} \end{bmatrix} = \begin{bmatrix} A_1 & A_2 & A_3 & 0 & 0 & 0 \\ A_4 & 0 & A_5 & 0 & 0 & 0 \\ -\Delta V_{PV} & 0 & 0 & 0 & 0 & 0 \\ 0 & -1 & 0 & 0 & 0 & 0 \\ 0 & K_{P1D} & 0 & K_{I1D} & 0 & 0 \\ 0 & 0 & 0 & 0 & 0 & 0 \end{bmatrix} \begin{bmatrix} \Delta I_{PV} \\ \Delta V_{DC} \\ \Delta V_{PVerr} \\ \Delta V_{DCerr} \\ \Delta I_{LDerr} \\ \Delta I_{LQerr} \end{bmatrix} + \begin{bmatrix} 0 & 0 & 0 & 0 & 0 \\ 0 & 0 & 0 & 0 & \frac{-1}{C_{DC}} \\ 1 & 0 & 0 & 0 & 0 \\ 0 & 0 & 0 & 0 & 0 \\ 0 & 1 & 0 & 0 & 0 \\ 0 & 0 & 0 & 0 & 0 \end{bmatrix} \begin{bmatrix} \Delta V_{ref} \\ \Delta I_{LD} \\ \Delta I_{LQ} \\ \Delta V_{DCref} \\ \Delta I_{DC} \\ 0 \end{bmatrix} \tag{3.57}$$

where,

$$A_1 = f(V_{PV})$$

$$A_2 = \frac{-1}{L_B(K_{PB}(V_{ref} - V_{PV}) + K_{IB}V_{PVerr})}$$

$$A_3 = \frac{(V_{PV0} - V_{DC0})K_{IB}}{L_B(K_{PB}(V_{ref} - V_{PV}) + K_{IB}V_{PVerr})^2}$$

$$A_4 = \frac{1}{C_{DC}}(K_{PB}V_{ref0} - K_{PB}V_{PV0} - K_{PB}I_{PV0}\Delta V_{PV})$$

$$A_5 = \frac{K_{IB}}{C_{DC}}$$

Equation (3.57) is expressed as $\dot{\Delta x} = A\Delta x + B\Delta u$

The state variables after linearization are

$$\Delta x = [\Delta I_{PV}\ \Delta V_{DC}\ \Delta V_{PVerr}\ \Delta V_{DCerr}\ \Delta I_{LDerr}\ \Delta I_{LQerr}]^T \tag{3.58}$$

3.7 Control Parameter Design

To study the stability of the grid connected PV system with and without energy storage, the control parameter settings have to be optimized. The linear model developed from the non-linear differential equations is used to study the stability of the system. The eigenvalues are used to check whether the system is stable or not and to move the poorly damped eigenvalues to the left to make the system more stable.

3.7.1 Objective Functions

For grid connected PV system the optimized parameters are K_{PB}, K_{IB}, K_{P1D}, K_{I1D}, K_{P2D}, K_{I2D}, K_{P2Q}, and K_{I2Q}. Eigenvalue based objective function is proposed to improve the system stability. The eigenvalue based objective function shown in equation 3.59 is proposed.

$$J_{linear\_model} = \max(\text{Real}(\lambda_i)) \tag{3.59}$$

Real (λ_i) is the real part of the i^{th} mode eigenvalue. In the optimization process, it is aimed to minimize J_{linear_model} in order to shift the poorly damped eigenvalues to the left in the S-plane. In this dissertation the control parameters determined using the linear model are used to study the nonlinear time simulation using RTDS.

3.7.2 Problem Constraints

The control parameters to be optimized for the grid connected PV system are restricted by their upper and lower limit values. For grid connected PV system constraints (3.60)-(3.67) are used.

$$K_{PB}^{\min} \le K_{PB} \le K_{PB}^{\max} \tag{3.60}$$

$$K_{IB}^{\min} \le K_{IB} \le K_{IB}^{\max} \tag{3.61}$$

$$K_{P1D}^{\min} \le K_{P1D} \le K_{P1D}^{\max} \tag{3.62}$$

$$K_{I1D}^{\min} \le K_{I1D} \le K_{I1D}^{\max} \tag{3.63}$$

$$K_{P2D}^{\min} \le K_{P2D} \le K_{P2D}^{\max} \tag{3.64}$$

$$K_{I2D}^{\min} \le K_{I2D} \le K_{I2D}^{\max} \tag{3.65}$$

$$K_{P2Q}^{\min} \le K_{P2Q} \le K_{P2Q}^{\max} \tag{3.66}$$

$$K_{I2Q}^{\min} \le K_{I2Q} \le K_{I2Q}^{\max} \tag{3.67}$$

3.7.3 Optimization Problem

The optimization problem can be formulated as:

$$\text{Minimize } (J_{\text{linear\_model}}) \tag{3.68}$$

Subject to constraints given from (3.60) to (3.67)

In this dissertation, PSO [142] is proposed to solve the above optimization problem to obtain the optimal parameters for the PI regulators to achieve the system stability to transfer the generated from the PV array to the grid. PSO has advantages over other traditional optimization techniques are summarized in [143]. The steps to implement the PSO technique are described in [144].

3.7.4 PSO Implementation

The PSO based approach to determine the control parameters is implemented using Matlab code. The initial PSO parameters are carefully chosen to improve the performance and the limits of the control parameters are set. The used PSO data are as follows:

- Population size, Pop=20;
- Acceleration constants, c_1 and c_2=2;
- Number of generation=80;
- Inertia weight factor, w=1;
- Decrement constant, α=0.98;
- Initial PSO control parameter settings:
    1. $K_{PB\_min}=0;\ K_{PB\_max}=1;$
    2. $K_{IB\_min}=0;\ K_{IB\_max}=1;$
    3. $K_{P1D\_min}=0;\ K_{P1D\_max}=1.5;$
    4. $K_{I1D\_min}=0;\ K_{I1D\_max}=1;$
    5. $K_{P2D\_min}=0;\ K_{P2D\_max}=1;$
    6. $K_{I2D\_min}=5;\ K_{I2D\_max}=25;$
    7. $K_{P2Q\_min}=0;\ K_{P2Q\_max}=15;$
    8. $K_{I2Q\_min}=0;\ K_{I2Q\_max}=1.5;$

The proposed PSO based optimization can be described in flow chart shown in Figure 3.15.

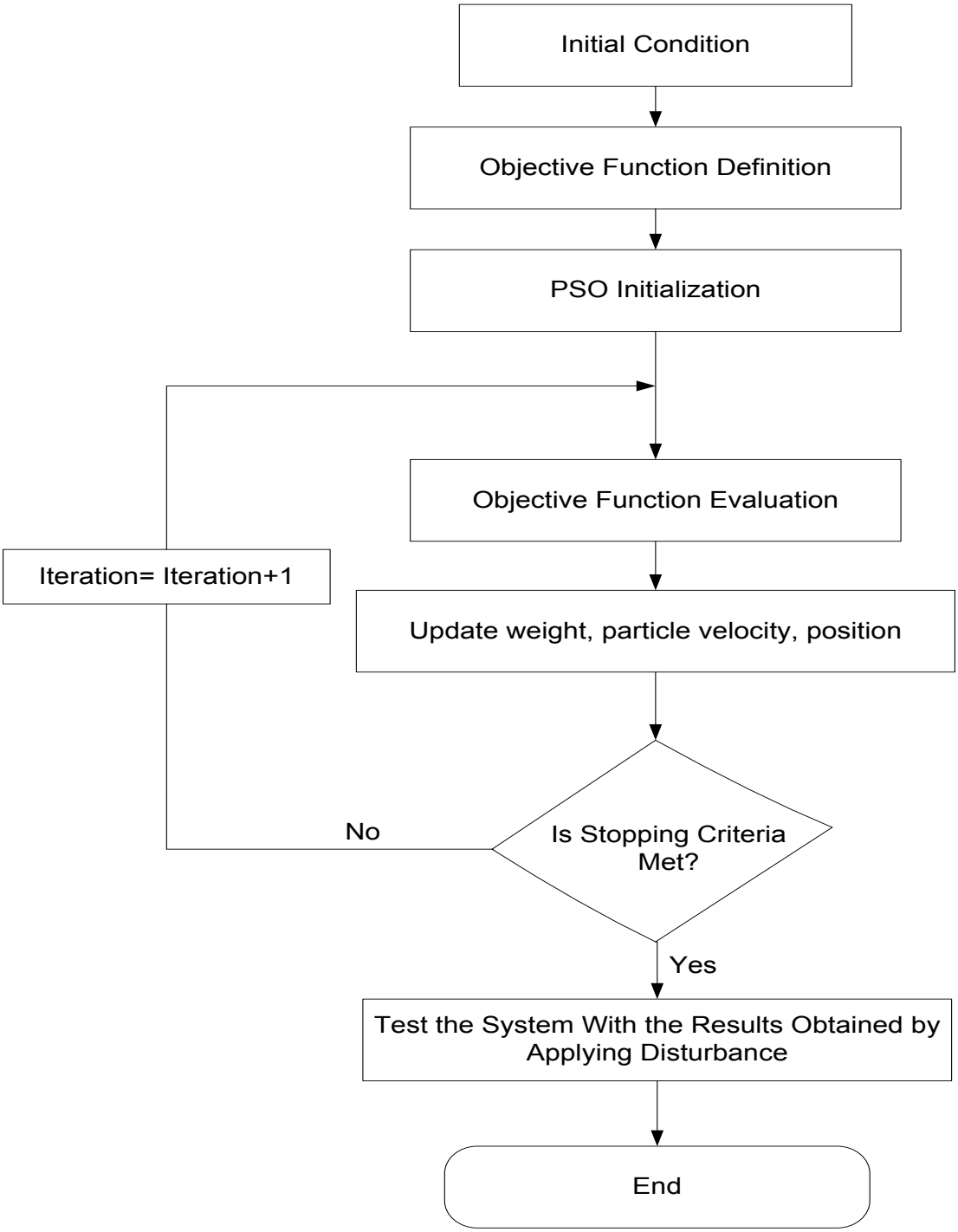

Figure 3.15: Flow chart of the proposed PSO based optimal parameter design

3.8 Real Time Digital Simulator (RTDS) Results and Discussions

A PV array with the specification given in Table 3.1 is developed on RTDS. It consists of 50 series and 20 parallel connected modules. For the reference solar intensity of 1000 W/m^2 and 25^{o}c, the operating voltage V_{PV} and current I_{PV} at the MPPT are 50×17.4 V=870 V, and 20×3.05 A=61A, respectively. The expected maximum output power at this operating point from this PV array is 53 kW (870V×61 A). The reference DC link voltage is designed to be 650 V. The rating of the coupling transformer is 100 kVA, 0.23/11 kV for 11 kV grid voltage.

The inductor L_B of the buck converter is designed using the values of the PV array parameters and using equations (3.13-3.16) to be 1.35mH. The DC link capacitor C_{DC} is also designed using equation (3.17) to have an approximate value of 80mF. The parameters of the components used for the grid connected PV system are shown in Table 3.2.

PSO technique is applied to the eigen value based objective function of eqn. (3.68) to search for the optimal parameters of the proposed controllers. The eigen values before and after optimization are tabulated in Table 3.3. The optimal settings obtained are:

- for the buck converter, K_{PB}=0.6 and K_{IB}=0.2,
- for the inverter: K_{P1D} =0.7, K_{I1D} =0.2, K_{P2D} =0.5, K_{I2D}=15, K_{P2Q} = 5, and K_{I2Q} =0.5.

Table 3.1: Parameter of a PV array and grid

Parameter	Value
Open circuit voltage	21.7 V
Short circuit current	3.35 A
Voltage at P_{MAX}	17.4 V
Current at P_{MAX}	3.05 A
Series connected modules(N_{SS})	50
Parallel connected modules(N_{PP})	20
PV array voltage at P_{MAX}	870 V
PV array current at P_{MAX}	61 A
PV array maximum power	53 kW
DC link voltage	650 V
Grid voltage	11 kV
Coupling transformer rating	100 kVA, 0.23/11 kV
Number of PV cells in each model	36
Ideality factor of PV diode, a	1.5
Temperature Dependency factor	3
Reference Temperature	25^{o}c
Temperature Coefficient of I_{SC}	0.065
Reference solar intensity	1000 W/m^2

The values of the system components used for grid connected PV system are tabulated in Table 3.2.

Table 3.2: Parameter of system components

Parameter	Value
Coupling inductance L	1.35mH
DC link capacitor C_{DC}	80mF
C_1	10mF
L_B	1.35 mH
Converter switching frequency	5 kHz

Table 3.3: Eigen value spectrum

Before Optimization		After optimization	
Real part	Imaginary part	Real part	Imaginary part
-85.854	$\pm 2619.94i$	-367.259	$\pm 8952.6i$
-0.21463	$\pm 3.8536i$	-24.9654	$\pm 354.41i$
-12.486		-39.52	
5.687		-84.6352	

Figure 3.16 shows the complete RTDS model of the grid connected PV system used in this dissertation. It consists of the PV array, the buck converter, the inverter, the transformer and the controller for the inverter and the buck converter. Figure 3.17 depicts the power electronics block inside the BRDG1. The power electronics blocks are modeled in small time step with a step time of 2 microseconds. The transformers used in this block are interface transformers to link the small time step to large step with step time of 50 microseconds. The controllers are modeled in large time step. The PLL and the ABC/DQ conversion in RTDS are shown in Figure 3.18. The buck converter and the

inverter controller in RTDS are shown in Figure 3.19 and 3.20 respectively. The coupling and feed-forward added to the inverter controller is presented in Figure 3.21.

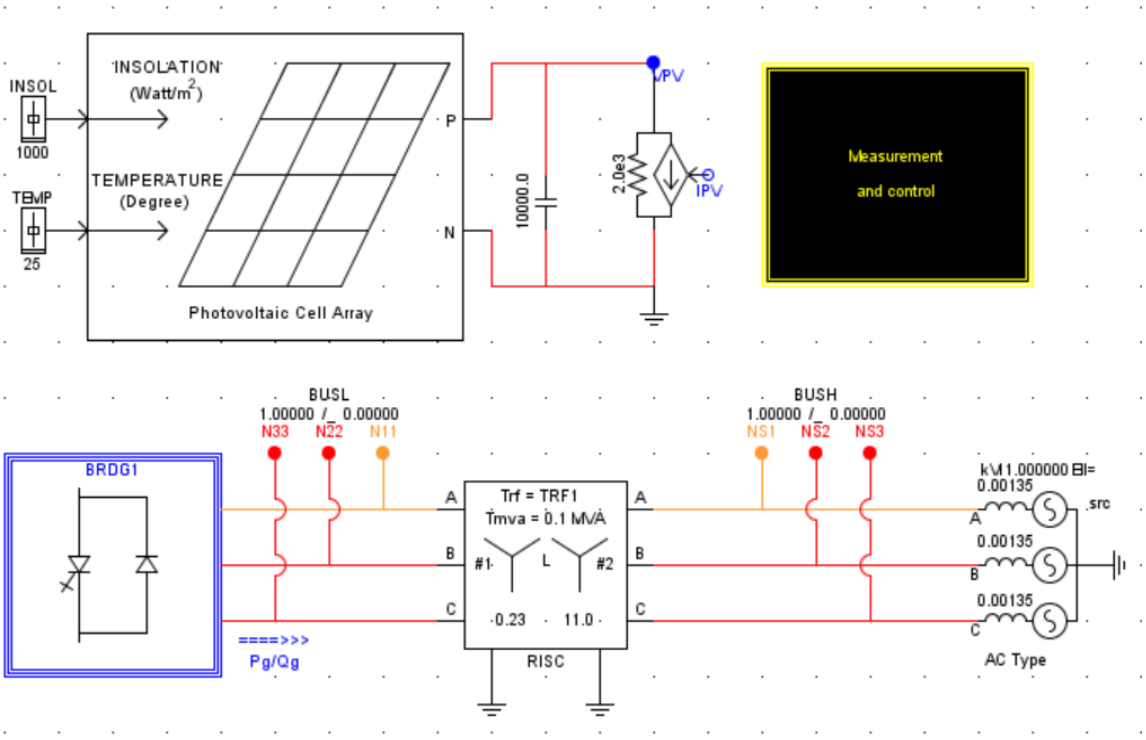

Figure 3.16: RTDS model of grid connected PV system

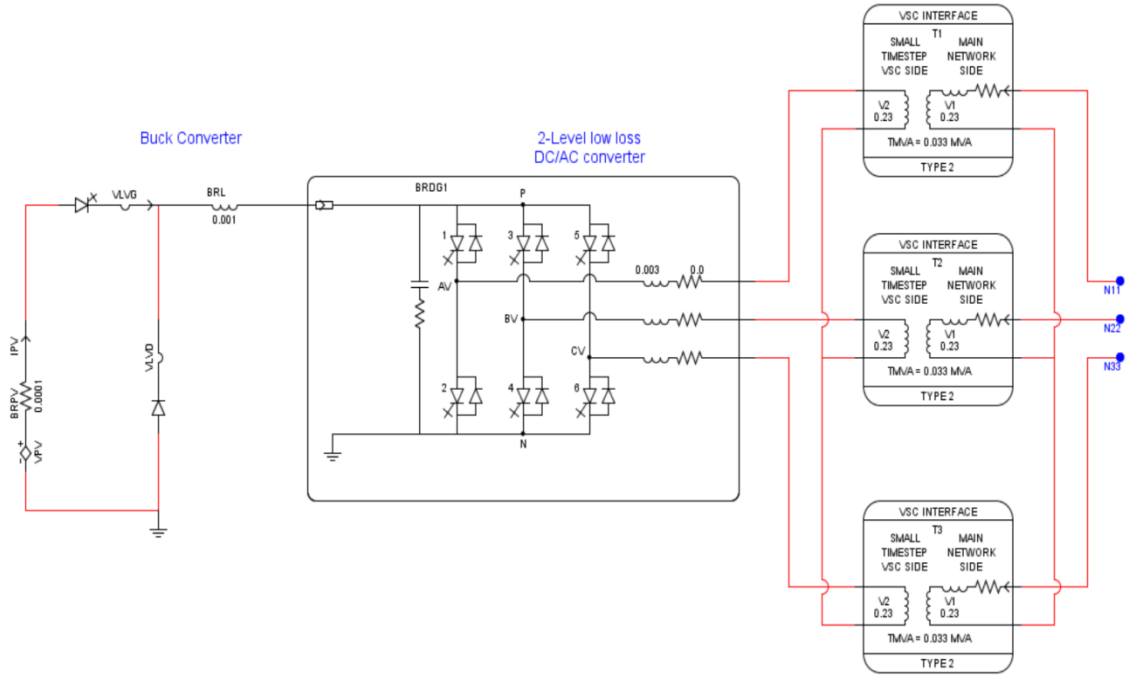

Figure 3.17: Inside BRDG1

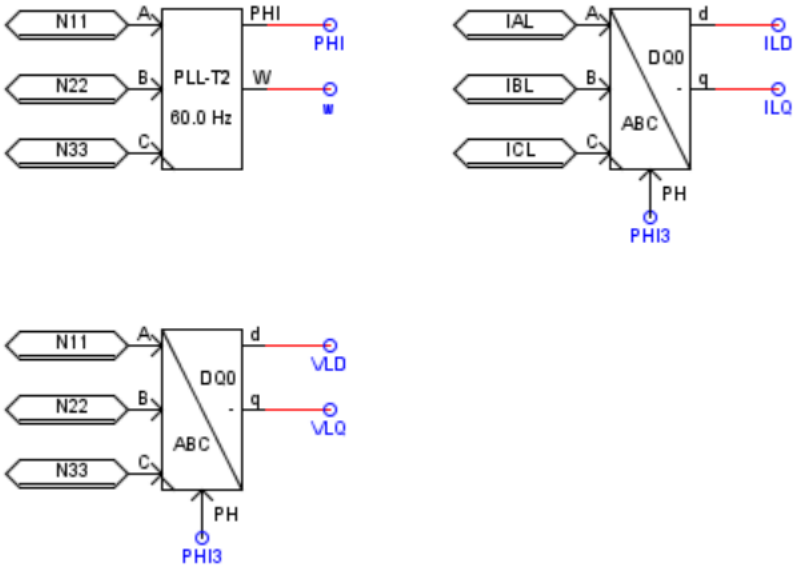

Figure 3.18: PLL and *ABC* to *DQ* conversion

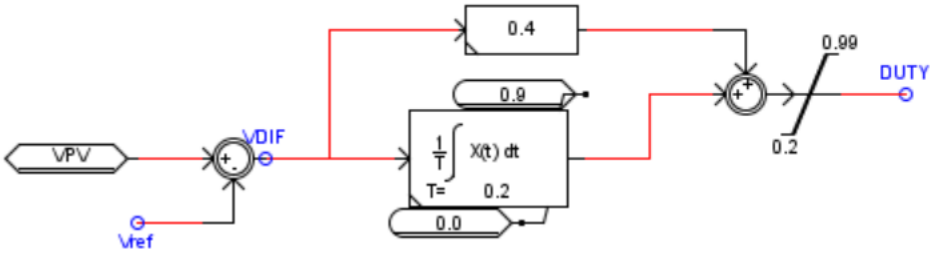

Figure 3.19: Buck converter controller in RTDS

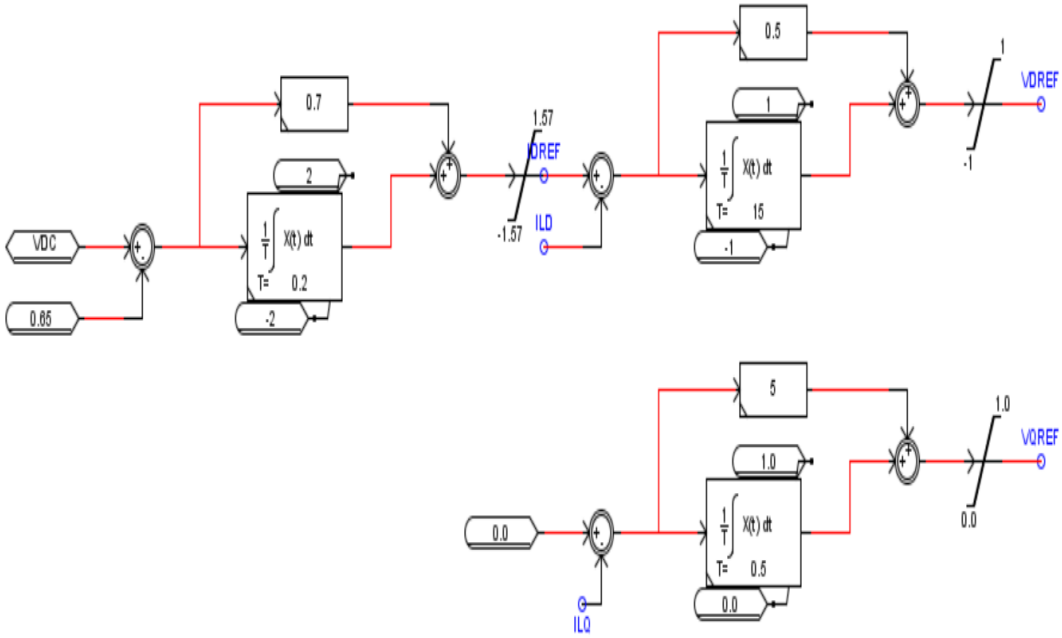

Figure 3.20 : Inverter controller

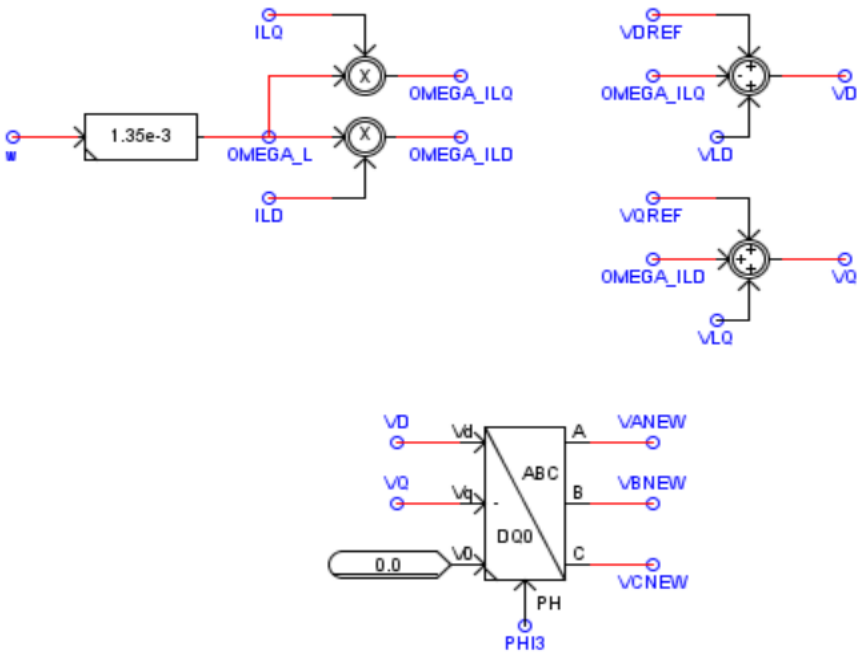

Figure 3.21: Coupling and feedforward

To demonstrate the effectiveness of the proposed IC based MPPT and grid connected PV system, the following tests have been applied.

a. Step change in irradiation from 500 to 1000 W/m^2
b. Step change in temperature from 25 to 50 ^{o}c
c. Multiple variations in input irradiation

3.8.1 Step Change in Irradiation

The first disturbance applied to check the efficiency of the proposed controllers is a step change in irradiation from 500 to 1000 W/m^2 keeping the temperature constant. The applied disturbance and response of the system are presented in Figures. 3.22-3.26. The proposed MPPT controller tracks the maximum voltage from the PV array and maximum

power P_{PV} is generated. The inverter controller is able to transfer the generated power from the PV array to the grid P_g as shown in the Figure 3.22. Figure 3.23 shows the output of the IC based MPPT controller output voltage V_{ref} and shows how the buck converter controller forces the PV array to track at a maximum PV array voltage V_{PV}. The DC link voltage is kept constant by the inverter controller with a reference 650 V as depicted in Figure 3.24. The *D*-axis current component is responsible for real power transfer to the grid and the inverter controller keeps error between the actual and reference *D*-axis current close to 0 as shown in Figure 3.25. The synchronization of the scaled grid voltage and inverter output voltage is shown in Figure 3.26 and the offset is removed by connecting a transformer between the inverter and the gird.

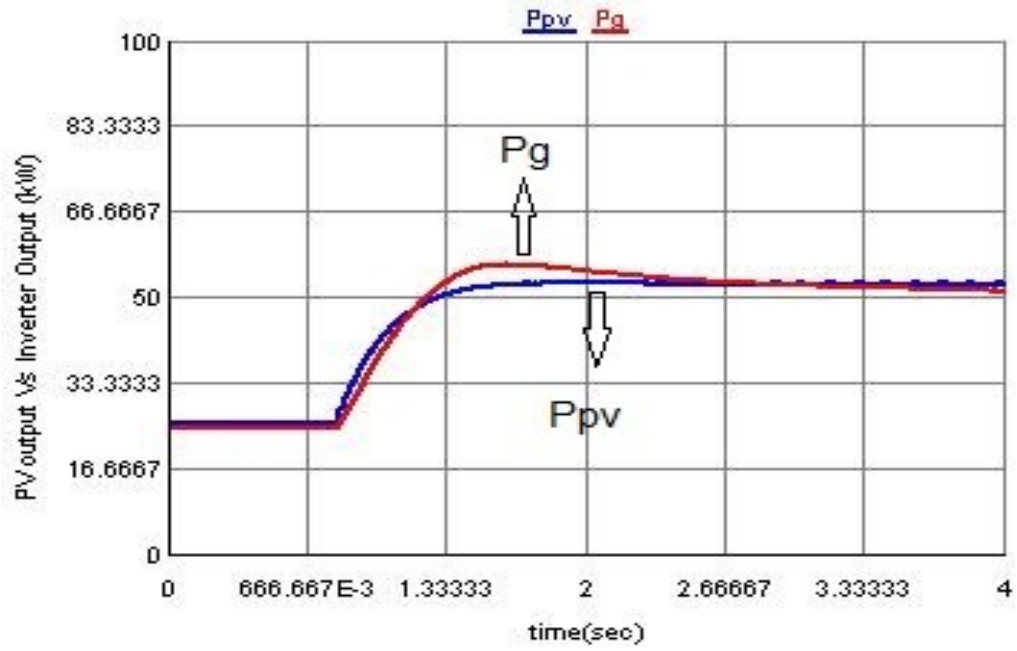

Figure 3.22: PV array output power P_{PV} and inverter output power P_g

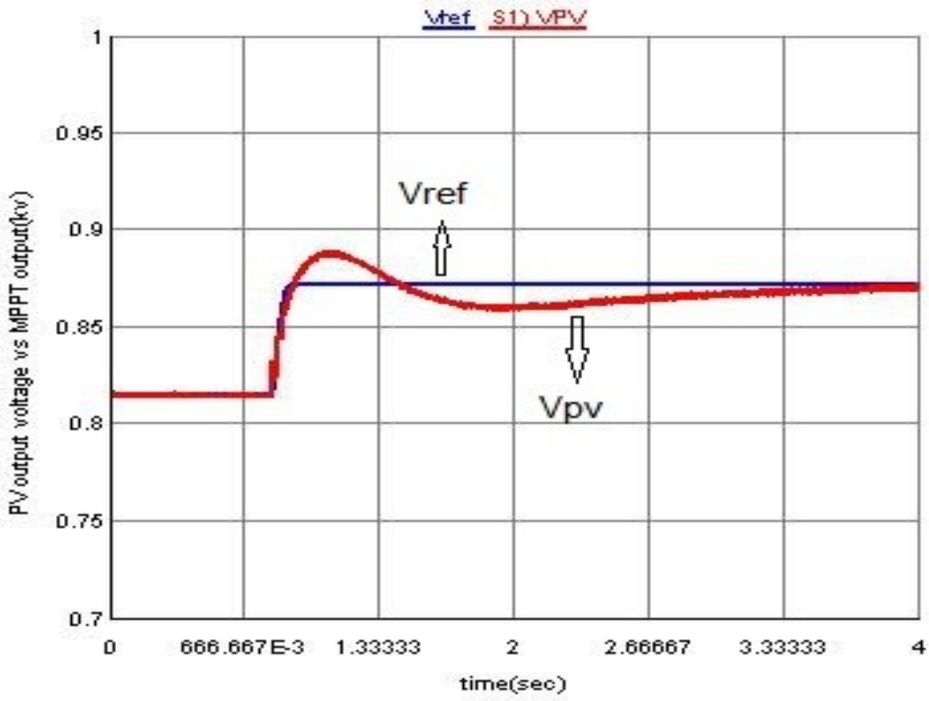

Figure 3.23: PV array output voltage V_{PV} and MPPT output voltage V_{ref}

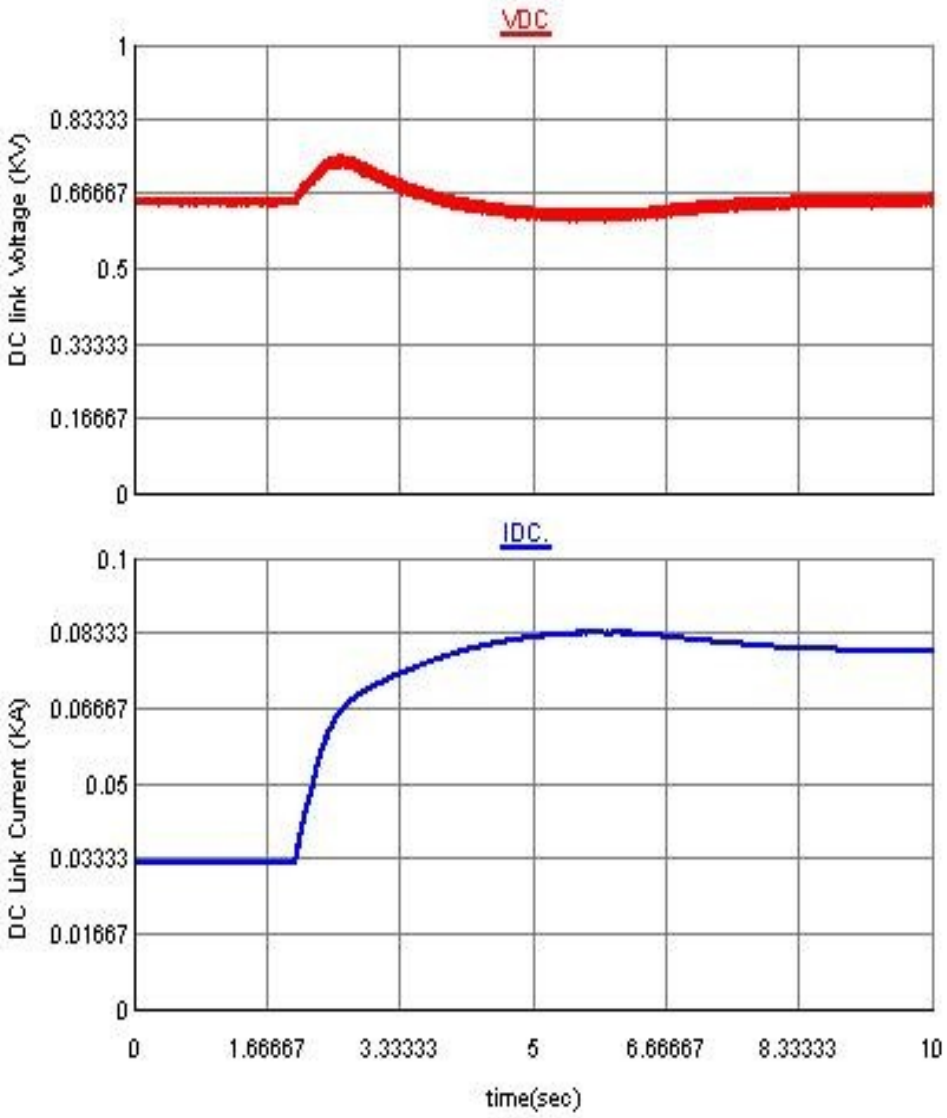

Figure 3.24: DC link voltage V_{DC} and current I_{DC}

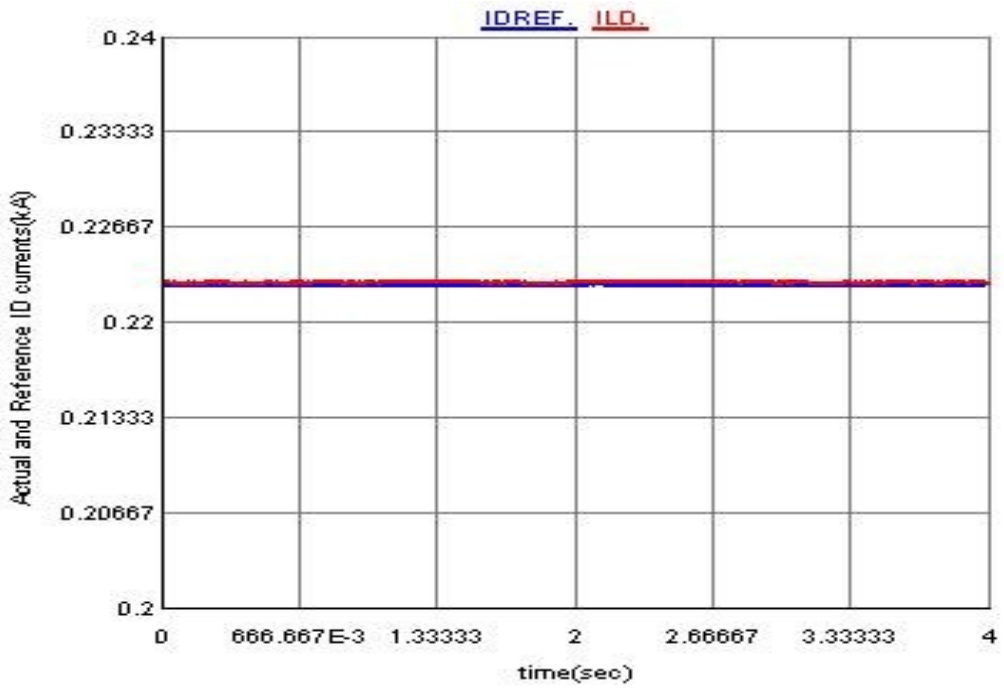

Figure 3.25: Actual and reference *D*-axis inverter currents

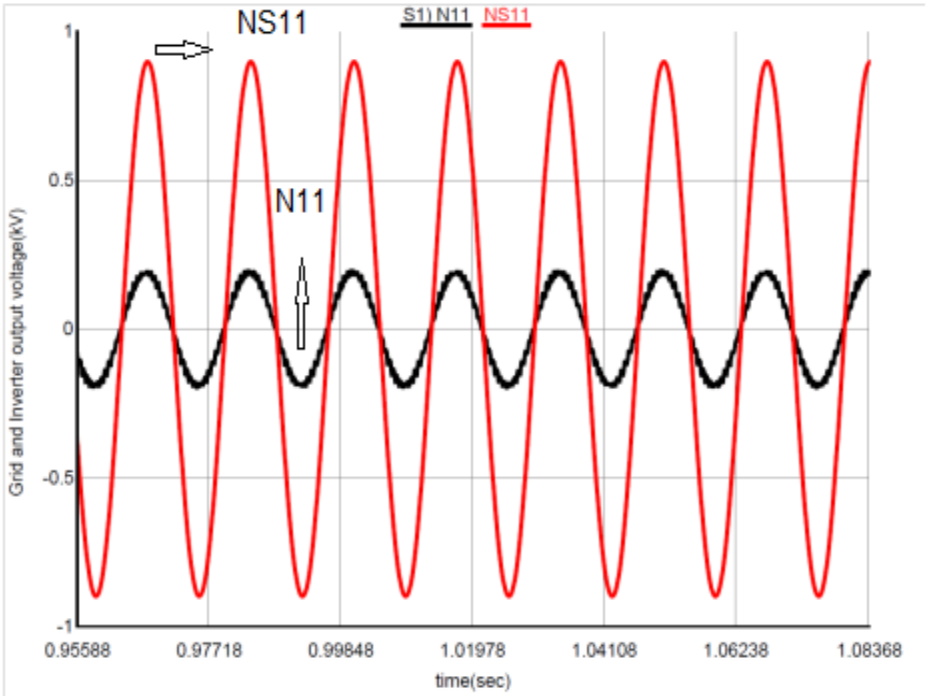

Figure 3.26: Grid *NS11* and inverter *N11* output voltages to show the synchronization

3.8.2 Step Change in Temperature

The second disturbance applied to check the robustness of the controller is a step change in temperature from 25 to 50^{o}c keeping the irradiation level at 1000W/m^{2}. From the PV array electrical characteristics, the output power gets reduced at higher temperature and results are provided through Figures 3.27-3.31. The grid power P_g follows the PV array output power P_{PV} as shown in Figure 3.27 and the value has decreased from the nominal 53 kW since the temperature has increased. Figure 3.28 shows the PV array output voltage and the MPPT voltage following each other as proposed by the controller. Similar to the irradiation change, the inverter controller keeps the DC link voltage constant for step change in temperature as shown in Figure 3.29. The inverter current controller keeps the error between the actual and measured *D*-axis current component approximately zero as presented in Figure 3.30. For unity power factor, the reference reactive power is kept 0 and from Figure 3.31 the actual measured reactive power Q_g is around 0.

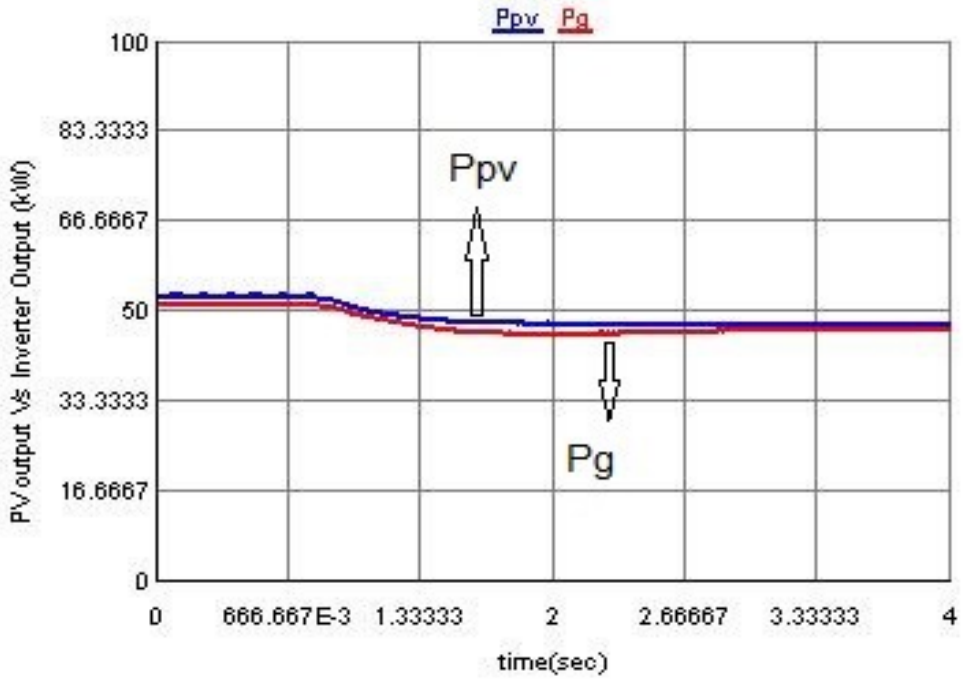

Figure 3.27: PV array output power P_{PV} and inverter output power P_g

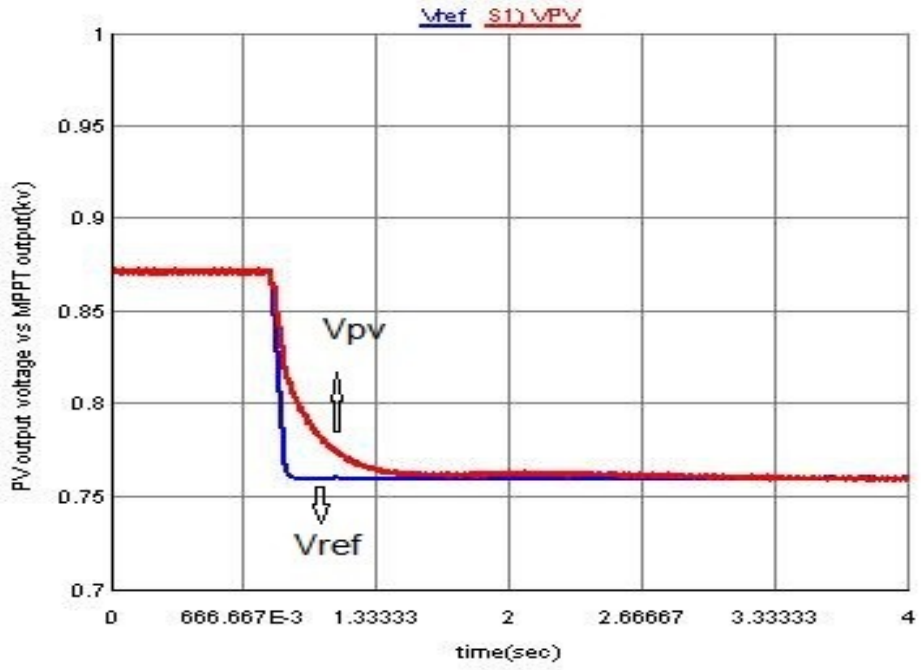

Figure 3.28: PV array output voltage V_{PV} and MPPT output voltage V_{ref}

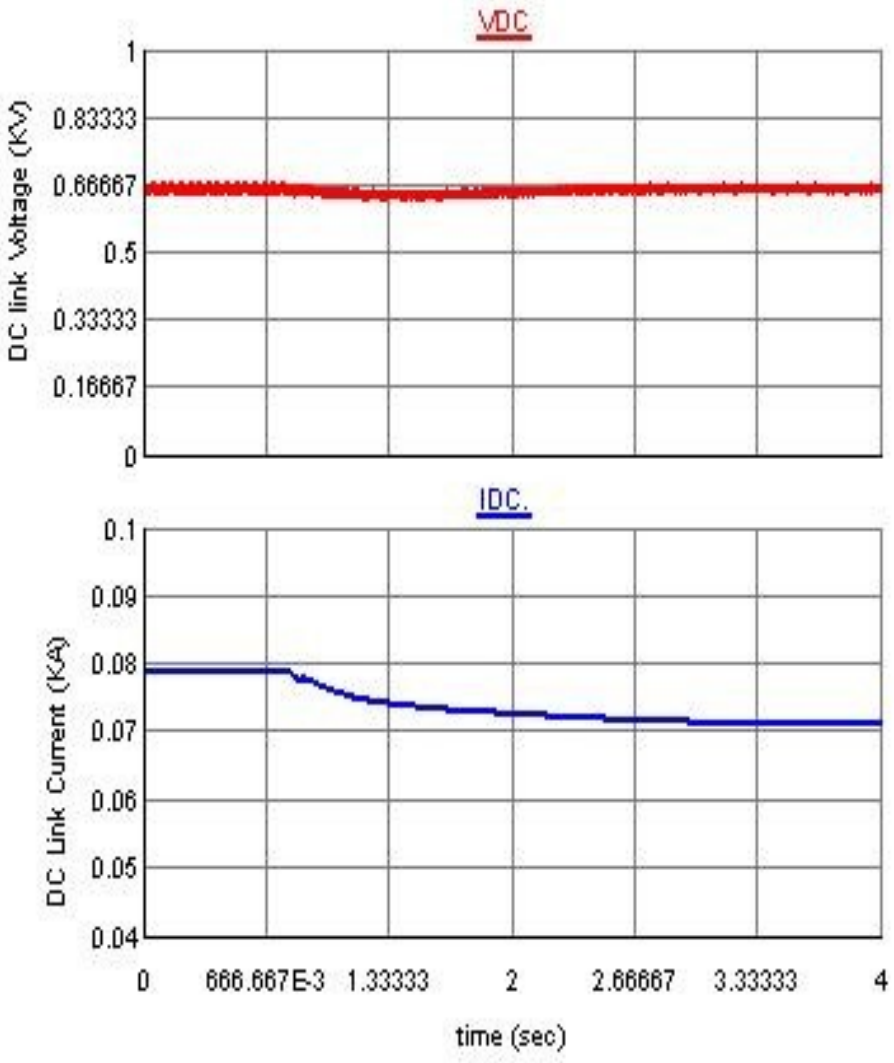

Figure 3.29: DC link voltage V_{DC} and current I_{DC}

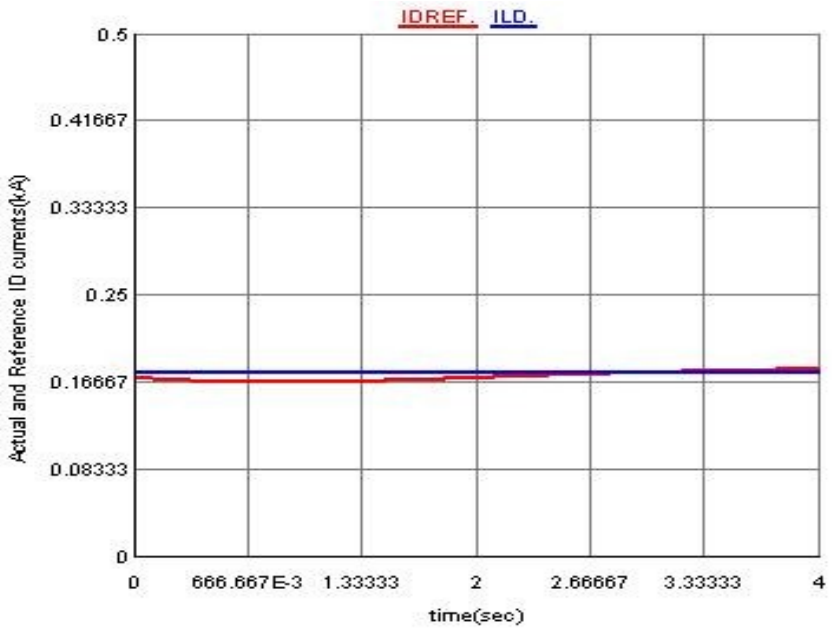

Figure 3.30: Actual and reference *D*-axis inverter currents

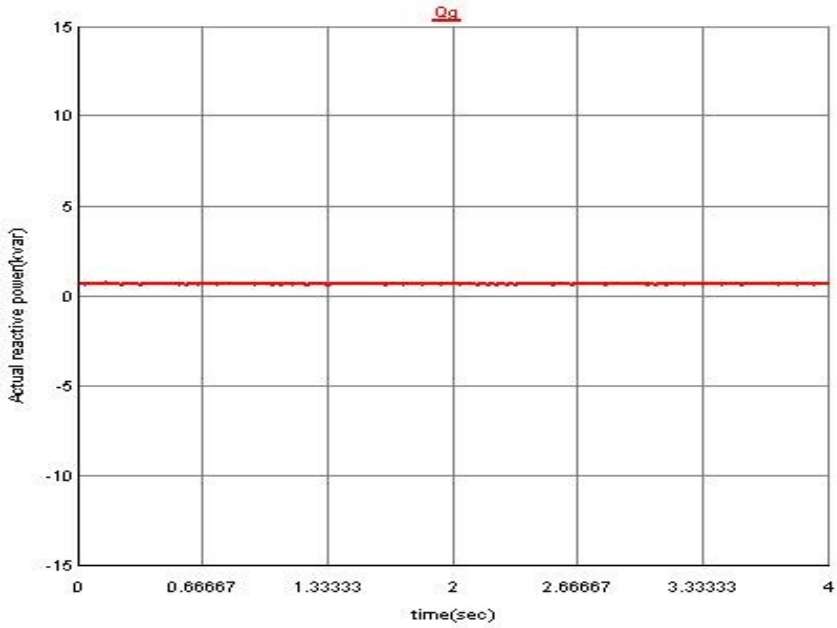

Figure 3.31: The actual reactive power Q_g from the grid side

3.8.3 Multiple Variations in Input Irradiation

The above disturbances applied are to check the controllers performance in the worst case but unexpected to happen in real environment. To check the performance of the controller for real environment change in the input parameters, a scheduled trapezoidal irradiation input shown in Figure 3.32 is applied. The response of the system for the applied disturbance is depicted from Figures 3.33-3.36. The grid power P_g follows the output PV power P_{PV} as shown in Figure 3.33. The DC link voltage is kept constant by the inverter controller irrespective of the variation in the input irradiation as shown in Figure 3.34. The proposed MPPT controller tracks the maximum voltage and the proposed buck converter ensures that the PV array output voltage and the MPPT output voltage are identical as shown in Figure 3.35. During the input irradiation variation, the IC based MPPT tracks the maximum voltage by changing the duty as shown in Figure 3.36.

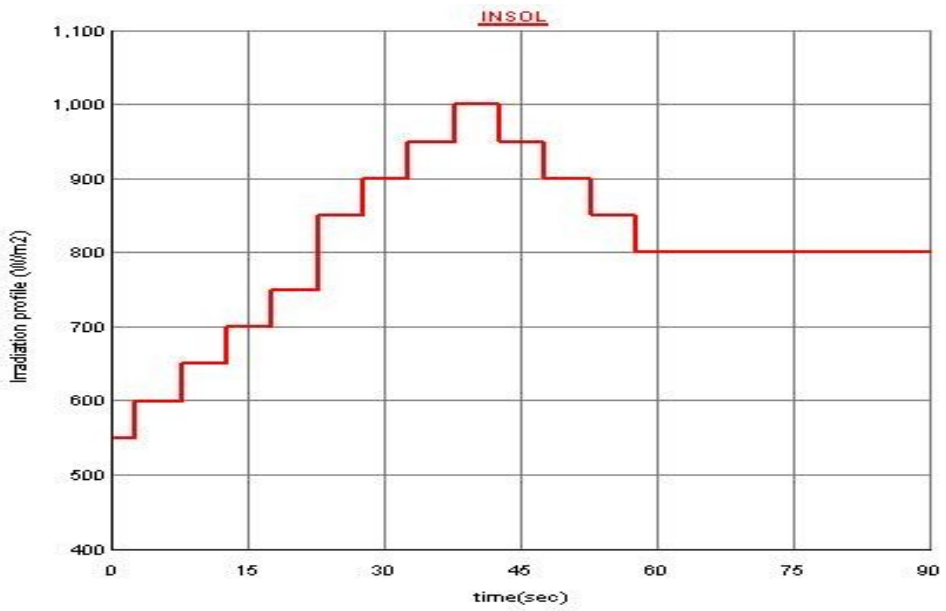

Figure 3.32: Trapezoidal irradiation input profile

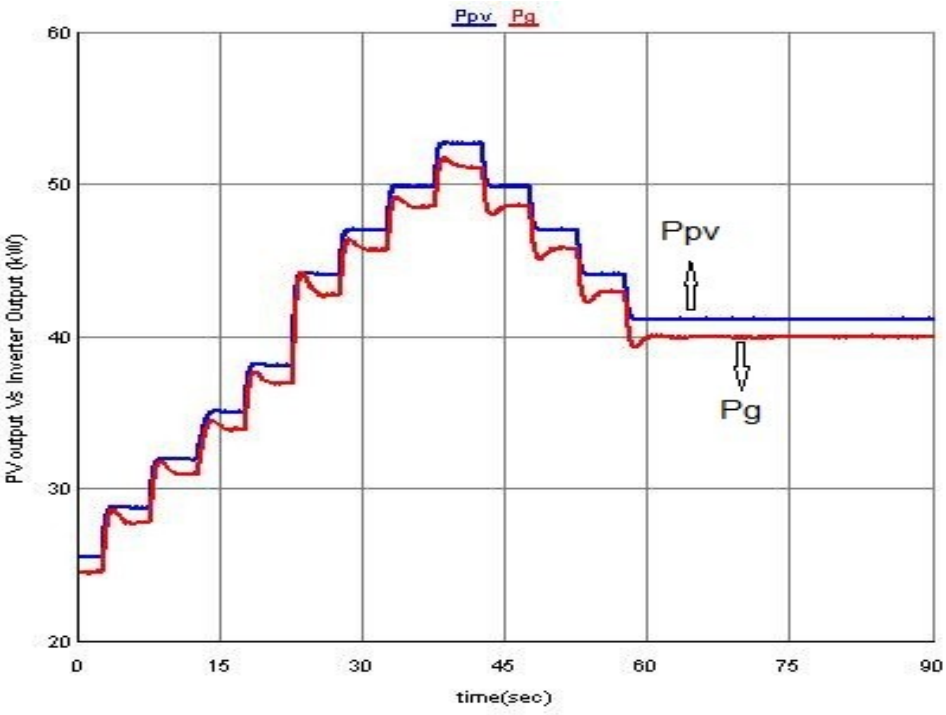

Figure 3.33: PV array output power P_{PV} and inverter output power P_g

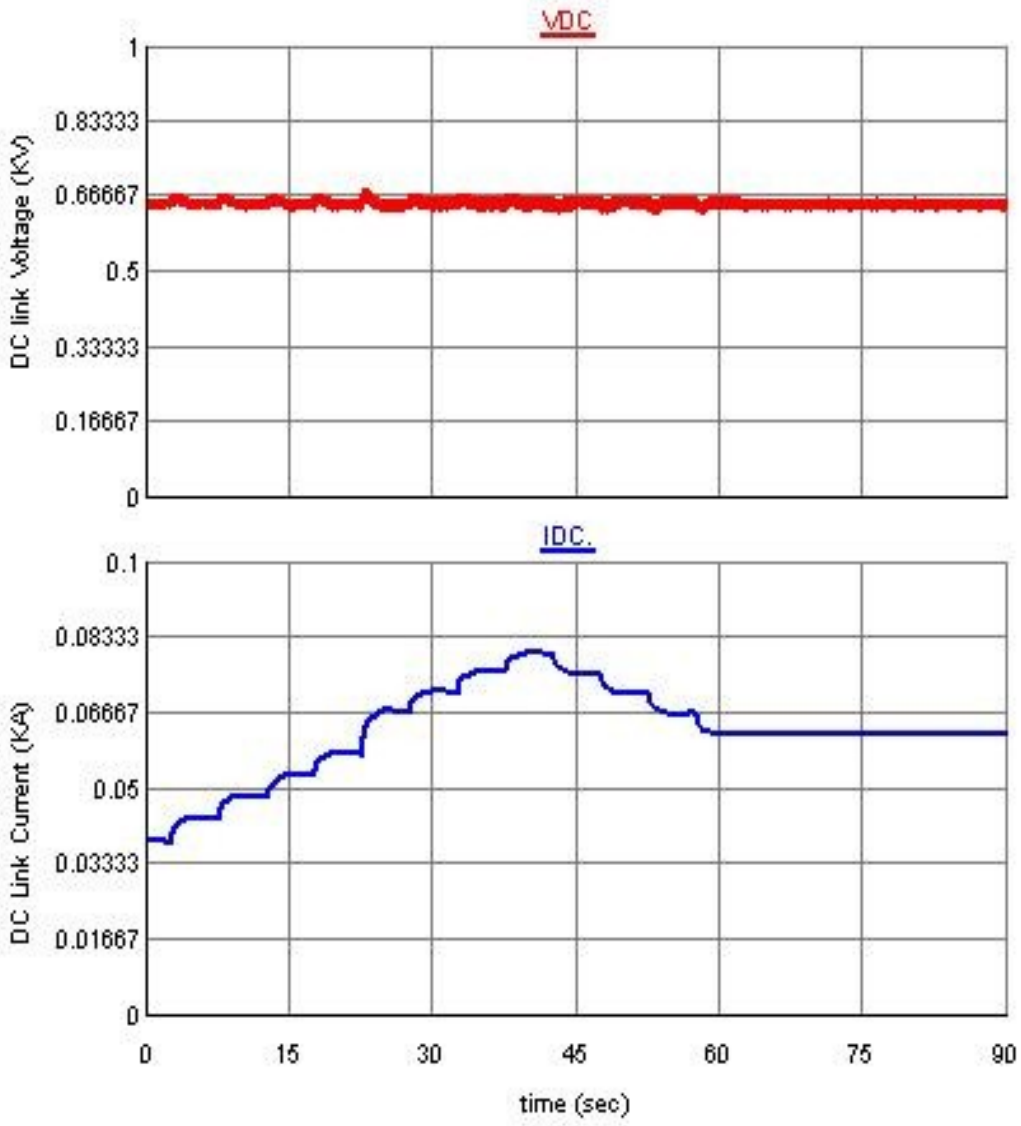

Figure 3.34: DC link voltage V_{DC} and current I_{DC}

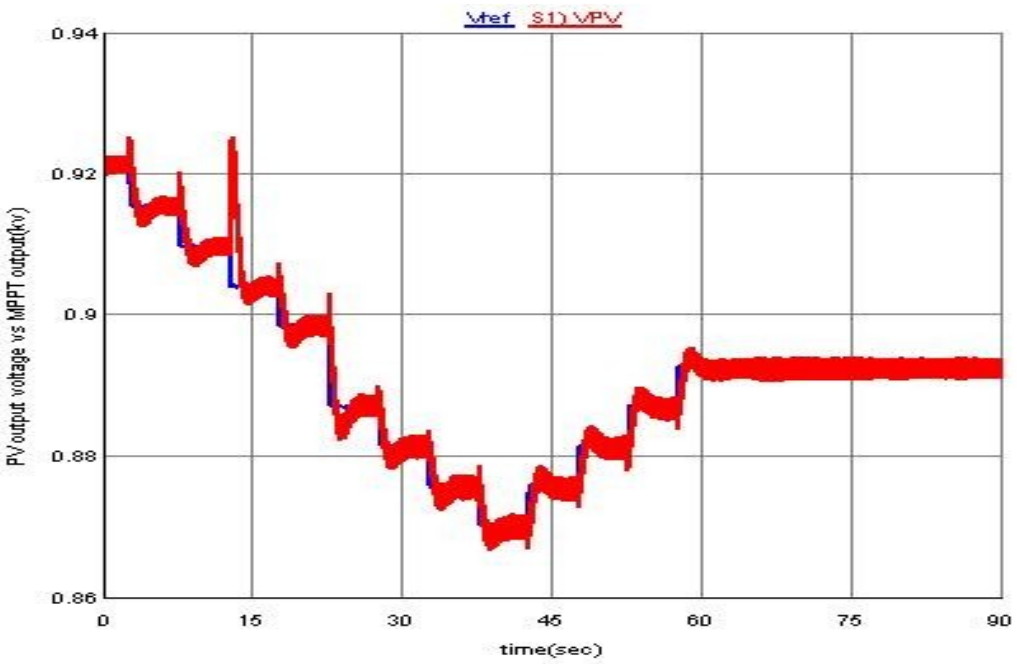

Figure 3.35: PV array output voltage V_{PV} and MPPT output voltage V_{ref}

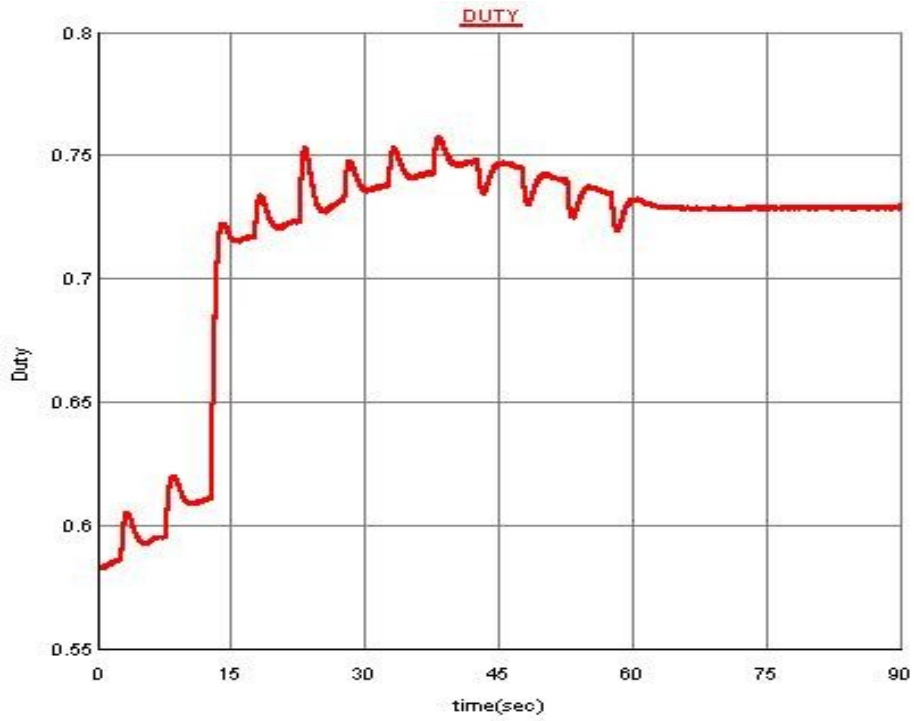

Figure 3.36: Duty cycle for the buck converter

3.9 CONCLUSION

This chapter presented real time simulation of grid connected PV system with efficient P-Q and IC based MPPT controller. An independent active and reactive P-Q controller is implemented to transfer the generated power from the PV array to the grid. The proposed IC-based MPPT controller implemented forces the PV array to work at the maximum power point. The generated DC power is connected to the grid using a voltage source converter. A vector controller is implemented in RTDS to control independently the active and reactive power. RTDS is used to assess the validity of the proposed controllers. Results show that the proposed controllers are efficient in delivering the maximum power from the PV to the grid.

CHAPTER 4 POWER FLUCTUATION MINIMIZATION OF PV SYSTEM USING SUPERCAPACITORS

This chapter presents grid connected PV system equipped with supercapacitor energy storage system to minimize the fluctuation caused by change in irradiation and temperature. A controller is designed to charge and discharge the supercapacitor and the optimal supercapacitance of the supercapacitor is determined. The results provided verify the superiority of the proposed controller in minimizing the fluctuation from the generated power.

4.1 Overview

Electrical energy in an AC system cannot be stored electrically. However, energy can be stored by converting the AC electricity and storing it electromagnetically, electrochemically, kinetically, or as potential energy. Each energy storage technology usually includes a power conversion unit to convert the energy from one form to another. Energy storage technology is used to make the electric power systems more reliable as well as making the broader use of renewable energy a reality. They can provide a wide array of solutions to key issues that are affecting the power system. Depending on the technology selected, they can provide spinning reserves, load leveling and shifting, load forecasting, frequency control, VAR support and voltage regulation, relief of overloaded transmission lines, release of system capacity, and enhance power quality. It also increases the overall efficiency of the power system. Large scale storage devices are

battery, compressed air, flywheel, pumped hydroelectric, superconducting magnetic, and supercapacitor.

Storage can be a useful addition to renewable resources such as wind and solar which may not be available when required. Storage technologies can help smooth the demand for electrical generation and thereby improve efficiency and reliability. During periods of low demand, excess generation can be used to charge an energy storage device. The stored energy can then be used to provide electricity during periods of high demand. Since storage is a tool for improving utility operation, it is very likely that most storage systems will be utility operated and that their scheduling will be well coordinated with the rest of the electric power system.

4.2 Grid Connected PV with Supercapacitor Energy Storage System (SCESS)

Despite all the benefits introduced by PV systems to electric utilities, these systems might lead to some operational problems. One of the main factors that lead to such problems is the fluctuations of the output power of PV systems due to the variations in the irradiation and temperature. Such fluctuations reduce their reliability in providing continuous power to customers and lead to several operational problems that make the output power forecast of PV systems a hard task.

To overcome this fluctuation, different energy storage devices are integrated to the PV system. The use of energy storage devices with PV systems is currently receiving a lot of attention, especially due to the fact that the power generated from these systems is intermittent. The installation of storage devices can enhance the performance of PV systems by bridging their power fluctuations, shifting the time of their peak generation,

supplying critical loads during power outages, and providing reactive power support. Among these, battery and supercapacitor energy storage system (SCESS) are used in the literature because of their high energy and power densities respectively.

In this dissertation SCESS is used to minimize the fluctuation as it has high power density and fast response as shown in Table 2.1 of chapter 2. Figure 4.1 depicts the configuration of grid integrated PV system with energy storage connected to the DC link. The modeling of the PV array and the function of the DC-DC converter (buck) is the same as that of grid connected PV discussed in chapter three. The energy storage is connected at the DC link between the buck converter and the inverter using a bidirectional buck boost converter. Unlike the grid connected PV system discussed in chapter three where the DC link voltage is controlled by the inverter, in this topology the DC link voltage is kept constant by the buck boost converter for real power delivery by absorbing any mismatch between the generated power and the power transferred to the grid. A constant P-Q control is implemented for the inverter to transfer the available power of the DC link to either an AC load or to the main grid.

In Figure 4.1,

P_{SC} : is the power exchanged between the DC link and the SCESS

C_{SC} : the supercapacitor capacitance

All the other parameters are described in Figure 3.1.

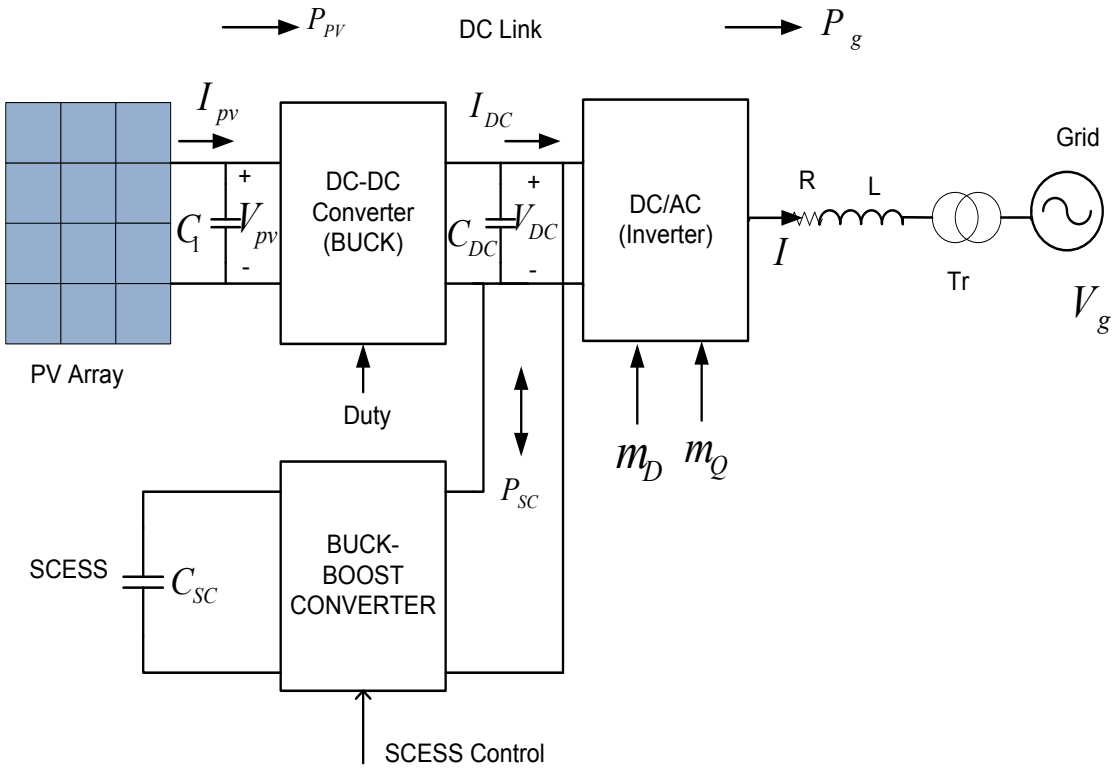

Figure 4.1: Grid connected PV system with energy storage

4.2.1 Bidirectional Buck-Boost Converter and Its Controller

The topology of the bi-directional buck-boost converter is shown in Figure 4.2. The bidirectional converter acts as a buck converter to charge the supercapacitors in one direction and as a boost converter to transfer energy to the DC link capacitor in the other direction. IGBTs are used as the switching devices in the circuit. The operation of the converter is controlled by the DC link voltage and the voltage of the supercapacitors. The main purpose of the bidirectional buck-boost converter is to maintain the voltage of the DC link relatively constant at a reference value. To make this converter controller stable, a lower limit is placed on the supercapacitor voltage which is 50% of the maximum value V_{SCmax}, where V_{SCmax} is the maximum supercapacitor voltage. The state of charge (SoC) controls the supercapacitor voltage to be between $0.5V_{SCmax}$ and V_{SCmax}. Between these

two voltages 75% of the energy stored can be utilized. The inductor L_{SC} is designed from the boost mode using a duty cycle of about 0.5 [145].

$$V_{DC} = \frac{V_{SC}}{1-d} \tag{4.1}$$

The inductor ripple current when switch S_2 is on is:

$$\Delta I_{LSC(on)} = (\frac{V_{SC}}{L_{SC}})T_{on} \tag{4.2}$$

And when it is off,

$$\Delta I_{LSC(off)} = (\frac{V_{SC} - \frac{V_{SC}}{1-d}}{L_{SC}})T_{off} \tag{4.3}$$

At steady state, $\Delta I_{LSC(on)} = \Delta I_{LSC(off)}$ and $T=T_{on}+T_{off}=1/f_s$

$$\Delta I_{LSC} = \frac{V_{SC}}{L_{SC}} dT \quad or \quad L_{SC} = \frac{V_{SC} dT}{\Delta I_{LSC}} \tag{4.4}$$

where,

V_{DC} : is the DC link voltage

V_{SC} : is the supercapacitor voltage

d : duty cycle of the buck boost converter IGBT

$\Delta I_{LSC(on)}$: inductor ripple current when S_2 is on

$\Delta I_{LSC(off)}$: inductor ripple current when S_2 is off

T_{on} : IGBT on period

T_{off} : IGBT off period

T : is the switching period and f_s is the switching frequency

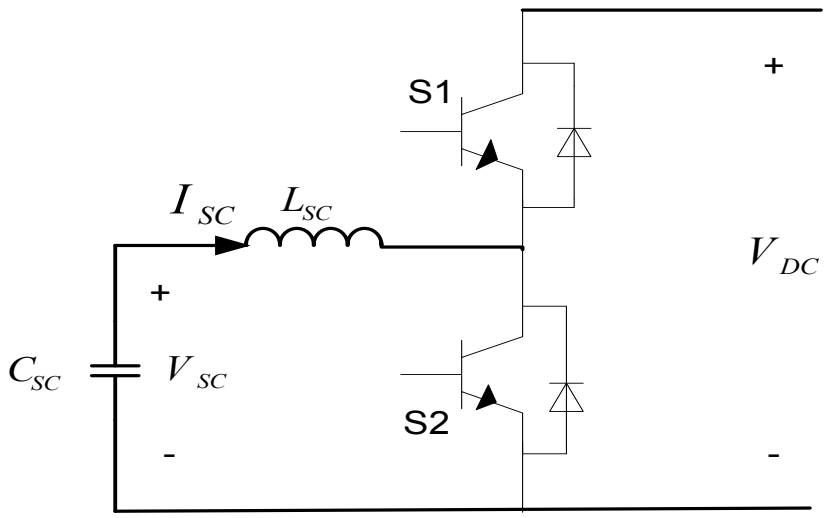

Figure 4.2: Buck boost converter to integrate the SCESS

4.2.2 DC-Link Capacitor Design

In the configuration of Figure 4.1, the DC link capacitor is only required to function as a smoothing capacitor in order to limit voltage ripple during boost mode. In buck mode, energy will be stored in supercapacitor modules. The design of the DC link capacitor for this case is then focused on boost mode operation. In boost mode when S_2 is ON, it is the DC link capacitor that supplies energy to the grid, the supercapacitors are transferring energy to L_{SC}. The amount of charge Q stored in the DC link capacitor decreases as it supplies the required real power via the inverter to the grid, and the DC link voltage drops. When S_2 is OFF, the DC link capacitor is charged from the C_{SC} (the stored energy in L_{SC}), and the DC link voltage increases. This cycle of store and supply charge causes a ripple voltage, ΔV, written in (4.5).

$$\Delta V = \frac{\Delta Q}{C_{DC}} = \frac{IdT}{C_{DC}} = \frac{P_{SC}dT}{C_{DC}V_{DC}} \tag{4.5}$$

$$C_{DC} = \frac{P_{SC}dT}{\Delta V V_{DC}} \tag{4.6}$$

where,

ΔV : is DC link ripple voltage, V.

ΔQ : is change in capacitor charge, Coulomb.

C_{DC} : is DC Link capacitor, F.

C_{SC} : the supercapacitor capacitance

I : is load current supplied to the grid, A.

In equation (4.5), if the maximum ripple voltage, ΔV_{max}, occurs when maximum power is supplied to the grid with a duty ratio d =1.0. Two cascaded loops are implemented for the buck boost converter as shown in Figure 4.3. The outer loop is a voltage control that regulates the DC link voltage by comparing the measured DC link voltage with the reference and generates the reference supercapacitor current I_{SCref}. This reference current is compared with the actual inductor current I_{SC} to generate the gating signals for the IGBTs.

Let

$$\dot{V}_{DCERR} = V_{DCref} - V_{DC}$$

$$I_{SCERR} = I_{SCref} - I_{SC}$$

The reference current I_{SCref} in Laplace transform is given as:

$$I_{SCref} = K_{PO}(V_{DC} - V_{DCref}) + K_{IO}V_{DCERR} \tag{4.7}$$

The control signal V_s in Laplace transform is given by

$$V_S = K_{PI}\,(I_{SCref} - I_{SC}) + K_{II}\,I_{SCERR} \tag{4.8}$$

where,

V_{DCERR} : is the state variable for the outer voltage controller

I_{SCERR} : is the state variable for the inner current controller

K_{PO} and K_{IO} : are the PI proportional and integral gains of the outer voltage control loop

K_{PI} and K_{II} : are the PI proportional and integral gains of the inner current control loop

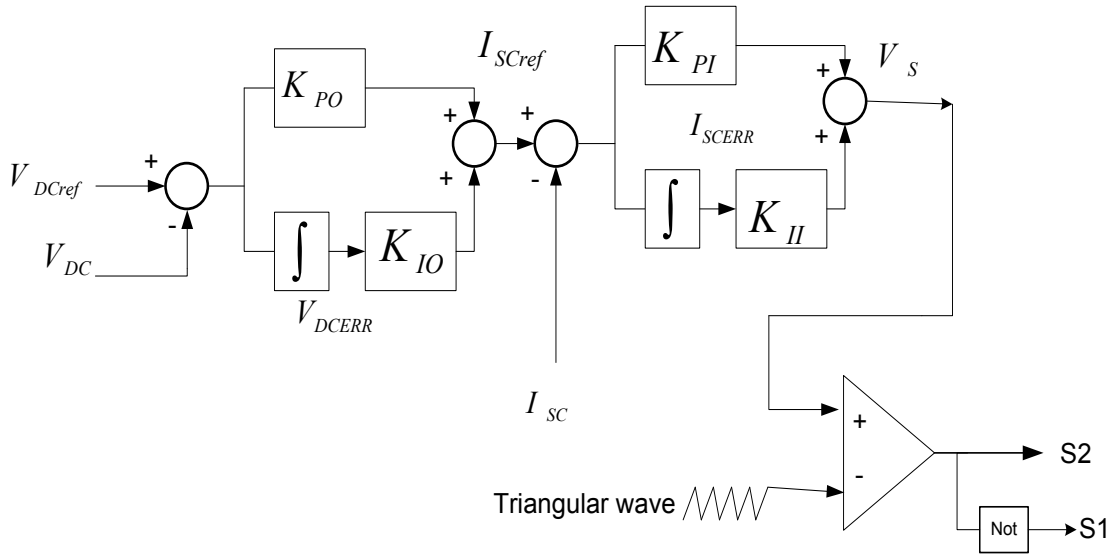

Figure 4.3: Controller for the buck boost converter

The size of the supercapacitor is chosen depending on the amount of energy required to minimize the fluctuation from the PV source. From Figure 4.1,

$$P_g = P_{pv} \pm P_{SC} \tag{4.9}$$

$$P_{SC} \times t = \frac{1}{2} C_{SC} V_{SC}^{\ 2} \tag{4.10}$$

where,

P_g : is the grid demand power,

P_{pv} : the maximum power generated from PV array

t : time required to support the system using SCESS

If the power demand from the grid or load connected to the AC side is less than the power generated from the PV array, the excess power is stored in the supercapacitor for later use when the power demand is high.

4.2.3 P-Q Controller for the Inverter

The inverter discussed in chapter three for grid connected PV controls the DC link voltage but in this case the buck-boost converter controls the DC link voltage. The inverter sends a constant power to the grid. Using synchronous rotating reference frame (D-Q axis), decoupled active and reactive current control technique is implemented using a PI controller.

$$\begin{aligned} P_g &= \frac{3}{2}(V_{LD}I_{LD} + V_{LQ}I_{LQ}) \\ Q_g &= \frac{3}{2}(V_{LQ}I_{LD} - V_{LD}I_{LQ}) \end{aligned} \tag{4.11}$$

The power reference signals for the active and reactive power controllers are obtained from the Power Management Control (PMC). If the reference active and reactive powers are known, the respective I_{DREF} and I_{QREF} currents are determined from equation (4.11) as:

$$I_{DREF} = \frac{2}{3}\left(\frac{P_{REF}V_{LD} - Q_{REF}V_{LQ}}{V_{LD}^{\ 2} + V_{LQ}^{\ 2}}\right) \tag{4.12}$$

$$I_{QREF} = \frac{2}{3}\left(\frac{P_{REF}V_{LQ} + Q_{REF}V_{LD}}{V_{LD}^{\ 2} + V_{LQ}^{\ 2}}\right) \tag{4.13}$$

The control scheme for the constant P-Q control is shown in Figure 4.4. Since the *D* and *Q* components are coupled, cross-coupling term and a feed forward voltage are used to improve the performance of the PI current controllers.

Let,

$$\dot{I}_{DERR} = I_{DREF} - I_{LD}$$
$$\dot{I}_{QERR} = I_{QREF} - I_{LQ}$$

The D-axis component control signal in the Laplace domain is:

$$m_D = K_{P1D}(I_{DREF} - I_{LD}) + K_{I1D} I_{DERR} + V_{LD} - \omega L I_{LQ} \tag{4.14}$$

And *Q*-axis component control signal in the Laplace domain is

$$m_Q = K_{P2Q}(I_{QREF} - I_{LQ}) + K_{I2Q} I_{QERR} + V_{LQ} + \omega L I_{LD} \tag{4.15}$$

where,

I_{DERR} : is the *D*-axis state variable

I_{QERR} : is the *Q*-axis state variable

K_{P1D} and K_{I1D} : are the *D*-axis PI regulator gains

K_{P2Q} and K_{I2Q} : are the *Q*-axis PI regulator gains

m_D : is the *D*-axis control signal

m_Q : is the *Q*-axis control signal

The control signals m_D and m_Q are then converted back using DQ/ABC and firing pulses are generated for the inverter using pulse width modulation (PWM).

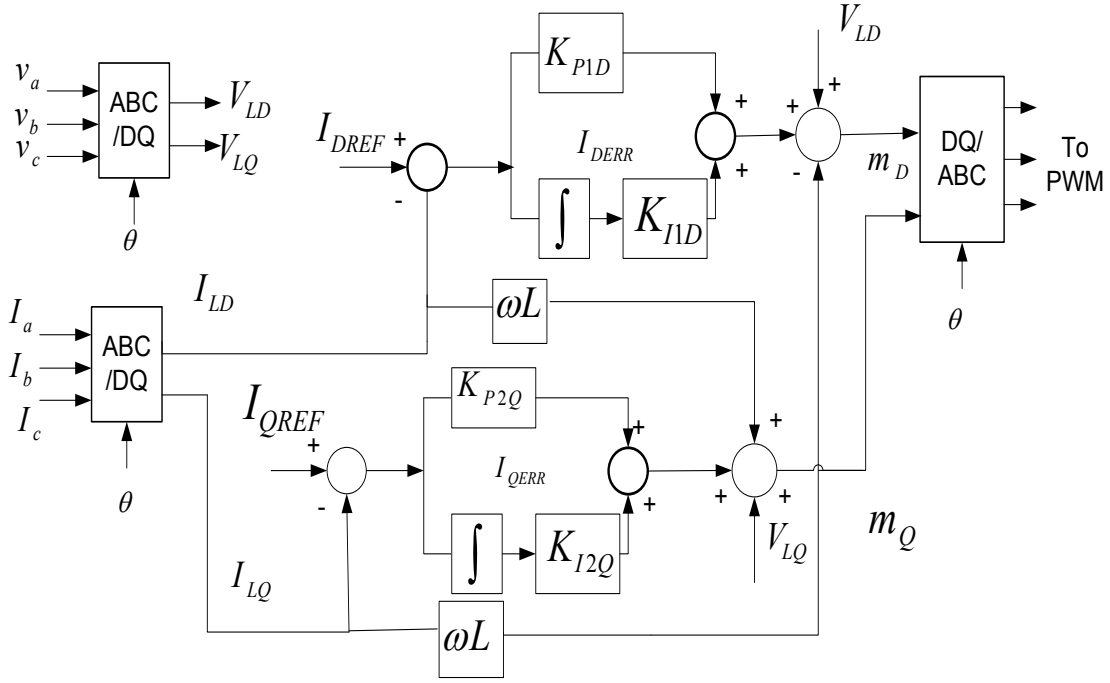

Figure 4.4: Decoupled P-Q inverter control

4.3 Problem Formulation and Control Parameter Design

The same technique applied in chapter three is used to determine the control parameters of grid connected PV system with SCESS. The same objective function is used. For grid connected PV system with supercapacitor energy storage system the optimized parameters are K_{PB}, K_{IB}, K_{PO}, K_{IO}, K_{PI}, K_{II}, K_{P1D}, K_{I1D}, K_{P2Q} and K_{I2Q}. The constraints are:

$$K_{PB}^{\min} \le K_{PB} \le K_{PB}^{\max} \tag{4.16}$$

$$K_{IB}^{\min} \le K_{IB} \le K_{IB}^{\max} \tag{4.17}$$

$$K_{P1D}^{\min} \le K_{P1D} \le K_{P1D}^{\max} \tag{4.18}$$

$$K_{I1D}^{\min} \le K_{I1D} \le K_{I1D}^{\max} \tag{4.19}$$

$$K_{P2D}^{\min} \le K_{P2D} \le K_{P2D}^{\max} \tag{4.20}$$

$$K_{I2D}^{\min} \le K_{I2D} \le K_{I2D}^{\max} \tag{4.21}$$

$$K_{PO}^{\min} \le K_{PO} \le K_{PO}^{\max} \tag{4.22}$$

$$K_{IO}^{\min} \le K_{IO} \le K_{IO}^{\max} \tag{4.23}$$

$$K_{PI}^{\min} \le K_{PI} \le K_{PI}^{\max} \tag{4.24}$$

$$K_{II}^{\min} \le K_{II} \le K_{II}^{\max} \tag{4.25}$$

The states are:

$$x=[I_{PV}\ \ V_{DC}\ \ V_{PVerr}\ \ V_{DCERR}\ \ I_{SCERR}\ \ I_{DERR}\ \ I_{QERR}]^T \tag{4.26}$$

4.4 RTDS BASED RESULTS AND DISCUSSIONS

A PV array with the same specification used in chapter three as given in Table 3.1 is developed in RTDS. It consists of 50 series and 20 parallel connected modules. The DC link capacitor designed in chapter three and eqn. (4.6) give the same capacitance of 80 mF for the PV array specification and DC link voltage provided. For the reference solar intensity of 1000 W/m^2 and temperature of 25^{o}c, the operating voltage V_{MP} and current I_{MP} at the MPPT is 50×17.4 V=870 V, and 20×3.05 A=61A, respectively. The expected maximum output power at this operating point from this PV array is 53 kW (870V×61 A). The SCESS is designed to have energy capacity of 10 kW for 120 seconds (1200 kJ) to minimize the fluctuation of the 53 kW PV system. Using a reference DC link voltage of 650 V and supercapacitor voltage of 325 V (0.5×650), the optimum supercapacitor capacitance C_{SC} is designed using equation (4.10) as 22.7 F. The inductor L_{SC} of the

SCESS is designed using equation (4.4) as 0.8 mH. The P-Q controller set points P_{REF} and Q_{REF} can be set depending on the amount of power to be transferred to the grid and to the SCESS. Taking into account the capacity of the supercapacitor for this particular case, P_{REF} and Q_{REF} are set as 50 kW and 0 var, respectively. Therefore, the inverter is transferring this amount of power to the grid. In case of higher values of PV generated power, the excess power is stored in the SCESS.

Applying PSO technique on the eigenvalue based objective function of eqn. (3.68) to search for the optimal parameters of the proposed controllers, the optimal settings obtained are:

- for the buck converter, K_{PB}=0.6 and K_{IB}=0.2,
- for the buck-boost converter, K_{PO} =0.4, K_{IO} =0.5, K_{PI} =0.5, and K_{II} =0.5,
- for the inverter: K_{P1D} =0.7, K_{I1D} =0.2, K_{P2Q} = 5, and K_{I2Q} =0.5.

The eigen values of before and after optimization are tabulated in Table 4.1.

Table 4.1: Eigen value spectrum with SCESS

Before Optimization		**After optimization**	
Real part	**Imaginary part**	**Real part**	**Imaginary part**
17.6980	$\pm 1025.8i$	**-191.74**	$\pm 4025.25i$
-19.1	$\pm 648.11i$	**-68.4785**	$\pm 1926.23i$
-4.486		**-19.07**	
-9.247		**--175.1282**	
0.521		**-28.3604**	

Figure 4.5 shows the complete RTDS model of the grid connected PV system with energy storage used in this dissertation. Figure 4.6 depicts the power electronics block inside the BRDG1 block. The constant P-Q controller implemented to generate reference currents for the inverter is shown in Figure 4.7. The inner current control loop of the P-Q controller for the inverter in RTDS is shown in Figure 4.8. The coupling and feed-forward added to the inverter controller is presented in Figure 4.9. The buck-boost converter controller is depicted in Figure 4.10.

To demonstrate the effectiveness of the proposed buck-boost, P-Q and IC based MPPT controller, the following tests have been applied.

a. Normal operation: Normal operation at 1000 W/m^2 and 25^{o}c, the grid demand power is set at 50 kW and 0 var.
b. Irradiation Increase and SCESS Charging: Step change in irradiation from 1000 to 1200 W/m^2 keeping the other parameters as in case a.
c. Irradiation Decrease and SCESS Discharging: Discharging the supercapacitor when the irradiation varies from 1200 to 800 W/m^2.
d. Trapezoidal change in input irradiation

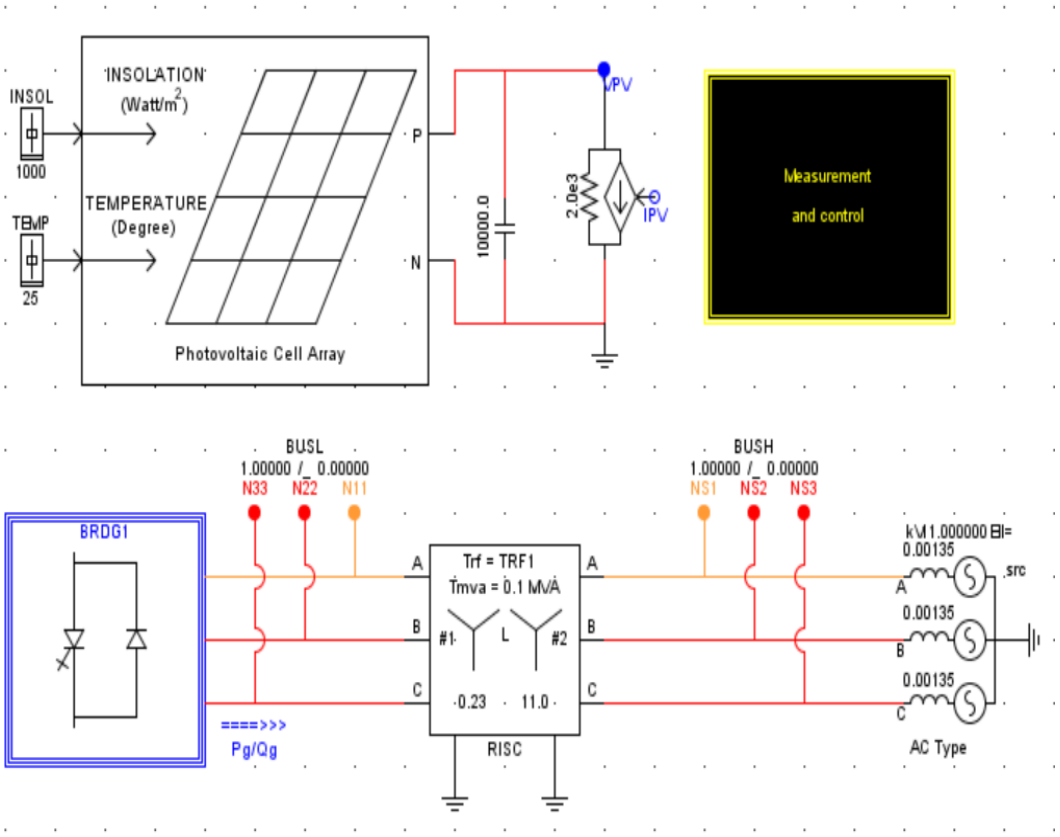

Figure 4.5: RSCAD model of grid connected PV system

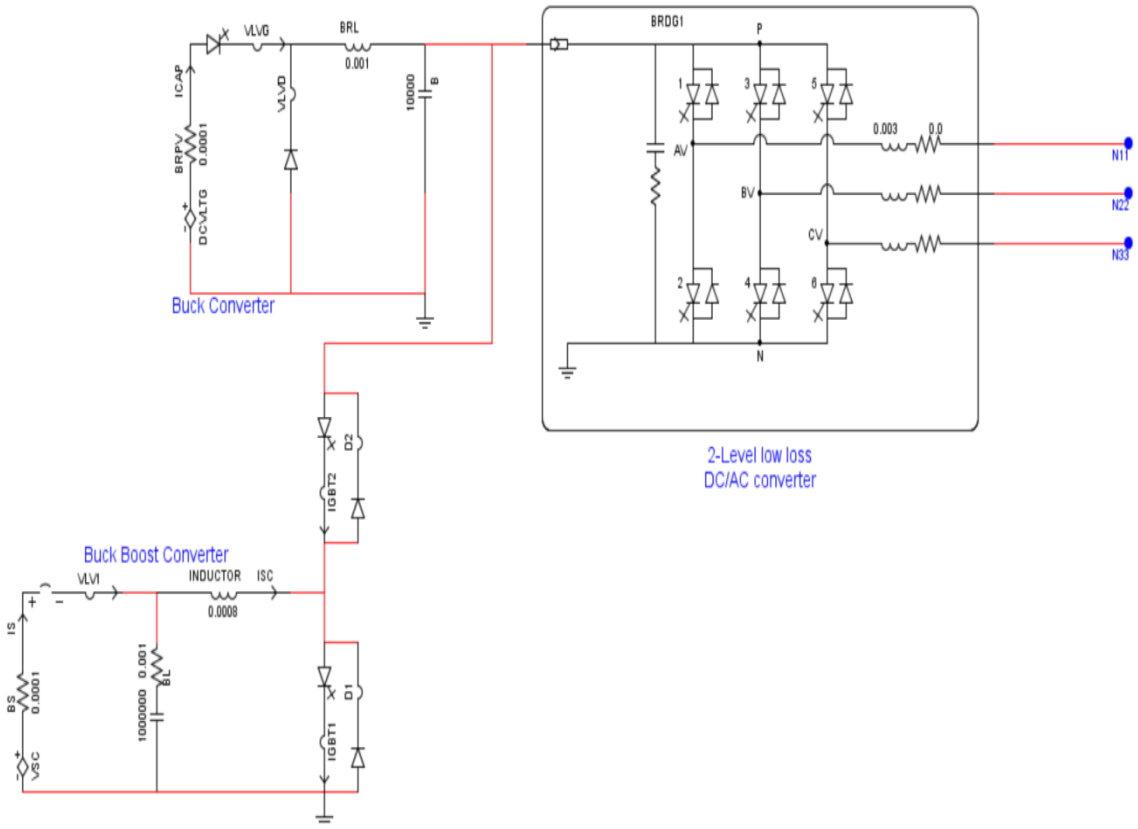

Figure 4.6: Configuration inside BRDG1

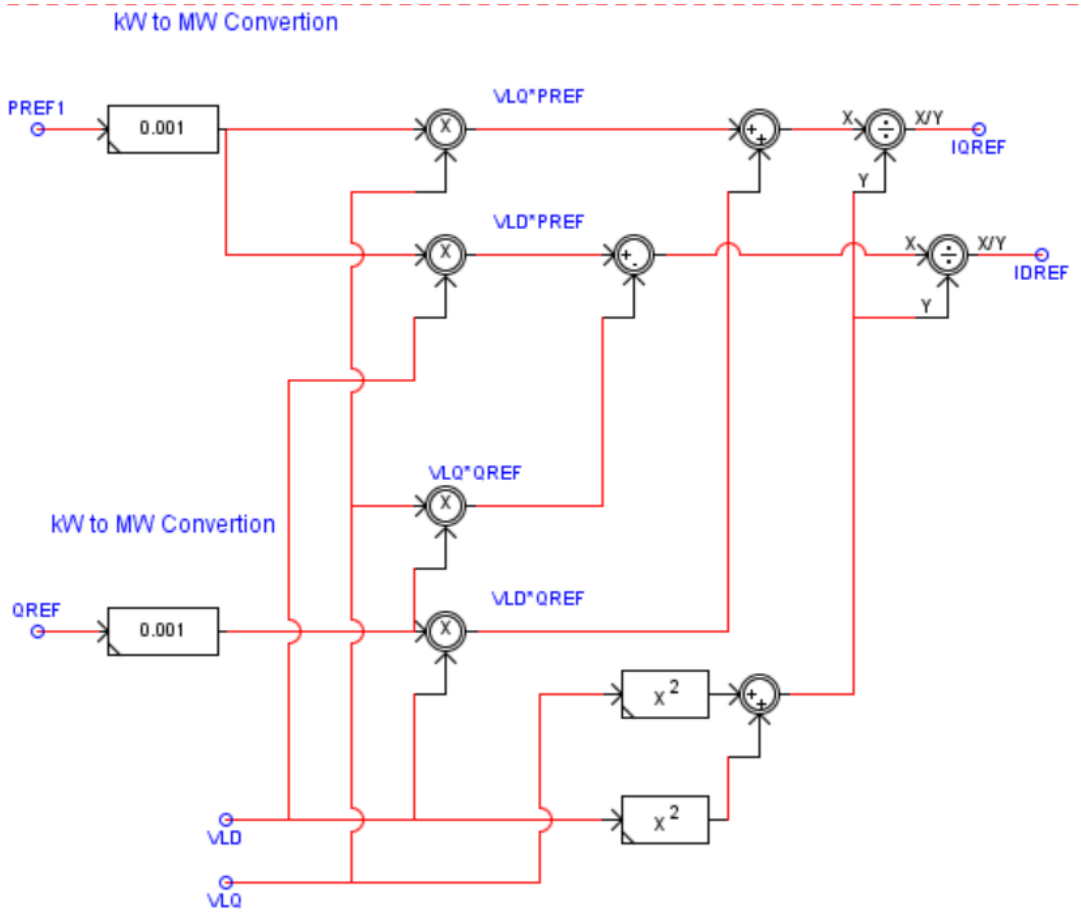

Figure 4.7: Constant P-Q control to generate reference currents for the inverter

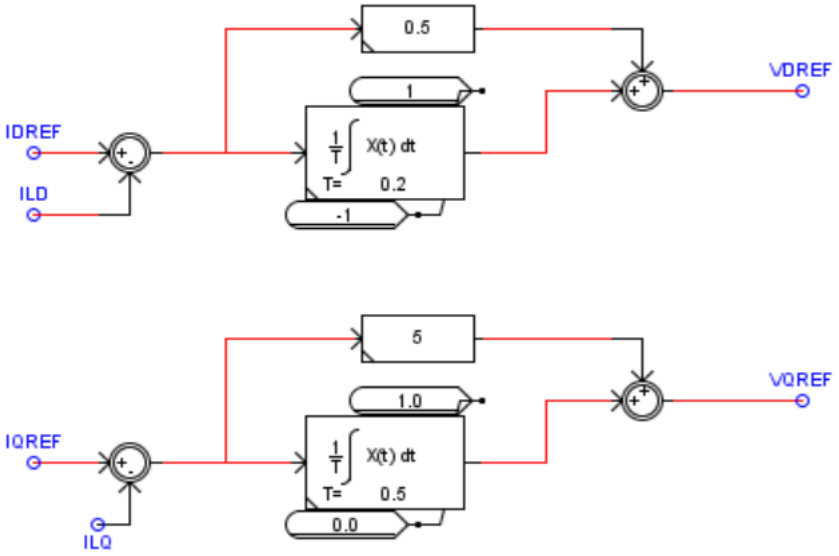

Figure 4.8: Inner current control loop

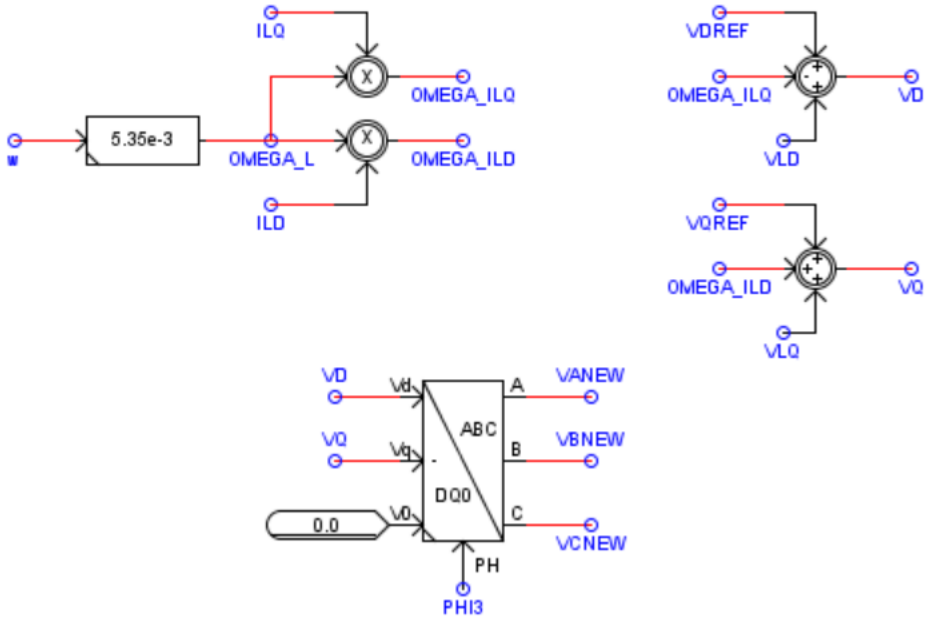

Figure 4.9: Feed forward and cross coupling

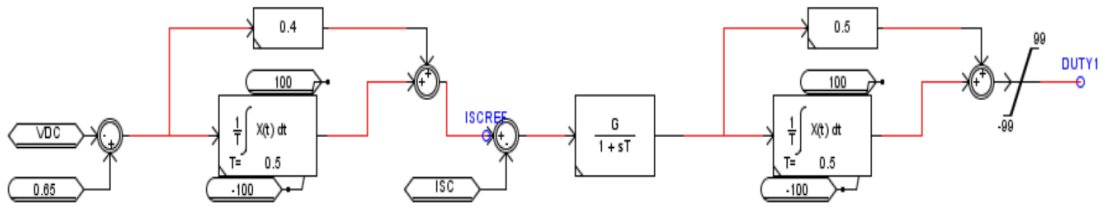

Figure 4.10: Buck boost converter controller

4.4.1 Normal Operation

For normal operation, the power generated from the PV array is directly transferred to the grid. Depending on the irradiation and temperature, the PMC will set the P-Q power set points for the inverter so that it can transfer the power generated directly to the grid. For this case, the irradiation is set at 1000 W/m^2 and the temperature at 25^{o}c that means the PV array is generating 53 kW. The P-Q controller set points are set to 50 kW and 0 var respectively. Only around 3kW is being exchanged between the DC link and the SCESS to compensate for the losses. The applied disturbance and response of the system are presented in Figures. 4.11-4.18. The proposed MPPT controller tracks the maximum voltage from the PV array and maximum power P_{PV} is generated. The P-Q controller for the inverter transfers the 50 kW to the grid as shown in Figure 4.11. Figure 4.12 shows the output of the IC based MPPT controller output voltage V_{ref} and shows how the buck converter controller forces the PV array to track at the maximum voltage V_{MP}. The DC link voltage which is common to both the inverter and the buck boost converter is the duty of the buck converter multiplied by the PV array output voltage V_{PV}. This DC link voltage is kept constant by the buck boost controller with a reference 650 V. The PV

array output power is always V_{PV} x I_{PV} and the P-Q controller transfers V_{DC} * I_{DC} as shown in Figure 4.13. The *D*-axis current component is responsible for real power transfer to the grid and the inverter controller keeps error between the actual and reference *D*-axis current close to 0 as shown in Figure 4.14. The synchronization of the scaled grid voltage and inverter output voltage is shown in Figure 4.15 and the offset is removed by connecting a transformer between the inverter and the grid. The duty cycle of the buck and buck-boost converters are depicted in Figure 4.16 and Figure 4.17 respectively. The firing pulses of the buck-boost converter is shown in Figure 4.18.

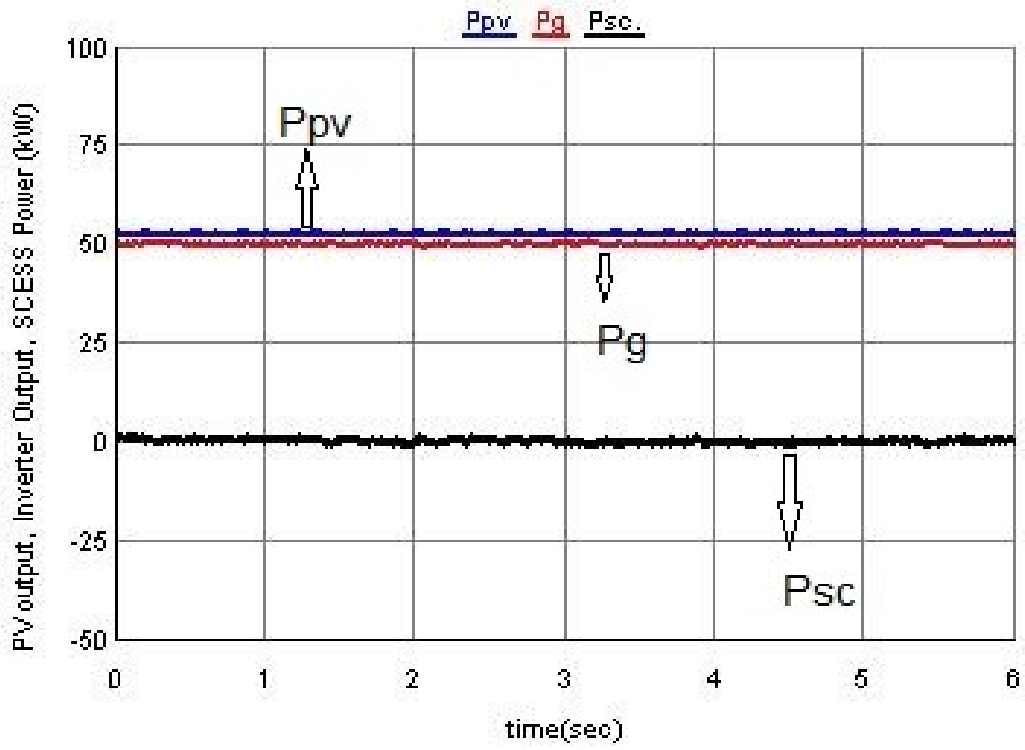

Figure 4.11: PV array output power P_{PV}, inverter output power P_g and supercapacitor power P_{sc}

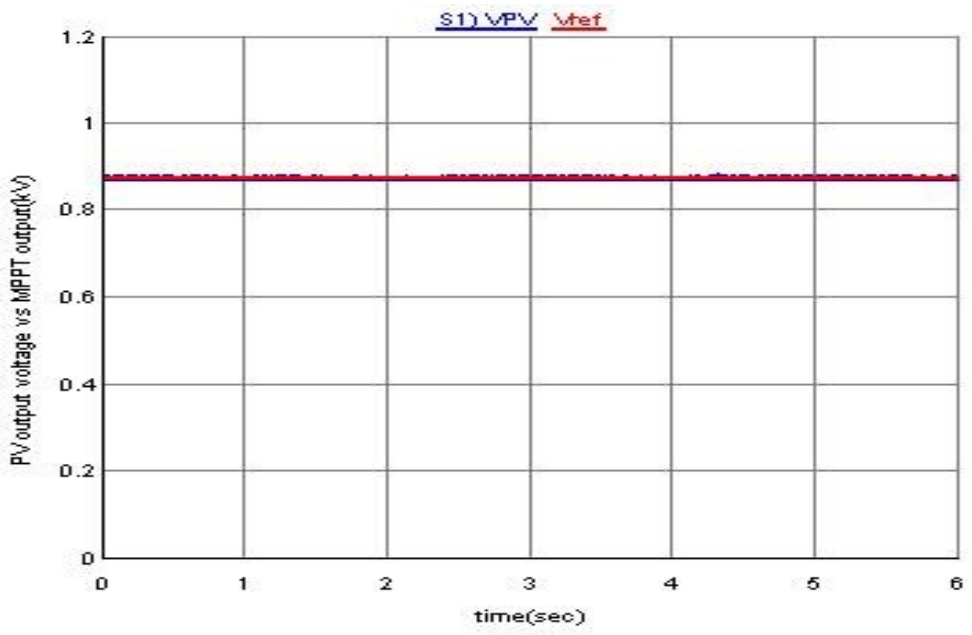

Figure 4.12: PV array output voltage V_{PV} and MPPT output voltage V_{ref}

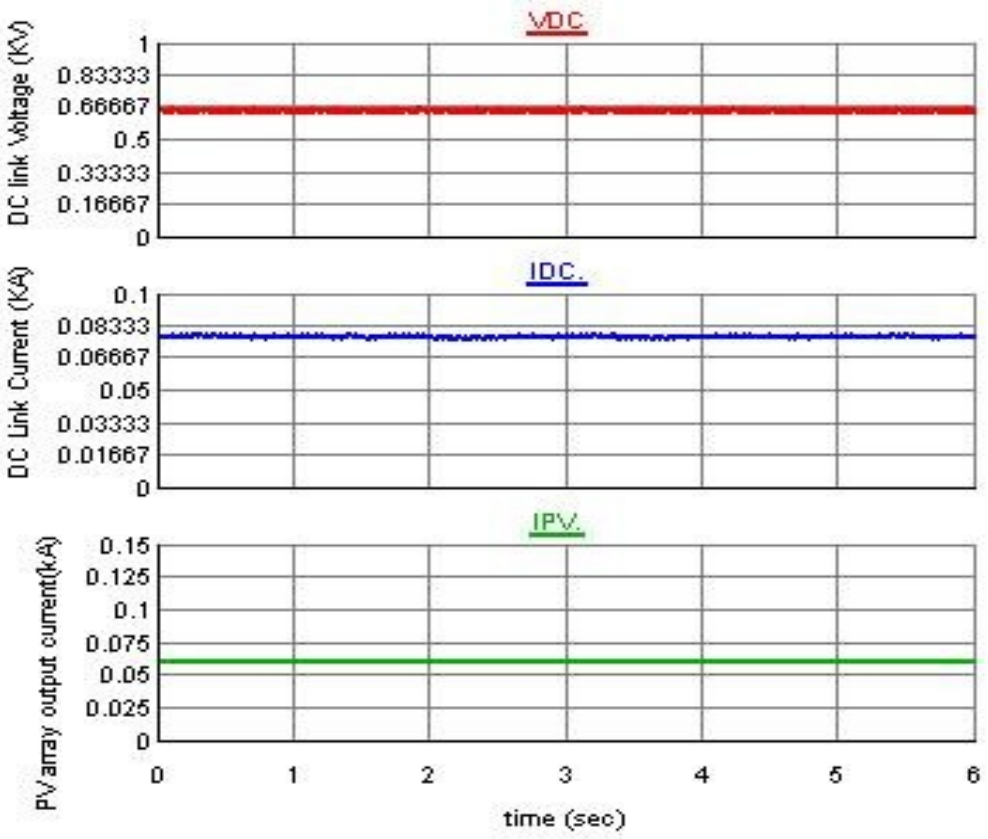

Figure 4.13: DC link voltage V_{DC}, DC link current I_{DC} and PV output current I_{PV}

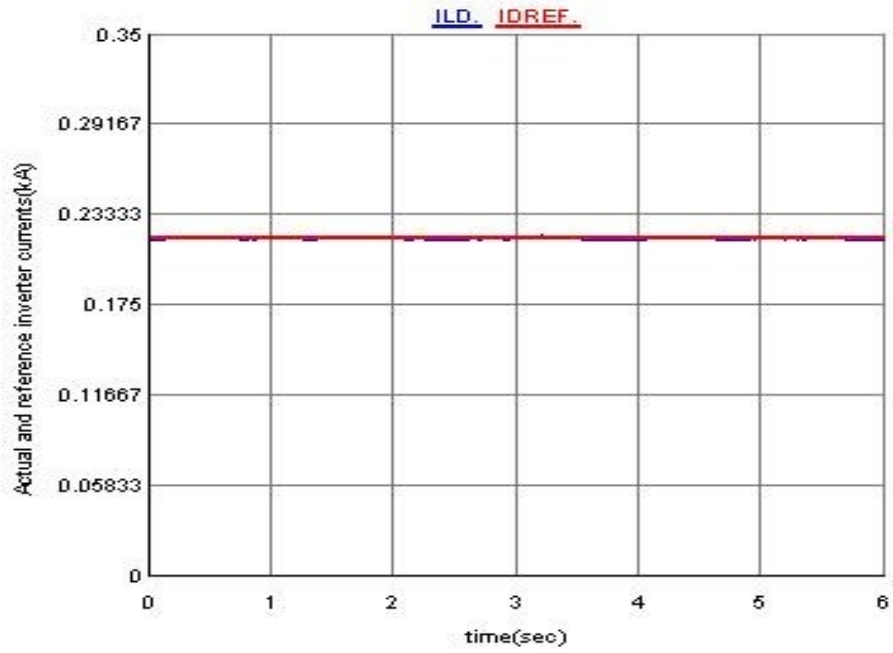

Figure 4.14: Actual I_{LD} and reference I_{DREF} inverter *D*-component inverter current

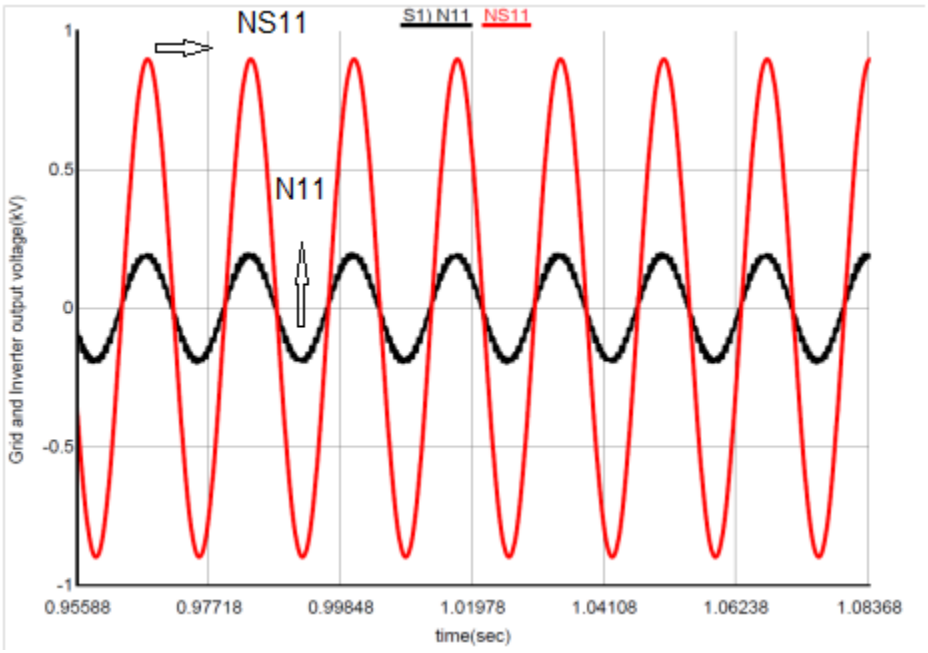

Figure 4.15: Grid *NS11* and inverter *N11* output voltages to show the synchronization

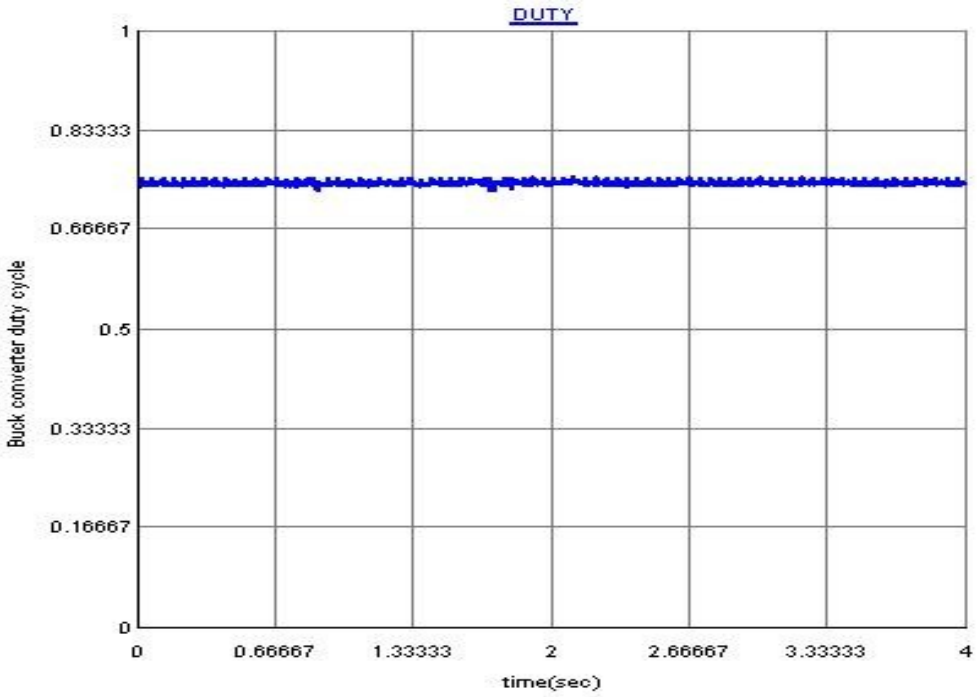

Figure 4.16: Buck converter duty cycle

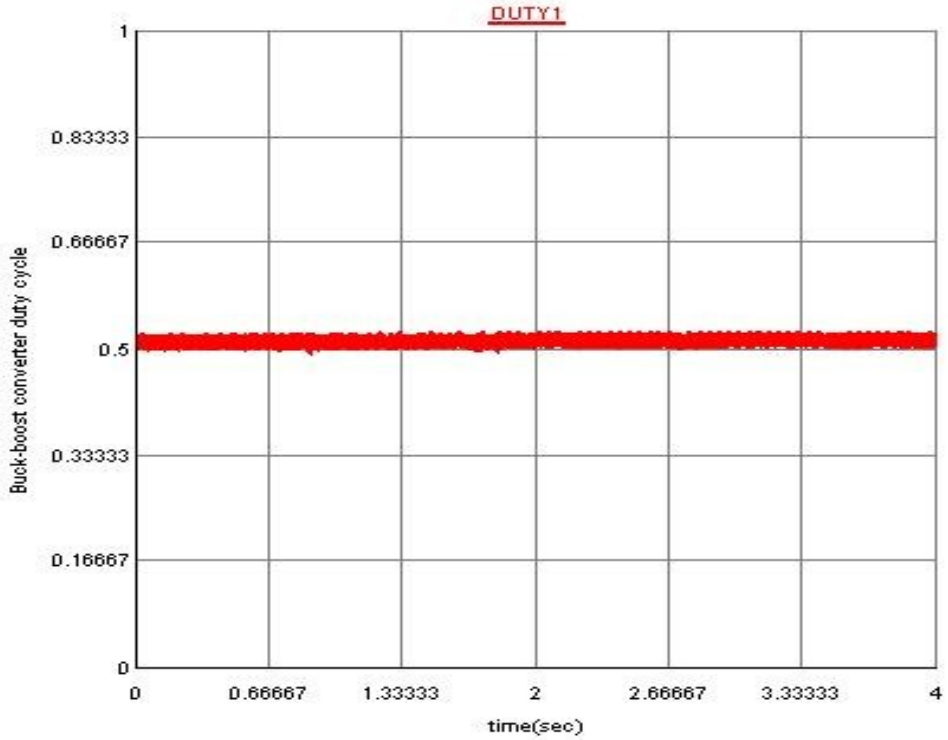

Figure 4.17: Buck-boost converter duty cycle

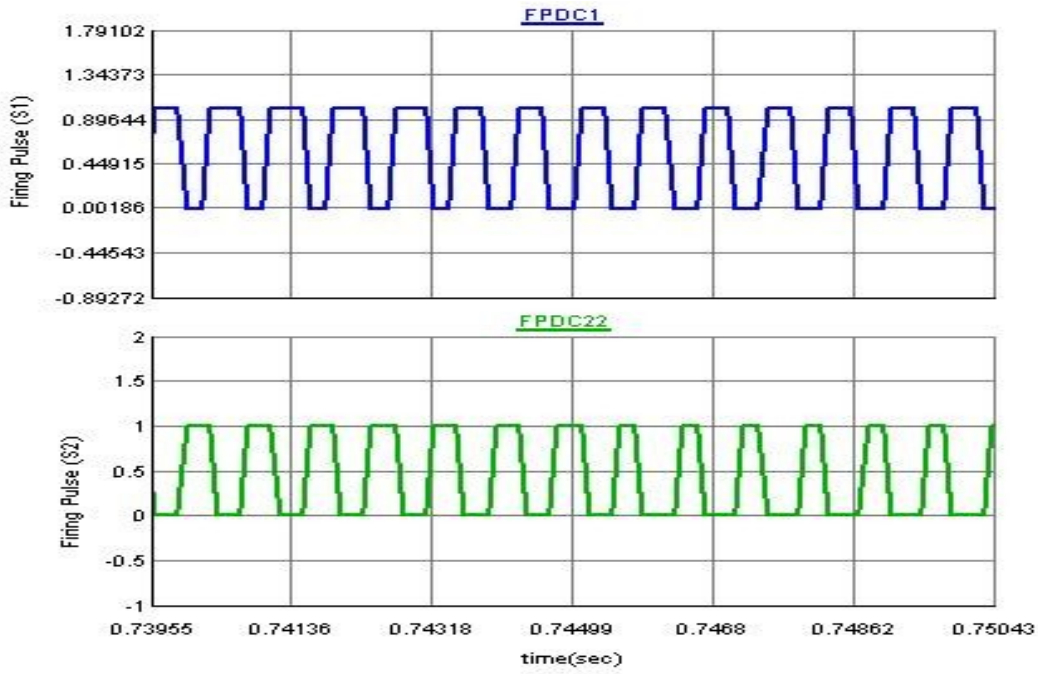

Figure 4.18: Firing pulses for the buck-boost converter

4.4.2 Increase Irradiation and SCESS Charging

When the irradiation increases from the normal operating point, the DC link voltage increases and since the inverter is transferring a constant power to the grid, this excess power goes to the SCESS to charge it for later use. The results for this disturbance are provided from Figures 4.19-4.24. As shown in Figure 4.19 the PV array is generating P_{PV} of around 62 kW and the inverter is transferring 50 kW, P_g, and the excess power is charging the supercapacitor, P_{SC}. To charge the SCESS, the buck boost converter works as buck mode and Figure 4.20 shows the actual and reference inductor current of the SCESS. Similar to the normal operation, the IC based MPPT controller tracks the maximum voltage and hence power from the PV array as depicted in Figure 4.21. For constant power transferred to the grid, V_{DC} and I_{DC} are maintained constant as the normal operation of case *A* but the PV array current varies depending on the irradiation as shown

in Figure 4.22. The duty cycle of the buck and the buck-boost converters are shown in Figure 4.23 and Figure 4.24 respectively.

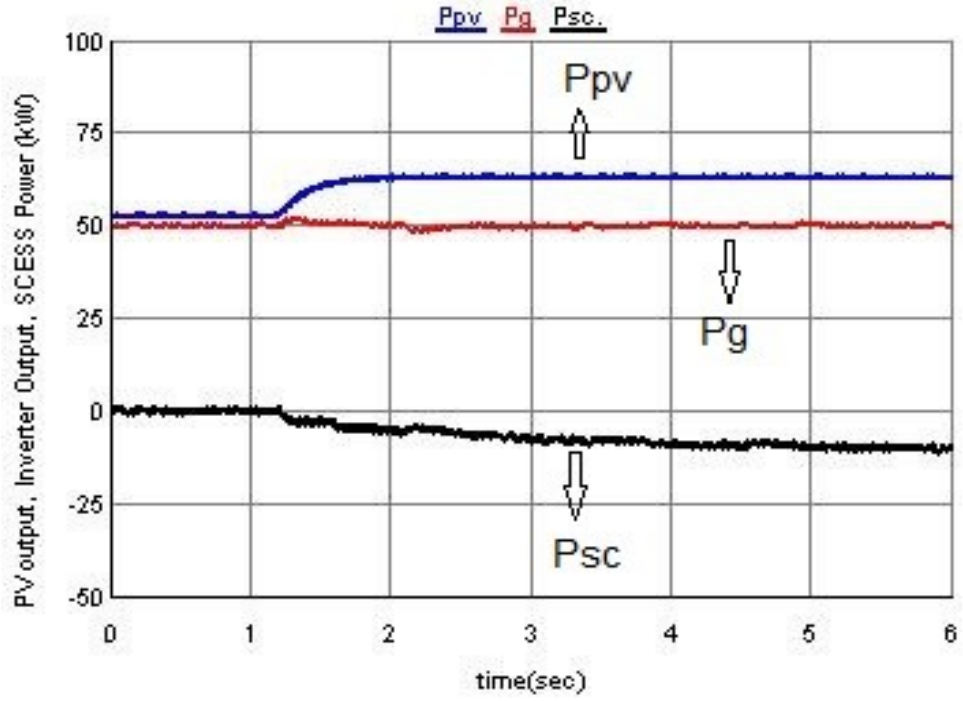

Figure 4.19: PV array output power P_{PV}, inverter output power P_g and supercapacitor power P_{sc}

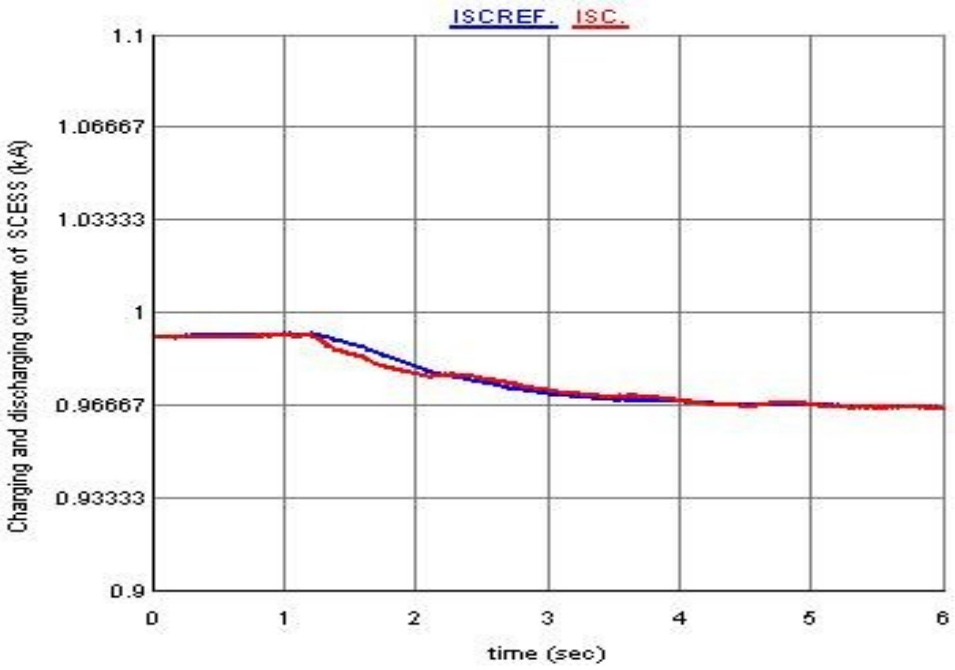

Figure 4.20: Actual I_{SC} and reference I_{SCREF} charging current of the SCESS.

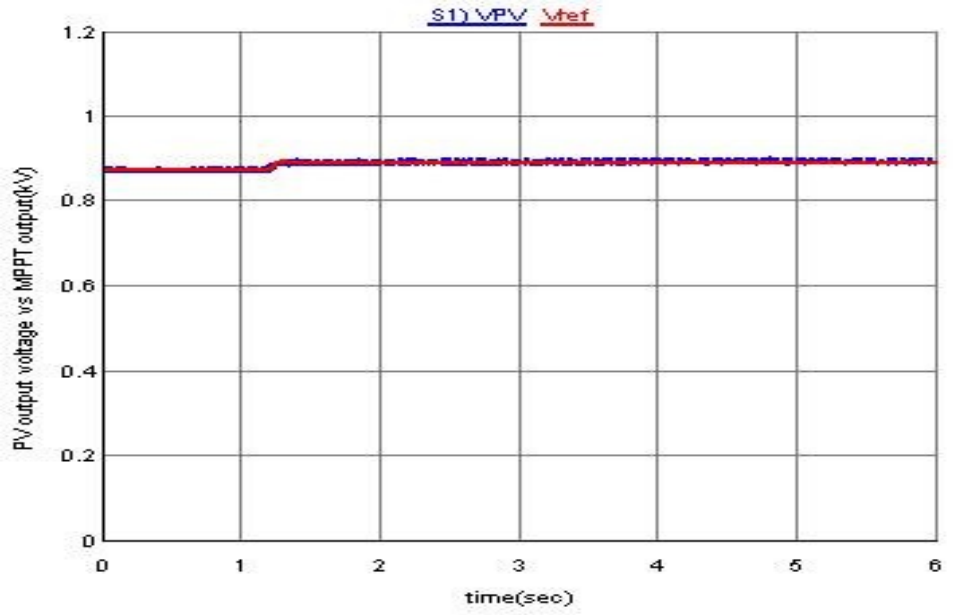

Figure 4.21: PV array output voltage V_{PV} and MPPT output voltage V_{ref}

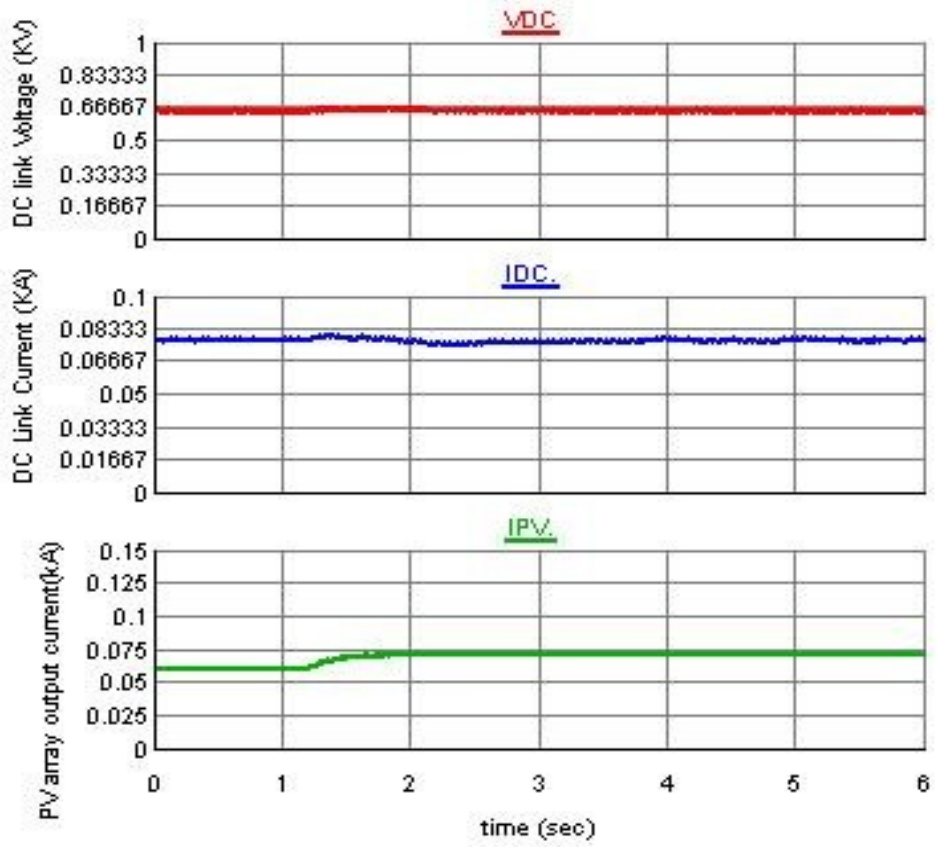

Figure 4.22: DC link voltage V_{DC}, DC link current I_{DC} and PV output current I_{PV}

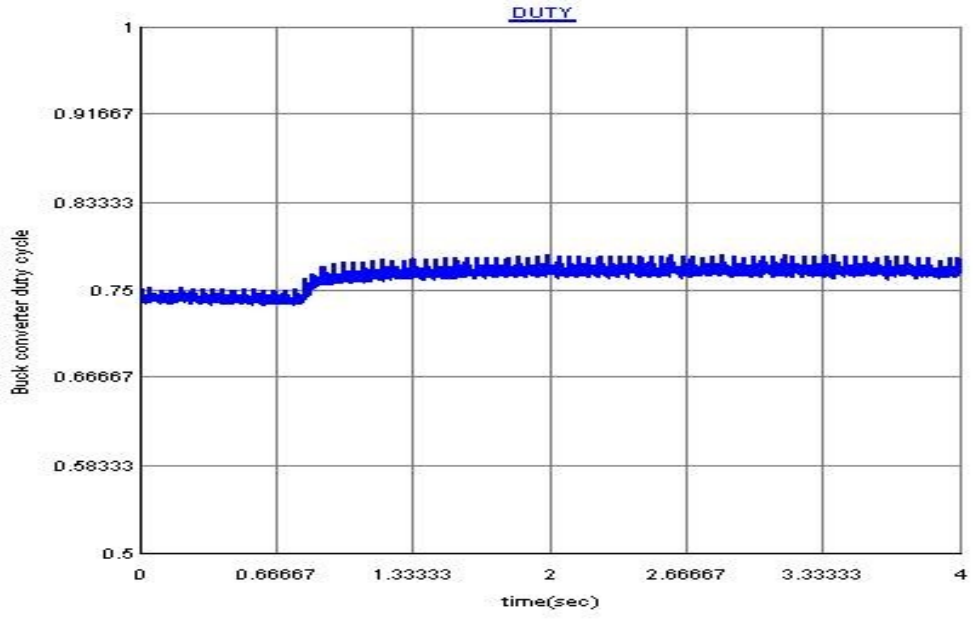

Figure 4.23: Buck converter duty cycle

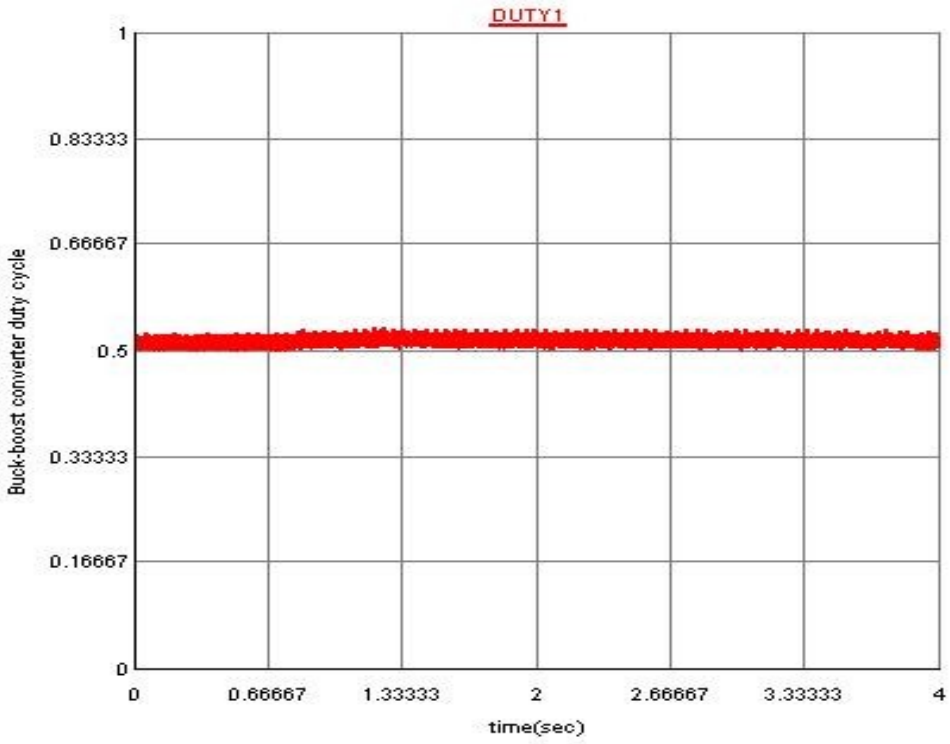

Figure 4.24: Buck-boost converter duty cycle

4.4.3 Irradiation Decrease and Discharging the SCESS

The controller's capability is further tested by applying an irradiation disturbance lower than the normal operating point. With the P-Q controller fixed like the other cases, a step irradiation from 1200 to 800 W/m^2 is applied and the response of the system is presented in Figures 4.25-4.30. The stored power in the SCESS is being utilized now as the irradiation is decreased. As shown in Figure 4.25 the inverter is transferring the constant 50 kW while the PV is generating around 40 kW this means that deficiency power is coming from the stored energy in the SCESS. Since the DC link voltage decreases from the reference value, the buck boost converter works in boost mode by sending a controlled current signal so that this voltage is restored back to its original value as

depicted in Figure 4.26. The IC MPPT controller tracks the maximum power from the PV array as depicted in Figure 4.27. Similar to the previous cases, Figure 4.28 shows the constant controlled DC link power and a varying PV array current I_{PV}. The duty cycle of the buck and buck-boost converters are shown in Figure 4.29 and Figure 4.30 respectively.

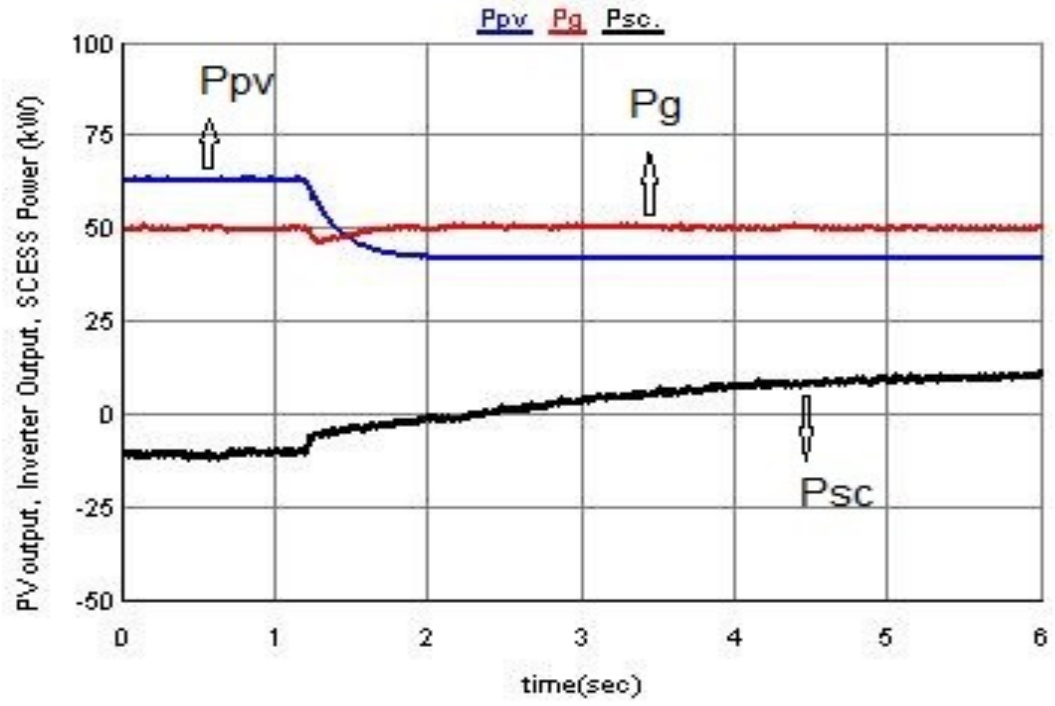

Figure 4.25: PV array output power P_{PV}, inverter output power P_g and supercapacitor power P_{sc}

Figure 4.26: Actual and reference charging current of the SCESS.

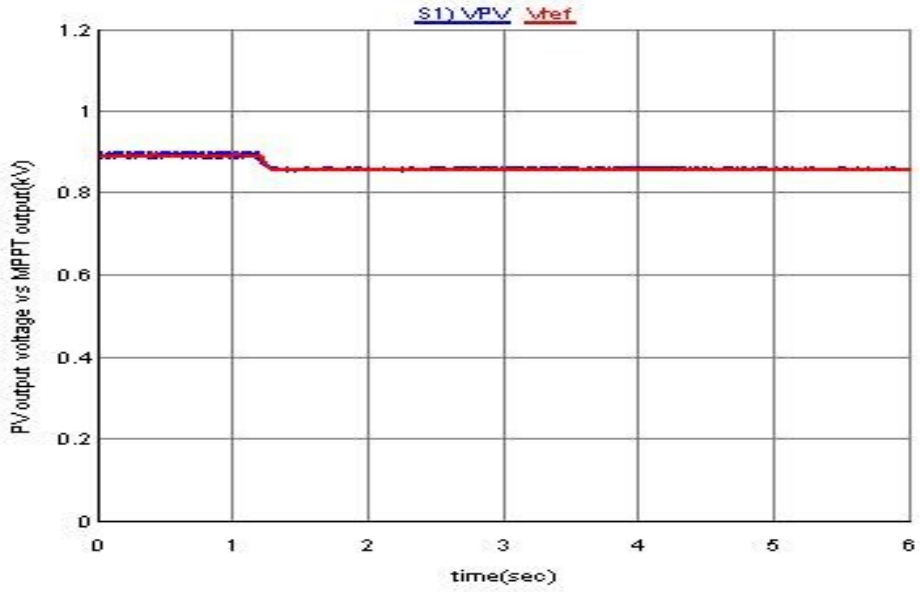

Figure 4.27: PV array output voltage V_{PV} and MPPT output voltage V_{ref}

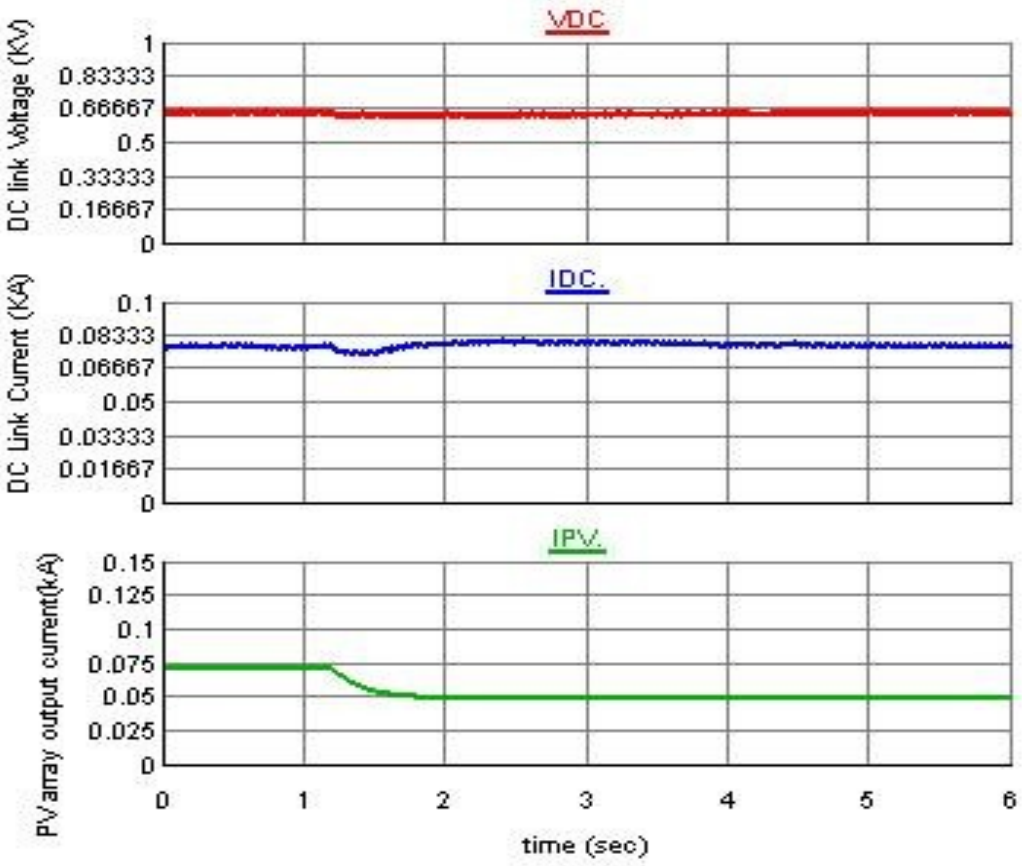

Figure 4.28: DC link voltage V_{DC}, DC link current I_{DC} and PV output current I_{PV}

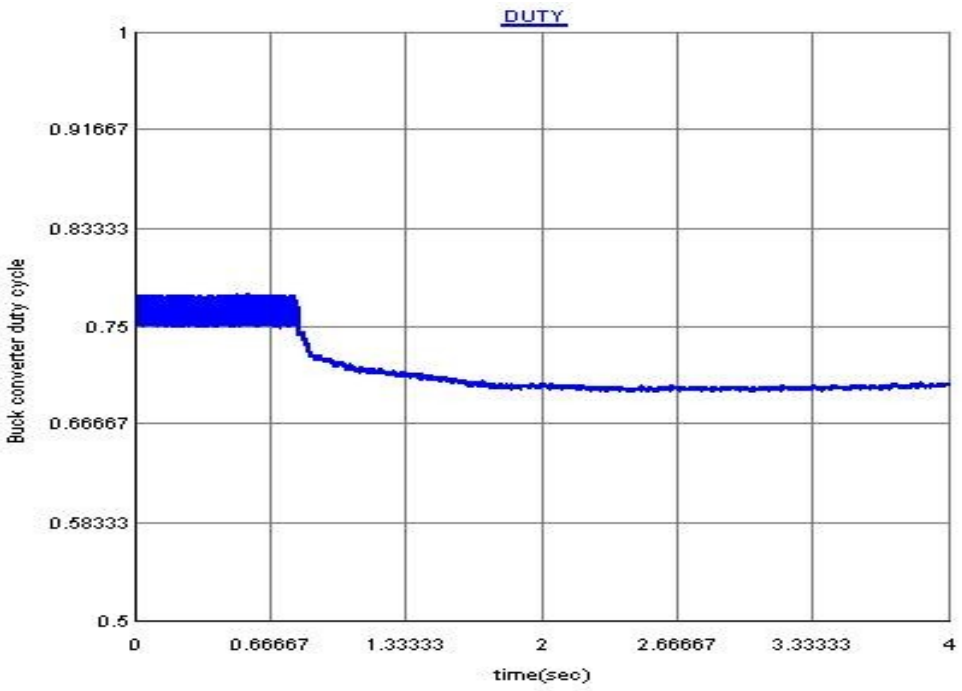

Figure 4.29: Buck converter duty cycle

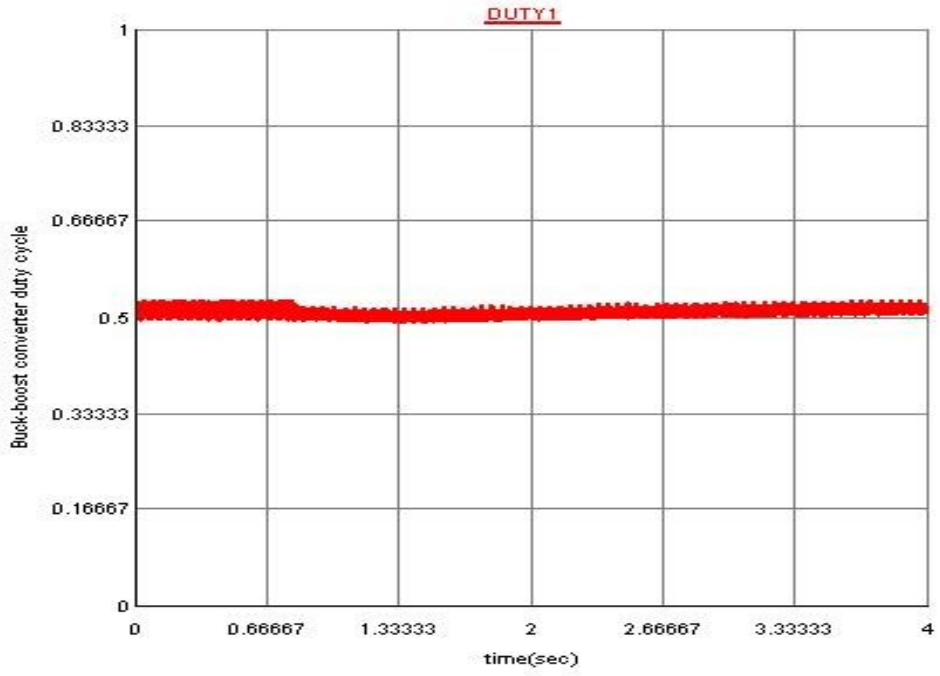

Figure 4.30: Buck-boost converter duty cycle

4.4.4 Trapezoidal Change in Input Irradiation

A scheduled input irradiation shown in Figure 4.31 is applied to the PV array and the response of the system is depicted from Figures 4.32-4.34. The PV array was generating around 53 kW for input irradiation of 1000 W/m^2. The P-Q set points are kept as before and when the irradiation increases the SCESS gets charged and the stored energy is used when the irradiation decreased as shown in Figure 4.32. As previous cases the DC link voltage is kept constant by the buck boost converter controller as shown in Figure 4.33. Figure 4.34 shows the output of the MPPT controller.

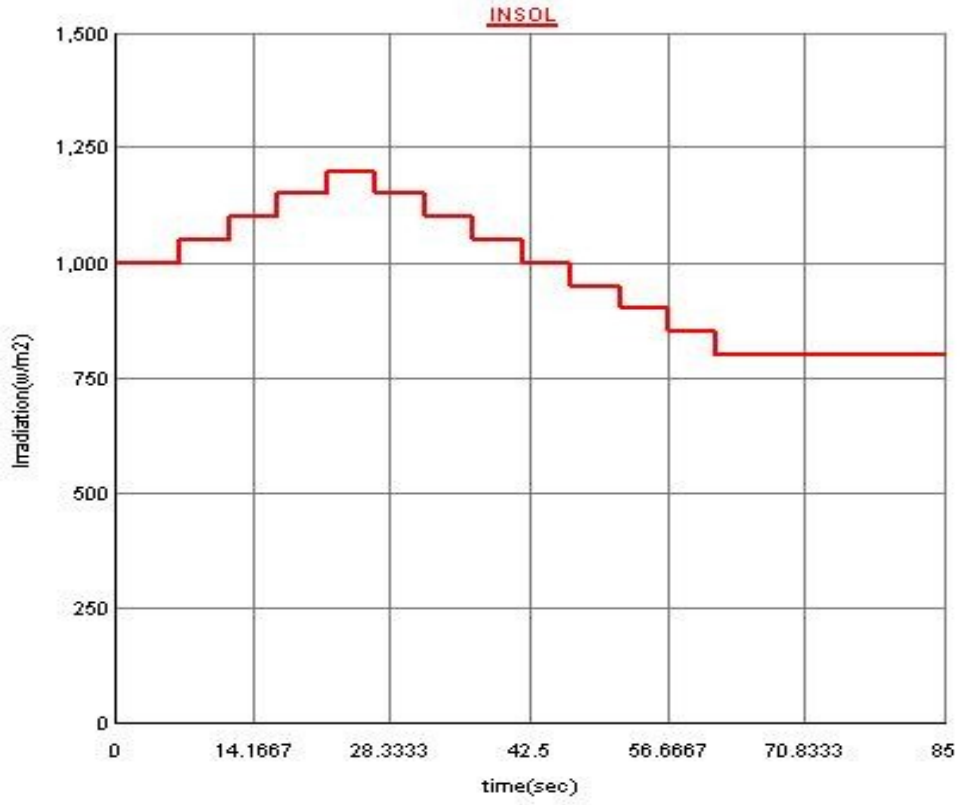

Figure 4.31: Scheduled irradiation input to the PV array

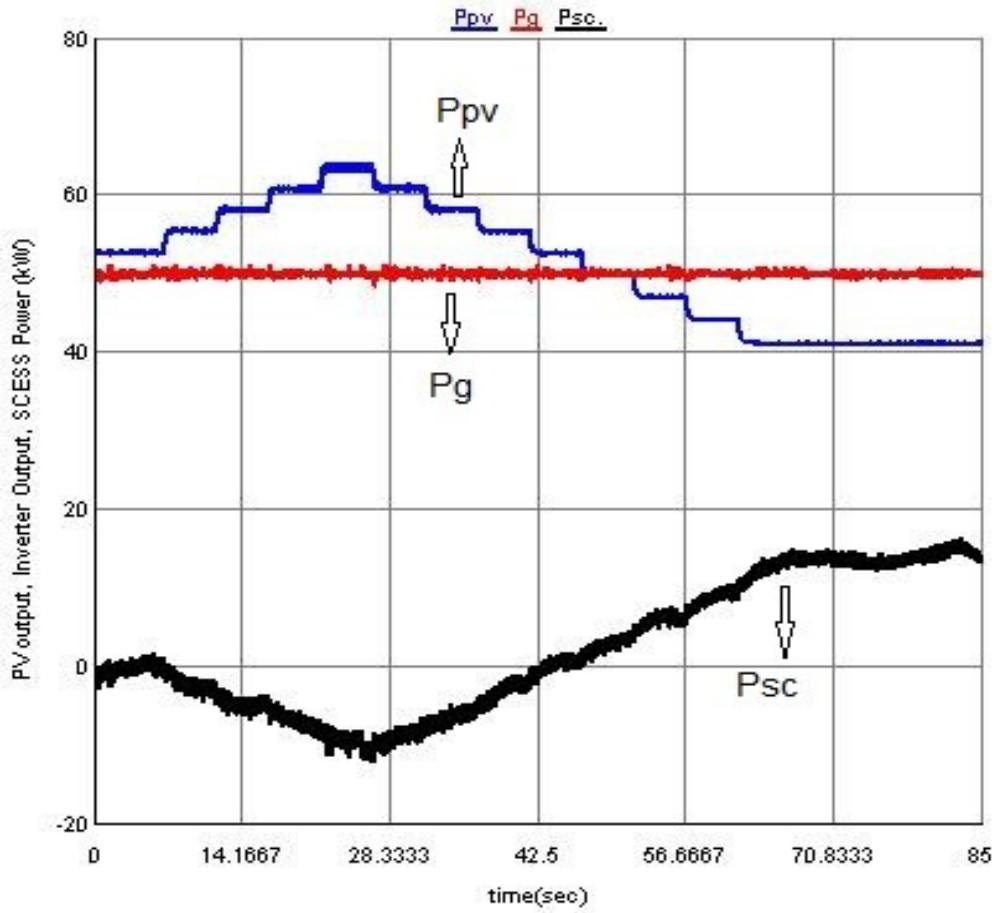

Figure 4.32: PV array output power P_{PV}, inverter output power P_g and supercapacitor power P_{sc}

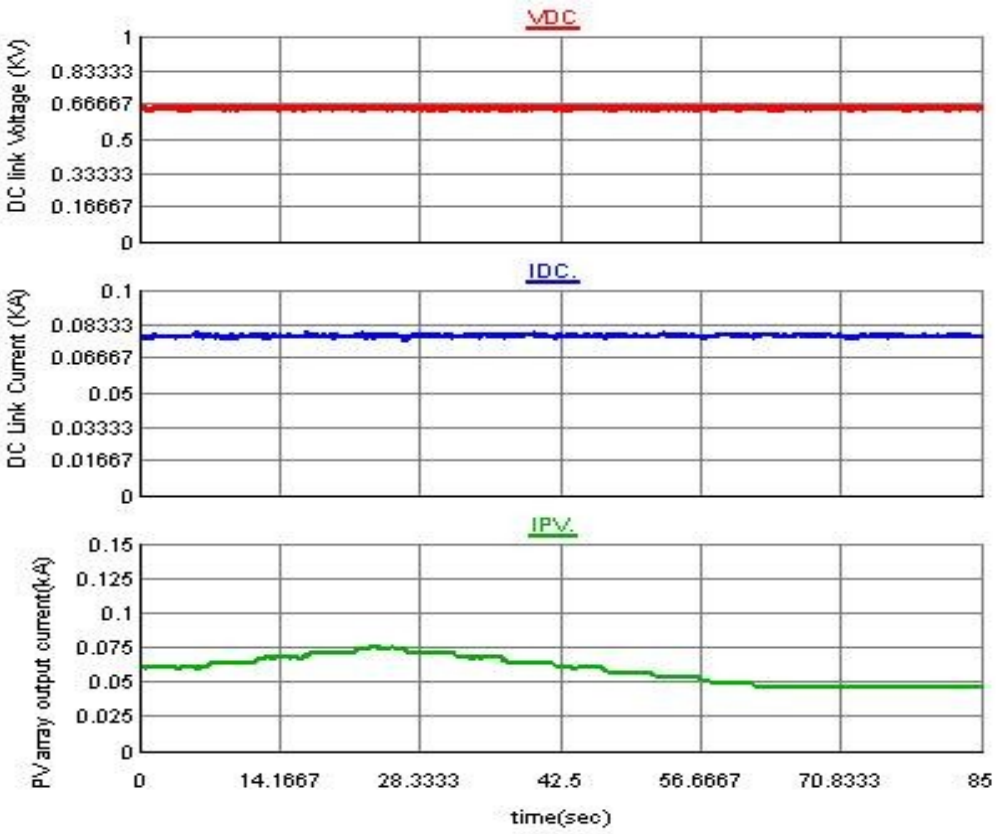

Figure 4.33: DC link voltage V_{DC}, DC link current I_{DC} and PV output current I_{PV}

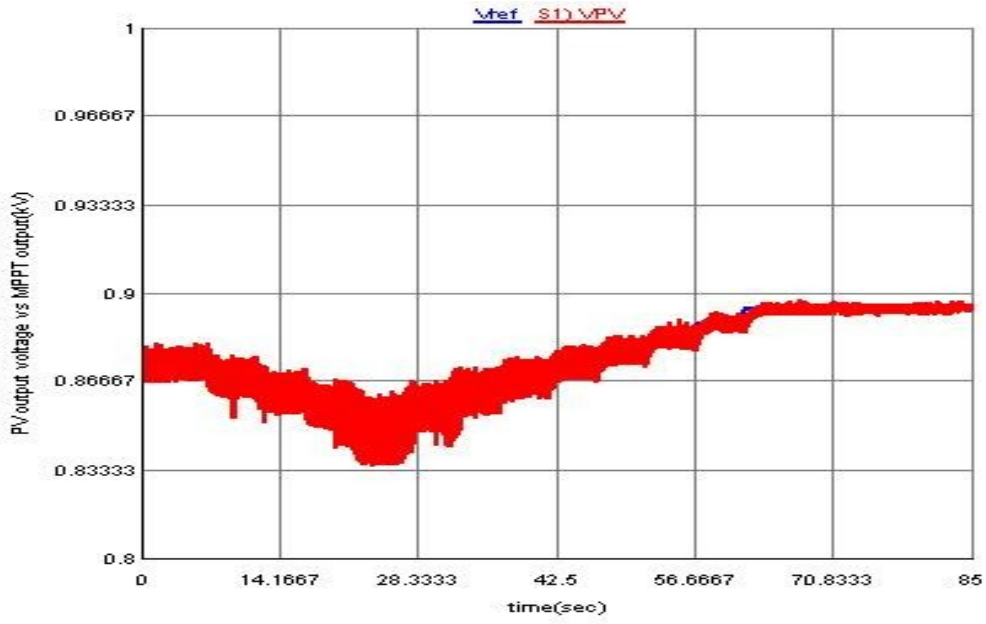

Figure 4.34: PV array output voltage V_{PV} and MPPT output voltage V_{ref}

4.5 CONCLUSION

This chapter presents grid connected PV system with supercapacitor energy storage system to minimize the power fluctuation. A P-Q controller is implemented to transfer the generated power from the PV array to both the grid and the SCESS. The IC based MPPT implemented in RTDS forces the PV array to work at the maximum power. The generated power is connected to the grid using a voltage source converter. The SCESS connected to the DC link is used to store the mismatch power from the PV array and the power demand by DC or AC load set by the power management control. The buck boost converter, which controls the DC link voltage, is used to connect the SCESS to the DC link. RTDS is used to check the validity of the controller and results show that the proposed controller minimizes the fluctuation from PV source that can help PV sources participate in the power markets.

CHAPTER 5 POWER FLUCTUATION MINIMIZATION IN WIND ENERGY USING SUPERCAPACITORS

In this chapter, wind turbine generator system based on permanent magnet synchronous generator equipped with supercapacitor energy storage system is presented. A controller is designed and implemented for the back to back connected three level neutral point clamped converters used to integrate the generated power from the wind to the grid. RTDS based results are provided to verify the controller's capability.

5.1 Introduction

Windmills have been used for many years to harness wind energy for mechanical work such as pumping water. Wind turbines were first used to produce utility power in Denmark during the Second World War. Power generation using wind turbine is becoming the main sources of the world energy market to tackle problems associated with price volatility and carbon impact of fossil fuels. A wind turbine is a machine for converting the kinetic energy in wind into mechanical energy. The working principle of a wind turbine encompasses two main conversion processes. The turbine consists of a rotor that extracts kinetic energy from the wind and converts it into a rotating movement which is then converted into electricity by a generator. Most of the wind turbines are variable speed to get more power from the same wind in comparison with fixed speed wind

turbines. They also mostly use either doubly fed induction generator or synchronous generator.

Variable speed wind turbines using direct drive permanent magnet synchronous generator (PMSG) is getting more attention in wind turbine applications because it is gear box free, does not need field excitation, has full controllability of the system. As compared to double fed induction generator (DFIG) wind turbine, PMSG wind turbine has better efficiency and reliability. The increasing penetration of wind power to the grid forces many countries to adopt and revise grid operating codes for wind farms specifying the fault condition under which a WTG should remain connected to the grid.

One concern of using wind as a power generation unit is that its output power is unpredictable as a result of varying wind speed. To overcome this fluctuation different energy storage devices are integrated to the WTG system. Among these, superconducting magnetic energy storage (SMES) and flywheel are used to minimize the fluctuation. Because of their high energy and power densities battery and supercapacitor energy storage system (SCESS) are commonly used [146].

PMSG based variable speed wind energy conversion system is depicted in Figure 5.1. The horizontal axis variable-speed wind turbine directly drives the rotor of a PMSG through a gearless drive train. Field excitation to the generator is obtained through permanent magnets mounted on the generator rotor. The PMSG based wind turbine generator (WTG) is connected to the grid using a fully controlled power converter system, a bidirectional buck boost converter, step-up transformer, and harmonic filter. To minimize the fluctuation and to ride through the fault, supercapacitor energy storage

system (SCESS) is connected to the DC link using a bidirectional buck boost converter. The power converter system comprises of two three-level neutral- point-clamped (NPC) back to back connected voltage source-converters (VSC). In the NPC the DC link capacitor split to form a zero neutral point. The maximum power from the wind turbine is tracked by adjusting the generator rotor speed controlled by the machine side converter (MSC). The other function of the MSC controller is to minimize the generator loss. The grid side converter (GSC) controls the active and reactive power flow to the grid. The buck boost converter keeps the DC link voltage to a constant value so that the GSC delivers the required power to the grid. By proper control of the buck boost converter, charging and discharging of the SCESS is achieved. Vector control is employed on the back-to-back connected NPCs in synchronously rotating reference frames.

In Figure 5.1,

P_{WT} : is power output of wind turbine,

P_M : is PMSG power output,

P_{DC} : is DC link power,

P_{SC} : is SCESS power,

P_{PCC} : is the PCC power,

P_G : is Power delivered to the gird and

T_r : is the step-up transformer.

m_d : is the d-axis machine side converter (MSC) modulation index

m_q : is the *q*-axis machine side converter (MSC) modulation index

m_{id} : is the *d*-axis grid side converter (GSC) modulation index

m_{iq} : is the *q*-axis grid side converter (GSC) modulation index

I_G : GSC output current

I : PMSG stator output current

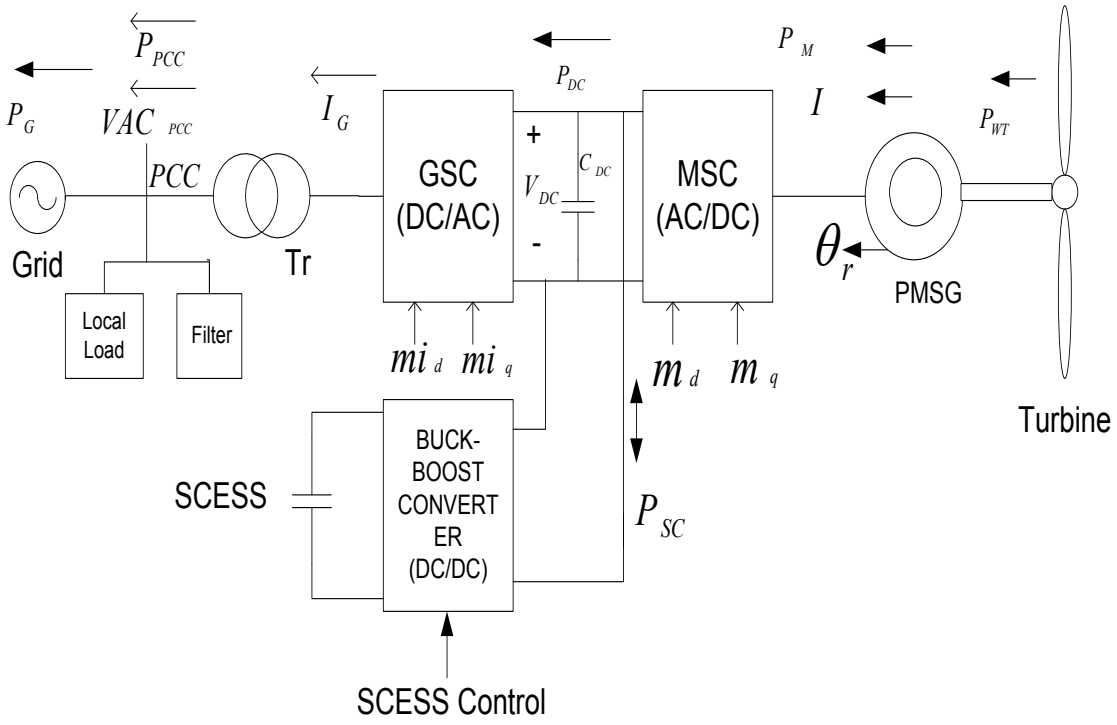

Figure 5.1: Grid connected variable speed wind energy conversion system using PMSG

5.2 Power in the Wind and Wind Turbine Model

Wind turbines convert the kinetic energy present in the wind into mechanical energy by means of producing torque and it is characterized by its power-speed characteristics. Since the energy contained by the wind is in the form of kinetic energy, its magnitude

depends on the air density and the wind velocity. The amount of power P_{WT} and torque T_{WT} a horizontal axis wind turbine capable of producing is given by:

$$P_{WT} = \frac{1}{2} C_p(\beta, \lambda) \rho A V^3 \tag{5.1}$$

$$T_{WT} = \frac{1}{2W_t} C_p(\beta, \lambda) \rho A V^3 \tag{5.2}$$

where,

ρ : is the density of the air in kg/m^3,

A : is the exposed area in m^2,

V : is the wind velocity in m/s,

W_t : is the turbine rotational speed (which is equal to w_r for gear less drive),

C_p : is the power coefficient,

β : is the pitch angle.

The tip speed ratio λ is defined as:

$$\lambda = \frac{W_t R_t}{V} \tag{5.3}$$

where,

R_t : is the turbine radius

C_p which is a nonlinear function of λ and β is given by:

$$C_p(\beta, \lambda) = 0.5176\left(\frac{116}{\lambda_i} - 0.4\beta - 5\right) e^{\frac{-21}{\lambda_i}} + 0.00668\lambda$$
$$\frac{1}{\lambda_i} = \frac{1}{\lambda + 0.08\beta} - \frac{0.035}{\beta^3 + 1} \tag{5.4}$$

A typical relationship between C_p and λ is shown in Figure 5.2. It is clear from this figure that there is a value of λ for which C_p is maximized thus maximizing the power for a given wind speed.

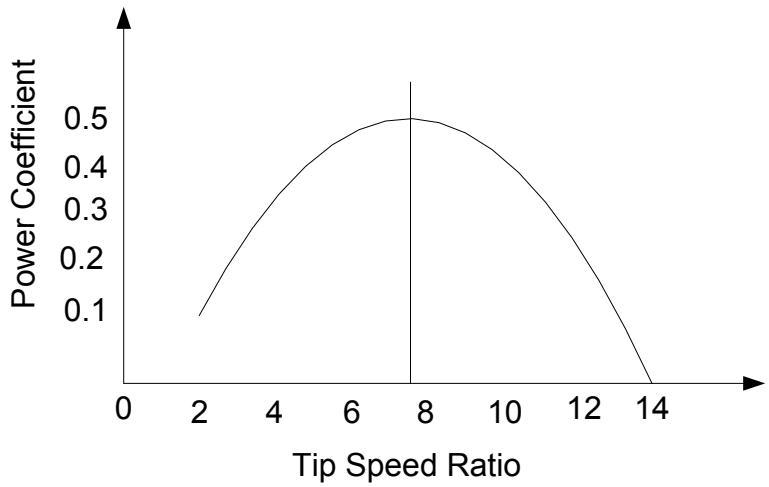

Figure 5.2: C_p vs λ Characteristics for 0 Pitch Angle

Because of the relationship between C_p and λ, as the turbine speed changes for a given wind velocity there is a turbine speed that gives a maximum output power. This is shown in Figure 5.3 for various wind speeds. As seen in the figure the peak power for each wind speed occurs at the point where C_p is maximized. The prime motivation for variable speed control of wind energy conversion system is to track the rotor speed with changing wind velocity that is always maintained at its maximum C_p value. To maximize the power generated it is therefore desirable for the generator to have a power characteristic that will follow the maximum C_p line.

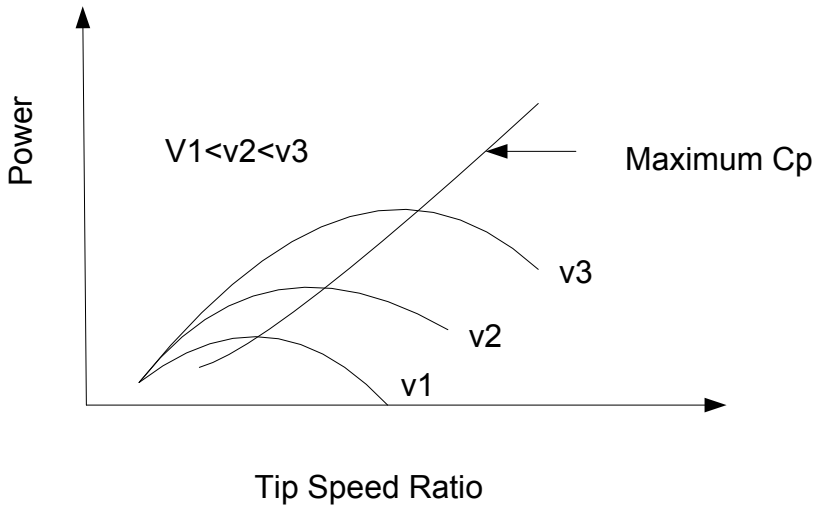

Figure 5.3: Typical turbine power relationship for various wind speeds

The drive train system of wind energy conversion system to be used in this study includes a two mass model as shown in Figure 5.4. The wind turbine constituting a greater mass having inertia of H_t connects the PMSG rotor with inertia of H_g. A mechanical shaft with a stiffness coefficient of K_s is used to couple the two masses. The damping coefficients for the turbine and generator are taken as D_t and D_g respectively.

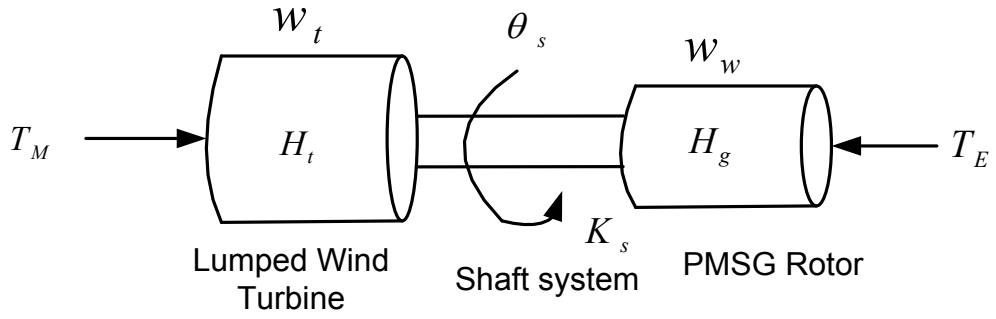

Figure 5.4: Two mass model of drive train

Four first order nonlinear ordinary differential equations describe the electromechanical dynamics of the drive train system in terms of the torsional angle θ_s, the turbine speed W_t, the PMSG rotor angle δ_w and the PMSG rotor speed W_w as:

$$\frac{d\theta_s}{dt} = w_0(w_t - w_w) \tag{5.5}$$

$$\frac{dw_t}{dt} = \frac{1}{2H_t}(P_{mw} - K_s\theta_s - D_t(w_t - 1) \tag{5.6}$$

$$\frac{d\delta_w}{dt} = w_0(w_w - 1) \tag{5.7}$$

$$\frac{dw_w}{dt} = \frac{1}{2H_g}(K_s\theta_s - P_{ew} - D_g(w_w - 1) \tag{5.8}$$

There is a range of methods for controlling aerodynamic forces on the turbine rotor and therefore limiting the peak power output of a turbine. The simplest is passive stall control in which the design of rotor aerodynamics causes the rotor to stall (loose power) when the wind velocities exceed a certain value. Other methods include yawing, in which the rotor is turned out of alignment with the wind by some mechanical device, when a given wind speed is exceeded. The most sophisticated method is active aerodynamic control, such as flaps or full span pitch control. The latter can be implemented as an emergency control method that only feathers the blades in an over speed condition. Alternatively, it can be a highly active method for starting the rotor and controlling power output over a wide range of wind speeds.

5.2.1 Pitch Control

The aerodynamic model of the wind turbine has shown that the aerodynamic efficiency is strongly influenced by variation of the blade pitch with respect to the direction of the wind or to the plane of rotation. Small changes in pitch angle can have a dramatic effect on the power output. In low to moderate wind speeds, the turbine should simply try to produce as much power as possible, so there is generally no need to vary the pitch angle. The pitch angle should only be at its optimum value to produce maximum power. In high wind speeds, pitch control provides a very effective means of regulating the aerodynamic power and loads produced by the rotor so that design limits are not exceeded. Figure 5.5 shows the relationship between C_p and λ for different values of pitch angle.

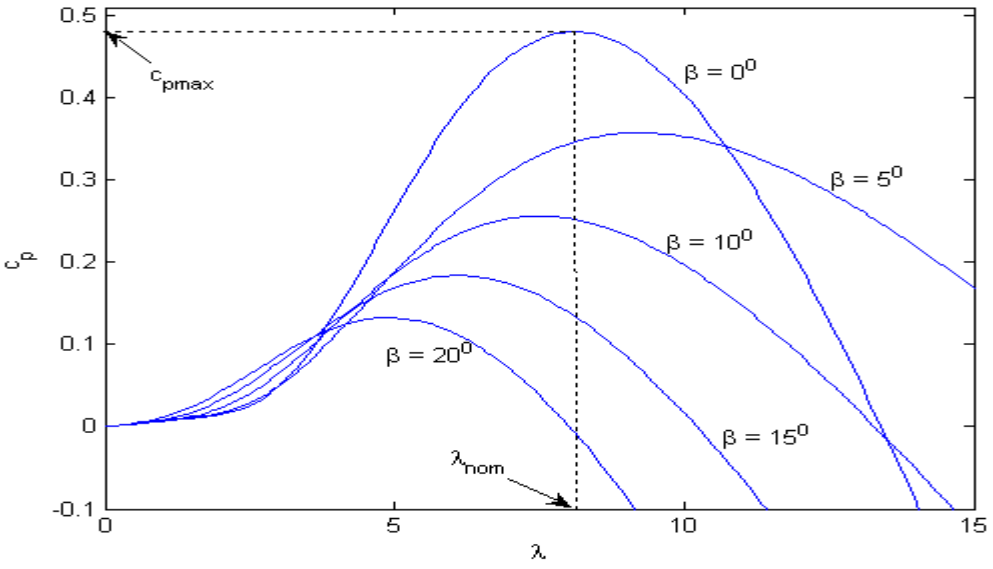

Figure 5.5: C_p vs λ characteristics for different value of pitch angle

5.3 The Permanent Magnet Synchronous Generator (PMSG)

PMSG is modeled as an interior magnet machine with sinusoidally distributed windings. By ignoring the damper windings, the machine is modeled in the rotor aligned synchronously rotating *dq* reference frame as:

$$\frac{1}{2} m_d V_{DC} = RI_d + (L_{Md} + L_{LS}) \frac{dI_d}{dt} - w_r (L_{Mq} + L_{LS}) I_q \tag{5.9}$$

$$\frac{1}{2} m_q V_{DC} = RI_q + (L_{Mq} + L_{LS}) \frac{dI_q}{dt} - w_r (L_{Md} + L_{LS}) I_d + w_r \psi_f \tag{5.10}$$

$$\frac{dw_r}{dt} = \frac{P}{2J} (T_{WT} - 1.5 \frac{P}{2} ((L_{Md} - L_{Mq}) I_d + \psi_f) I_q \tag{5.11}$$

where,

d and q : are direct and quadrature components,

m : is the MSC modulation index,

V_{DC} : is the DC link voltage,

L_{Md}, L_{Mq} : are mutual inductances,

R : is the stator resistance

L_{LS} : is the stator leakage inductance,

ψ_f : is the permanent magnet flux,

I : is the PMSG stator current,

P : is the number of machine poles,

w_r : is the rotor electrical speed,

J : is moment of inertia of turbine and rotor,

T_{WT} : is the mechanical turbine torque.

Developed torque has two components: The first component is the component due to field flux, and the other component is due to reluctance torque. The general expression is

$$T_e = 1.5(\hat{\psi}_f I_q + (L_{Md} - L_{Mq}) I_d I_q \quad (5.12)$$

where,

$\hat{\psi}_f = \sqrt{2}\psi_f$ is the peak permanent flux, and

T_e is the developed torque.

For an interior magnet machine

$$L_{Mq} > L_{Md} \quad (5.13)$$

Which means I_d reduces the overall electrical torque. Also if saliency is neglected, the torque expression in equation (5.12) reduces to

$$T_e = 1.5(\hat{\psi}_f I_q) \quad (5.14)$$

In this case, torque is a function of quadrature axis stator current I_q alone.

5.4 Machine Side Converter (MSC) and Its Controller

To generate the maximum available power from continually varying wind speed, the generator rotor speed is optimally adjusted by the machine side converter controller. One of the primary functions of the MSC is to control stator current so that it is 180 degrees out of phase with the stator voltage in order to maximize PMSG efficiency. The torque or *q* axis component of stator current is maintained to match the power requirements of the wind turbine. By measuring the power produced by the wind turbine over a range of wind speeds, an optimum rotor speed w_{ropt}, versus power relationship can be derived. The I_q

current or torque reference can then be created from the measured power by regulating the rotor speed.

The *d* axis component controls the armature reaction flux and is varied to keep the reactive power at a minimum as long as the power output of the machine is 1 per unit or less. The *d* axis current contributes to the magnetizing flux and as the torque increase from zero to rated, both I_d and I_q increase. The reference for the *d* axis current is stored in a function (y = f(x) component), where the output is a function of machine speed. This function is derived by reducing the reactive power output from the PMSG to approximately zero, thus minimizing losses. The content of the function are approximated in Figure 5.6. The control signals m_d and m_q in Laplace domain for the MSC are shown in Figure 5.7 and are given by:

$$m_d = (I_{dREF} - I_d)(K_{p2d} + \frac{K_{I2d}}{s}) - w_r I_q (L_{Mq} + L_{LS}) \tag{5.15}$$

$$m_q = [(w_{ropt} - w_r)(K_{p1q} + \frac{K_{I1q}}{s}) - I_q)](K_{p2q} + \frac{K_{I2q}}{s}) + w_r I_d (L_{Mq} + L_{LS}) \tag{5.16}$$

where,

K_{p2d} and K_{I2d} : are *d*-axis proportional and integral constants of the PI regulator

K_{p1q} and K_{I1q} : are the *q*-axis outer loop proportional and integral constants of the PI regulator.

K_{p2q} and K_{I2q} : are the *q*-axis inner loop proportional and integral constants of PI regulator.

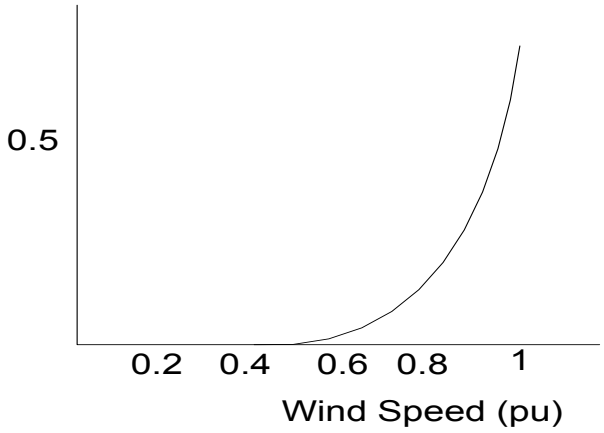

Figure 5.6: Look up table for I_{dREF} generation

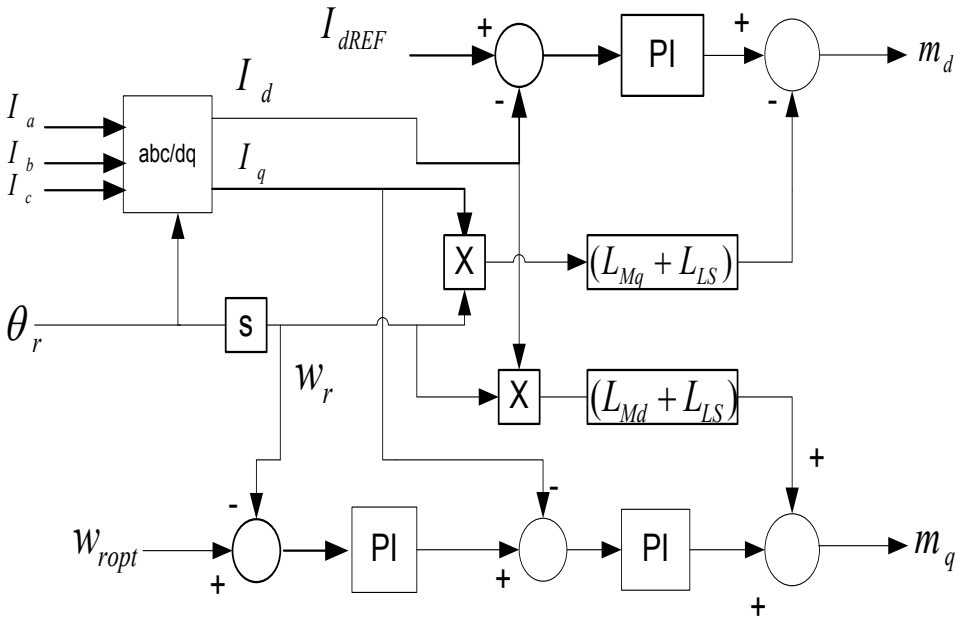

Figure 5.7: Machine side converter controller

5.5 Grid Side Converter (GSC) Controller

The function of the grid side converter (GSC) is to control the active and reactive power exchanged between the PCC and the main grid. Using a synchronously rotating dq reference frame with the PCC ac voltage vector (V_{ACPCC}), the equations describing the GSC and PCC are:

$$\frac{1}{2} m_{id} V_{DC} = VAC_{PCCd} + R_C I_{Gd} - wL_T I_{Gq} + L_T \frac{dI_{Gd}}{dt} \tag{5.17}$$

$$\frac{1}{2} m_{iq} V_{DC} = VAC_{PCCq} + R_C I_{Gd} + wL_T I_{Gd} + L_T \frac{dI_{Gq}}{dt} \tag{5.18}$$

$$P_{PCC} = \frac{3}{2}(VAC_{PCCd} I_{Gd} + VAC_{PCCq} I_{Gq}) \tag{5.19}$$

$$Q_{PCC} = \frac{3}{2}(VAC_{PCCq} I_{Gd} - VAC_{PCCd} I_{Gq}) \tag{5.20}$$

where,

m_i : is the GSC modulation index,

L_T : is transformer leakage inductance,

R_C : is to represent converter losses,

I_G : is GSC ac current,

w : is the grid frequency,

P_{PCC} and Q_{PCC} : are the active and reactive power at the PCC.

A phase locked loop (PLL) is implemented to track the grid frequency ($\omega=2\pi f$) and phase angle Θ that will be used for *abc* to *dq* conversion. The control scheme for the GSC P-Q controller is shown in Figure 5.8. Since the *d* and *q* components are coupled, cross-coupling term and feed forward voltage are used to improve the performance of the PI current controllers. The reference grid power P_{GREF} is determined by the power management control depending on the grid power or AC load demand.

The *d*-axis component control signal in the Laplace domain is:

$$mi_d = [(P_{GREF} - P_{PCC})(K_{P3d} + \frac{K_{I3d}}{s}) - I_{Gd})](K_{P4d} + \frac{K_{I4d}}{s}) + VAC_{PCCd} - \omega L_T I_{Gq} \quad (5.21)$$

And *q*-axis component control signal in the Laplace domain is:

$$mi_q = (K_{P4q} + \frac{K_{I4q}}{s})(I_{GqREF} - I_{Gq}) + VAC_{PCCq} + \omega L_T I_{Gd} \quad (5.22)$$

where,

K_{p3d} and K_{I3d} : are *d*-axis outer proportional and integral constants of the PI regulator

K_{p4d} and K_{I4d} : are the *d*-axis inner loop proportional and integral constants of the PI regulator.

K_{p4q} and K_{I4q} : are the *q*-axis proportional and integral constants of PI regulator.

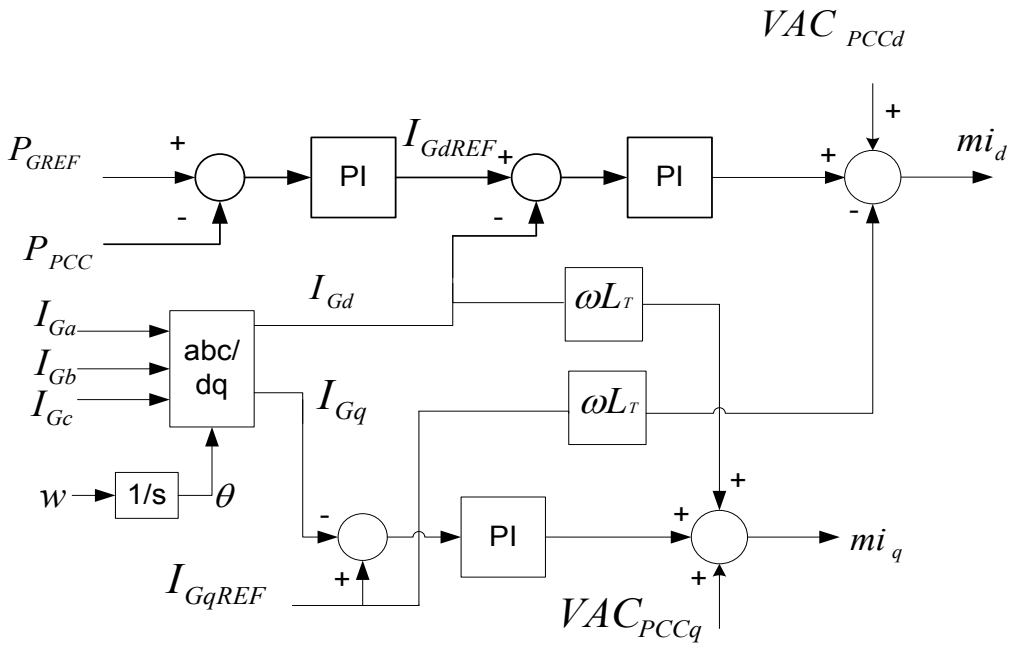

Figure 5.8: Grid side converter vector control

5.6 Buck Boost Converter Controller

The function of the buck-boost converter is similar to the one used in chapter four. The designs of the converter and controller parameters are obtained using the same procedure and will not be discussed in this chapter.

5.7 RTDS BASED RESULTS AND DISCUSSION

A variable speed direct driven permanently excited 4kV, 22 pole, 60Hz, 2MW wind turbine generator has been modeled in RTDS as shown in Figure 5.9. The parameters of the PMSG and other system parameters are tabulated in Table 5.1. The interfacing transformer is a 2.5 MVA 4kV/33 kV. The system is working at rated speed of 12 m/s

and is generating the rated 2 MW power. Both the GSC and the MSC are voltage source converters (VSC) and are Neutral Point Clamped (NPC) three level types joined together back to back on the DC link side through small reactors. The buck-boost converter controller built in RTDS is shown in Figure 5.10. The GSC controller and the abc/dq conversion of this converter are depicted in Figure 5.11 and 5.12 respectively. The MSC controller built in RTDS is presented in Figure 5.13.

Table 5.1: Parameter of a PMSG and other system components [107]

Parameter	Value
Rated stator voltage	4 kV
Rated MVA of the machine	2 MVA
Stator leakage reactance	0.1 pu
D-axis unsaturated magnetic reactance	0.65 pu
D-axis damper leakage reactance	2.5 pu
Q-axis magnetizing reactance	1 pu
Q-axis damper leakage reactance	2.5 pu
Stator resistance	0.01 pu
Inertia constant	3.5
Rated wind speed	12 m/sec
DC link voltage	7.6 kV
Grid voltage	33 kV
Coupling transformer rating	2.5 MVA, 4/33 kV
Transformer leakage reactance	0.15 pu
L_{SC}	0.0096 H
C_{SC}	7.5 F
C_{DC}	10 mF

The same technique is applied to find the parameters of the PI gains for the buck boost converter controller. The values obtained are:

- For the MSC: K_{P2d} =0.4, K_{I2d}=0.125, K_{P1q}=0.01, K_{I1q}=0.5, K_{P2q}=0.4, K_{I2q}=0.125
- For the GSC: K_{P3d}=5, K_{I3d}=0.125, K_{P4d}=0.4, K_{I4d}=0.05, K_{P4q}=0.4, K_{I4q}=0.05
- For the buck-boost converter: K_{PO} =5, K_{IO} =0.05, K_{PI} =0.562, and K_{II} =0.05

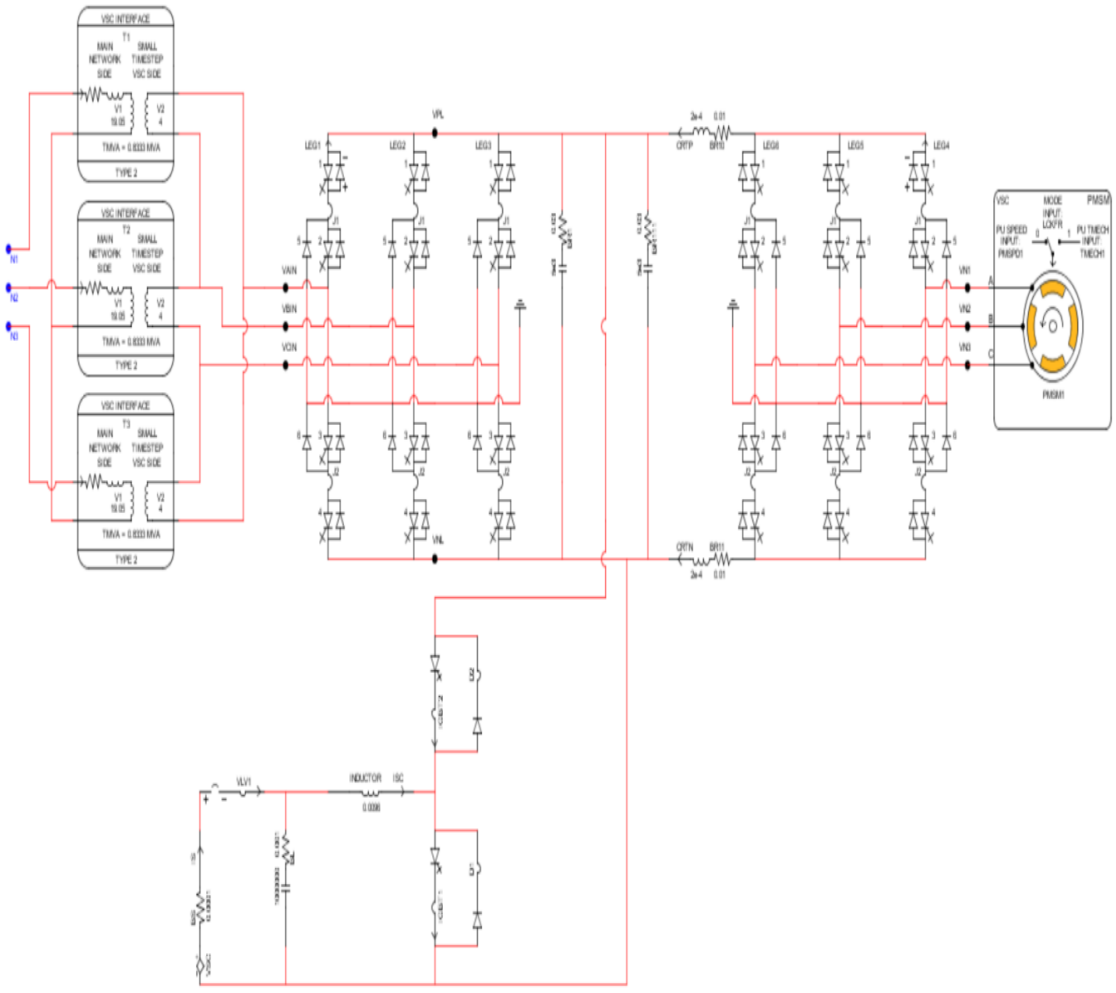

Figure 5.9: Complete RTDS model of three level neutral point clamped grid connected PMSG.

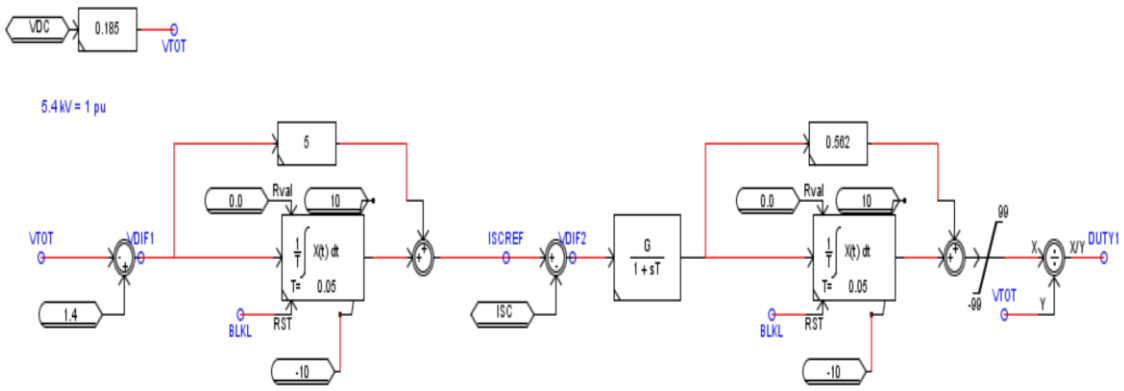

Figure 5.10: Buck boost converter controller in RTDS

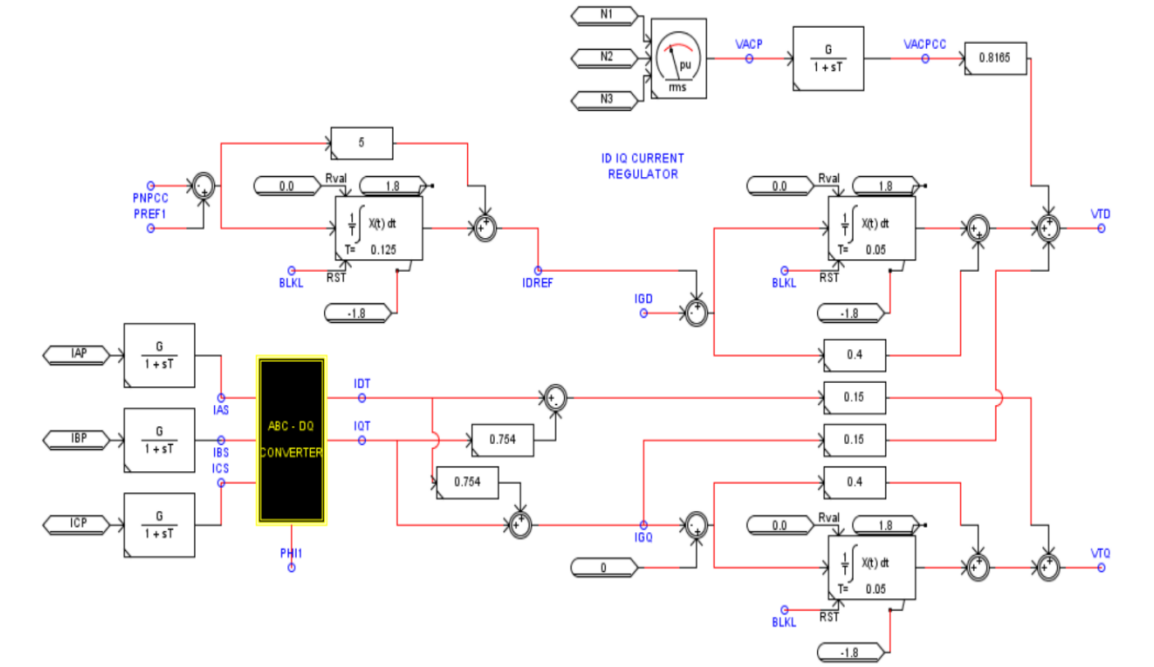

Figure 5.11: Grid side converter controller in RTDS

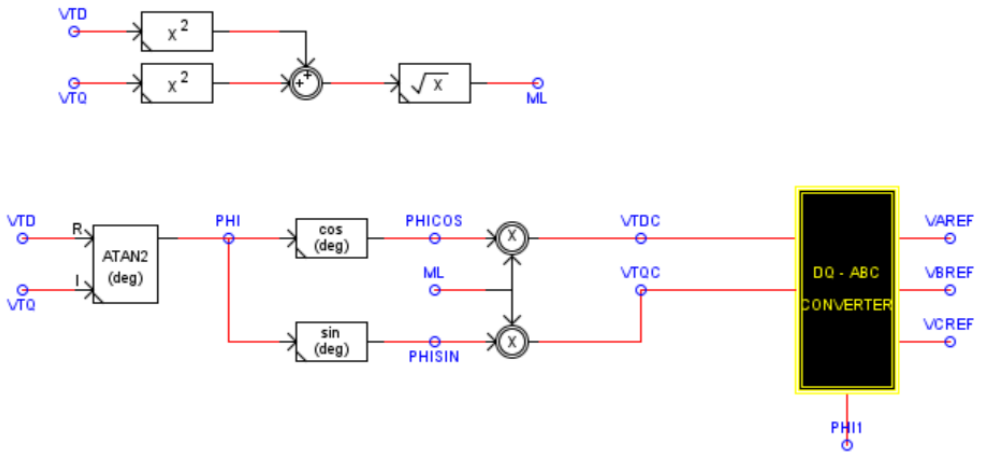

Figure 5.12: Grid side converter dq/abc conversion in RTDS

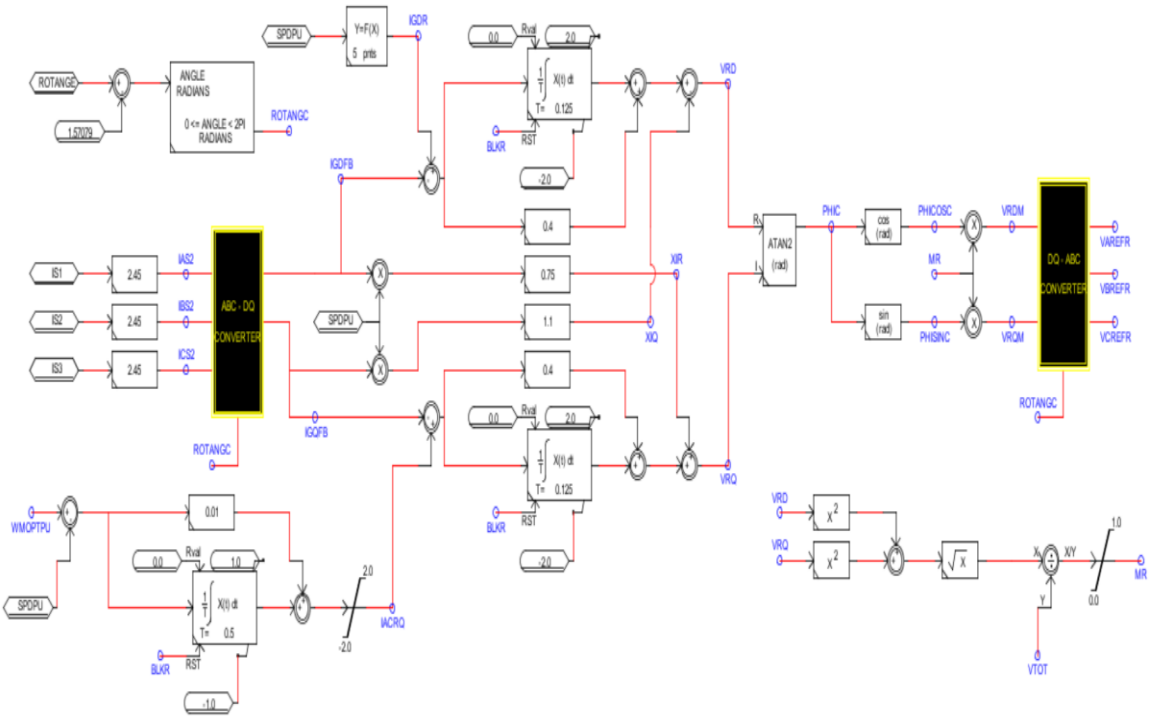

Figure 5.13: Machine side converter controller built in RTDS

To verify the effectiveness of the controller's capability, the developed system has been tested for power smoothing. The wind speed profile and the reference active power and reactive power of the grid side converter are varied to test the charging and discharging capability of the SCESS. The SCESS is designed to have energy capacity of 15 kWh to minimize the fluctuation for the 2 MW WTG system. Using a reference DC link voltage of 7.6 kV and supercapacitor voltage of 3.8 kV (0.5×7.6 kV), the optimum supercapacitor capacitance C_{SC} is designed using equation (4.10) as 7.5 F. The P-Q controller set point P_{GREF} can be set depending on the amount of power to be transferred to the grid and to the SCESS. Taking into account the capacity of the supercapacitor, P_{GREF} has to be set accordingly. In case of higher values of WTG generated power, the excess power is

stored in the SCESS and is used when the generated power is less. The applied disturbances for power smoothing control are:

a. Normal Operation
b. Charging the Supercapacitor
c. Variation in Wind Speed Input

The applied disturbance and results of the system for the above cases are explained below.

5.7.1 Normal Operation

For normal operation the system is generating the rated 2MW power at the rated speed of 12 m/sec. The generated power is directly transferred to the grid. The supercapacitor is only used to minimize small power oscillation. The system response for this case is depicted from Figures 5.14-5.20. Figure 5.14 shows the generator power from the PMSG P_M, the DC link power P_{DC}, the PCC active power P_{NPCC} and the supercapacitor power P_{SC}. As can be seen from the figure, the PMSG generates the rated power from the rated wind speed and is directly transferred to the grid. Neglecting all the losses, the generated power from the PMSG is actually equal to the transferred power to the grid. While working at the rated wind speed the PMSG electrical torque T_e and the PU speed are 1 PU as shown in figure 5.15. The PCC PU voltage V_{ACPCC} and one of the phase voltages N_1 are shown in figure 5.16 and the PU voltage is kept at 1 PU by the grid side converter controller. The supercapacitor voltage V_{SC} and the DC link voltage V_{DC} are depicted in figure 5.17. Since the generated power is directly transferred to the grid, the supercapacitor voltage V_{SC} remains almost constant. The DC link voltage V_{DC} is controlled by the buck-boost converter to a constant reference value and as can be seen

from Figure 5.17 this voltage is kept constant with reference value of 7.6 kV. The d-component current is responsible to control the active power exchanged between the PCC and the grid side converter. The actual and reference component of this current is depicted in Figure 5.18 and are identical. Figure 5.19 shows the actual and reference supercapacitor currents. The PCC reactive power Q_{NPCC} and grid reactive power after the high pass filter Q_S are shown in Figure 5.20.

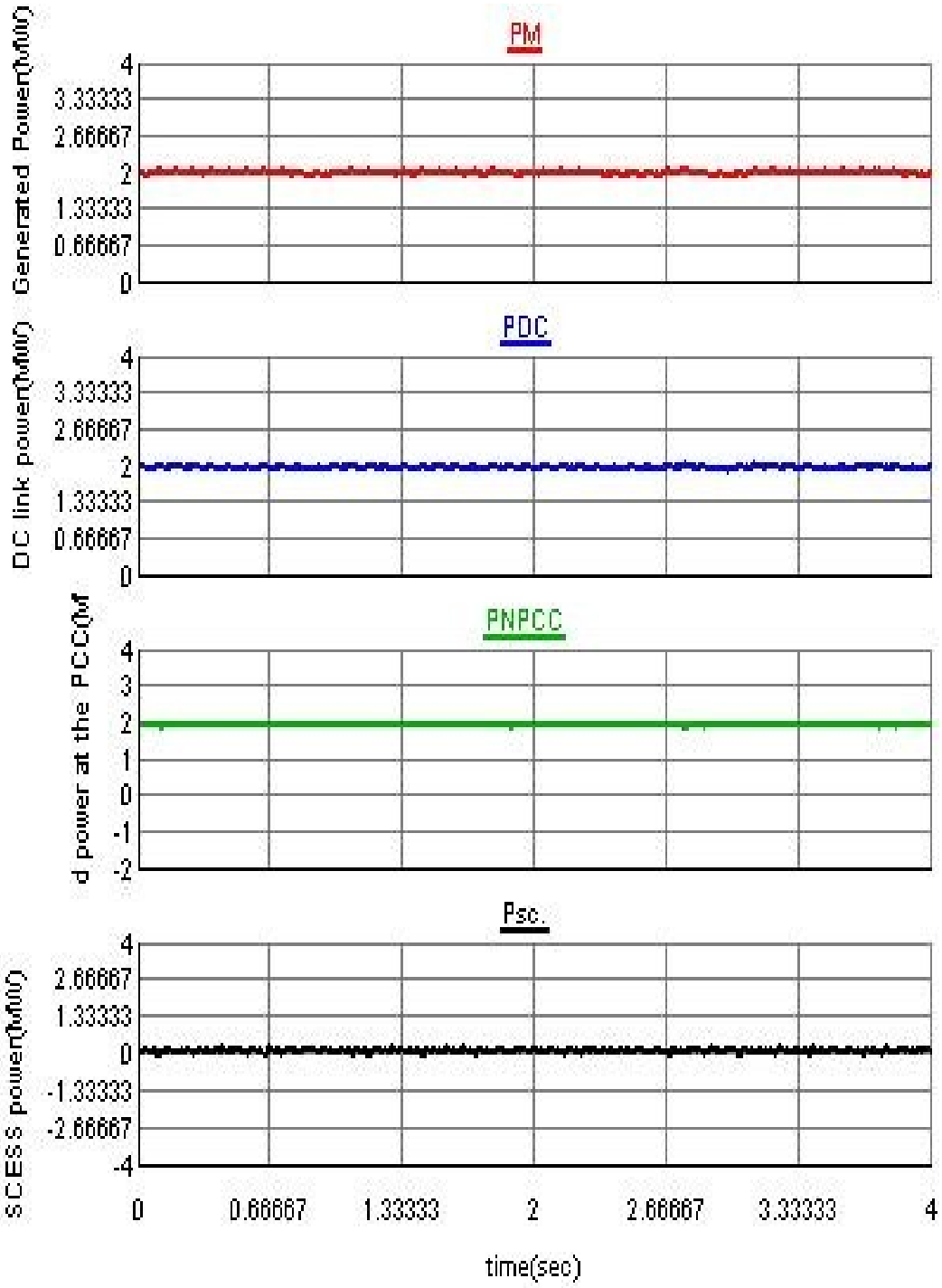

Figure 5.14: PMSG generated power P_M, DC link power P_{DC}, PCC active power P_{NPCC} and SCESS power P_{SC}.

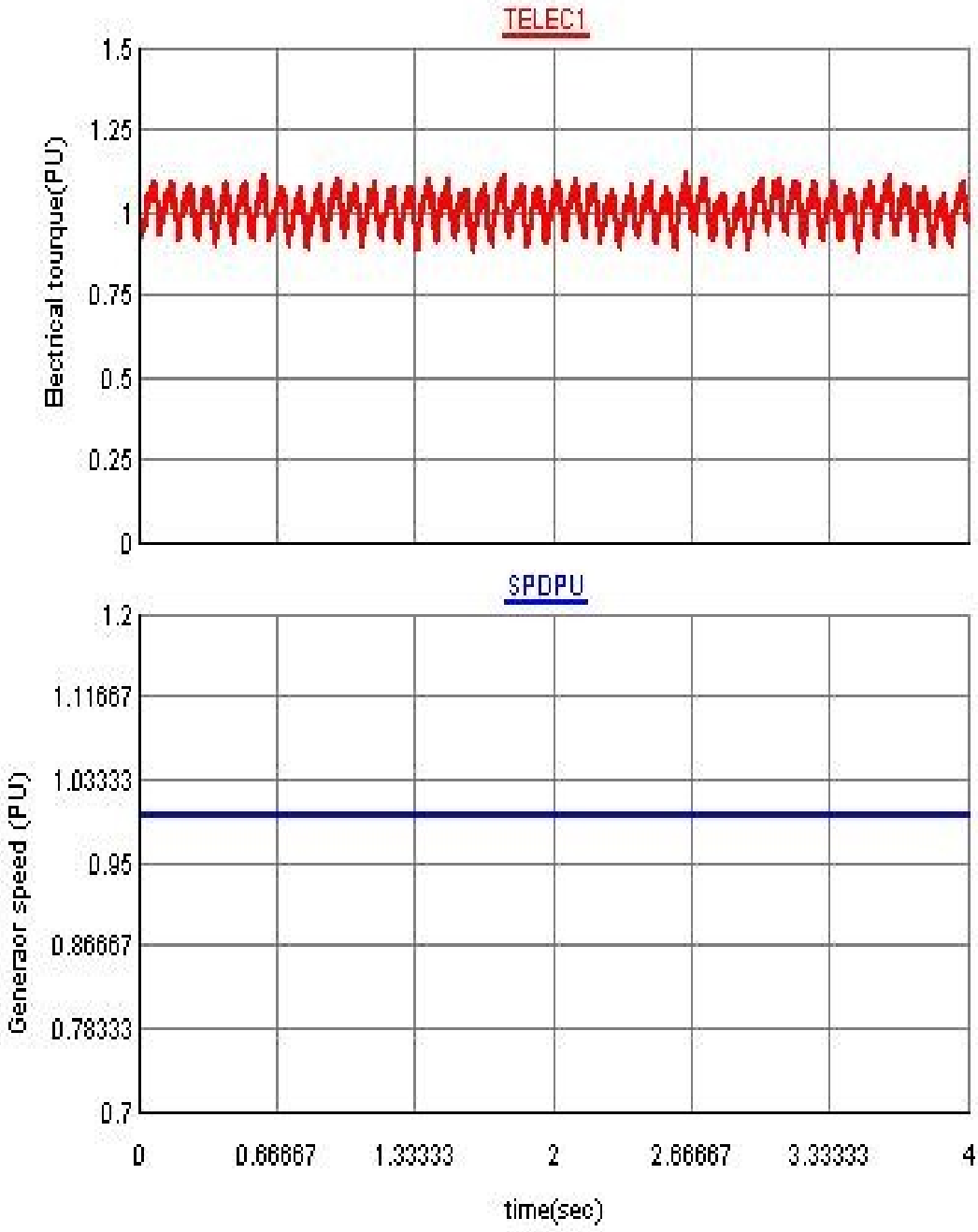

Figure 5.15: PMSG electrical torque T_{ELEC} and generator per unit speed *SPDPU*

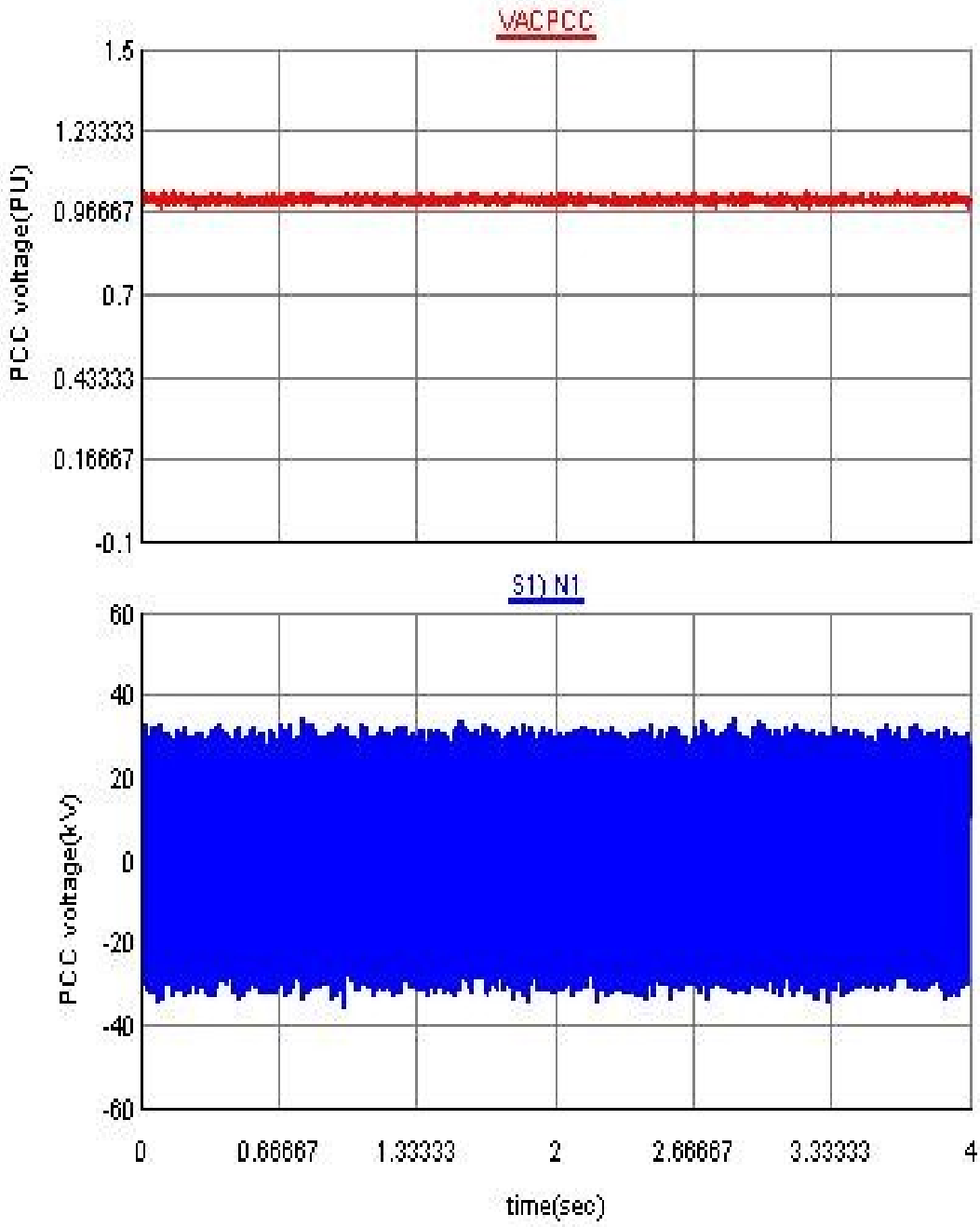

Figure 5.16: PCC PU voltage V_{ACPCC} and phase *a* voltage N_1

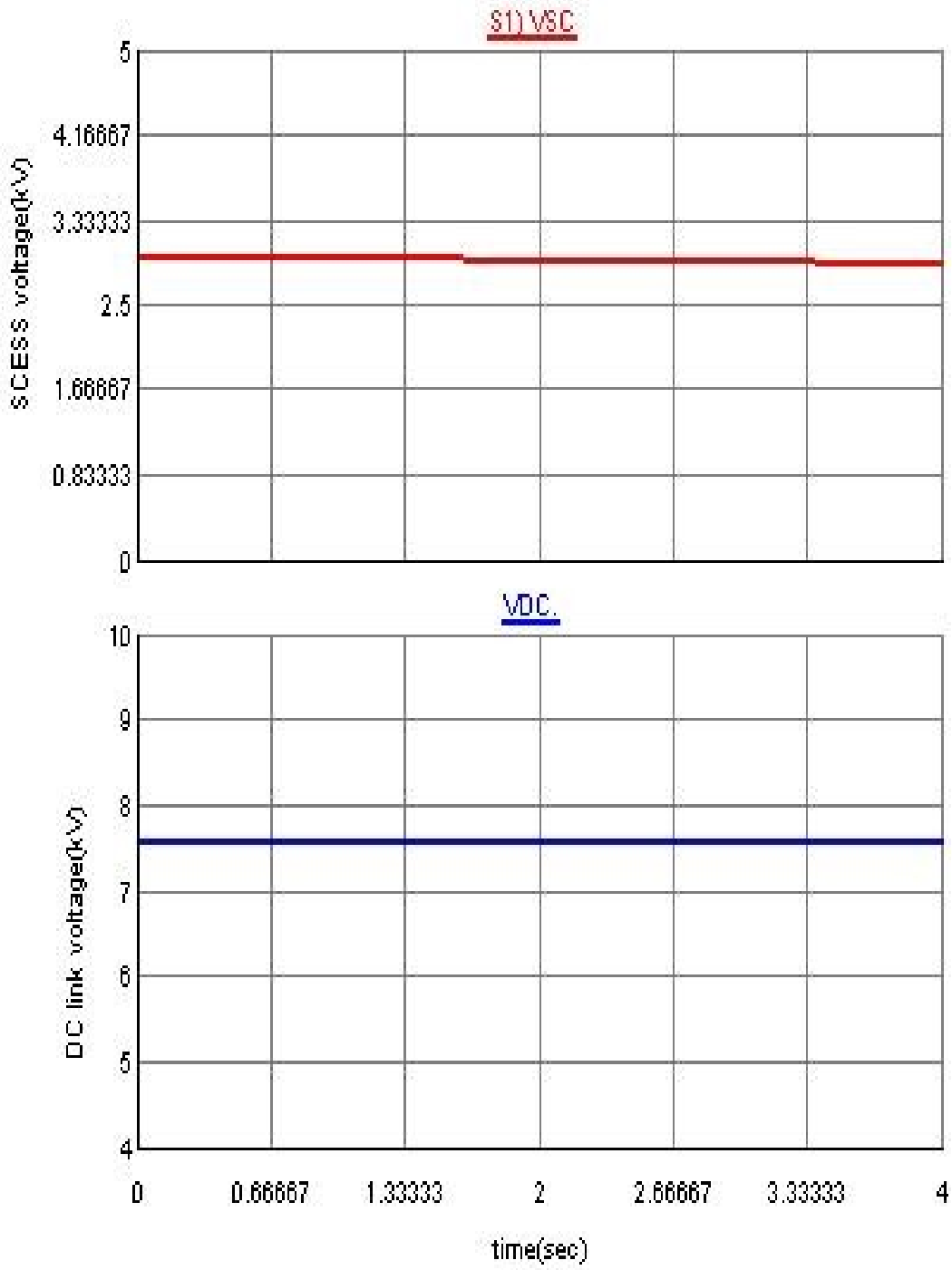

Figure 5.17: The supercapacitor voltage V_{SC} and DC link voltage V_{DC}

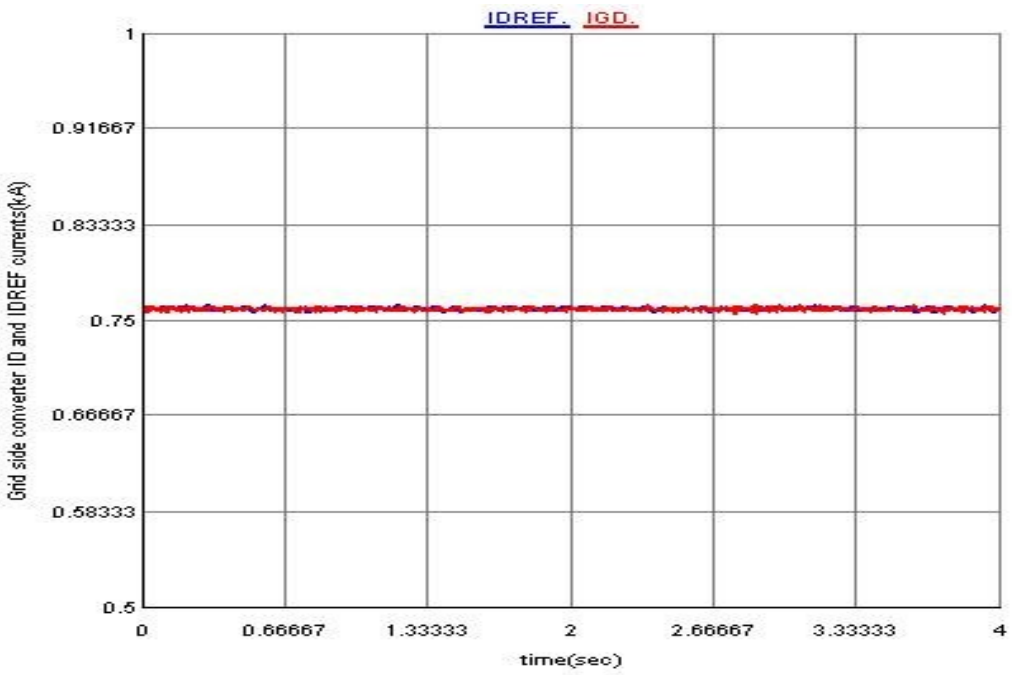

Figure 5.18: Grid side converter reference I_{DREF} and actual I_{GD} inductor currents

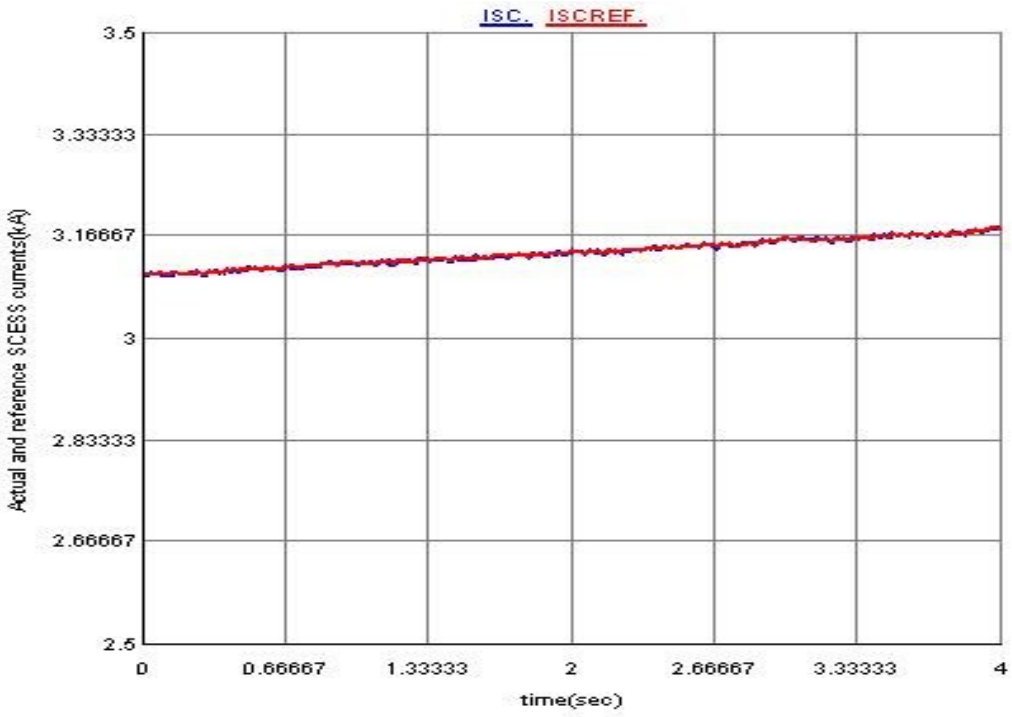

Figure 5.19: Actual I_{SC} and reference I_{SCREF} supercapacitor currents

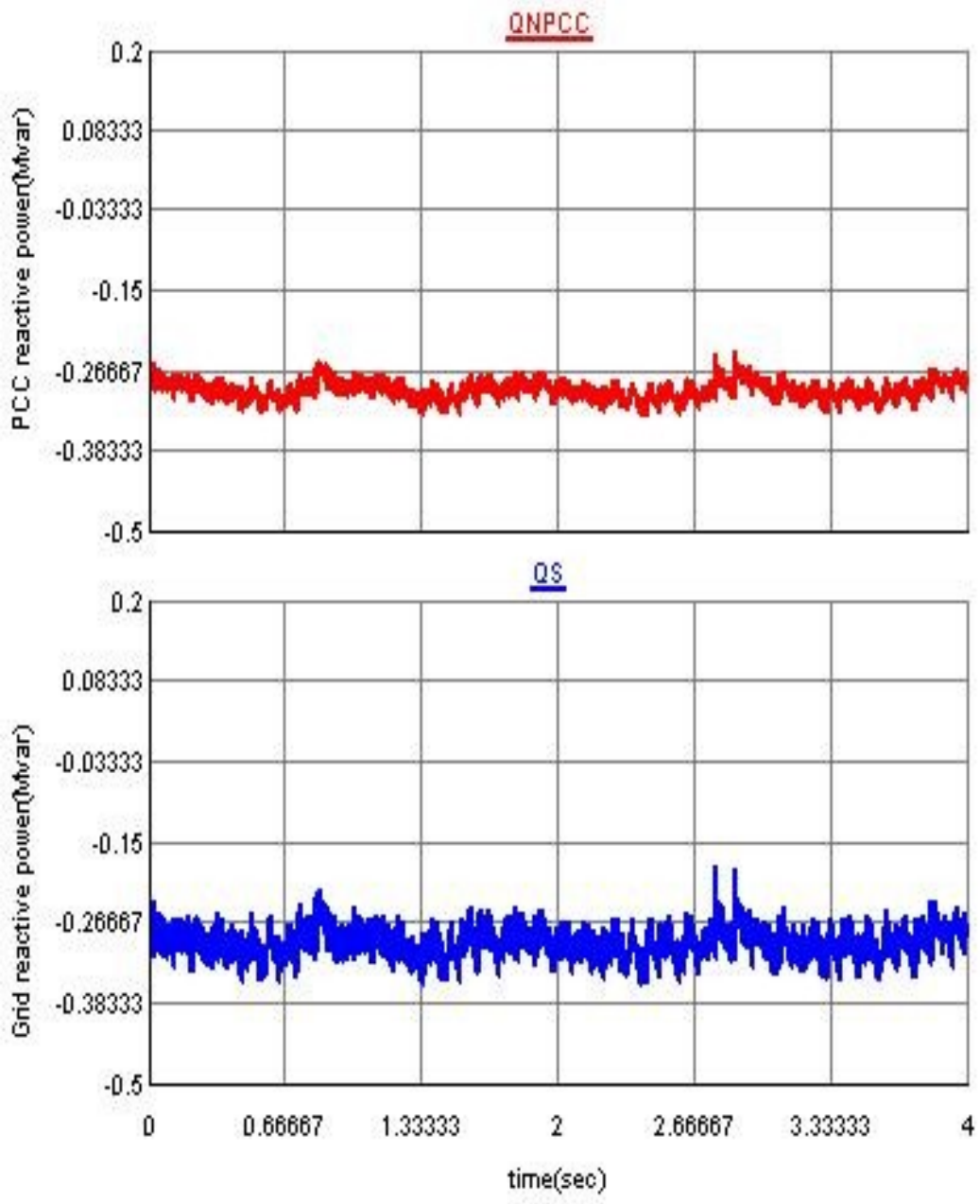

Figure 5.20: PCC reactive power Q_{NPCC} and grid reactive power after the filter Q_S

5.7.2 Charging the Supercapacitor

The supercapacitor can be charged when the power generated by the PMSG is greater than the power transferred to the grid. The PMSG generated its rated power of 2 MW with a wind speed of 12 m/sec. At higher wind speeds, pitch control should be activated to limit the amount of power at the rated PMSG value. The supercapacitor can handle only the fraction of the rated power. To demonstrate the controller's capability in charging the supercapacitor, two cases are conducted.

1. Case 1: Charging the Supercapacitor at Rated Wind Speed

For this case the wind speed is kept at 12m/sec that means the PMSG is generating the rated 2MW. The P_{GREF} of the grid side converter is set at 1MW. The other 1MW is used to charge the supercapacitor energy storage system. The applied disturbance and response of the system are shown from figures 5.21- 5.27. Figure 5.21 shows the generator power from the PMSG PM, the DC link power P_{DC}, the PCC active power P_{NPCC} and the supercapacitor power P_{SC}. As can be seen from the figure, the PMSG generates the rated 2 MW power from the rated wind speed and the grid side converter is transferring only 1 MW of the generated power. The other 1 MW is used to charge the SCESS which can be used later when the wind speed falls down or the grid demand power is high. Figure 5.22 shows the PU electrical torque and speed of the PMSG kept at their corresponding rated values for the applied rated wind speed. Similar to the normal operation the PU voltage at the PCC is kept at its rated 1 PU values as depicted in figure 5.23. The reactive power at the PCC and grid are shown in Figure 5.24. Figure 5.25 shows the supercapacitor voltage V_{SC} and DC link voltage V_{DC} controlled by their respective controller accordingly. The actual and reference inductor currents of the grid side converter are shown in Figure 5.26.

The magnitude of these currents corresponds to the 1MW power transferred to the grid by the grid side converter. Figure 5.27 depicts the actual and reference charging supercapacitor current.

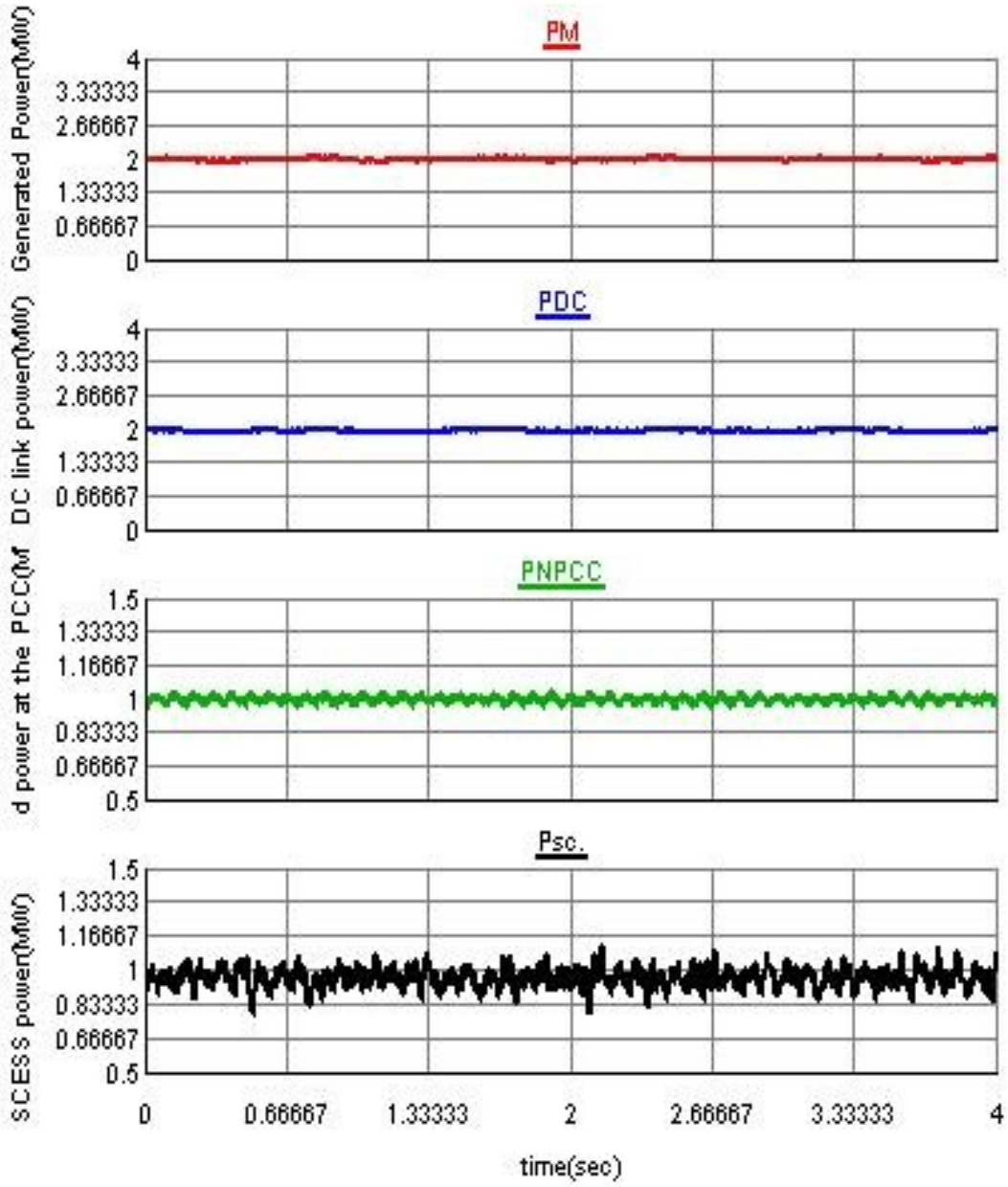

Figure 5.21: PMSG generated power P_M, DC link power P_{DC}, PCC active power P_{NPCC} and SCESS power P_{SC}.

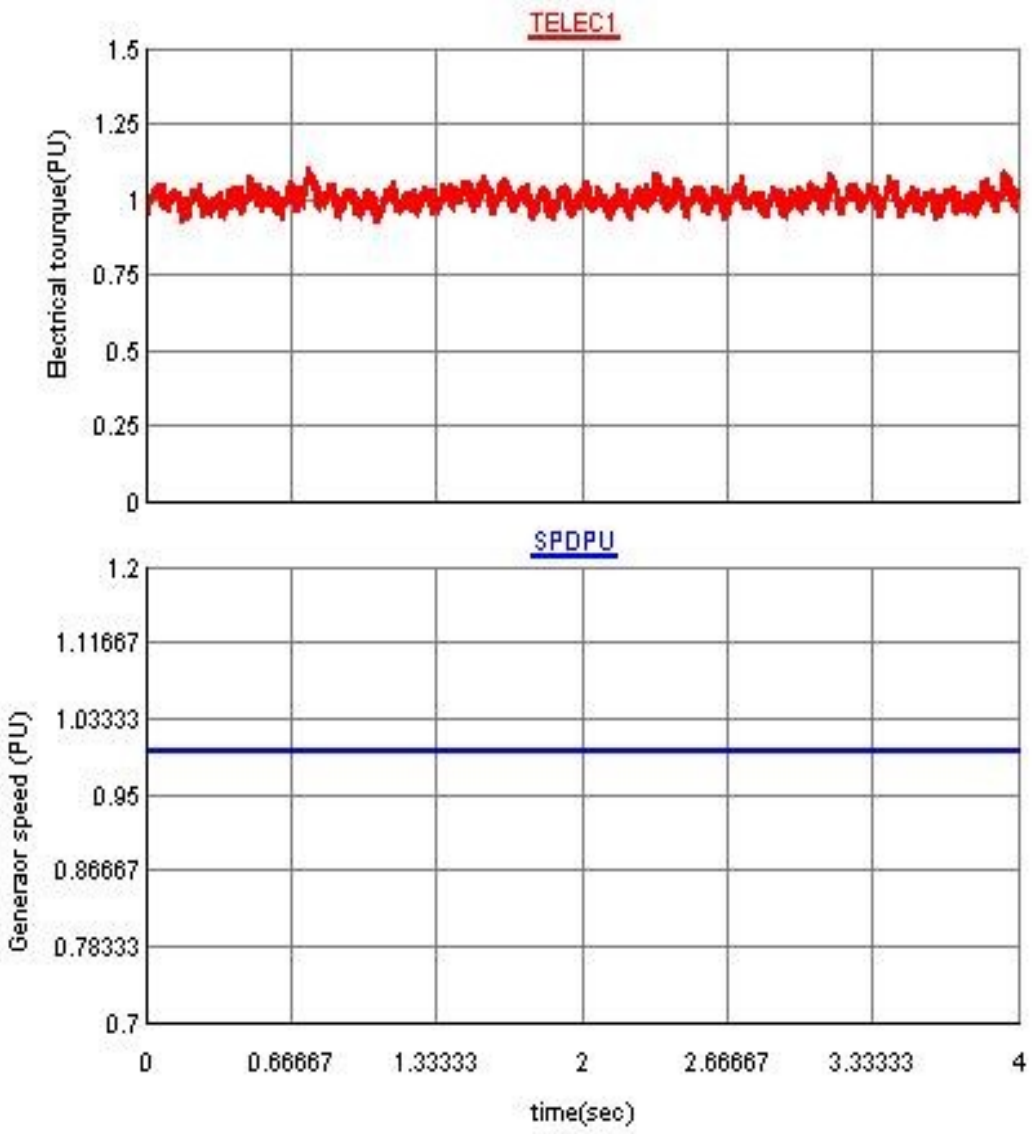

Figure 5.22: PMSG electrical torque T_{ELEC} and generator per unit speed *SPDPU*

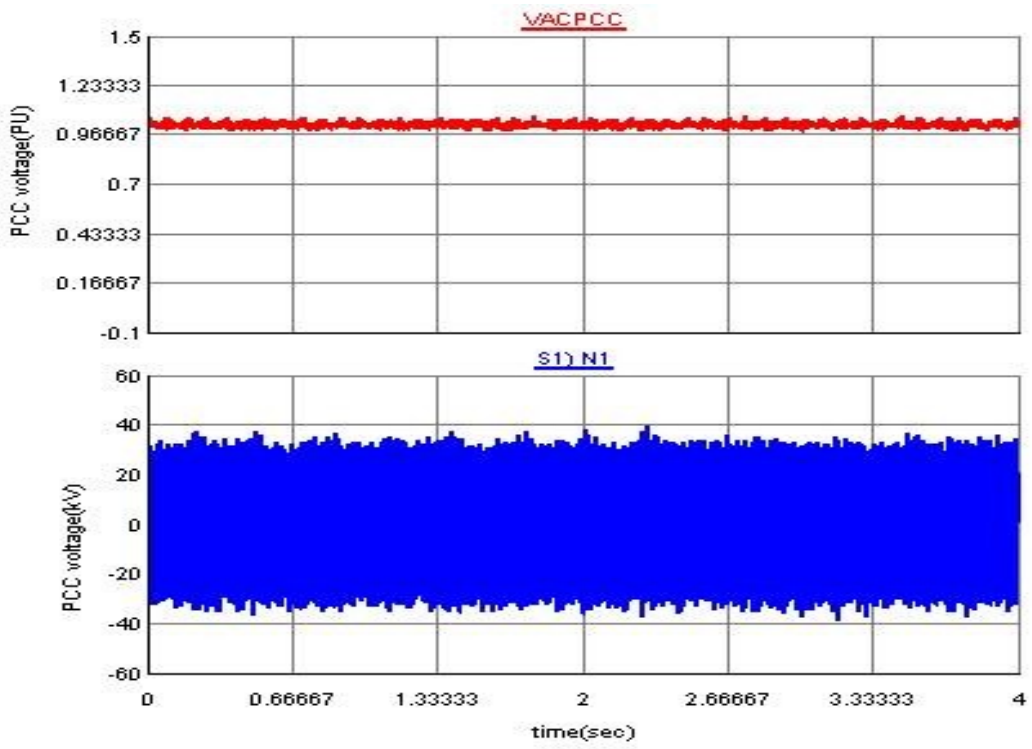

Figure 5.23: PCC PU voltage V_{ACPCC} and phase *a* voltage N_1

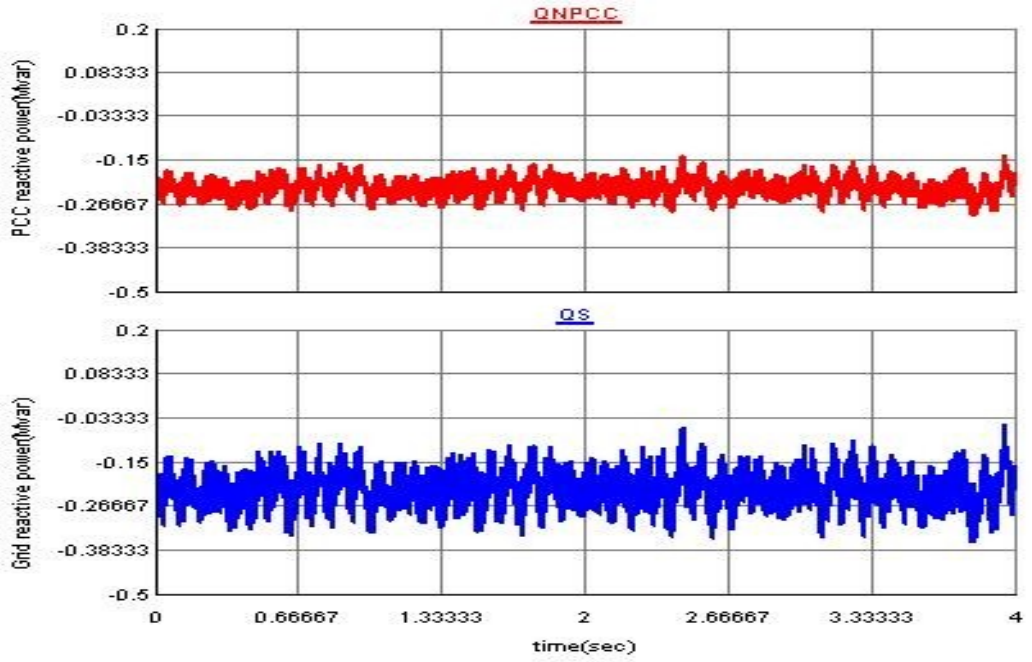

Figure 5.24: PCC reactive power Q_{NPCC} and grid reactive power after the filter Q_S

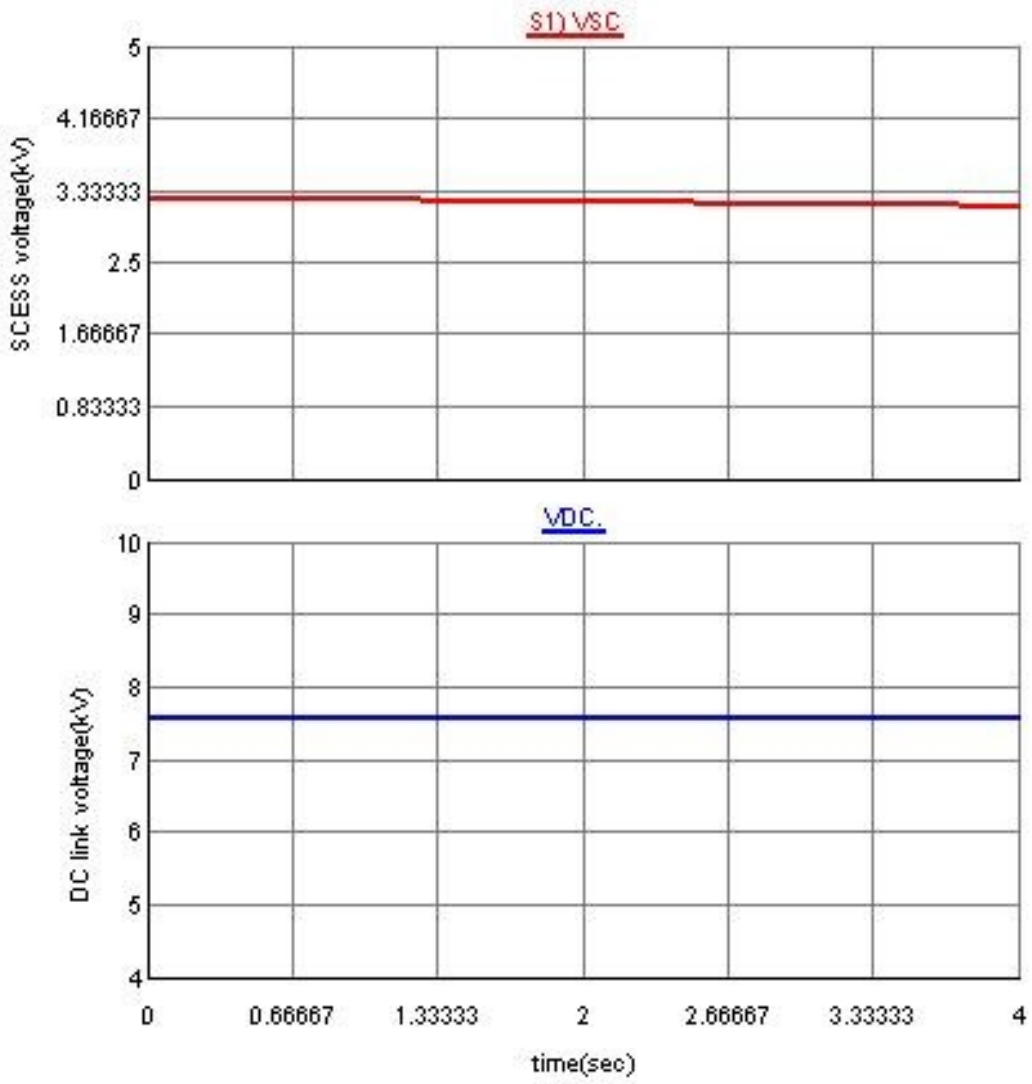

Figure 5.25: The supercapacitor voltage V_{SC} and DC link voltage V_{DC}

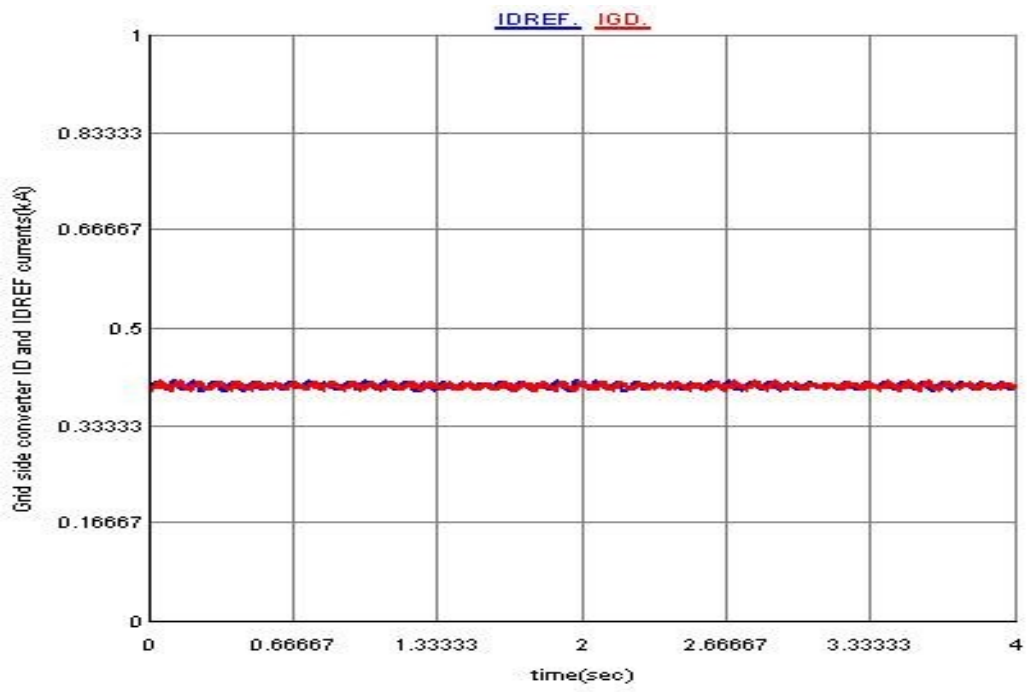

Figure 5.26: Grid side converter reference I_{DREF} and actual I_{GD} inductor currents

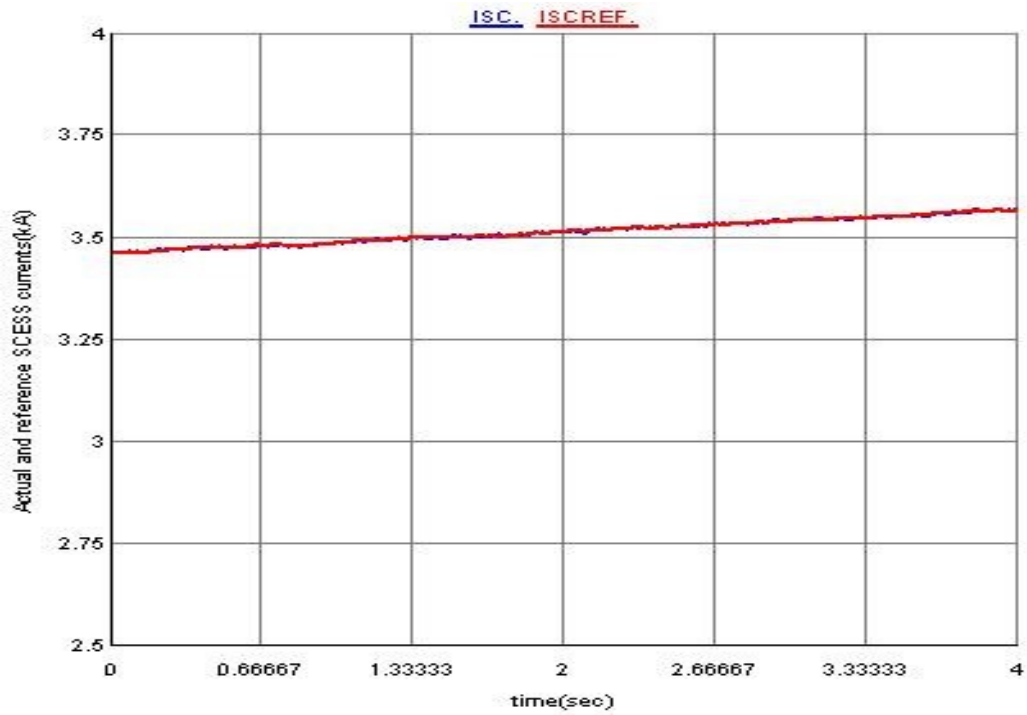

Figure 5.27: Actual I_{SC} and reference I_{SCREF} supercapacitor currents

2. Case 2: Charging the Supercapacitor By Varying the Reference Power

To further demonstrate the efficiency of the controller, another case has been performed where the PMSG is generating the rated power of 2MW from the rated wind speed of 12 m/sec but the reference active power P_{GREF} is changed to 1.5 MW. For this particular case the 0.5 MW is used to charge the SCESS. Figure 5.28 shows the PMSG generating the rated power P_M, the grid side converter transferring the set 1.5 MW to the PCC P_{NPCC} and the supercapacitor getting charged by 0.5 MW P_{SC}. The corresponding supercapacitor charging current is shown in Figure 5.29. Figure 5.30 depicts the PCC voltage response for the applied disturbance and Figure 5.31 demonstrates the controller's capability in keeping the DC link voltage constant. The actual and reference inductor currents corresponding to the set P_{GREF} is shown in Figure 5.32.

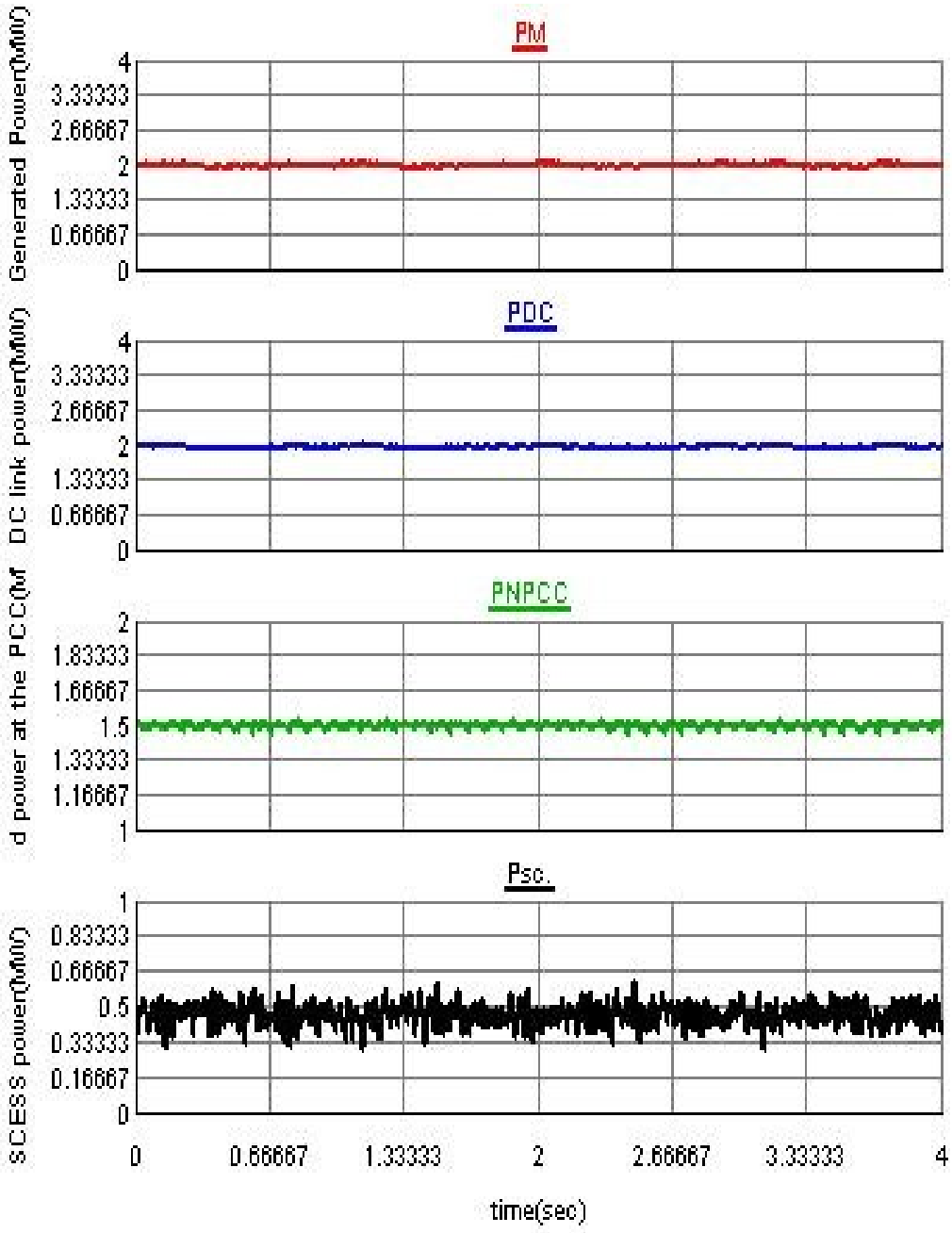

Figure 5.28: PMSG generated power P_M, DC link power P_{DC}, PCC active power P_{NPCC} and SCESS power P_{SC}.

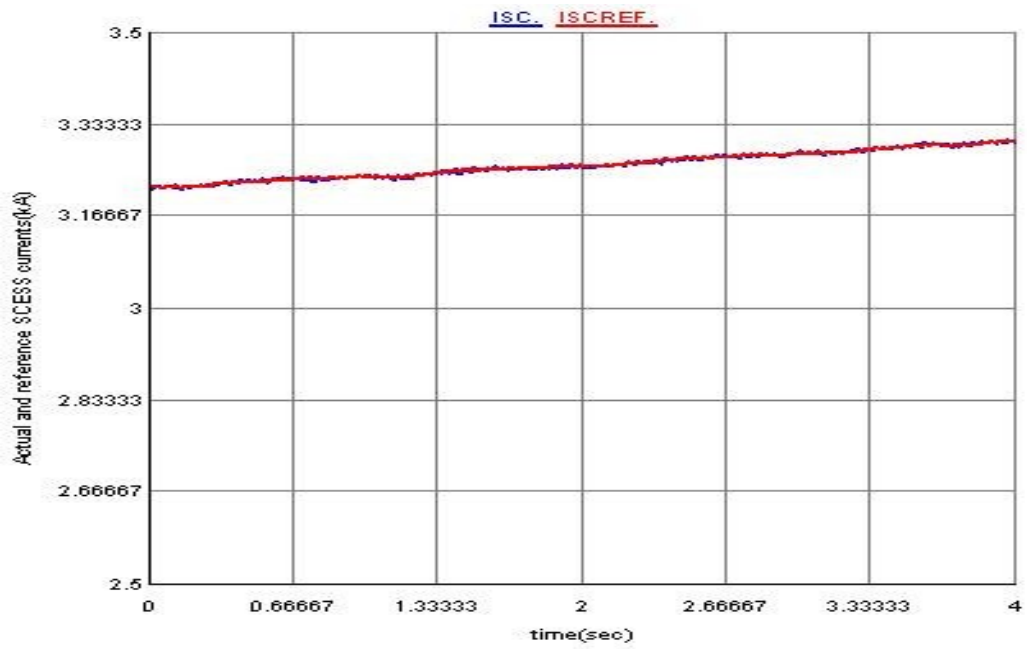

Figure 5.29: Actual I_{SC} and reference I_{SCREF} supercapacitor currents

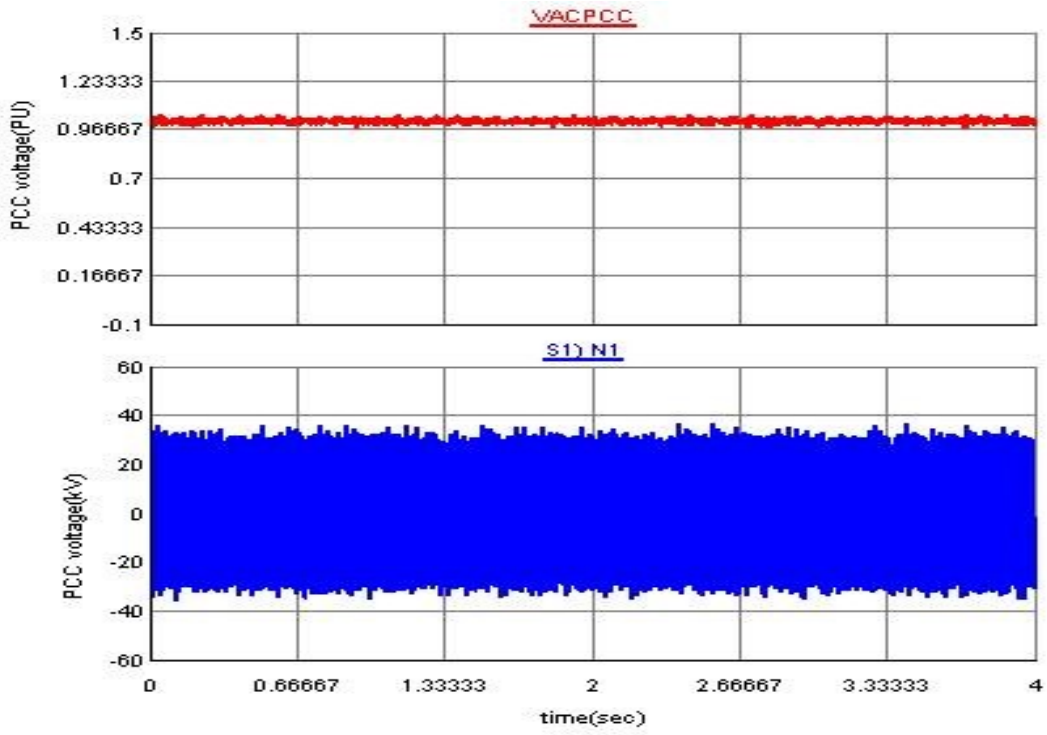

Figure 5.30: PCC PU voltage V_{ACPCC} and phase *a* voltage N_1

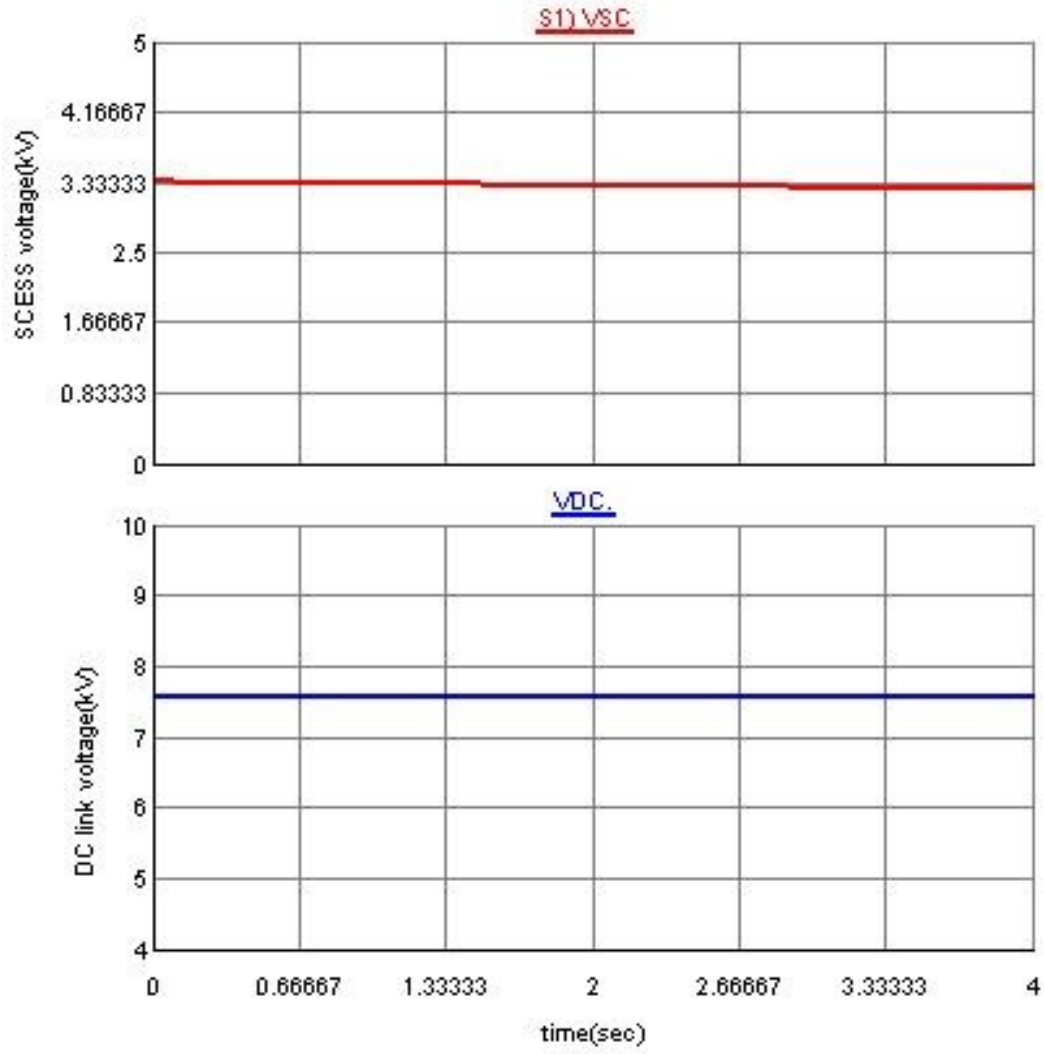

Figure 5.31: The supercapacitor voltage V_{SC} and DC link voltage V_{DC}

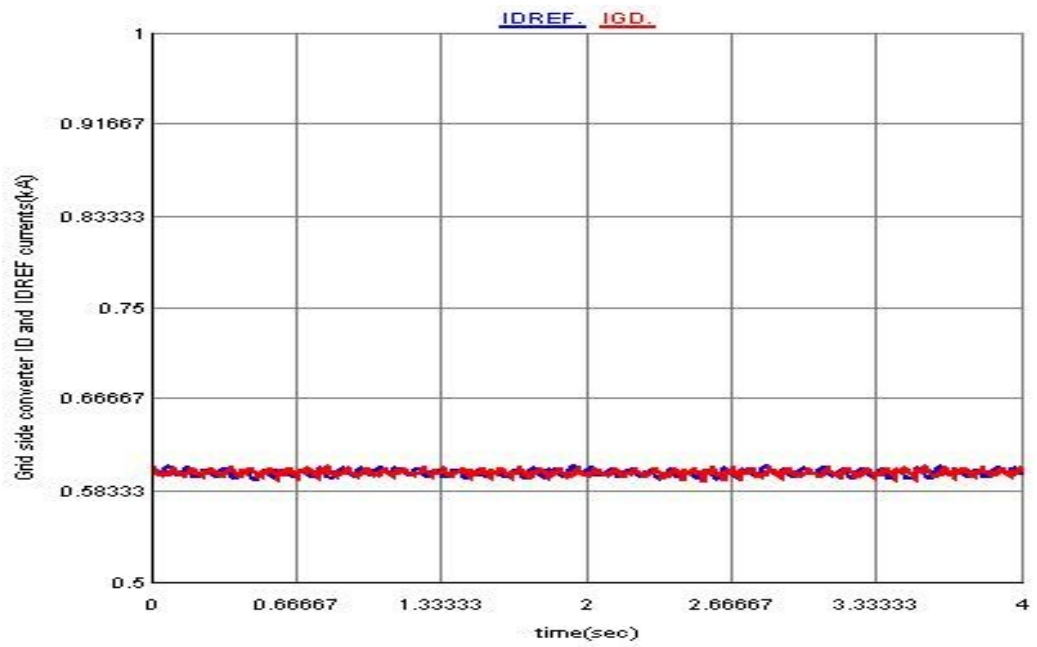

Figure 5.32: Grid side converter reference I_{DREF} and actual I_{GD} inductor currents

5.7.3 Variation in Wind Speed Input

To further demonstrate the controller's capability, a scheduled wind speed input shown in Figure 5.33 is applied as a disturbance input. The response of the system is shown from figures 5.34-5.38. Initially the wind speed was 11 m/sec and the PMSG was generating 1.5 MW. The reference active power P_{GREF} for the grid side converter was 1.5 MW and the controller was able to transfer the same amount to the grid. When the wind speed jumps to 12 m/sec the PMSG now generates 2 MW but since P_{GREF} is kept at 1.5 MW, the excess power goes to the SCESS to charge it. At t=12.5 sec, the wind drops back to 11 m/sec and the corresponding power is generated. When the wind speed drops further to 10 m/sec, the stored energy in the SCESS is now utilized to support the grid as shown in Figure 5.34. The PU electrical torque and speed of the machine during this varying wind speed is depicted in Figure 5.35. The PU PCC voltage V_{ACPCC} and one of the phase

voltage N_1 during the disturbance is shown in Figure 5.36 and are kept at their rated values. As shown in Figure 5.37, the DC link voltage V_{DC} is kept constant in spite of the change in the generated and DC link power because of the change in the wind speed. Figure 5.37 also shows the SCESS voltage V_{SC} during the process of charging and discharging cycle. The actual and reference SCESS currents are depicted in Figure 5.38.

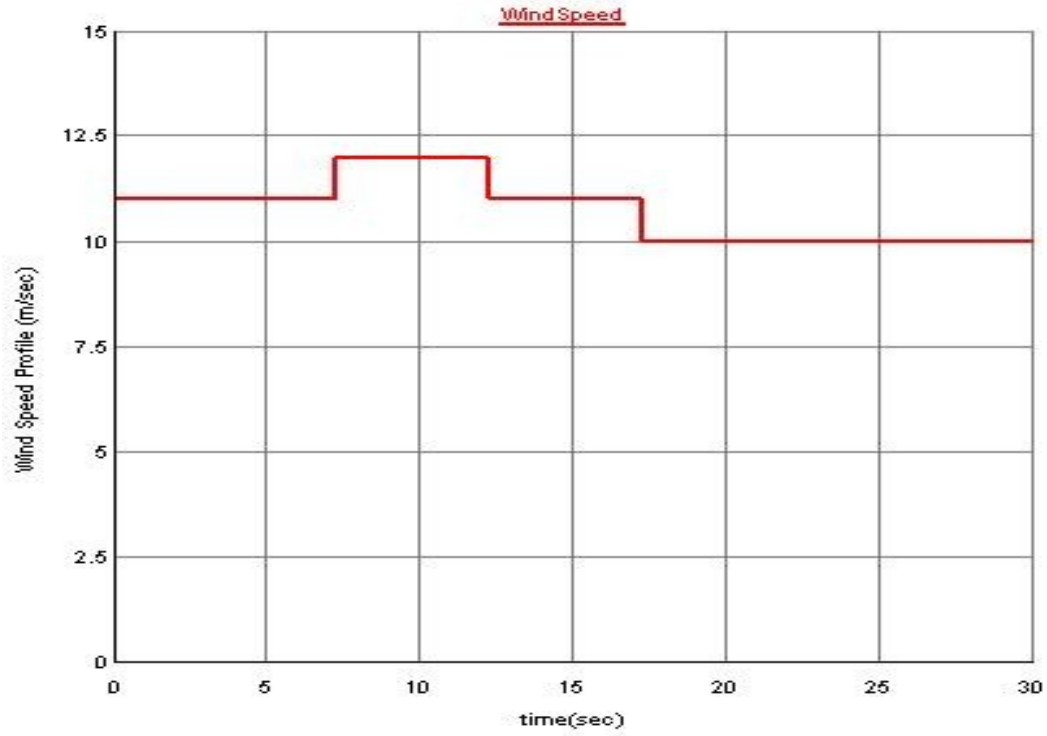

Figure 5.33: Scheduled input wind speed

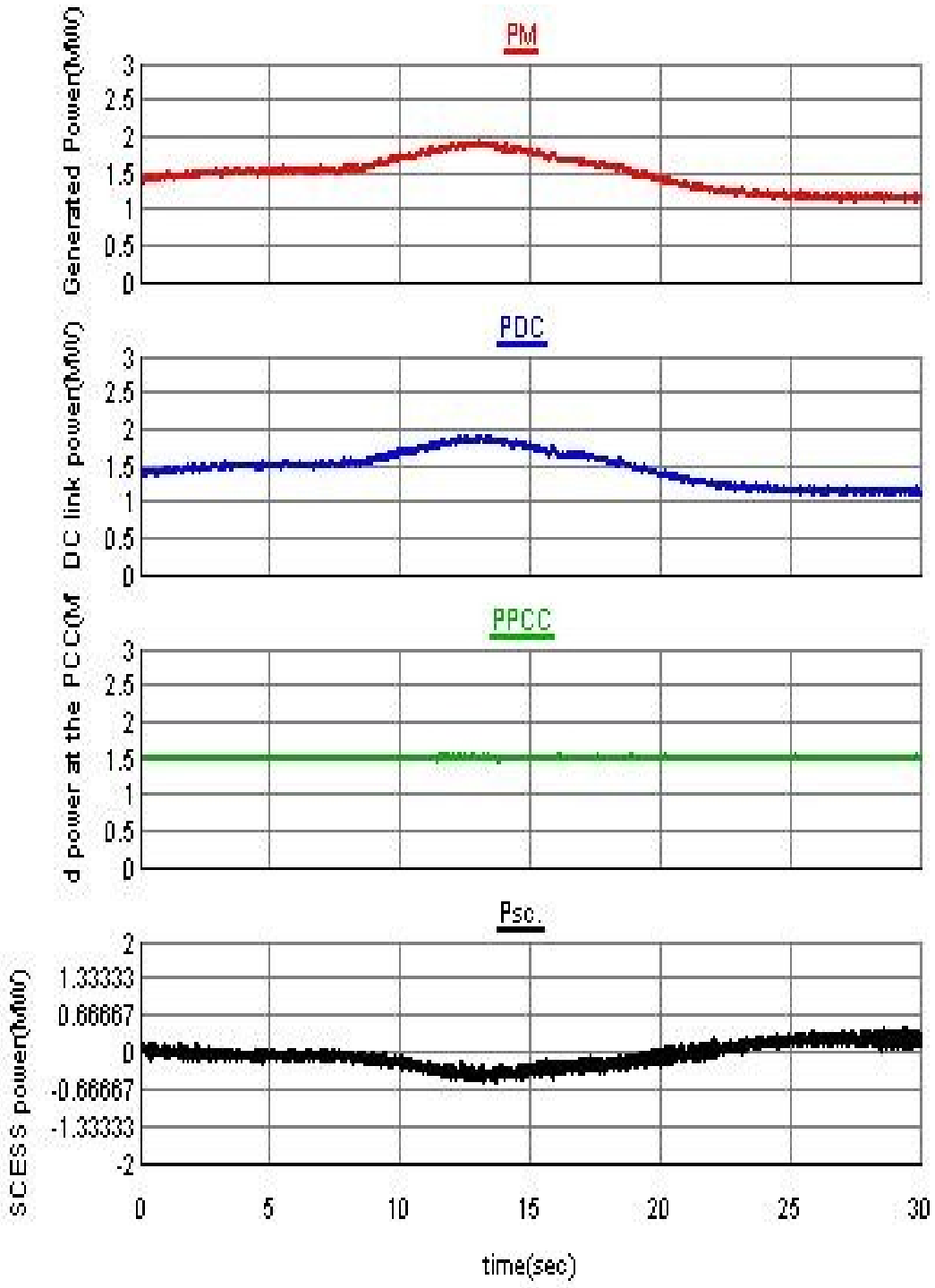

Figure 5.34: PMSG generated power P_M, DC link power P_{DC}, PCC active power P_{NPCC} and SCESS power P_{SC}.

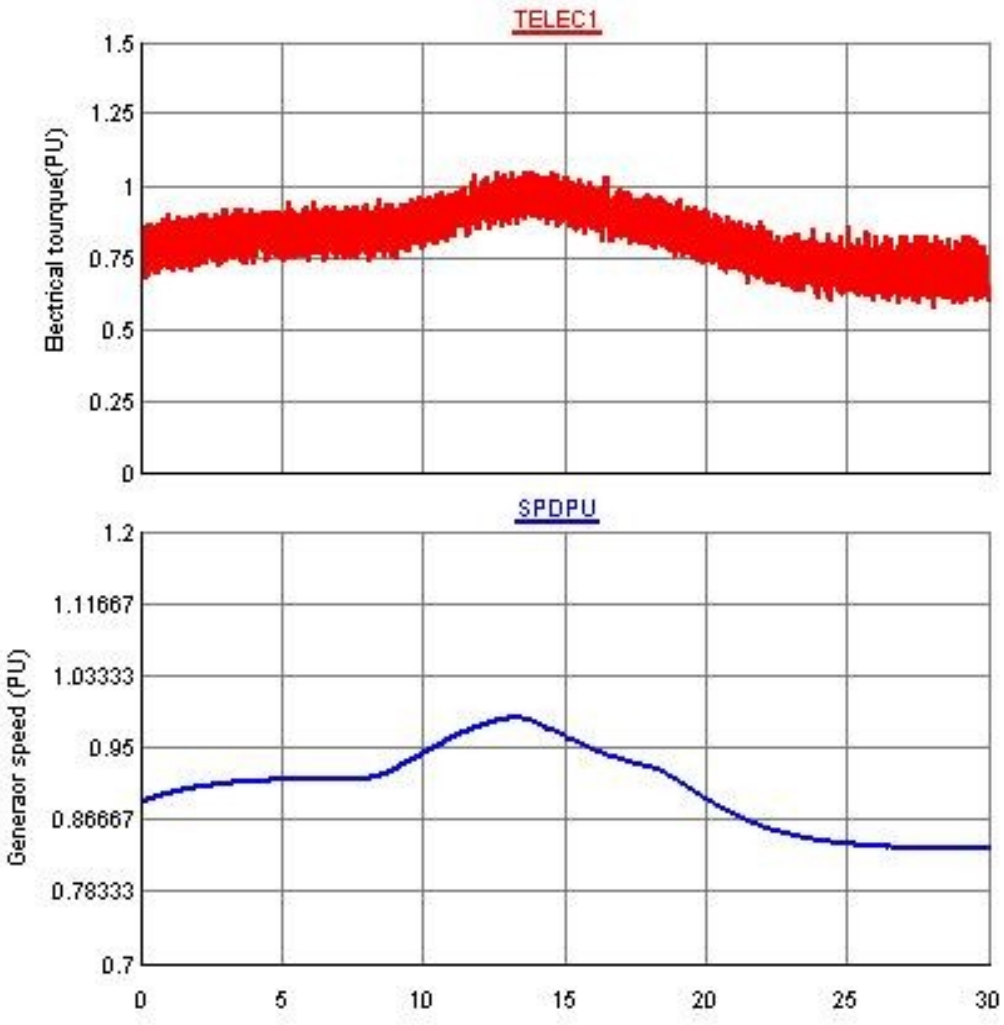

Figure 5.35: PMSG electrical torque T_{ELEC} and generator per unit speed *SPDPU*

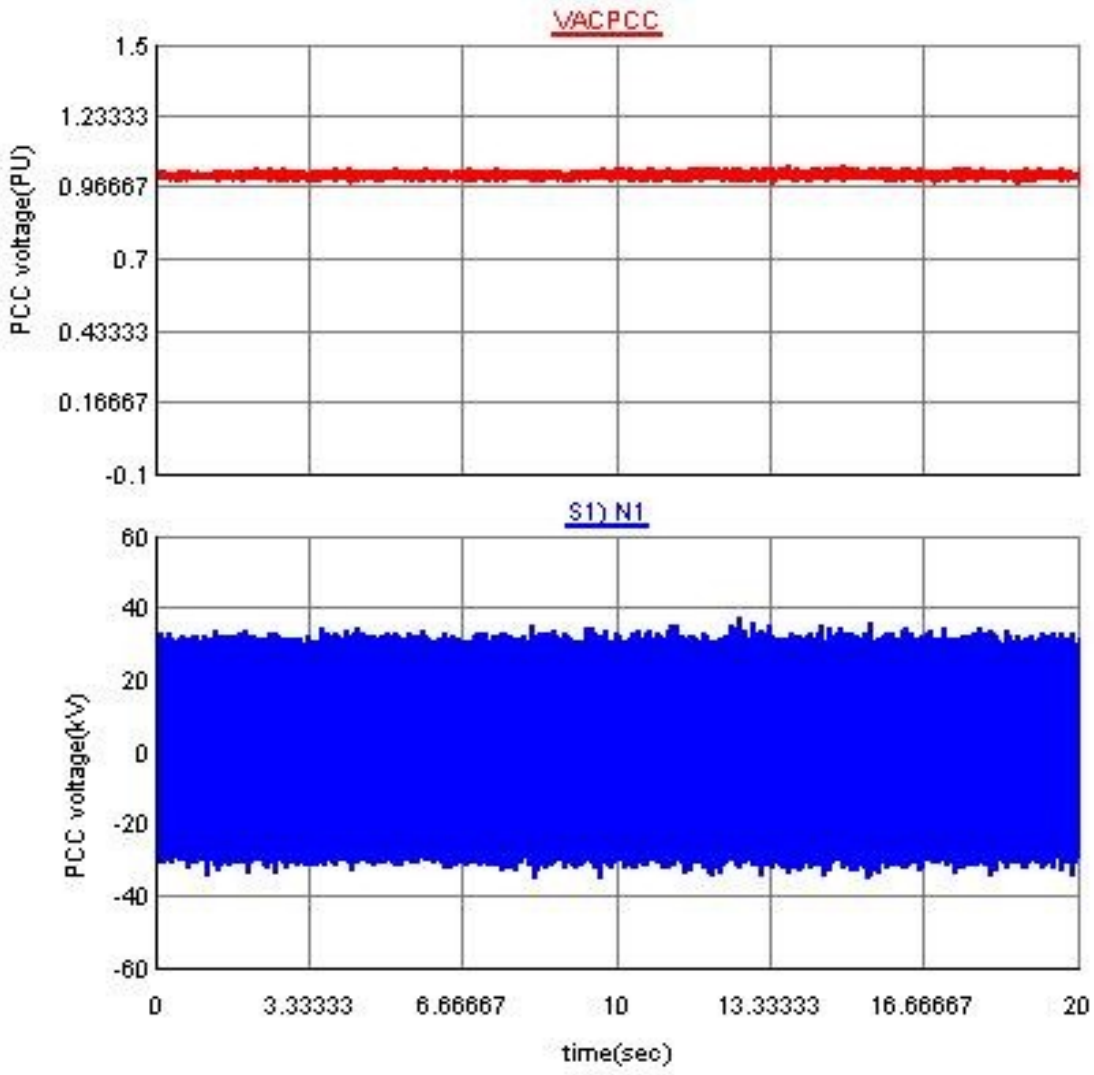

Figure 5.36: PCC PU voltage V_{ACPCC} and phase *a* voltage N_1

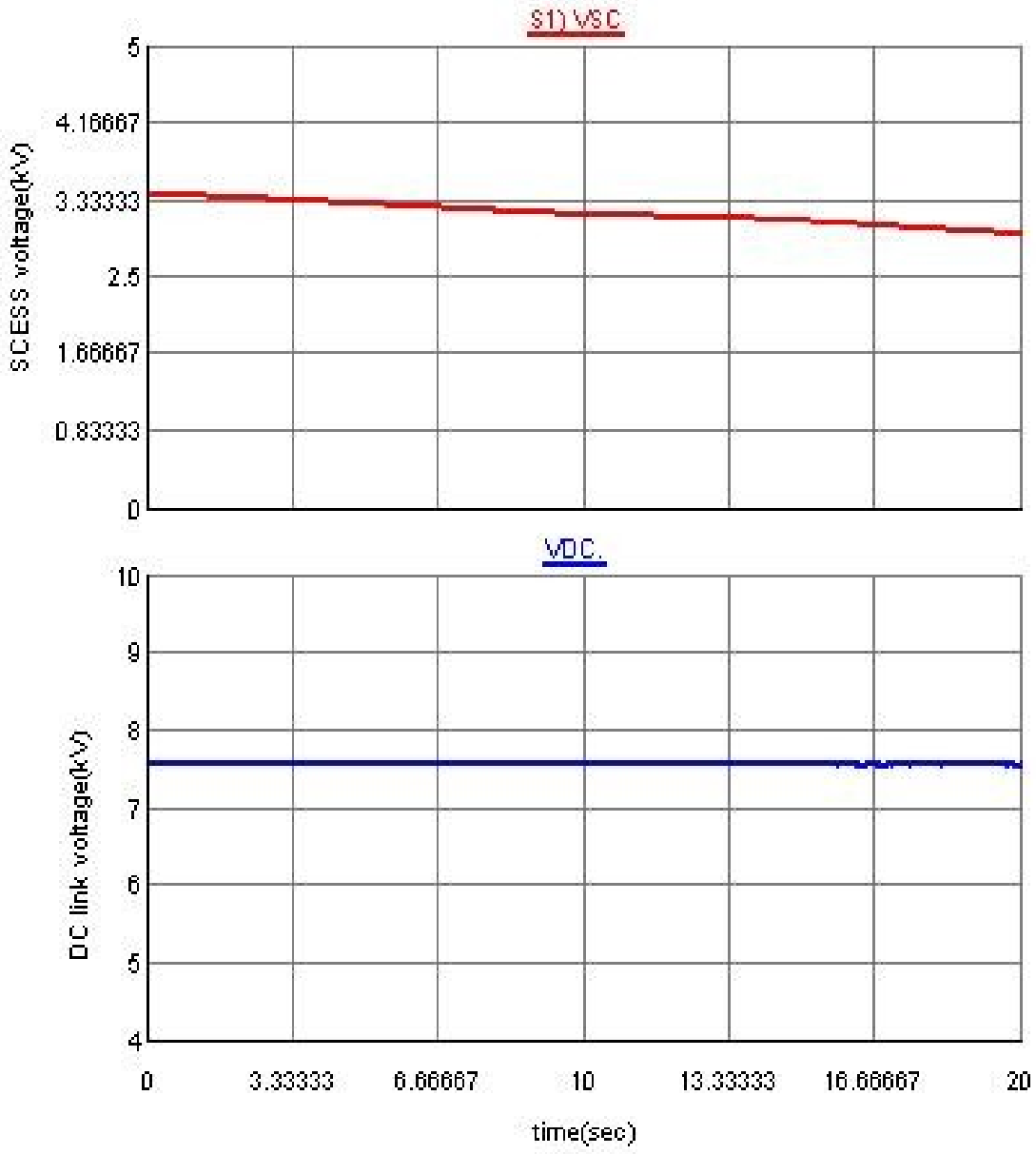

Figure 5.37: The supercapacitor voltage V_{SC} and DC link voltage V_{DC}

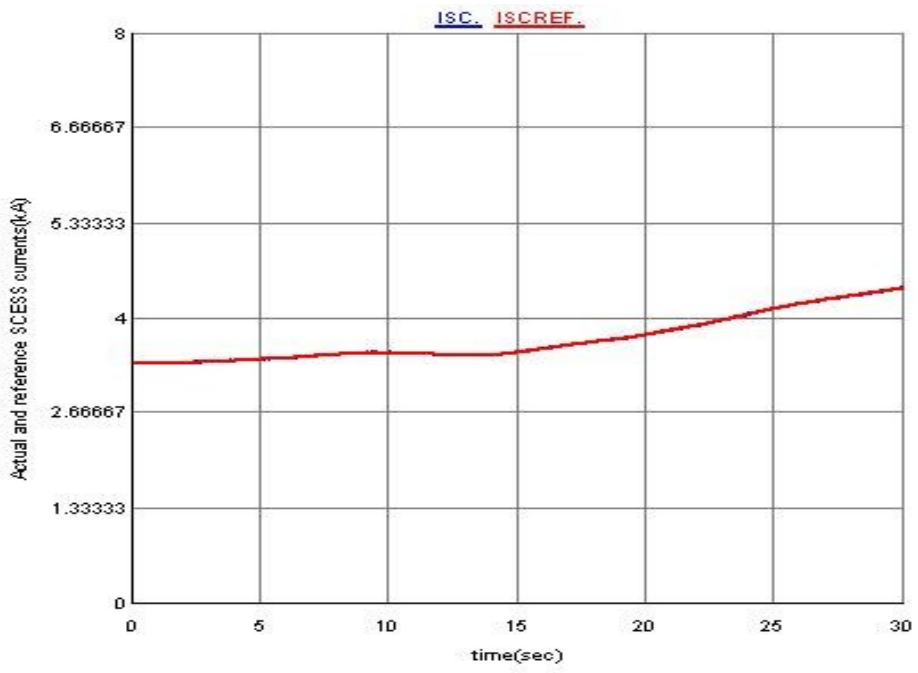

Figure 5.38: Actual I_{SC} and reference I_{SCREF} supercapacitor currents

5.8 CONCLUSION

This chapter proposed an efficient control scheme to demonstrate the potential of supercapacitor energy storage system to minimize the power fluctuation of grid connected wind turbine generator. The proposed power smoothing capability of controller is examined by varying the input wind speed. Three independent controllers are proposed and implemented. The buck boost converter controller proposed and employed controls the DC link voltage to a constant reference value for real power delivery to the grid by charging and discharging the SCESS. A P-Q controller is implemented to transfer the DC link power to the grid using the MSC. The GSC controls the generator rotor speed to generate maximum power from the wind and it simultaneously controls the generator to decreases its losses. During normal operation the proposed controller uses the SCESS to minimize the fluctuation caused by varying wind

speed. RTDS based results show the validity and effectiveness of the proposed controllers.

CHAPTER 6 FAULT RIDE THROUGH OF RENEWABLE ENERGY SOURCES USING ENERGY STORAGE SYSTEM

In this chapter, the fault ride through of PV and wind system equipped with supercapacitor energy storage system is presented. A controller is proposed and implemented to store the generated power from the renewable sources during the fault duration. The proposed controller is verified by applying a three phase fault at the grid side.

6.1 Fault Ride Through of PV systems using SCESS

As the capacity of PV systems are growing significantly, the impact of PV modules on power grid can't be ignored. They can cause problems on the grid like flicker, increase of harmonics, and aggravated stability of the power system. To both increase the capacity of PV arrays and maintain power quality, it's necessary to comply with the technique requirements of the PV system, such as fault-ride-through capability and harmonic current regulation. Especially when a large scale PV module is connected to the grid, the effects on the grid may be quite severe. Therefore, the system operation and system stability under fault conditions should be examined when PV modules are interface with power grid.

A. Three Phase Grid Fault

The complete model of the grid connected system for fault ride through study is depicted in Figure 6.1. The fault controller is shown in Figure 6.2. The limiting curve of the power plant is shown in Figure 6.3 [147]. For fault duration of ≤150 ms, the power plant must remain online for a voltage drop down of 0 pu. For zones A and B the plant should remain online. In zone C, a short-time disconnection can be carried out and no requirement for the plant to remain online for zone D.

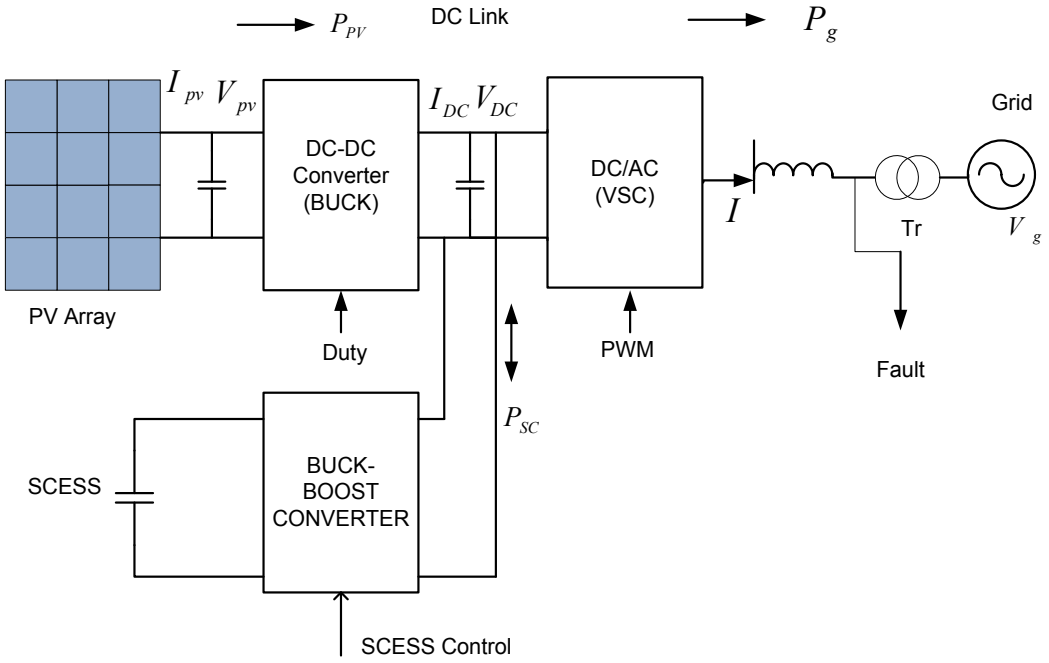

Figure 6.1: Grid connected PV system with energy storage

A three phase fault of nine cycles (150msec) shown in Figure 6.3 is applied on the grid side. For comparison, two systems have been developed one with SCESS and the other without energy storage in RTDS. The response of the system for the applied fault is depicted from Figures 6.4-6.14. The grid voltage after the described fault is shown in Figure 6.4. Since power is being exchanged between the PV array and the SCESS, the

power generated from the PV array, P_{PV} is unaffected because of the fault at the grid side and is stored in the SCESS P_{SC} as shown in Figure 6.5. The oscillation of the grid power because of the fault is reduced for a system having a SCESS than without energy storage as shown in Figure 6.6. Figure 6.7 shows the power stored in the SCESS which is generated by the PV array during the fault. The inverter and fault currents during the applied fault are shown in Figure 6.8. The reactive power set point prior to the fault is zero but during the fault, the SCESS participates in riding the fault by increasing the reactive power Q_g as shown in Figure 6.9. The DC link voltage is controlled by the buck boost converter for the system having the SCESS but the inverter controls this voltage if there is no energy storage. As can be seen from Figure 6.10 the DC link voltage is kept constant to its reference value of 650 V for a system equipped with SCESS. The operation of the PV array is unaffected if the system has energy storage as shown in Figures.6.11-6.12. The PV array MPPT tracks the maximum voltage in spite of the fault as shown in Figure 6.13. The actual and reference charging current of the SCESS is shown in Figure 6.14.

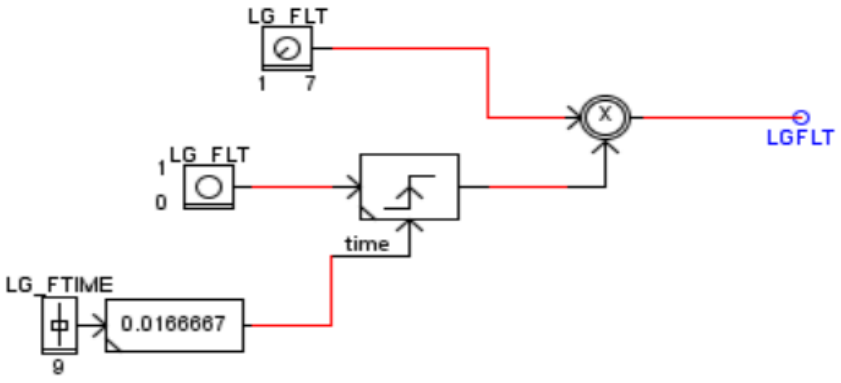

Figure 6.2: Applied three phase to ground fault controller

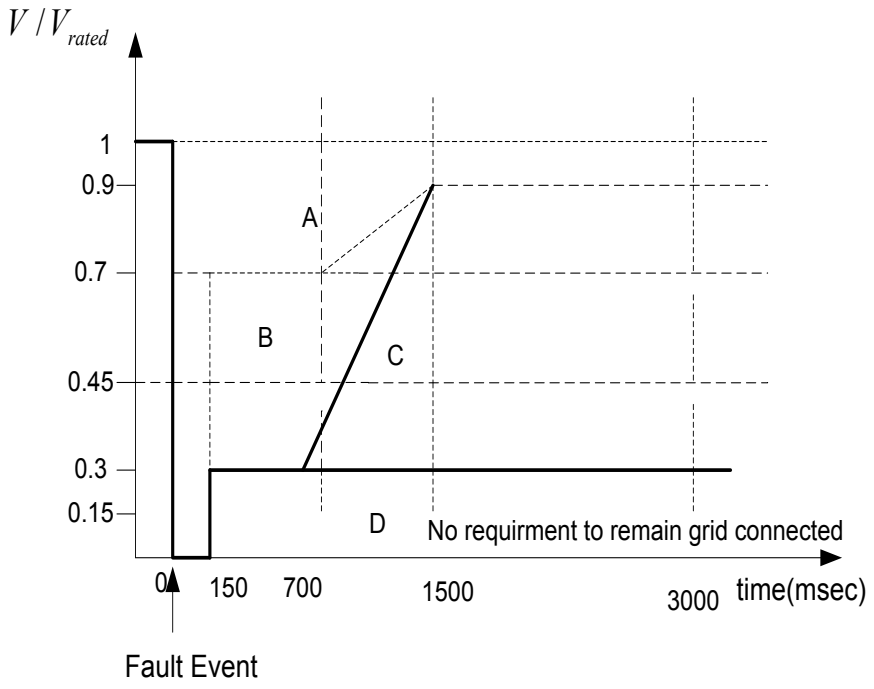

Figure 6.3: Low voltage ride through (LVRT) curve

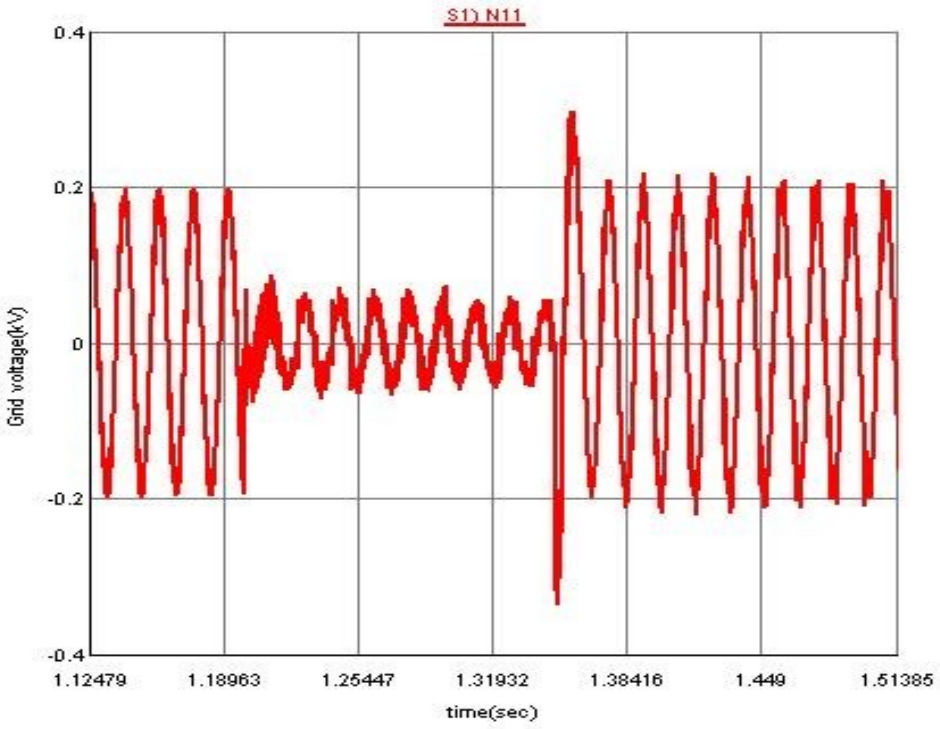

Figure 6.4: Grid voltage after three phase fault is applied

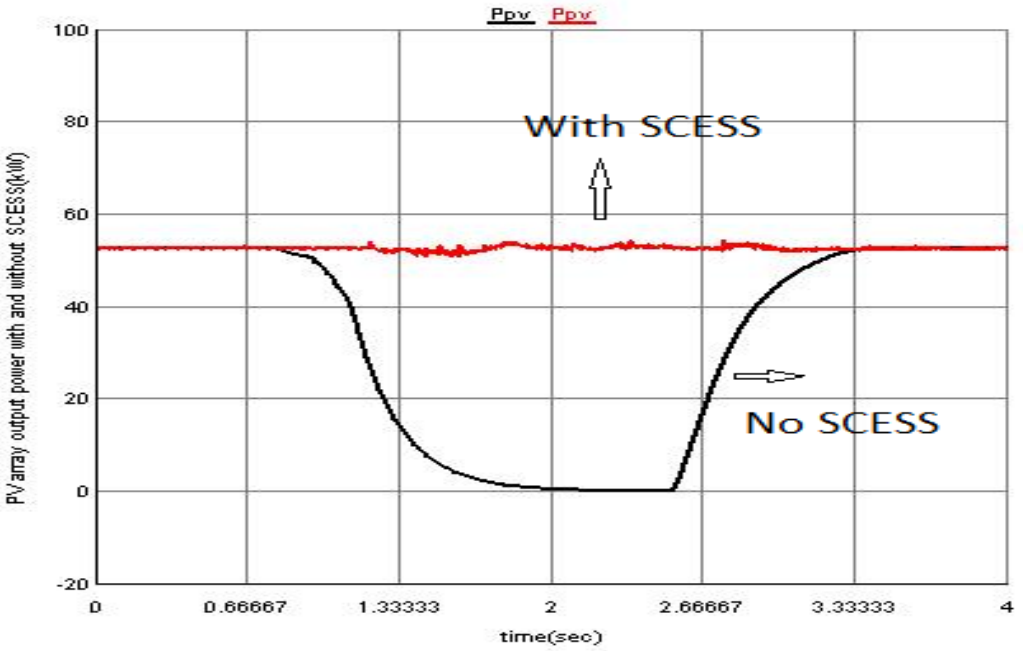

Figure 6.5: PV array power P_{PV} with SCESS and with no energy storage

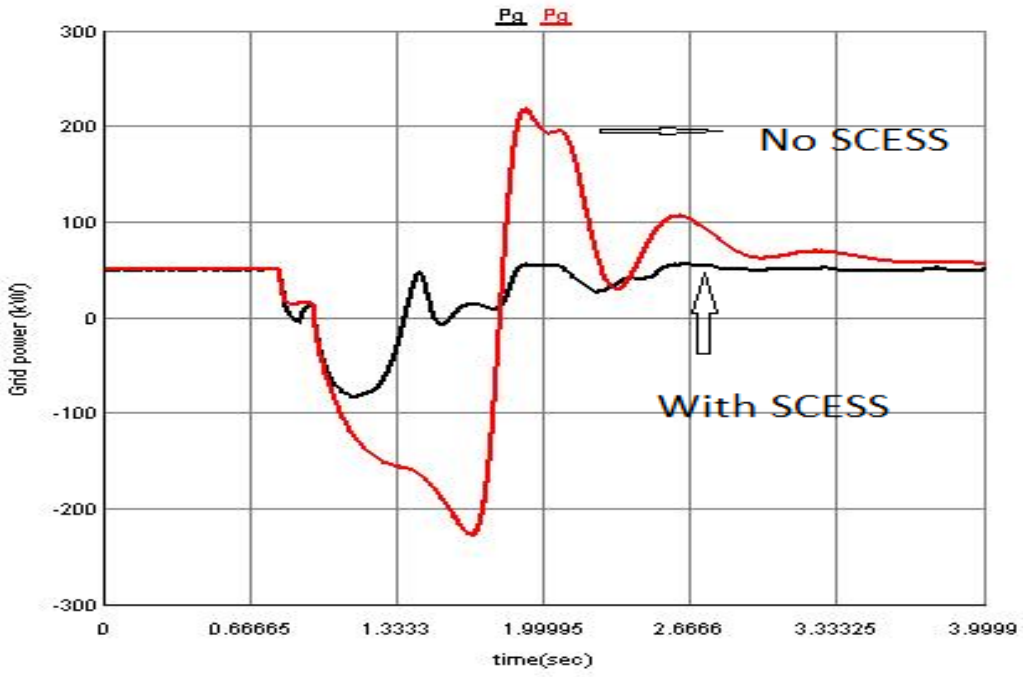

Figure 6.6: Grid active power P_g for a three phase fault with and without energy storage

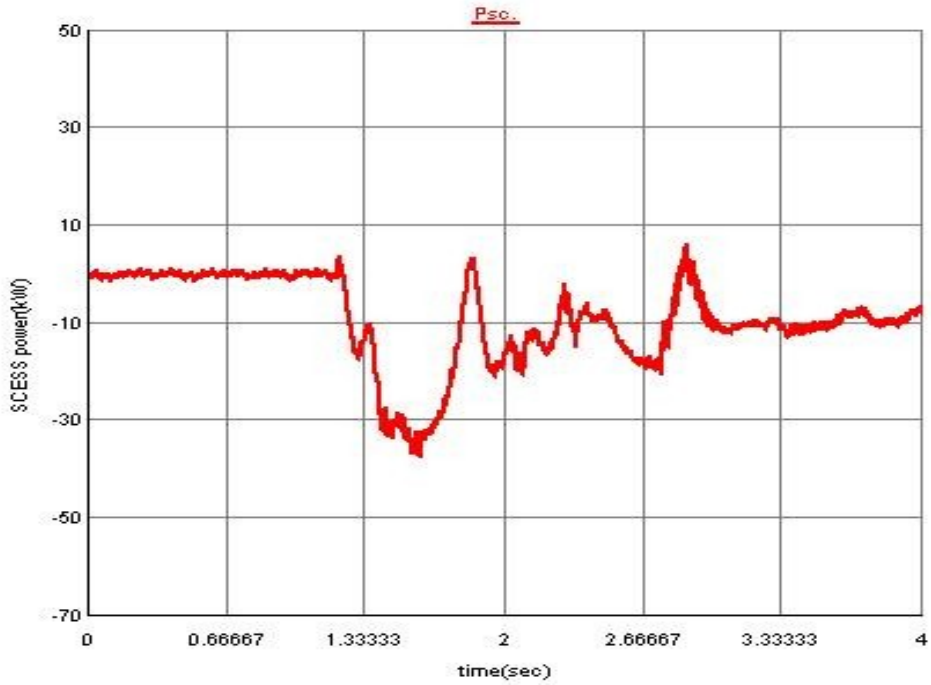

Figure 6.7: SCESS power P_{SC} for the applied fault on the grid side

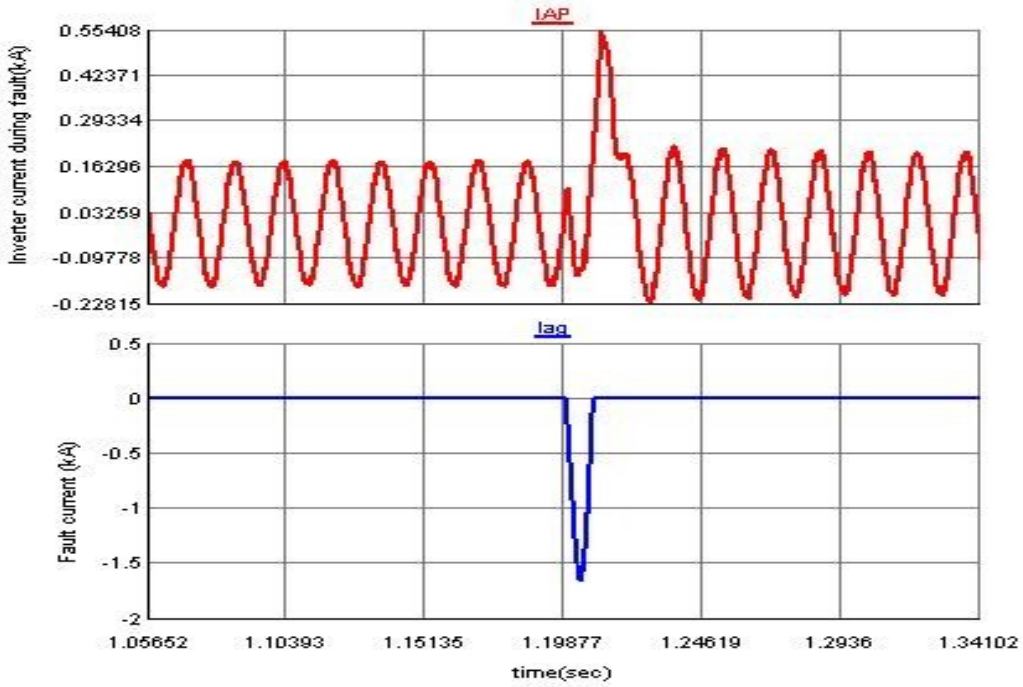

Figure 6.8: Inverter and fault currents

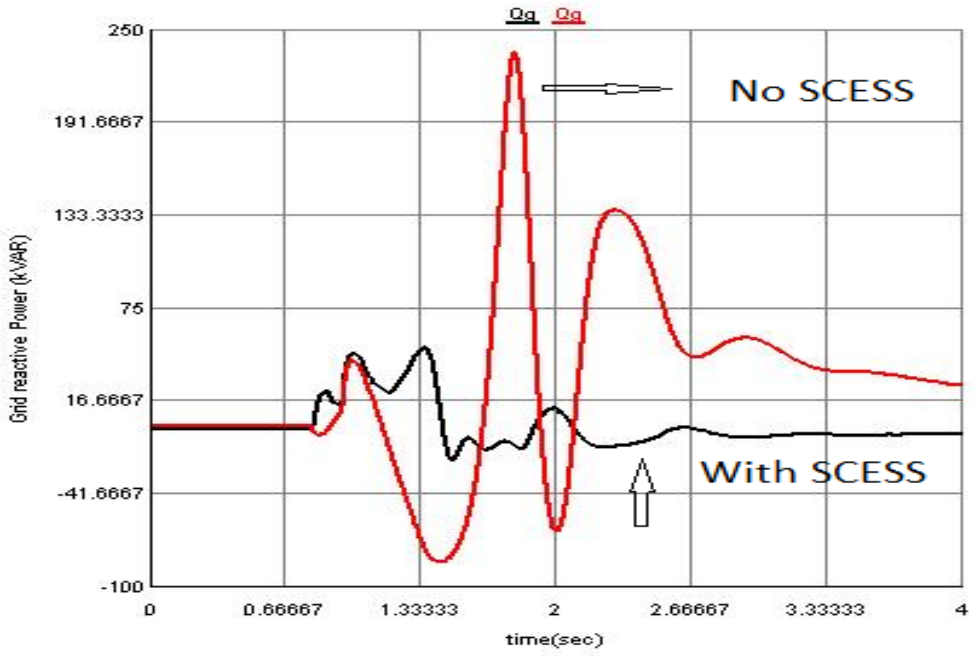

Figure 6.9: Grid reactive power Q_g during three phase fault

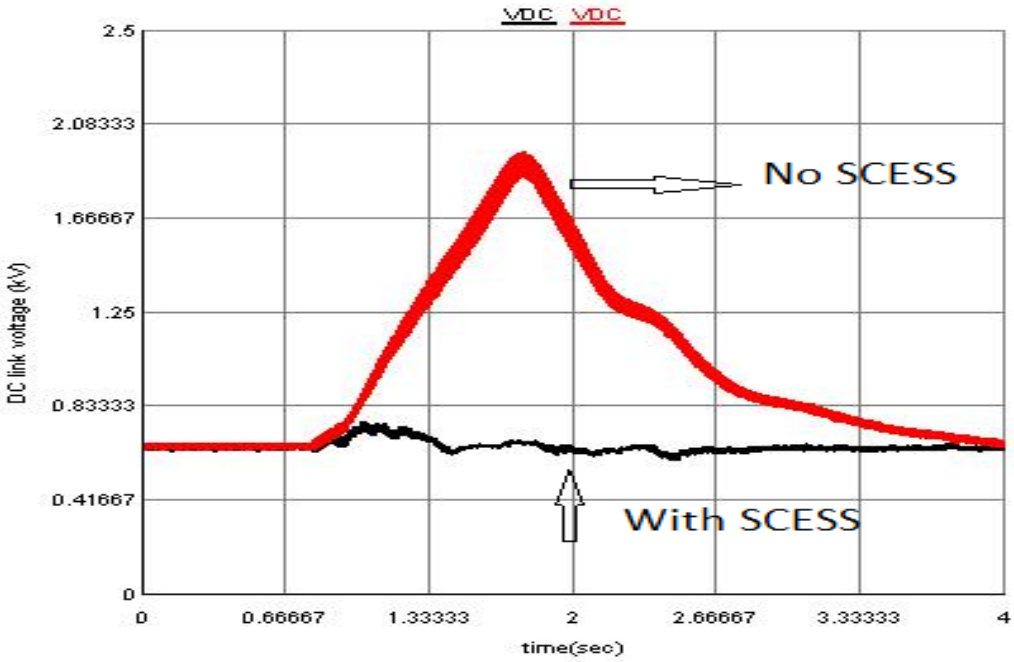

Figure 6.10: DC link voltage for the applied fault

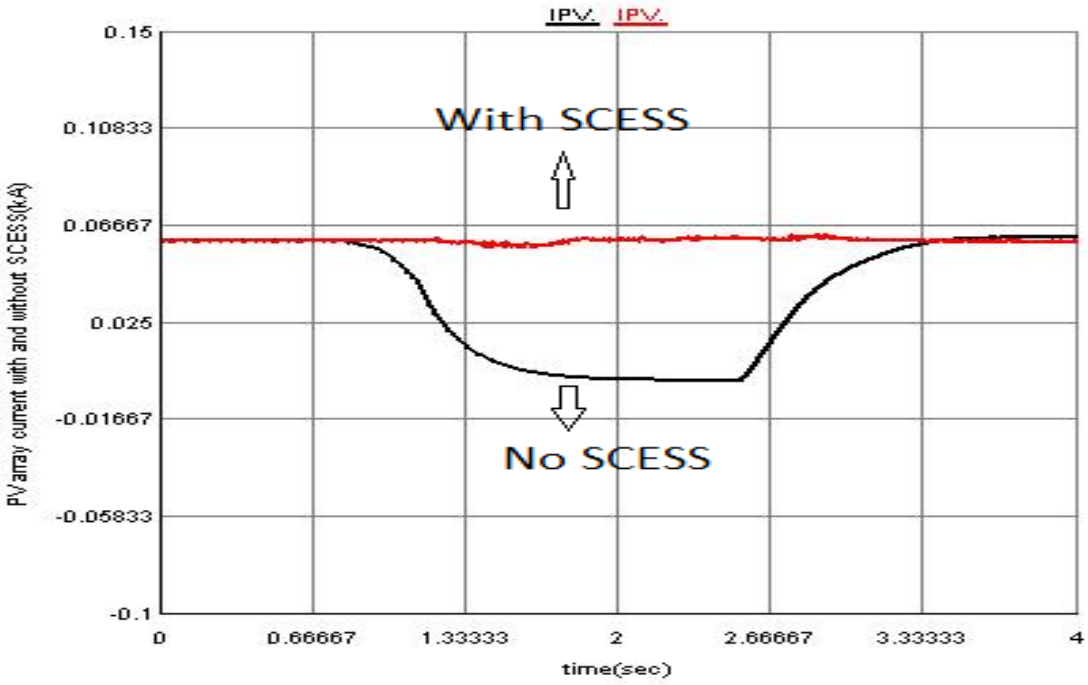

Figure 6.11: PV output current I_{PV} after three phase fault

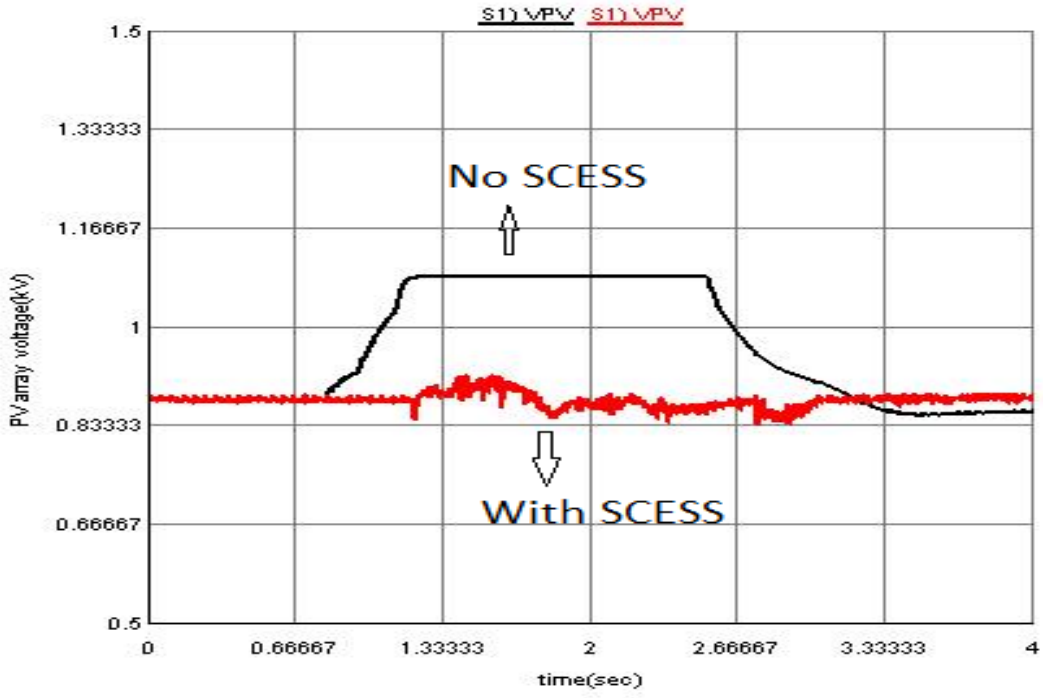

Figure 6.12: PV array voltage V_{PV} during three phase fault

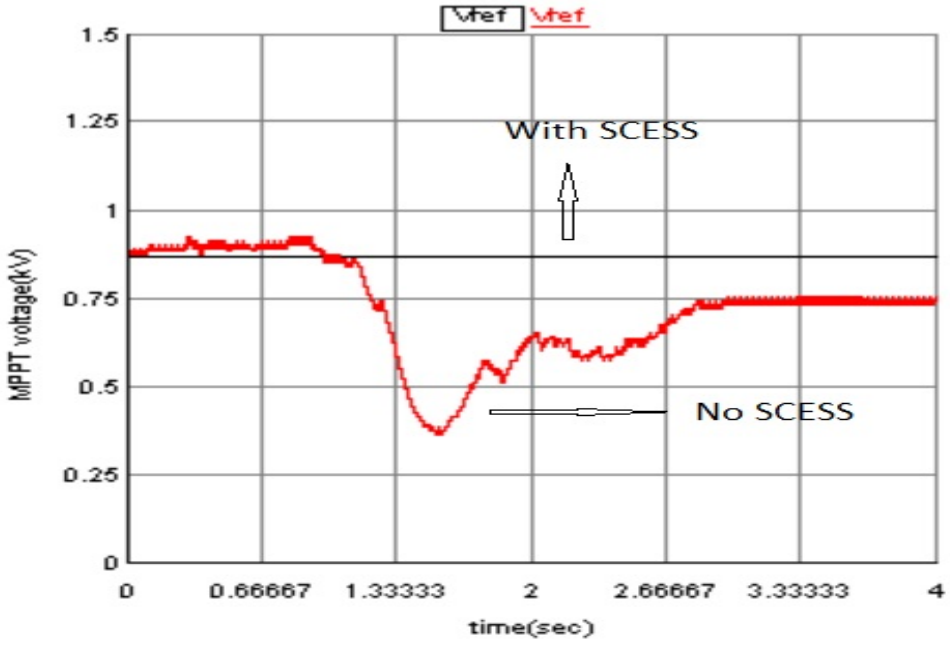

Figure 6.13: MPPT output voltage V_{ref} for the applied fault

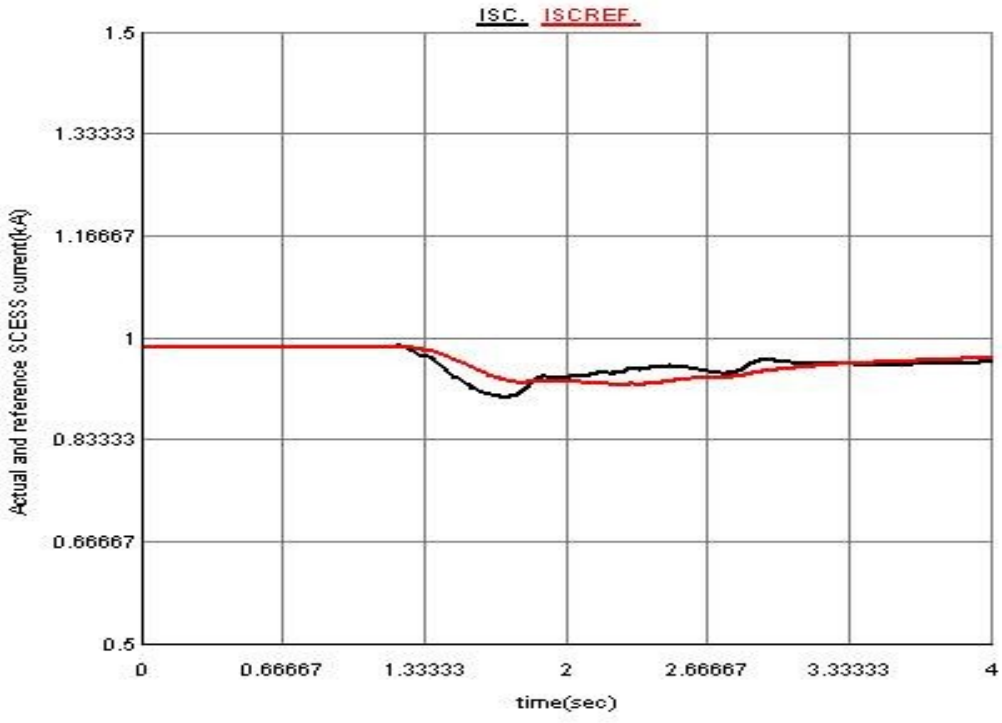

Figure 6.14: Actual and reference SCESS current during three phase fault

6.2 Fault Ride Through of Wind Turbine Generator using SCESS

The complete model adopted for fault ride through study of PMSG based wind turbine generator system using SCESS is presented in Figure 6.15. The same type of fault controller used for PV system is also applied here. During grid faults the speed of the generators increase causing offline tripping. Different countries have grid codes for LVRT standards having low voltage duration in the rage of 100-250 ms [148]. The German E.ON Netz GmbH's grid code for fault ride through is shown in Figure 6.16.

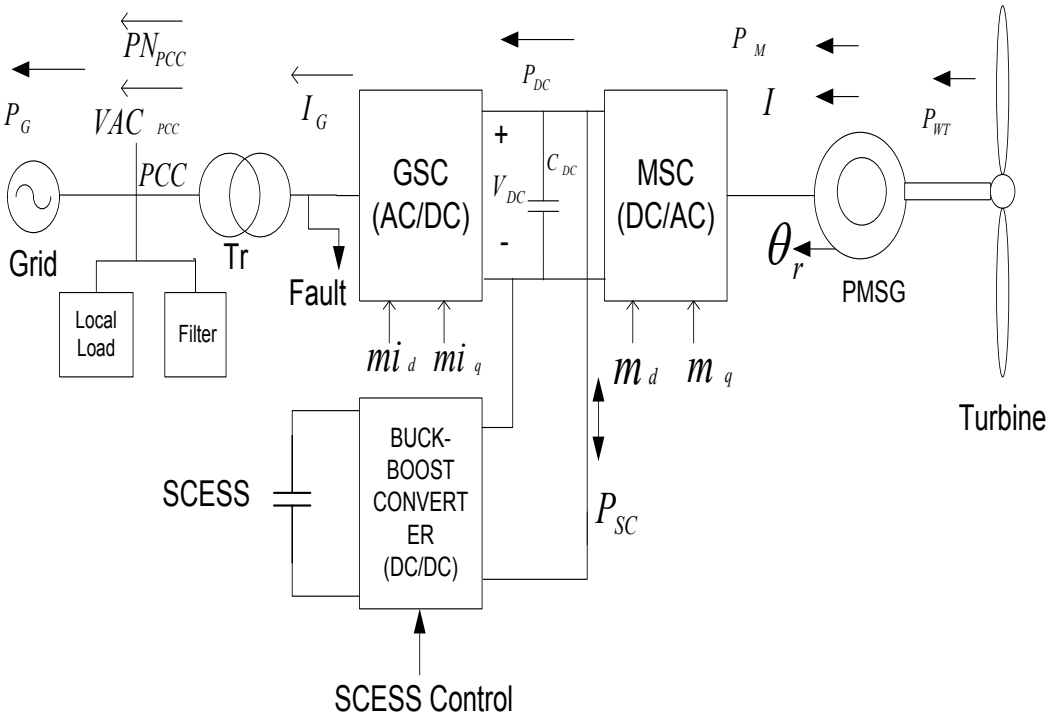

Figure 6.15: PMSG based WTG with the applied fault

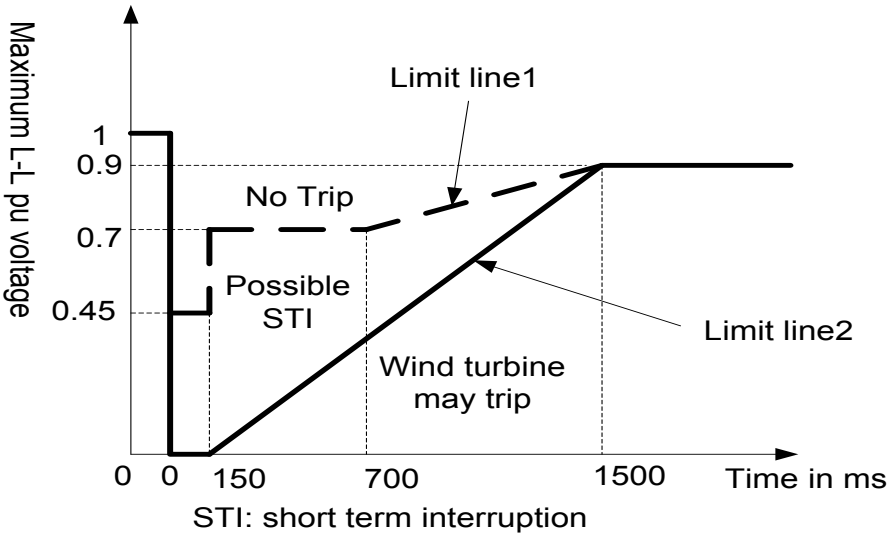

Figure 6.16: Fault ride through requirement in E.ON Netz GmbH's grid code

A severe three phase fault of sixty cycles (1sec) is applied on the grid side at t=0.8s and is cleared at t=1.8s. The response of the system for the applied fault is depicted from Figures 6.17-6.22. The PCC per unit (pu) V_{ACPCC} and phase N_1 voltages during the applied symmetrical fault is depicted in Figure 6.17. The fault is cleared with small spike at breaker closing. Figure 6.18 illustrates the generated power P_M, the DC link power P_{DC}, the PCC power P_{PCC} and the SCESS power P_{SC}. The generated power during the fault is stored in the SCESS and is transferred when the fault is cleared. The operation of the WTG is unaffected by the fault and is alive during the fault. Figure 6.19 illustrates the electrical torque T_e and generator speed w_e in pu. The DC link voltage is controlled to be constant with a reference value of 7.6 kV by the buck boost converter and except with small fluctuation, it is stable during the fault as can be seen from Figure 6.20. The figure also shows the SCESS voltage V_{SC} during the fault. The reactive power set point prior to the fault is zero but during the fault, the SCESS participates in riding the fault by

increasing the reactive power Q_{PCC} as shown in Figure 6.21. Q_s in Figure 6.21 is the grid reactive power after the filter. The charging and discharging currents of the SCESS during the three phase short circuit fault is depicted in Figure 6.22.

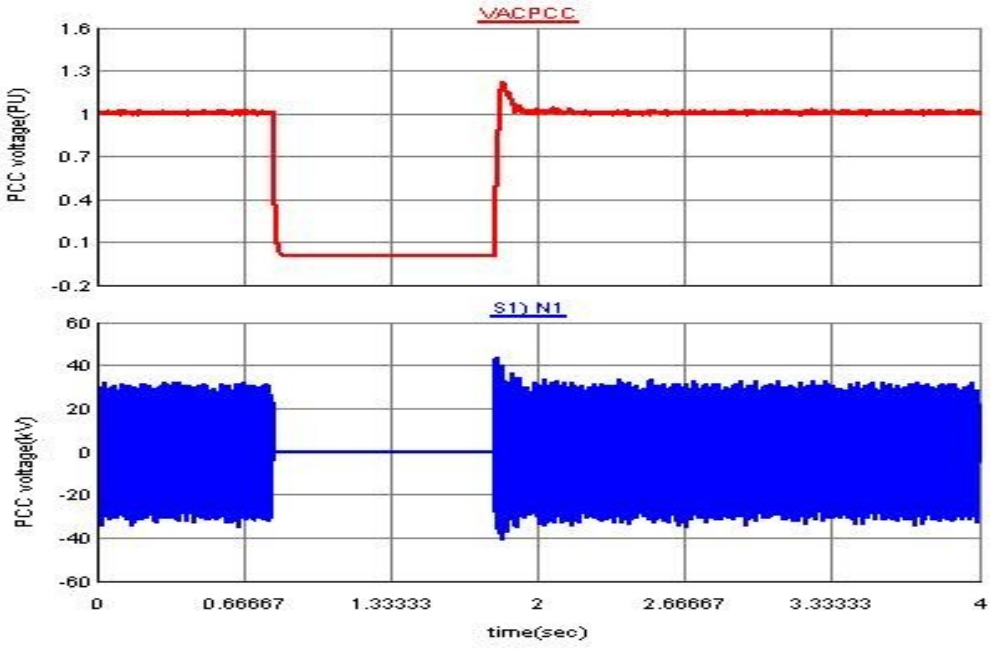

Figure 6.17: PCC pu voltage VAC_{PCC} and phase voltage N_1

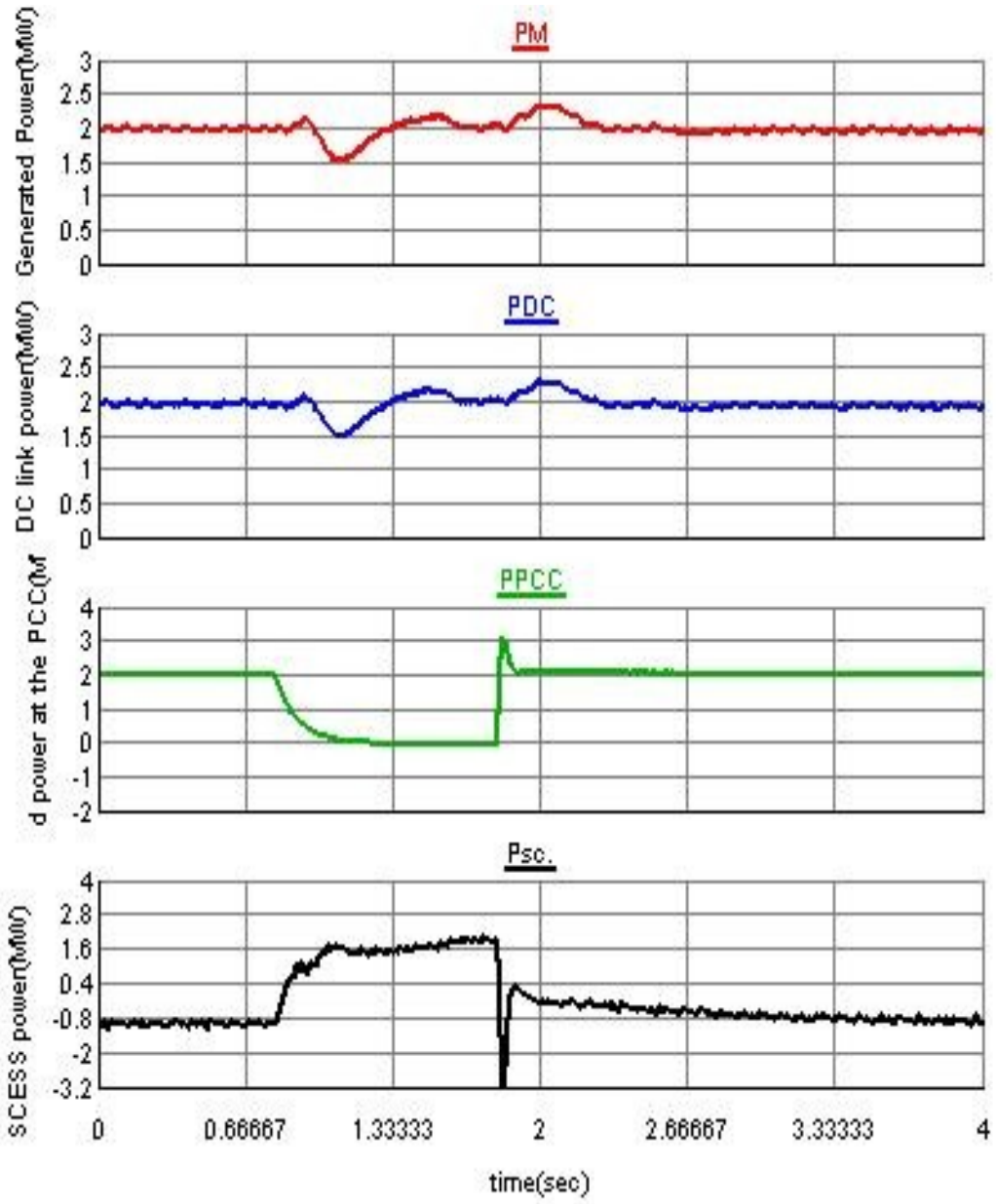

Figure 6.18: Generated power P_M, DC link power P_{DC}, PCC power P_{PCC} and SCESS power P_{SC}.

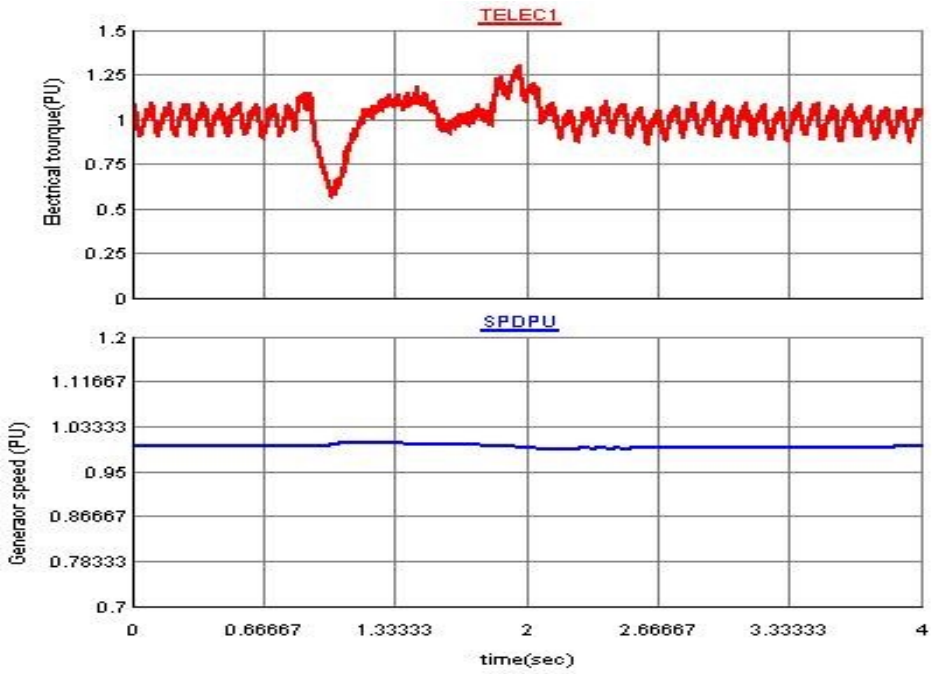

Figure 6.19: Electrical torque T_e, and generator speed w_e in pu

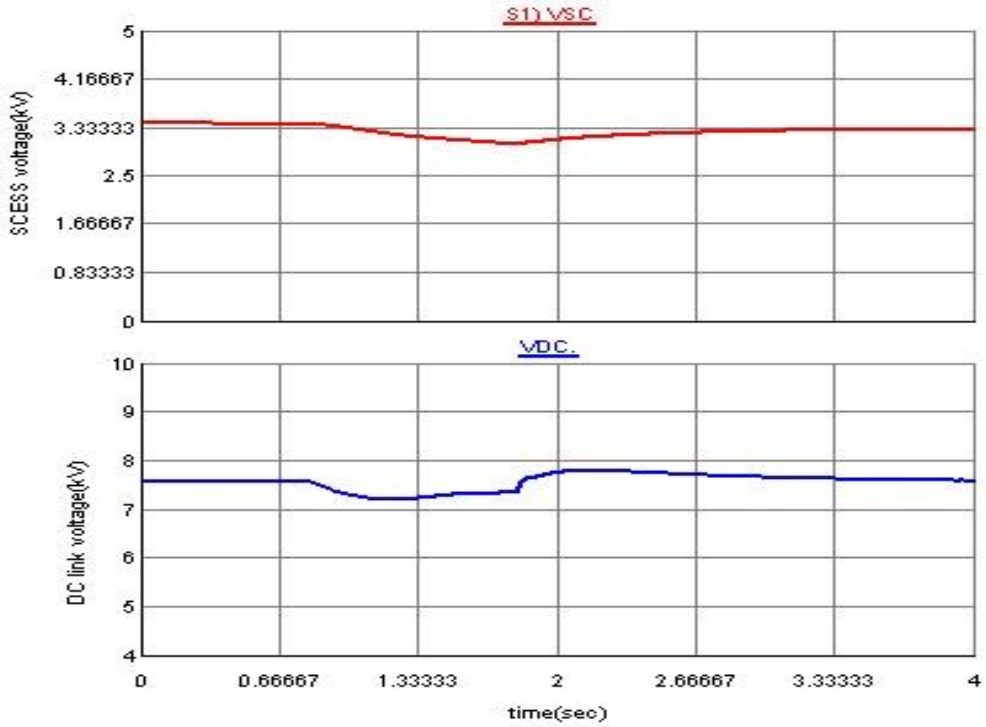

Figure 6.20: SCESS voltage V_{SC} and DC link voltage V_{DC}

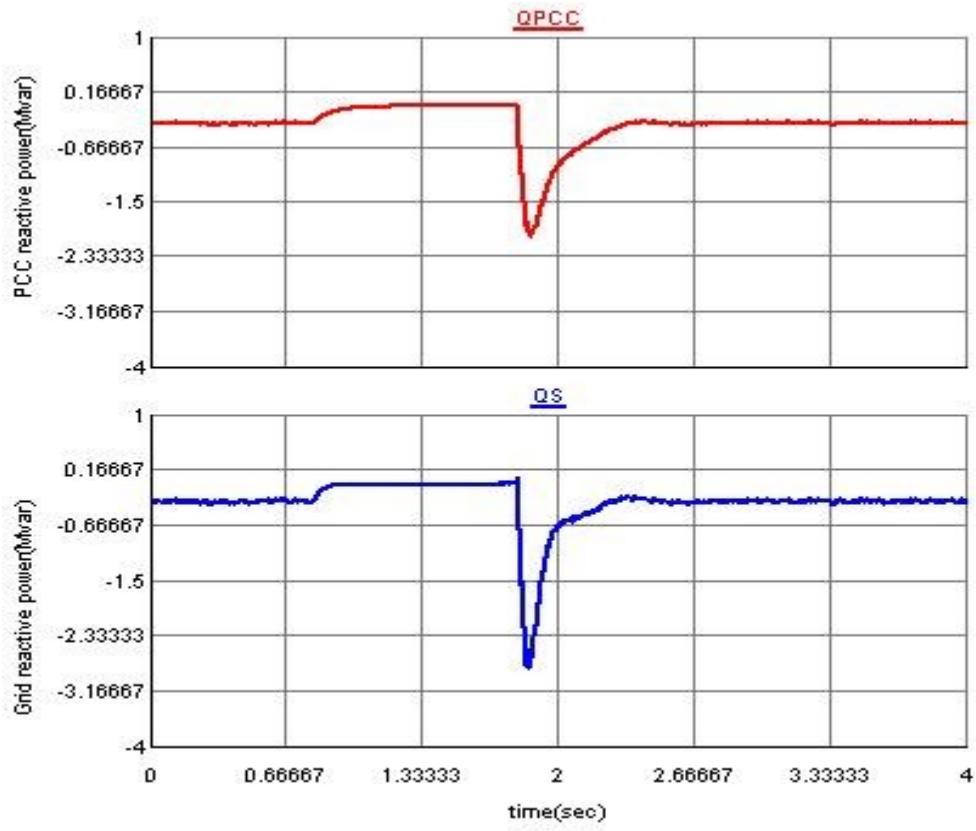

Figure 6.21: PCC reactive power Q_{PCC} and grid reactive power Q_S

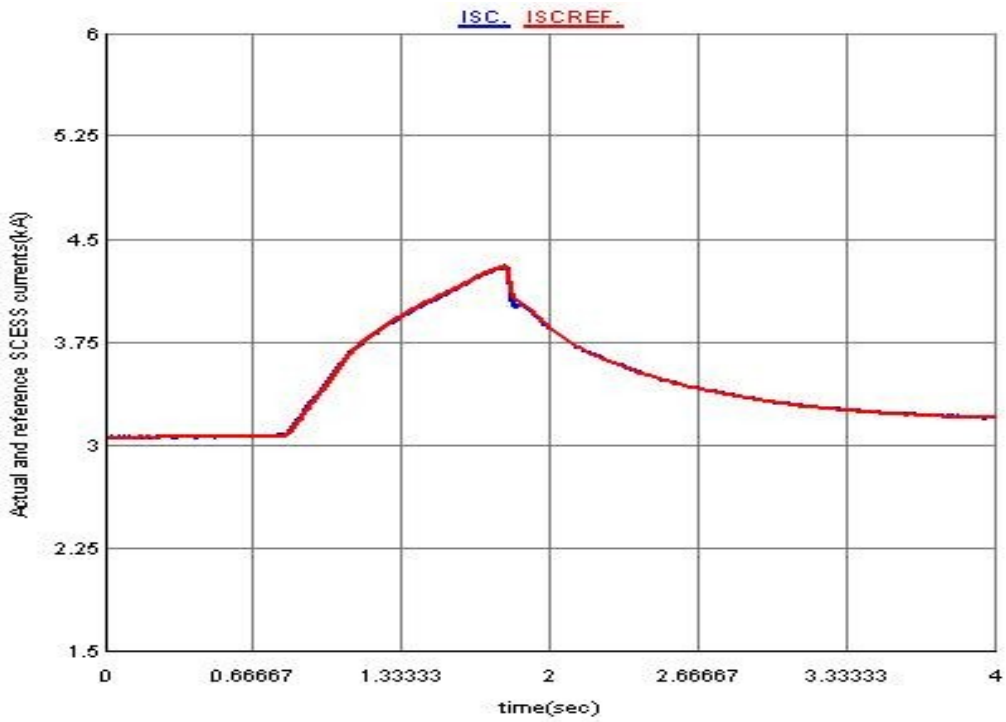

Figure 6.22: Actual and reference SCESS currents during the fault

6.3 CONCLUSION

This chapter presented the fault ride through capability of the system equipped with supercapacitor energy storage system (SCESS). The power generated during the fault duration in the renewable sources is stored in the SCESS that helps the system ride through the fault by providing both active and reactive power. The power generation system is unaffected because of the fault.

CHAPTER 7 CONCLUSIONS AND FUTURE WORK

CONCLUSIONS

A new control technique to minimize the fluctuation of the power generated from the renewable sources using supercapacitor energy storage system (SCESS) is presented in this dissertation. By varying the input parameters of the renewable sources, the controller is able to minimize the fluctuation by charging and discharging the SCESS. The SCESS is also used to provide the fault ride through capability of the system by storing the power generated in the SCESS during the fault duration. PV and wind are considered as renewable sources to study the effect of using SCESS in minimizing the power generation and for fault ride through.

PV SYSTEM

Grid connected PV system with and without energy storage system is investigated.

For grid connected PV system without energy storage:

- A multistage power converter using buck converter and an inverter are used to transfer the generated power to the grid.
- Maximum power point tracking (MPPT) control using incremental conductance is employed to generate the maximum power from the PV array using a buck converter. The duty of the buck converter is controlled to ensure that the PV array is generating the maximum available power.
- The optimal system parameters of the buck converter including the capacitor and inductor are designed.

- A P-Q controller is employed for the inverter to transfer the power from the DC link to the grid.
- The linear and non-linear models of the PV system are developed to design the control parameters of the PI regulators of the MPPT and P-Q controllers and to study the stability of the system using the Eigen value analysis.
- PSO is employed to optimize the controller parameters to shift the poorly damped poles to the left to make the system more stable.
- The proposed controller is tested by varying the input irradiation and temperature and the controller is able to transfer the generated power from the PV array directly to the grid.

For grid connected PV system using supercapacitor energy storage system:

- To minimize the fluctuation of the power generated from the PV array a supercapacitor energy storage system is connected at the DC link of the multistage PV system used in the grid connected PV system. The SCESS is connected to the DC link using a bidirectional buck boost converter.
- The optimal capacitance of the supercapacitor is designed. The capacitance is designed by taking into account the storage capacity with respect to the PV array capacity. The other system components of the buck boost converter are also designed.
- The optimal control parameters for the buck boost converter are obtained using the linear model developed.

- A controller is implemented to control the DC link voltage by the buck boost converter. The function of the buck converter remains the same to locate the maximum power point.
- A constant P-Q controller is implemented for the inverter to transfer the available DC link power to the grid. Set points are provided to transfer specific power to the grid and the rest to charge and discharge the SCESS.
- The performance of the system is evaluated by varying the irradiation and temperature. The obtained results proved the capacity of the SCESS to minimize the fluctuation of the generated power from the PV array.

WIND SYSTEM

Grid connected wind turbine generator (WTG) using permanent magnet synchronous generator (PMSG) is considered. The power generated from the WTG system is connected to the grid using a two three level neutral point clamped voltage source converters. The SCESS is connected to the DC link using a buck boost converter similar to the PV configuration.

- The PMSG is modeled as an interior magnet with sinusoidally distributed windings.
- The controller proposed and implemented for the machine side converter ensures that the PMSG is generating the maximum available power from the varying wind speed.
- The controller proposed and implemented for the grid side converter is responsible to transfer the available DC link power to the grid.

- The controller employed for the buck boost converter minimizes the fluctuation generated from the WTG by charging and discharging the SCESS.
- The developed system has been tested and the results verified the proposed controller's capability in minimizing the fluctuation in wind sources.

FAULT RIDE THROUGH

The developed power generation model using PV array and WTG has been tested for fault ride through enhancement. One requirement of power generation using renewable sources is that they need to have a fault ride through capability. The system has to be connected to the grid according to the fault ride through curve provided by grid code.

- For the PV system, two models are developed to study the fault ride through capability: one with energy storage and the other one without. The capacitance of the SCESS is designed to handle the generated power during the fault. A three phase fault has been applied on the grid side and the performance of the system has been reported. For the system equipped with SCESS, the operation of the PV array is unaffected as power is exchanged between the SCESS and the PV array. The system was able to ride through the fault as the SCESS has participated by providing active and reactive power. The operation of the inverter is also protected as the DC link voltage is controlled by the buck boost converter.

- For the WTG based on PMSG, a three phase fault is applied at the grid side similar to the PV case and the system can ride through the fault even if the fault duration is more than five seconds.

FUTURE WORK

The work presented in this dissertation can be extended in the future by addressing topics such as:

- The set points of the P-Q controller for the inverter are obtained manually in this dissertation. This work can be extended by obtaining the set points in closed loop depending on the power generated from the PV, WTG and the SCESS power.
- Different control techniques such as sliding mode, optimal control can be implemented.
- Different optimization techniques can be implemented to find the optimal control parameters.
- The grid connected and island modes can be implemented in the same model and a controller can be proposed to shift from grid mode to island mode depending on the control strategy. The transient analysis can be performed on the developed model.

References

[1] I. Confederation and E. Regulators, "International Confederation of Energy Regulators REPORT on Renewable Energy and Distributed Generation : International Case Studies on Technical and Economic Considerations Ref : I12-CC-17-03," no. February, pp. 1–154, 2012.

[2] P. Basak, S. Chowdhury, S. Halder Nee Dey, and S. P. Chowdhury, "A literature review on integration of distributed energy resources in the perspective of control, protection and stability of microgrid," Renew. Sustain. Energy Rev., vol. 16, no. 8, pp. 5545–5556, 2012.

[3] H. Jiayi, J. Chuanwen, and X. Rong, "A review on distributed energy resources and MicroGrid," Renew. Sustain. Energy Rev., vol. 12, no. 9, pp. 2465–2476, 2008.

[4] J. H. Jeon, J. Y. Kim, H. M. Kim, S. K. Kim, C. Cho, J. M. Kim, J. B. Ahn, and K. Y. Nam, "Development of hardware in-the-loop simulation system for testing operation and control functions of microgrid," IEEE Trans. Power Electron., vol. 25, no. 12, pp. 2919–2929, 2010.

[5] R. Majumder, A. Ghosh, G. Ledwich, and F. Zare, "Power management and power flow control with back-to-back converters in a utility connected microgrid," IEEE Trans. Power Syst., vol. 25, no. 2, pp. 821–834, 2010.

[6] F. Katiraei and M. R. Iravani, "Power Management Strategies for a Microgrid With Multiple Distributed Generation Units.Pdf," vol. 21, no. 4, pp. 1821–1831, 2006.

[7] D. Singh, D. Singh, and K. S. Verma, "Multiobjective optimization for DG planning with load models," IEEE Trans. Power Syst., vol. 24, no. 1, pp. 427–436, 2009.

[8] J. P. Barton and D. G. Infield, "Energy storage and its use with intermittent renewable energy," IEEE Trans. Energy Convers., vol. 19, no. 2, pp. 441–448, 2004.

[9] P. F. Ribeiro, B. K. Johnson, M. L. Crow, a Arsoy, and Y. Liu, "Energy storage systems for advanced power applications," Proc. IEEE, vol. 89, no. 12, pp. 1744–1756, 2001.

[10] J. M. Carrasco, L. G. Franquelo, J. T. Bialasiewicz, S. Member, E. Galván, R. C. P. Guisado, S. Member, M. Ángeles, M. Prats, J. I. León, and N. Moreno-alfonso,

"Power-Electronic Systems for the Grid Integration of Renewable Energy Sources : A Survey," Ieee Trans. Ind. Electron., vol. 53, no. 4, pp. 1002–1016, 2006.

[11] J. Z. J. Zhang, "Research on Super Capacitor Energy Storage System for Power Network," 2005 Int. Conf. Power Electron. Drives Syst., vol. 2, pp. 1366–1369, 2005.

[12] Chi-Jui Wu and Yuang-Shung Lee, "Application of superconducting magnetic energy storage unit to improve the damping of synchronous generator," IEEE Trans. Energy Convers., vol. 6, pp. 573–578, 1991.

[13] S. F. O. R. Analysis, "Application of supercondricting magnet energy storage," vol. 3, no. 4, pp. 1418–1425, 1988.

[14] T. Ise, Y. Murakami, and K. Tsuji, "Simultaneous active and reactive power control of superconducting magnet energy storage using GTO converter," Trans. Power Deliv. IEEE, vol. PWRD-1, no. 1, pp. 143–150, 1986.

[15] S. C. Banerjee, S., Chatterjee, J. K., and Tripathy, "Application of Magnetic Energy Storage Unit as Load-Frequency Stabilizer," IEEE Trans. Energy Converions., vol. 5, no. 1, pp. 46–51, 1990.

[16] a P. V. G. System, "A Study on Optimal Sizing of Superconducting Magnetic Energy Storage in Distribution Power System," IEEE Trans. Appl. Supercond., vol. 22, no. 3, pp. 5701004–5701004, 2012.

[17] C. a. Hill, M. C. Such, D. Chen, J. Gonzalez, and W. M. Grady, "Battery energy storage for enabling integration of distributed solar power generation," IEEE Trans. Smart Grid, vol. 3, no. 2, pp. 850–857, 2012.

[18] P. Mercier, R. Cherkaoui, and A. Oudalov, "Optimizing a battery energy storage system for frequency control application in an isolated power system," IEEE Trans. Power Syst., vol. 24, no. 3, pp. 1469–1477, 2009.

[19] L. Wang, J.-Y. Yu, and Y.-T. Chen, "Dynamic stability improvement of an integrated offshore wind and marine-current farm using a flywheel energy-storage system," IET Renew. Power Gener., vol. 5, no. January, p. 387, 2011.

[20] M. Martinez, M. G. Molina, F. Frack, and P. E. Mercado, "Dynamic Modeling, Simulation and Control of Hybrid Energy Storage System Based on Compressed Air and Supercapacitors," Lat. Am. Trans. IEEE (Revista IEEE Am. Lat., vol. 11, no. 1, pp. 466–472, 2013.

[21] S. Lemofouet and a. Rufer, “A Hybrid Energy Storage System Based on Compressed Air and Supercapacitors With Maximum Efficiency Point Tracking (MEPT),” IEEE Trans. Ind. Electron., vol. 53, no. 4, pp. 1105–1115, 2006.

[22] D. J. Swider, “Compressed air energy storage in an electricity system with significant wind power generation,” IEEE Trans. Energy Convers., vol. 22, no. 1, pp. 95–102, 2007.

[23] G. L. Bullard, H. B. Sierra-Alcazar, H. L. Lee, and J. L. Morris, “Operating principles of the ultracapacitor.,” IEEE Trans. Magn., vol. 25, no. 1, pp. 102–106, 1989.

[24] M. U. D. Mufti, S. A. Lone, S. J. Iqbal, M. Ahmad, and M. Ismail, “Super-capacitor based energy storage system for improved load frequency control,” Electr. Power Syst. Res., vol. 79, pp. 226–233, 2009.

[25] T. Wei, S. Wang, and Z. Qi, “Design of supercapacitor based ride through system for wind turbine pitch systems,” Proceeding Int. Conf. Electr. Mach. Syst. ICEMS 2007, pp. 294–297, 2007.

[26] K. Sahay and B. Dwivedi, “Supercapacitors Energy Storage System for Power Quality Improvement : An Overview,” Quality, vol. 5, 2009.

[27] S. S. Choi, K. J. Tseng, S. Member, D. M. Vilathgamuwa, and T. D. Nguyen, “Energy Storage Systems in Distributed Generation Schemes,” Practice, pp. 1–8, 2008.

[28] A. Virtanen and H. Tuusa, “Power compensator for high power fluctuating loads with a supercapacitor bank energy storage,” PECon 2008 - 2008 IEEE 2nd Int. Power Energy Conf., no. PECon 08, pp. 977–982, 2008.

[29] S. M. Halpin, “Revisions to IEEE Standard 519-1992,” pp. 1–3, 1992.

[30] X. Chen and Y. Li, “An Islanding Detection Algorithm for Inverter-Based Distributed Generation Based on Reactive Power Control,” IEEE Trans. Power Electron., vol. 29, no. 9, pp. 4672–4683, 2014.

[31] T. S. Basso and R. DeBlasio, “IEEE 1547 series of standards: Interconnection issues,” IEEE Trans. Power Electron., vol. 19, no. 5, pp. 1159–1162, 2004.

[32] Ieee, IEEE Application Guide for IEEE Std 1547(TM), IEEE Standard for Interconnecting Distributed Resources with Electric Power Systems, no. April. 2009.

[33] IEEE.Standards-1547.6, IEEE Recommended Practice for Interconnecting Distributed Resources with Electric Power Systems Distribution Secondary N

etworks IEEE Standards Coordinating Committee 21 Sponsored by the, no. September. 2011.

[34] S. Electricity, The Saudi Arabian Distribution Code, no. November. 2008, pp. 1–87.

[35] K. Ishaque and Z. Salam, “A review of maximum power point tracking techniques of PV system for uniform insolation and partial shading condition,” Renew. Sustain. Energy Rev., vol. 19, pp. 475–488, 2013.

[36] A. Reza Reisi, M. Hassan Moradi, and S. Jamasb, “Classification and comparison of maximum power point tracking techniques for photovoltaic system: A review,” Renew. Sustain. Energy Rev., vol. 19, pp. 433–443, 2013.

[37] B. Subudhi and R. Pradhan, “A comparative study on maximum power point tracking techniques for photovoltaic power systems,” IEEE Trans. Sustain. Energy, vol. 4, no. 1, pp. 89–98, 2013.

[38] S. Qin, M. Wang, T. Chen, and X. Yao, “Comparative analysis of incremental conductance and perturb-and-observation methods to implement MPPT in photovoltaic system,” 2011 Int. Conf. Electr. Control Eng. ICECE 2011 - Proc., pp. 5792–5795, 2011.

[39] A. Safari and S. Mekhilef, “Simulation and hardware implementation of incremental conductance MPPT with direct control method using cuk converter,” IEEE Trans. Ind. Electron., vol. 58, no. 4, pp. 1154–1161, 2011.

[40] M. a. S. Masoum, H. Dehbonei, and E. F. Fuchs, “Theoretical and experimental analyses of photovoltaic systems with voltageand current-based maximum power-point tracking,” IEEE Trans. Energy Convers., vol. 17, no. 4, pp. 514–522, 2002.

[41] B. Alajmi, K. Ahmed, S. Finney, and B. Williams, “Fuzzy logic controlled approach of a modified hill climbing method for maximum power point in microgrid stand-alone photovoltaic system,” IEEE Trans. Power Electron., vol. 26, no. 4, pp. 1022–1030, 2011.

[42] Y. Zheng, C. Wei, and S. Lin, “A maximum power point tracking method based on tabu search for PV systems under partially shaded conditions,” IET Conf. Renew. Power Gener. (RPG 2011), pp. 52–52, 2011.

[43] R. Ramaprabha, V. Gothandaraman, K. Kanimozhi, R. Divya, and B. L. Mathur, “Maximum power point tracking using GA-optimized artificial neural network for Solar PV system,” 2011 1st Int. Conf. Electr. Energy Syst., no. 1, pp. 264–268, 2011.

[44] N. Khaehintung, P. Sirisuk, and a Kunakorn, “Grid-connected Photovoltaic System with Maximum Power Point Tracking using Self-Organizing Fuzzy Logic Controller,” 2002 IEEE Power Eng. Soc. Winter Meet. Conf. Proc. Cat No02CH37309, vol. 1, pp. 372–377, 2002.

[45] J. S. R. Jang, “ANFIS: adaptive-network-based fuzzy inference system,” IEEE Trans. Syst. Man Cybern., vol. 23, no. 3, pp. 665–685, 1993.

[46] A. M. S. Aldobhani, “Maximum power point tracking of PV system using ANFIS prediction and fuzzy logic tracking.,” vol. II, pp. 19–21, 2008.

[47] F. Mayssa and L. Sbita, “Advanced ANFIS-MPPT control algorithm for sunshine photovoltaic pumping systems,” 2012 1st Int. Conf. Renew. Energies Veh. Technol. REVET 2012, pp. 167–172, 2012.

[48] N. Femia, G. Petrone, G. Spagnuolo, and M. Vitelli, “Optimization of perturb and observe maximum power point tracking method,” IEEE Trans. Power Electron., vol. 20, no. 4, pp. 963–973, 2005.

[49] D. Sera and R. Teodorescu, “Optimized maximum power point tracker for fast changing environmental conditions,” Ind. Electron. IEEE Trans., pp. 2401–2407, 2008.

[50] M. a. Elgendy, B. Zahawi, and D. J. Atkinson, “Assessment of perturb and observe MPPT algorithm implementation techniques for PV pumping applications,” IEEE Trans. Sustain. Energy, vol. 3, no. 1, pp. 21–33, 2012.

[51] E. S. Sreeraj, K. Chatterjee, and S. Bandyopadhyay, “One-Cycle-Controlled Single-Stage Single-Phase Voltage-Sensorless Grid-Connected PV System,” vol. 60, no. 3, pp. 1216–1224, 2013.

[52] G. Tsengenes and G. Adamidis, “Investigation of the behavior of a three phase grid-connected photovoltaic system to control active and reactive power,” Electr. Power Syst. Res., vol. 81, no. 1, pp. 177–184, 2011.

[53] A. Yazdani, A. R. Di Fazio, H. Ghoddami, M. Russo, M. Kazerani, J. Jatskevich, K. Strunz, S. Leva, and J. a. Martinez, “Modeling guidelines and a benchmark for power system simulation studies of three-phase single-stage photovoltaic systems,” IEEE Trans. Power Deliv., vol. 26, no. 2, pp. 1247–1264, 2011.

[54] G. Velasco-Quesada, F. Guinjoan-Gispert, R. Piqué-López, M. Román-Lumbreras, and A. Conesa-Roca, “Electrical PV array reconfiguration strategy for energy extraction improvement in grid-connected PV systems,” IEEE Trans. Ind. Electron., vol. 56, no. 11, pp. 4319–4331, 2009.

[55] F. Ruz, a. Rey, J. M. Torrelo, a. Nieto, and F. J. Cánovas, “Real time test benchmark design for photovoltaic grid-connected control systems,” Electr. Power Syst. Res., vol. 81, no. 4, pp. 907–914, 2011.

[56] X. Guo, J. Chen, and Q. Liu, “Real-time and grid-connected control of PV power system,” APAP 2011 - Proc. 2011 Int. Conf. Adv. Power Syst. Autom. Prot., vol. 2, pp. 923–928, 2011.

[57] J. Selvaraj and N. a. Rahim, “Multilevel Inverter For Grid-Connected PV System Employing Digital PI Controller,” IEEE Trans. Ind. Electron., vol. 56, no. 1, pp. 149–158, 2009.

[58] G. Spagnuolo, J. Jatskevich, and S. Member, “Efficient Approaches for Modeling and Simulating Photovoltaic Power Systems,” vol. 3, no. 1, pp. 500–508, 2013.

[59] C. Luo, H. Banakar, B. Shen, and B.-T. Ooi, “Strategies to Smooth Wind Power Fluctuations of Wind Turbine Generator,” IEEE Trans. Energy Convers., vol. 22, no. 2, pp. 341–349, 2007.

[60] A. Woyte, V. Van Thong, R. Belmans, and J. Nijs, “Voltage fluctuations on distribution level introduced by photovoltaic systems,” IEEE Trans. Energy Convers., vol. 21, no. 1, pp. 202–209, 2006.

[61] X. Tan, Q. Li, and H. Wang, “Advances and trends of energy storage technology in Microgrid,” Int. J. Electr. Power Energy Syst., vol. 44, no. 1, pp. 179–191, 2013.

[62] A. Rufer, D. Hotellier, and P. Barrade, “A supercapacitor-based energy storage substation for voltage compensation in weak transportation networks,” IEEE Trans. Power Deliv., vol. 19, no. 2, pp. 629–636, 2004.

[63] Y. Cheng, “Assessments of energy capacity and energy losses of supercapacitors in fast charging-discharging cycles,” IEEE Trans. Energy Convers., vol. 25, no. 1, pp. 253–261, 2010.

[64] Z. Yang, C. Shen, L. Zhang, M. L. Crow, and S. Atcitty, “Integration of a StatCom and battery energy storage,” IEEE Trans. Power Syst., vol. 16, no. 2, pp. 254–260, 2001.

[65] M. M. Mahmoud, “On the storage batteries used in solar electric power systems and development of an algorithm for determining their ampere-hour capacity,” Electr. Power Syst. Res., vol. 71, no. 1, pp. 85–89, 2004.

[66] S. I. Gkavanoudis and C. S. Demoulias, “A combined fault ride-through and power smoothing control method for full-converter wind turbines employing

Supercapacitor Energy Storage System," Electr. Power Syst. Res., vol. 106, pp. 62–72, 2014.

[67] a. H. M. a Rahim and E. P. Nowicki, "Supercapacitor energy storage system for fault ride-through of a DFIG wind generation system," Energy Convers. Manag., vol. 59, pp. 96–102, 2012.

[68] N. a. Ahmed, a. K. Al-Othman, and M. R. Alrashidi, "Development of an efficient utility interactive combined wind/photovoltaic/fuel cell power system with MPPT and DC bus voltage regulation," Electr. Power Syst. Res., vol. 81, no. 5, pp. 1096–1106, 2011.

[69] B. Bahmani-Firouzi and R. Azizipanah-Abarghooee, "Optimal sizing of battery energy storage for micro-grid operation management using a new improved bat algorithm," Int. J. Electr. Power Energy Syst., vol. 56, pp. 42–54, 2014.

[70] H. Jia, Y. Mu, and Y. Qi, "A statistical model to determine the capacity of battery-supercapacitor hybrid energy storage system in autonomous microgrid," Int. J. Electr. Power Energy Syst., vol. 54, pp. 516–524, 2014.

[71] H. Kanchev, D. Lu, F. Colas, V. Lazarov, and B. Francois, "Energy management and operational planning of a microgrid with a PV based active generator for smart grid applications," IEEE Trans. Ind. Electron., vol. 58, no. 10, pp. 4583–4592, 2011.

[72] E. Perez, H. Beltran, N. Aparicio, and P. Rodriguez, "Predictive power control for PV plants with energy storage," IEEE Trans. Sustain. Energy, vol. 4, no. 2, pp. 482–490, 2013.

[73] P. Thounthong, "Model based-energy control of a solar power plant with a supercapacitor for grid-independent applications," IEEE Trans. Energy Convers., vol. 26, no. 4, pp. 1210–1218, 2011.

[74] H. Fakham, D. Lu, and B. Francois, "Power control design of a battery charger in a hybrid active PV generator for load-following applications," IEEE Trans. Ind. Electron., vol. 58, no. 1, pp. 85–94, 2011.

[75] J. G. Slootweg and W. L. Kling, "The impact of large scale wind power generation on power system oscillations," Electr. Power Syst. Res., vol. 67, no. 1, pp. 9–20, 2003.

[76] B. H. Chowdhury and S. Chellapilla, "Double-fed induction generator control for variable speed wind power generation," vol. 76, pp. 786–800, 2006.

[77] L. Fan, H. Yin, and Z. Miao, “A novel control scheme for DFIG-based wind energy systems under unbalanced grid conditions,” Electr. Power Syst. Res., vol. 81, no. 2, pp. 254–262, 2011.

[78] G. M. As, “Doubly fed induction generator uising back-to-back PWM converters and its application to variable- speed wind-energy generation,” 1996.

[79] T. F. Chan and L. L. Lai, “Permanent-magnet machines for distributed power generation: A review,” 2007 IEEE Power Eng. Soc. Gen. Meet. PES, pp. 6–11, 2007.

[80] H. Polinder, S. W. H. De Haan, M. R. Dubois, and J. G. Slootweg, “Basic operation principles and electrical conversion systems of wind turbines,” EPE J. (European Power Electron. Drives Journal), vol. 15, no. 4, pp. 43–50, 2005.

[81] C. Cárdenas, D. Gomez, J. Bécares, a Morejón, L. Gorostiaga, and E. Moya, “Control of a variable speed and permanent magnet wind turbine : GARBI 150,” Int. Conf. Renew. Energies Power Qual., 2010.

[82] M. Chinchilla, S. Arnaltes, and J. C. Burgos, “Control of permanent-magnet generators applied to variable-speed wind-energy systems connected to the grid,” IEEE Trans. Energy Convers., vol. 21, no. 1, pp. 130–135, 2006.

[83] H. Li, Z. Chen, and H. Polinder, “Optimization of multibrid permanent-magnet wind generator systems,” IEEE Trans. Energy Convers., vol. 24, no. 1, pp. 82–92, 2009.

[84] D. Bang and H. Polinder, “Review of generator systems for direct-drive wind turbines,” Eur. Wind Energy …, pp. 1–11, 2008.

[85] Y. Yuan, X. Zhang, P. Ju, K. Qian, and Z. Fu, “Applications of battery energy storage system for wind power dispatchability purpose,” Electr. Power Syst. Res., vol. 93, pp. 54–60, 2012.

[86] B. Ge, W. Wang, D. Bi, C. B. Rogers, F. Z. Peng, A. T. De Almeida, and H. Abu-Rub, “Energy storage system-based power control for grid-connected wind power farm,” Int. J. Electr. Power Energy Syst., vol. 44, no. 1, pp. 115–122, 2013.

[87] H. S. Krishnamoorthy, D. Rana, P. Garg, P. N. Enjeti, and I. J. Pitel, “Wind turbine generator-battery energy storage utility interface converter topology with medium-frequency transformer link,” IEEE Trans. Power Electron., vol. 29, no. 8, pp. 4146–4155, 2014.

[88] L. Jerbi, L. Krichen, and A. Ouali, “A fuzzy logic supervisor for active and reactive power control of a variable speed wind energy conversion system

associated to a flywheel storage system," Electr. Power Syst. Res., vol. 79, no. 6, pp. 919–925, 2009.

[89] G. O. Suvire and P. E. Mercado, "DSTATCOM with Flywheel Energy Storage System for wind energy applications: Control design and simulation," Electr. Power Syst. Res., vol. 80, no. 3, pp. 345–353, Mar. 2010.

[90] M. Saejia and I. Ngamroo, "Stabilization of microgrid with intermittent renewable energy sources by SMES with optimal coil size," Phys. C Supercond. its Appl., vol. 471, no. 21–22, pp. 1385–1389, 2011.

[91] J. Shi, Y. Tang, Y. Xia, L. Ren, and J. Li, "SMES based excitation system for doubly-fed induction generator in wind power application," IEEE Trans. Appl. Supercond., vol. 21, no. 3 PART 2, pp. 1105–1108, 2011.

[92] S. T. Kim, B. K. Kang, S. H. Bae, and J. W. Park, "Application of SMES and Grid Code Compliance to Wind/Photovoltaic Generation System," Ieee Trans. Appl. Supercond., vol. 23, no. 3, p. 4, 2013.

[93] D. Kairous and R. Wamkeue, "DFIG-based fuzzy sliding-mode control of WECS with a flywheel energy storage," Electr. Power Syst. Res., vol. 93, pp. 16–23, 2012.

[94] a. Abdel-Khalik, a. Elserougi, a. Massoud, and S. Ahmed, "A power control strategy for flywheel doubly-fed induction machine storage system using artificial neural network," Electr. Power Syst. Res., vol. 96, pp. 267–276, 2013.

[95] A. Rabiee, H. Khorramdel, and J. Aghaei, "A review of energy storage systems in microgrids with wind turbines," Renew. Sustain. Energy Rev., vol. 18, pp. 316–326, 2013.

[96] A. Evans, V. Strezov, and T. J. Evans, "Assessment of utility energy storage options for increased renewable energy penetration," Renew. Sustain. Energy Rev., vol. 16, no. 6, pp. 4141–4147, 2012.

[97] M. Beaudin, H. Zareipour, A. Schellenberglabe, and W. Rosehart, "Energy storage for mitigating the variability of renewable electricity sources: An updated review," Energy Sustain. Dev., vol. 14, no. 4, pp. 302–314, 2010.

[98] a. Etxeberria, I. Vechiu, H. Camblong, and J. M. Vinassa, "Comparison of three topologies and controls of a hybrid energy storage system for microgrids," Energy Convers. Manag., vol. 54, no. 1, pp. 113–121, 2012.

[99] G. L. Park, A. I. Schäfer, and B. S. Richards, "Renewable energy-powered membrane technology: Supercapacitors for buffering resource fluctuations in a

wind-powered membrane system for brackish water desalination," Renew. Energy, vol. 50, pp. 126–135, 2013.

[100] G. Xu, J. Morrow, and L. Xu, "Power oscillation damping using wind turbines with energy storage systems," IET Renew. Power Gener., vol. 7, no. 5, pp. 449–457, 2013.

[101] C. Abbey and G. Joos, "Supercapacitor energy storage for wind energy applications," IEEE Trans. Ind. Appl., vol. 43, no. 3, pp. 769–776, 2007.

[102] L. Qu and W. Qiao, "Constant power control of DFIG wind turbines with supercapacitor energy storage," IEEE Trans. Ind. Appl., vol. 47, no. 1, pp. 359–367, 2011.

[103] S. M. Muyeen, R. Takahashi, T. Murata, and J. Tamura, "Integration of an energy capacitor system with a variable-speed wind generator," IEEE Trans. Energy Convers., vol. 24, no. 3, pp. 740–749, 2009.

[104] S. Li, T. a. Haskew, and L. Xu, "Conventional and novel control designs for direct driven PMSG wind turbines," Electr. Power Syst. Res., vol. 80, no. 3, pp. 328–338, 2010.

[105] H.-W. Kim, S.-S. Kim, and H.-S. Ko, "Modeling and control of PMSG-based variable-speed wind turbine," Electr. Power Syst. Res., vol. 80, no. 1, pp. 46–52, 2010.

[106] D. V. W. P. Unit, A. Yazdani, and R. Iravani, "A Neutral-Point Clamped Converter System for," vol. 21, no. 2, pp. 596–607, 2006.

[107] N. P. W. Strachan and D. Jovcic, "Stability of a variable-speed permanent magnet wind generator with weak AC grids," IEEE Trans. Power Deliv., vol. 25, no. 4, pp. 2779–2788, 2010.

[108] Z. Chen and F. Blaabjerg, "Wind farm-A power source in future power systems," Renew. Sustain. Energy Rev., vol. 13, no. 6–7, pp. 1288–1300, 2009.

[109] B. Singh and S. N. Singh, "Wind Power Interconnection into the Power System: A Review of Grid Code Requirements," Electr. J., vol. 22, no. 5, pp. 54–63, 2009.

[110] A. Mullane, G. Lightbody, and R. Yacamini, "Wind-turbine fault ride-through enhancement," IEEE Trans. Power Syst., vol. 20, no. 4, pp. 1929–1937, 2005.

[111] S. M. Muyeen, R. Takahashi, T. Murata, and J. Tamura, "A Variable Speed Wind Turbine Control Strategy to Meet Wind Farm Grid Code Requirements," IEEE Trans. Power Syst., vol. 25, no. 1, pp. 331–340, 2010.

[112] M. Mohseni, M. a S. Masoum, and S. M. Islam, “Low and high voltage ride-through of DFIG wind turbines using hybrid current controlled converters,” Electr. Power Syst. Res., vol. 81, no. 7, pp. 1456–1465, 2011.

[113] M. Rahimi and M. Parniani, “Grid-fault ride-through analysis and control of wind turbines with doubly fed induction generators,” Electr. Power Syst. Res., vol. 80, no. 2, pp. 184–195, 2010.

[114] T. Karaipoom and I. Ngamroo, “Optimal Superconducting Coil Integrated Into DFIG Wind Turbine for Fault Ride Through Capability Enhancement and Output Power Fluctuation Suppression,” vol. 6, no. 1, pp. 28–42, 2015.

[115] J. Morren and S. W. H. de Haan, “Ridethrough of wind turbines with doubly-fed induction generator during a voltage dip,” IEEE Trans. Energy Convers., vol. 20, no. 2, pp. 435–441, 2005.

[116] M. J. H. H. R. P. R. A. Ramos, “Improved low-voltage-ride-through capability of fixed- speed wind turbines using decentralised control of STATCOM with energy storage system,” no. July 2011, pp. 719–730, 2012.

[117] M. M. a Mahfouz and M. a H. El-Sayed, “Static synchronous compensator sizing for enhancement of fault ride-through capability and voltage stabilisation of fixed speed wind farms,” Iet Renew. Power Gener., vol. 8, no. 1, pp. 1–9, 2014.

[118] T. H. Nguyen and D. C. Lee, “Advanced fault ride-through technique for PMSG wind turbine systems using line-side converter as STATCOM,” IEEE Trans. Ind. Electron., vol. 60, no. 7, pp. 2842–2850, 2013.

[119] M. E. Elshiekh, D. a. Mansour, and a. M. Azmy, “Improving Fault Ride-Through Capability of DFIG-Based Wind Turbine Using Superconducting Fault Current Limiter,” IEEE Trans. Appl. Supercond., vol. 23, no. 3, pp. 5601204–5601204, 2013.

[120] W. Guo, L. Xiao, and S. Dai, “Enhancing low-voltage ride-through capability and smoothing output power of DFIG with a superconducting fault-current limiter-magnetic energy storage system,” IEEE Trans. Energy Convers., vol. 27, no. 2, pp. 277–295, 2012.

[121] I. Ngamroo and T. Karaipoom, “Improving Low-Voltage Ride-Through Performance and Alleviating Power Fluctuation of DFIG Wind Turbine in DC Microgrid by Optimal SMES With Fault Current Limiting Function,” vol. 24, no. 5, 2014.

[122] I. Ngamroo and T. Karaipoom, “Cooperative Control of SFCL and SMES for Enhancing Fault Ride Through Capability and Smoothing Power Fluctuation of DFIG Wind Farm,” vol. 24, no. 5, 2014.

[123] M. a Pedrasa and T. Spooner, “A survey of techniques used to control microgrid generation and storage during island operation,” Proc. Aust. Univ. Power Eng. Conf.(AUPEC), pp. 10–13, 2006.

[124] J. a P. Lopes, C. L. Moreira, and a. G. Madureira, “Defining control strategies for microgrids islanded operation,” IEEE Trans. Power Syst., vol. 21, no. 2, pp. 916–924, 2006.

[125] G. Modes, A. Mehrizi-sani, G. S. Member, and R. Iravani, “Potential-Function Based Control of a Microgrid in,” vol. 25, no. 4, pp. 1883–1891, 2010.

[126] K. De Brabandere, K. Vanthournout, J. Driesen, G. Deconinck, and R. Belmans, “Control of microgrids,” 2007 IEEE Power Eng. Soc. Gen. Meet. PES, pp. 1–7, 2007.

[127] I. J. Balaguer, U. Supatti, Q. Lei, N. S. Choi, and F. Z. Peng, “Intelligent control for intentional islanding operation of microgrids,” 2008 IEEE Int. Conf. Sustain. Energy Technol. ICSET 2008, pp. 898–903, 2008.

[128] M. N. Marwali and a. Keyhani, “Control of distributed generation systems-Part I: Voltages and currents control,” IEEE Trans. Power Electron., vol. 19, no. 6, pp. 1541–1550, 2004.

[129] C. V. Dobariya and S. a. Khaparde, “Decoupled power controller for inverter-interfaced distributed generation system,” 2007 IEEE Power Eng. Soc. Gen. Meet. PES, pp. 1–6, 2007.

[130] C. T. Lee, C. C. Chuang, C. C. Chu, and P. T. Cheng, “Control strategies for distributed energy resources interface converters in the low voltage Microgrid,” 2009 IEEE Energy Convers. Congr. Expo. ECCE 2009, no. 1, pp. 2022–2029, 2009.

[131] W. De Soto, S. a. Klein, and W. a. Beckman, “Improvement and validation of a model for photovoltaic array performance,” Sol. Energy, vol. 80, no. 1, pp. 78–88, 2006.

[132] C. Carrero, J. Amador, and S. Arnaltes, “A single procedure for helping PV designers to select silicon PV modules and evaluate the loss resistances,” Renew. Energy, vol. 32, no. 15, pp. 2579–2589, 2007.

[133] S. Liu, R. a Dougal, and S. Member, “Dynamic Multiphysics Model for Solar Array Dynamic Multiphysics Model for Solar Array,” vol. 17, no. 2, pp. 285–294, 2002.

[134] M. G. Villalva, J. R. Gazoli, and E. R. Filho, “Comprehensive Approach to Modeling and Simulation of Photovoltaic Arrays,” Power Electron. IEEE Trans., vol. 24, no. 5, pp. 1198–1208, 2009.

[135] R. Ramaprabha and B. L. Mathur, “A comprehensive review and analysis of solar photovoltaic array configurations under partial shaded conditions,” Int. J. Photoenergy, vol. 2012, 2012.

[136] L. Gao, R. a. Dougal, S. Liu, and A. P. Iotova, “Parallel-connected solar PV system to address partial and rapidly fluctuating shadow conditions,” IEEE Trans. Ind. Electron., vol. 56, no. 5, pp. 1548–1556, 2009.

[137] S. M. MacAlpine, R. W. Erickson, and M. J. Brandemuehl, “Characterization of power optimizer potential to increase energy capture in photovoltaic systems operating under nonuniform conditions,” IEEE Trans. Power Electron., vol. 28, no. 6, pp. 2936–2945, 2013.

[138] M. G. Villalva, T. G. de Siqueira, and E. Ruppert, “Voltage regulation of photovoltaic arrays: small-signal analysis and control design,” IET Power Electron., vol. 3, no. 6, p. 869, 2010.

[139] Muhammed Y Worku and M. Abido, “Real-Time Implementation of Grid-Connected PV System with Decoupled P-Q Controllers,” in 2014 22nd Mediterranean Conference on Control and Automation (MED) University of Palermo. June 16-19, 2014. Palermo, Italy, 2014.

[140] F. Liccardo, P. Marino, and G. Raimondo, “Robust and fast three-phase PLL tracking system,” IEEE Trans. Ind. Electron., vol. 58, no. 1, pp. 221–231, 2011.

[141] B. Singh and J. Solanki, “A Comparison of Control Algorithms for DSTATCOM,” IEEE Trans. Ind. Electron., vol. 56, no. 7, pp. 2738–2745, 2009.

[142] J. Kennedy, “The particle swarm: social adaptation of knowledge,” Proc. 1997 IEEE Int. Conf. Evol. Comput. (ICEC ’97), pp. 303–308, 1997.

[143] P. J. Angeline, “Evolutionary optimization versus particle swarm optimization: Philosophy and performance differences,” Lect. Notes Comput. Sci. Evol. Program. VII, vol. 1447, pp. 601–610, 1998.

[144] L. Zhang, H. Yu, and S. Hu, “Optimal choice of parameters for particle swarm optimization,” J. Zhejiang Univ. Sci., vol. 6A, no. 6, pp. 528–534, 2005.

[145] P. Srithorn, M. Sumner, L. Yao, and R. Parashar, “Power system stabilisation using STATCOM with supercapacitors,” Conf. Rec. - IAS Annu. Meet. (IEEE Ind. Appl. Soc., pp. 1–8, 2008.

[146] Muhammed Y Worku and M. Abido, “Supercapacitors for wind power application,” in International Conference on Renewable Energy Research and Applications, Madrid, Spain, 20-23 October 2013, 2013, no. October, pp. 20–23.

[147] Y. Bae, T. K. Vu, and R. Y. Kim, “Implemental control strategy for grid stabilization of grid-connected PV system based on German grid code in symmetrical low-to-medium voltage network,” IEEE Trans. Energy Convers., vol. 28, no. 3, pp. 619–631, 2013.

[148] M. Tsili and S. Papathanassiou, “A review of grid code technical requirements for wind farms,” IET Renew. Power Gener., vol. 3, no. 3, p. 308, 2009.

Vitae

Name	:Muhammed Yibre Worku
Nationality	:Ethiopian
Date of Birth	:12/29/1982
Email	:muhammedw@kfupm.edu.sa; muhammed251@gmail.com
Address	:Addis Ababa, Ethiopia
Academic Background	:Received Master of Technology (M.TECH) in Electrical Engineering with specialization in Power Apparatus and Electrical Drives from Indian Institute of Technology Roorkee (IITR) in June 2008

PUBLICATIONS

Patents

1. M.A.Abido, Muhammed Y. Worku, "Design and Real-Time Implementation of ANFIS-Based MPPT with Decoupled P-Q Controllers for a PV System," *Patent Application*, Docket # 37000.02, April 1, 2014.
2. M.A.Abido, Muhammed Y. Worku, "Fault Ride Through and Power Smoothing in Grid-Connected PV Array with Supercapacitor Energy Storage,". *Patent Application*, Docket # 37000.29, April 1, 2014.

Journal Publications

1. Muhammed Y.Worku, M.A. Abido and M.S.Khalid, "Minimization of Power Fluctuation in Grid-Connected PV Array Using Supercapacitor Energy Storage System", International Journal of Electrical Power and Energy Systems.(Second Revision)
2. M.A. Abido, M. Sheraz Khalid and Muhammed Y. Worku, "An Efficient ANFIS-Based Maximum Power Point Tracking for PV Systems", The Arabian Journal for Science and Engineering. (Accepted)
3. Muhammed Y.Worku, and M.A. Abido, "Fault Ride Through and Power Smoothing in Grid-Connected PV System with Supercapacitor Energy Storage System, IET, Generation, Transmission & Distribution. (Under Review)
4. Muhammed Y.Worku, M. A. Abido, M.S.Khalid, M. A. Hassan, I.M.Elamin and A. H. A. Rahim, "Real Time Modeling and Control of Grid Connected PV System", Electric Power Components and Systems.(Under Review)

Conference Publications

1. Muhammed Y. Worku, M.A.Abido, "Supercapacitor Energy Storage System for Fault Ride through in Grid-Connected PV Array", Saudi Arabia Smart Grid Conference and Exhibition, Jeddah, Saudi Arabia, December 14-17,2014.***(Won the Best Paper Award)***
2. Muhammed Y. Worku, and M.A. Abido, "Real-Time Implementation of Grid-Connected PV System with Decoupled P-Q Controllers",22nd IEEE Mediterranean Conference on Control and Automation, MED'14 Palermo, Italy, June 16-19, 2014.
3. Muhammed Yibre, M.A.Abido, "SUPERCAPACITORS For Wind Power Application", 2nd International Conference on Renewable Energy Research and Applications Madrid, Spain, 20-23 October 2013.
4. Muhammed Y. Worku, M.A.Abido, "Grid-Connected PV Array with Supercapacitor Energy Storage System for Fault Ride Through," 2015 IEEE International Conference on Industrial Technology, Sevilla, Spain March 17-19, 2015.
5. Muhammed Yibre, M.A.Abido, "Supercapacitors Coupled With DSTATCOM for Stability of Wind Power Generation", Saudi Arabia Smart Grid Conference and Exhibition, Jeddah, Saudi Arabia,November 24-27,2013.
6. Muhammed Yibre, M.A.Abido, "Active And Reactive Power Control Of Grid Integrated DFIG For Variable Speed Wind Power Generation", Saudi Arabia Smart Grid Conference and Exhibition, Jeddah, Saudi Arabia, December 08-11,2012.